Fire Performance of Reinforced Concrete Slabs

By

Adam Levesque

A Thesis

Submitted to the Faculty

of the

WORCESTER POLYTECHNIC INSTITUTE

in partial fulfillment of the requirements for the

Degree of Master of Science

in

Civil Engineering

May 2006

APPROVED:

Professor Leonard D. Albano, Major Advisor
Civil and Environmental Engineering

Professor Robert W. Fitzgerald, Co-Advisor
Civil and Environmental Engineering

Professor Fredrick L. Hart, Head of Department
Civil and Environmental Engineering

Acknowledgements

I would like to thank my advisor Professor Leonard D. Albano for giving me the opportunity to carry out research work related to the field of structural engineering and fire protection. I am extremely grateful for his valuable thoughts and other contributions towards the development of my thesis.

I would like to thank Professor Robert W. Fitzgerald for his guidance in developing research strategies for me to implement in the completion this thesis.

I would also like to thank Jeremy Cote for helping me with the TAS simulations. He saved me many hours in the lab trying to understand the software.

Most importantly I would like to thank my parents, Deborah and Paul Levesque, for their continued support. I could not have completed this thesis without them, thank you.

Abstract

In the United States design for fire safety follows a prescriptive code-based approach. Building codes detail the types of construction materials, assemblies, and fire suppression systems that are required for various building types. This prescriptive method has prevented structural engineers from exposure to performance-based design approaches for fire safety.

The motivation for this thesis was to increase the awareness of the structural engineering field to the concepts behind structural design for fire safety. Extensive research has been published on the performance of structural steel in fire conditions, and simplified design tools already exist to describe its behavior. Such tools do not exist for reinforced concrete structures. Research on concrete has been more focused on material properties rather than structural performance.

This thesis presents a simplified design tool which assesses the fire performance of reinforced concrete. An Excel-based spreadsheet application was developed for thermal analysis of concrete slabs. It accounts for different aggregate types, slab thicknesses, and fire exposures. Several analyses were performed with the spreadsheet application to examine the affect slab thickness and aggregate types have on the fire performance of concrete slabs in standard and natural fires. The results were compared with published test data and finite element software simulations to benchmark the accuracy of the proposed tool. Furthermore, methods for the design of reinforced concrete slabs in fire conditions are presented.

Table of Contents

Table of Figures

1 Introduction

The objective of fire safety is to protect life and property. Fires can occur at any time in buildings, and the safety of occupants and maintaining the integrity of the structure are of major importance. Building codes prescribe detailed measures for the fire safety of structural members because when other means for containing a fire fail, such as a fire suppression system ,structural integrity is the last line of defense. Code-based structural fire safety requirements refer to fire resistance which is defined as the ability of a structural element to maintain its load-bearing functions under standard fire conditions. The fire resistance rating of a structural member is the elapsed time it exhibits resistance with respect to structural integrity, stability, and temperature transmission while exposed to standard fire conditions. The measured fire resistance of a structural member or assembly is dependent on the geometry of elements, materials used in construction, load intensity, fire exposure, and the characteristics of a given furnace.

Testing for the fire resistance of materials is done in laboratories by exposing elements to fire conditions and monitoring their performance. Numerical and analytical methods were developed based on these fire tests as an economical alternative to laboratory testing. Over the past two decades there has been a widespread use of finite element programs to determine structural performance in both standard and natural fire conditions.

The above methods for predicting fire resistance do not increase the awareness of structural engineers to the concepts of design for fire conditions. They are either prescriptive in their application to design or being performed by the

materials and fire communities whose interests are geared towards properties of materials in fire conditions and complicated performance-based analyses of structural elements. From a design standpoint it is not sensible for a practicing structural engineer to use finite element software to analyze structural fire performance because analyses are time consuming and the use of these programs requires a strong background in fire protection engineering which most structural engineers do not have.

The motivation for this thesis was to increase the awareness of the structural engineering field to the concepts behind structural design for fire safety. The development of simplified design tools that predict the fire performance of structural elements is of utmost importance to practicing structural engineers. These tools address structural fire performance from an applied design approach similar to those which exist for the effects of wind and earthquake loads. Extensive research has been published on the performance of structural steel in fire conditions, and simplified design tools already exist to describe its behavior. However, such tools do not exist for reinforced concrete structures where research has been focused on the material properties of concrete in fire conditions rather than structural performance.

1.1 Objective

The objectives of this thesis are to categorize the research and to explore a simplified design tool that can be used by practicing structural engineers to assess the performance of concrete elements during fire conditions. Also, through the application of the design tool the user will gain an understanding of concretes thermal properties and basic principles of heat transfer.

1.2 Scope of Work

The following is a list of activities that define the scope of this work:

- Investigate literature covering the performance of reinforced concrete elements exposed to fire conditions and create an annotated bibliography of works relevant to the topic
- Investigate concepts of heat transfer in concrete and their application to one-dimensional thermal analyses.
- Develop a spreadsheet tool that calculates cross-section temperature distributions in concrete slabs.
- Perform studies of the fire performance of concrete slabs with varying aggregates and thicknesses against different fire exposures.
- Benchmark the use of the spreadsheet tool for analysis of heat transfer in concrete slabs with the use of TAS (Thermal Analysis Software), a finite element program.
- Explore case studies involving the failures of reinforced concrete roof and floor slabs during fires.

2 Literature Review

This section provides an overview of published research on the structural fire performance of reinforced concrete elements. The techniques used to assess concrete fire performance are detailed as well as the publications that were critical to the development of this thesis.

2.1 Performance of Concrete Elements in Fire Conditions

The measures used to assess the fire performance of concrete elements remain the traditional practice of fire testing along with numerical and analytical methods and finite element software; all of which have been developed to simulate fire testing results. Sensory and optical techniques have been developed to determine the post-fire material properties of concrete (Cruz 1962; Benedetti 1998). However, these methods are used in the evaluation of fire damage and cannot be applied to the assessment of concrete performance during fire conditions.

2.1.1 Fire Tests

Fire tests represent the oldest method to evaluate the fire endurance of structural elements. As early as 1918, fire tests were being performed on building columns at the Underwriters' Laboratories (1918). Fire tests expose structural elements to different fire severities and are either performed within a furnace or on full-scale buildings. Many countries use full-scale fire resistance tests to evaluate the fire performance of structural elements. Full-scale tests are preferred for the study of structural elements and assemblies of a relatively small extent because they give a more accurate representation of the various phenomena that occur during fire conditions such as the effects of thermal expansion and deformation under load.

2.1.1.1 Furnace Testing

Test furnaces are the most common method used to evaluate the fire resistance of structural elements. The furnaces' chamber is heated either electronically or by burning liquid fuel. The temperature history in the furnace is controlled by a designated fire curve, typically those of "standard fires". Usually, furnaces are equipped with devices to measure temperatures, and deformations, and to load test specimens.

Furnaces follow different testing specifications depending on the laboratory and are specially constructed for their purpose. There are vertical furnaces that are constructed for testing vertical partitions such as walls and doors; horizontal furnaces are used for testing horizontal partitions such as floors and roofs. Also, there are special beam and columns furnaces, although they are often tested in horizontal furnaces. Some furnaces are even designed so that all types of building elements can be tested.

Fire tests in furnaces are carried out by exposing certain surfaces of a test specimen to heating in a manner that simulates its exposure to heating in a fire (Abrams & Gustaferro 1968; Wade 1992). Generally, test specimens are construction elements for which a fire resistance classification is desired. Specimens are tested under conditions that are similar to those in service such as loading and restraint. Thermocouples are placed in the furnace and within specimens to measure temperatures. A specimen is considered fire resistant during a test up until the point it does not satisfy certain testing criteria with respect to stability, integrity, and thermal insulation.

2.1.1.2 Full-Scale Fire Tests

Occasionally full-scale fire tests are performed on structural systems. These tests give a more realistic representation of fire performance because they simulate the performance of a system as opposed to the study of discrete elements or small-scale assemblies. The major drawback of full-scale testing is that it is extremely expensive in comparison with furnace testing.

The most comprehensive full-scale testing completed took place in 1995 in Cardington, England. A series of fire tests were carried out on an eight-storey, steel-concrete composite structure. As an outgrowth of the Cardington tests, numerous numerical and theoretical models have been developed to simulate the performance of the structure. The test results and the subsequent models have deepened understanding of the mechanical behavior of highly redundant structures in extreme fires.

2.1.1.3 Standard Fires

Most fire resistance tests follow time-temperature curves that serve as "standard fires" which are idealized simulations of room fires. Since the tests follow established time-temperature curves, the heat load imposed on a test specimen is calculable at any point during testing. Standard fire test time-temperature curves for various countries can be seen in Figure 2.1 (Lie 1992). The most widely used standard test conditions are the ASTM E119 (United States and Canada) and ISO 834 (Australia, New Zealand, and England) (Buchanan 2001).

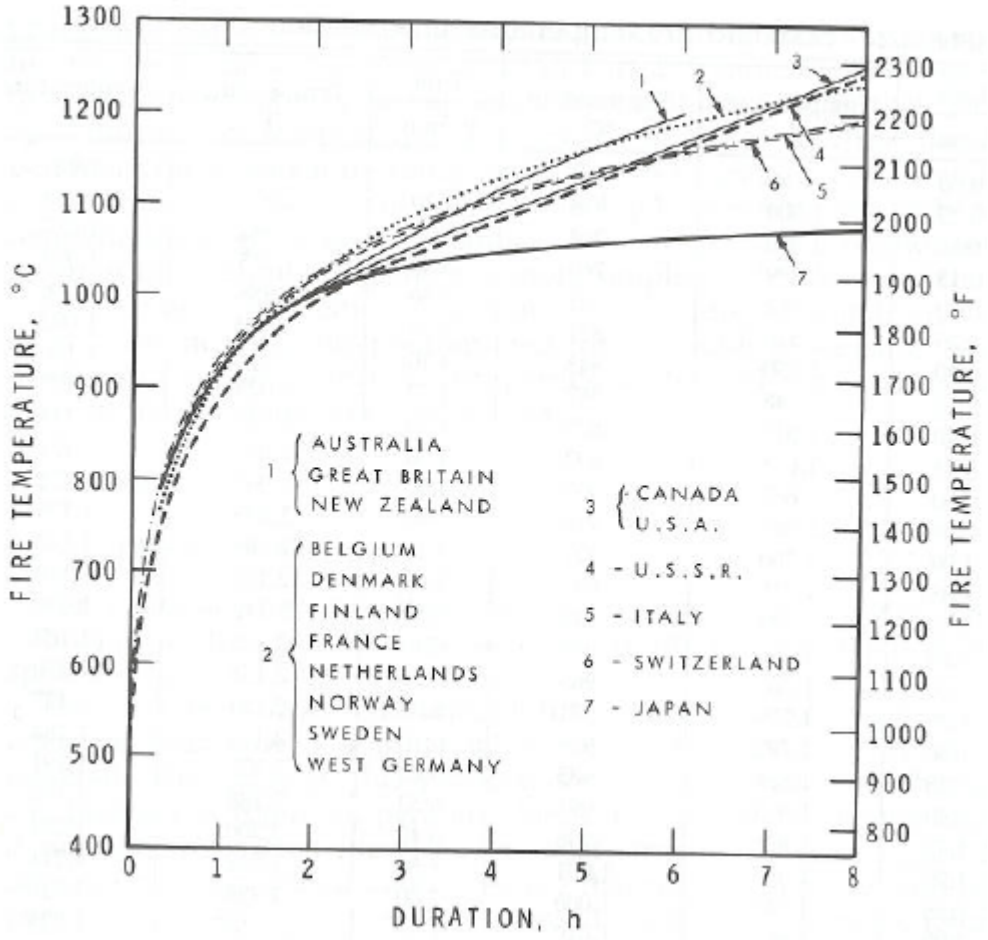

Figure 2.1: Standard Fire Temperature-Time Curves for Various Countries (as taken from Lie 1992)

Temperature values, T (ºC), for the ISO 834 fire follow the equation:

$$T = 345\log_{10}(8t+1) + T_o \text{ ,} \quad \textbf{(Equation 2.1)}$$

where t (minutes) is the time and T_o (ºC) is the ambient temperature. Failure criteria for the ISO 834 fire are (Malhotra 1982):

- Collapse or the downward deformation of flexural members exceeding L/30 where L is the span
- Ignition of a cotton pad held close to an opening for 10 seconds
- Temperature of the unexposed face rising more than 140ºC as an average or by more than 180ºC at any point

The ASTM E119 curve is defined by discrete points which can be seen in Table 2.1 along with the corresponding ISO 834 temperatures. A simplified equation that approximates the ASTM E119 curve is given by (Lie 1992):

$$T = 750\left[1 - e^{-3.79553\sqrt{t_h}}\right] + 170.41\sqrt{t_h} + T_o, \quad \textbf{(Equation 2.2)}$$

where t_h (hours) is the time. The conditions for failure for reinforced concrete components exposed to the ASTM E119 protocol are (Ellingwood & Shaver 1979):

- Collapse of the component or failure to inhibit passage of flame or hot gases
- Attainment of the limiting average temperature of 593ºC in reinforcement
- Rise of 139ºC in the average temperature of the unexposed surface of the test component.

Table 2.1: ISO 834 and ASTM E119 Time-Temperature Curves at Various Points

Time (minutes)	ASTM E119 Temperature (ºC)	ISO 834 Temperature (ºC)
0	20	20
5	538	576
10	704	678
30	843	842
60	927	945
120	1010	1049
240	1093	1153
480	1260	1257

2.1.1.4 Natural Fires

Standard fires are suitable for comparison purposes but do not provide a true indication of how structural components and assemblies will behave in an actual fire. Other than collapse the failure criteria for both the ISO 834 and ASTM E199 tests are not related to any physical limit state performance. Their increasing temperatures do not reflect the fact that natural fires, also known as compartment fires, decrease in

intensity once the fuel in the compartment has been burned. Furthermore, the standard fire curves do not account for material composition within the compartment, the boundary construction of the compartment, or ventilation effects.

Compartment fires have been utilized to better represent the conditions of natural fires within furnace testing (Ellingwood & Shaver 1979). Fire curves that portray compartment fires characterize the fuel and dimensions in typical room compartments. The two significant factors affecting fire curves are the fire load, q (MJ/m^2), and the ventilation or opening factor, φ ($m^{1/2}$), described as:

$$\varphi = \frac{A_o \sqrt{h}}{A_t}, \quad \textbf{(Equation 2.3)}$$

where A_o (m^2) is the total area of window and door openings, h (m) is the weighted average of height openings, and A_t (m^2) is the total area of compartment bounding surfaces.

In 1976 the National Bureau of Standards completed a survey of fire and live loads in office buildings in the U.S., and the compiled fire load data can be seen in Figure 2.2 (Ellingwood & Shaver 1979). The SDHI-M and SDHI-95 curves are for general clerical offices. The SDHI-95 represents the 95 percentile of severity while LDMI-M curve represents file and storage rooms for government and private offices. These fire curves are similar to those experienced in compartment tests and contribute to better understanding the performance of structural elements and assemblies in actual fires.

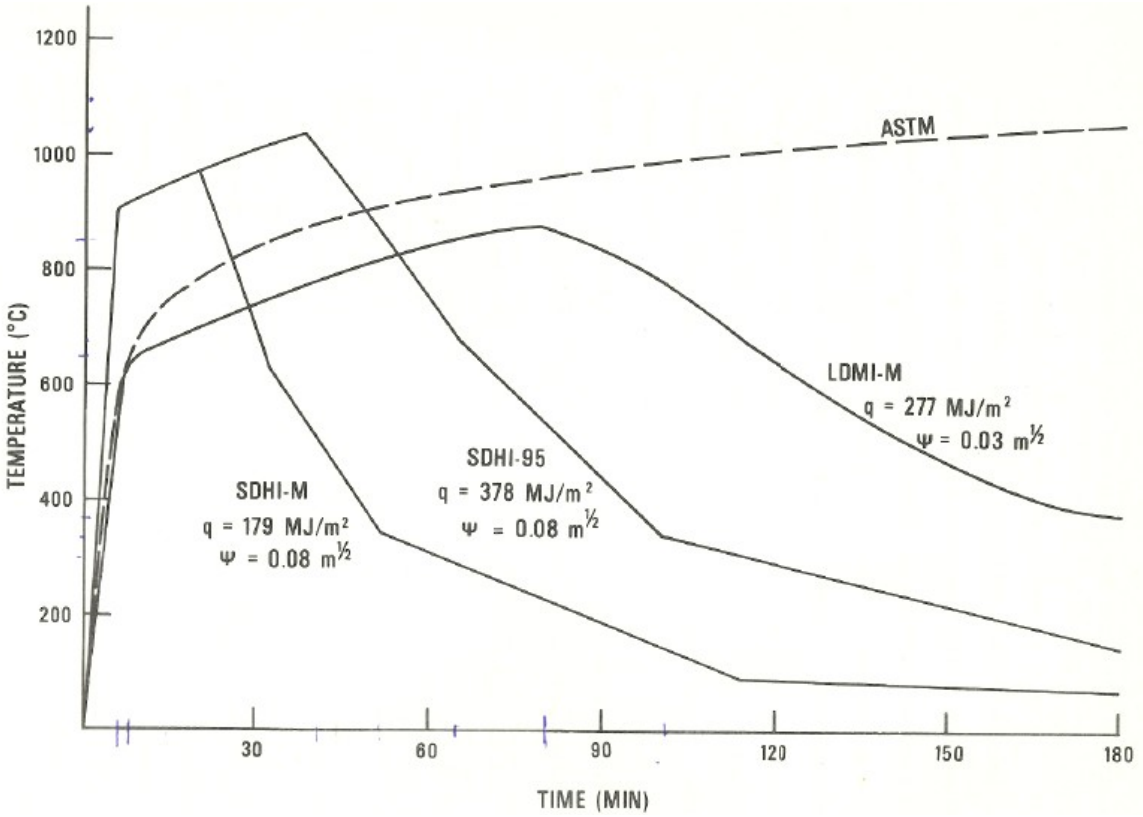

Figure 2.2: Comparison of Computed Natural Fire Curves with ASTM E119 (as taken from Ellingwood & Shaver 1979)

2.1.2 Numerical and Analytical Methods

Due to the costs involved in performing fire tests, numerical and analytical methods have been developed as an economic alternative for determining fire resistance. These methods have proven to be successful in predicting the fire resistance of structural elements (Lie 1972; Lie 1992), and the application and limitations of each are explained.

The main advantage of analytical methods is that simple graphs and formulae can be used to estimate the fire resistance (Bushev, Pchelintsev, Fedorenko, & Yakovlev 1972; Lie 1972; Malhotra 1982; Wade 1991). These techniques eliminate the need for computers and special testing devices, and estimations can be done

quickly without much effort by applying simple algebra. However, analytical procedures are less accurate in determining temperatures in structural elements than numerical and testing procedures because their application is limited to specific conditions and assumptions.

Numerical methods, albeit more complicated, have several advantages over their analytical counterparts (Harmathy 1979; Hertz 1981; Munukutla 1989; Lie 1992). For instance, they enable the solution of complex heat transfer problems for which analytical solutions have not yet been developed. Additionally, solving the governing heat transfer equations numerically allows for the implementation and investigation of temperature- dependent material properties. On the other hand, use of numerical methods is more complicated and time consuming than the use of analytical methods. Time is needed to develop and input the model as well as to review and interpret the body of results. Computers have reduced calculation time significantly but the preparation phase before execution is still cumbersome and involves programming equations into software applications as well as determining material properties as a function of time.

2.1.3 Special-Purpose Finite Element Software

Advancements in computer capabilities led to the development of special-purpose finite element software programs such as SAFIR, FEAST, and TAS (Wang 2002; Thermal Analysis Software) that model the performance of structural elements in fire conditions. These programs adhere to numerical methods and also consider the effects of restraint, loading, and deformation which allow for incredibly realistic simulations. Entire structural systems can be analyzed with these powerful programs.

The drawbacks of finite element software packages are that they are expensive, their interface is difficult to learn, and analyses are time consuming.

2.2 Distribution of Research

This section classifies the scope of published research on the structural fire performance of concrete elements. The distribution of publications for various structural elements can be seen in Figure 2.3 while Figure 2.4 characterizes the bodies of work in the aforementioned areas of special-purpose finite element software, fire tests, and numerical and analytical methods. Studies of specific structural elements are characterized in Figures 2.5, 2.6, and 2.7 while a research timeline is presented in Figure 2.8.

Figure 2.3 shows that little work has been done on the performance of reinforced concrete systems in fire conditions. Research has been more focused on the performance of individual structural elements so the performance of concrete structures and frames in fire conditions remains unknown. It is important to note that approximately half of the fire test data after the year 1996 is related to the Cardington fires. All of the publications summarized in the figures appear in Appendix A in an annotated bibliography.

The primary databases used to compile the literature were ScienceDirect (Elsevier B. V. 2006) and Civil Engineering Database (American Society of Civil Engineers 2006) which consists of publications by the ASCE with the keywords used in searches being “concrete”, “fire”, and “reinforced”. WPI subscribed journals in the discipline of fire protection engineering and the library catalog were explored using the same keywords. Additionally, the websites for Universities and Research

Institutions which produced multiple publications were searched to find further work on the subject of the fire performance of concrete elements.

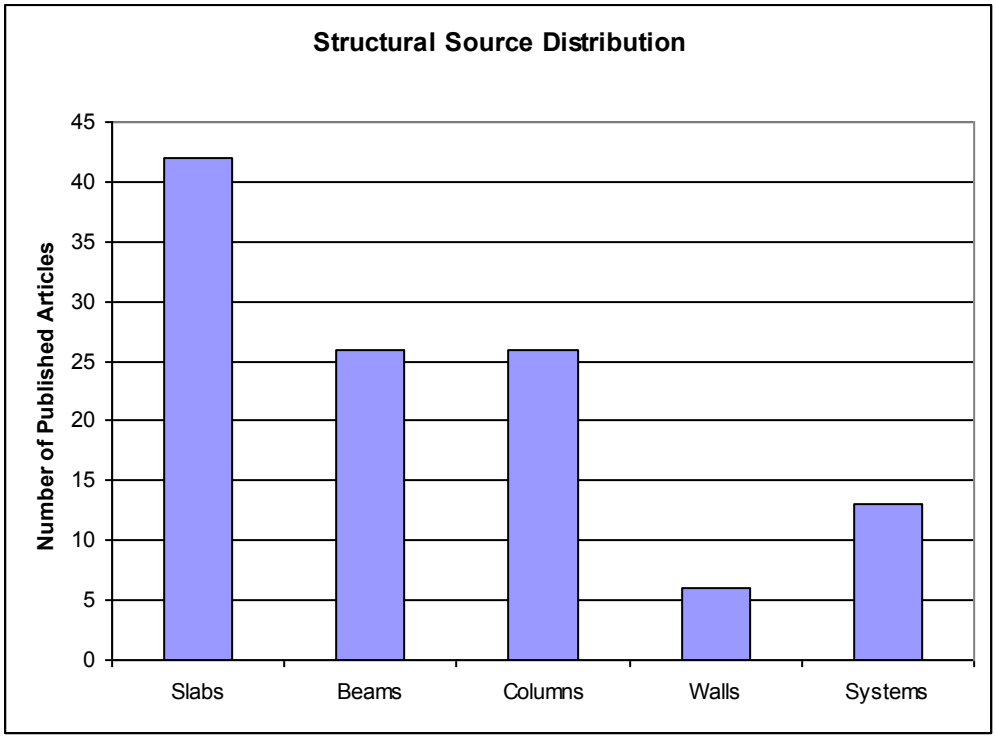

Figure 2.3: Source Distribution for Structural Elements (n = 95)

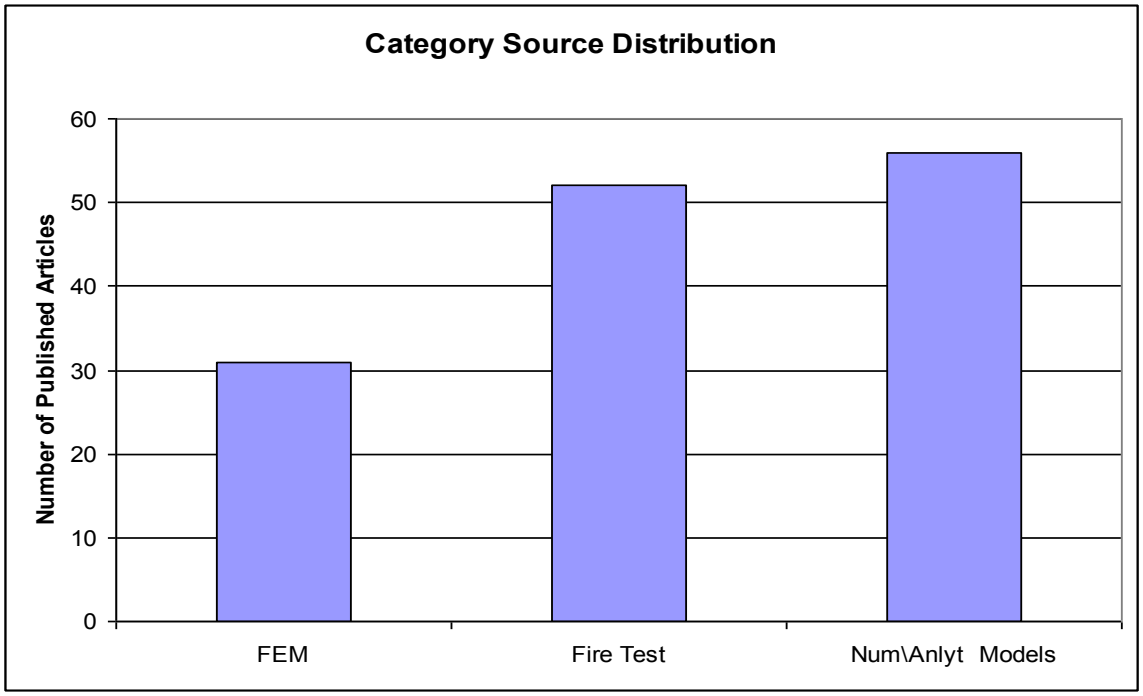

Figure 2.4: Characterized Research on Structural Elements (n = 95)

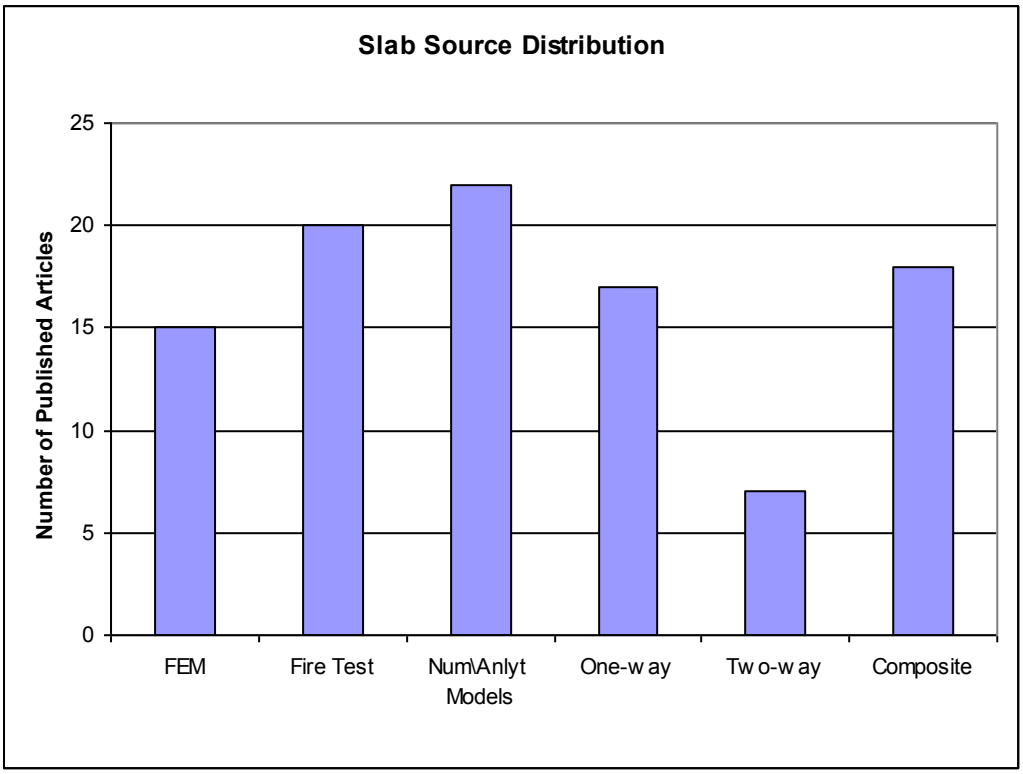

Figure 2.5: Source Distribution for Reinforced Concrete Slabs (n = 42)

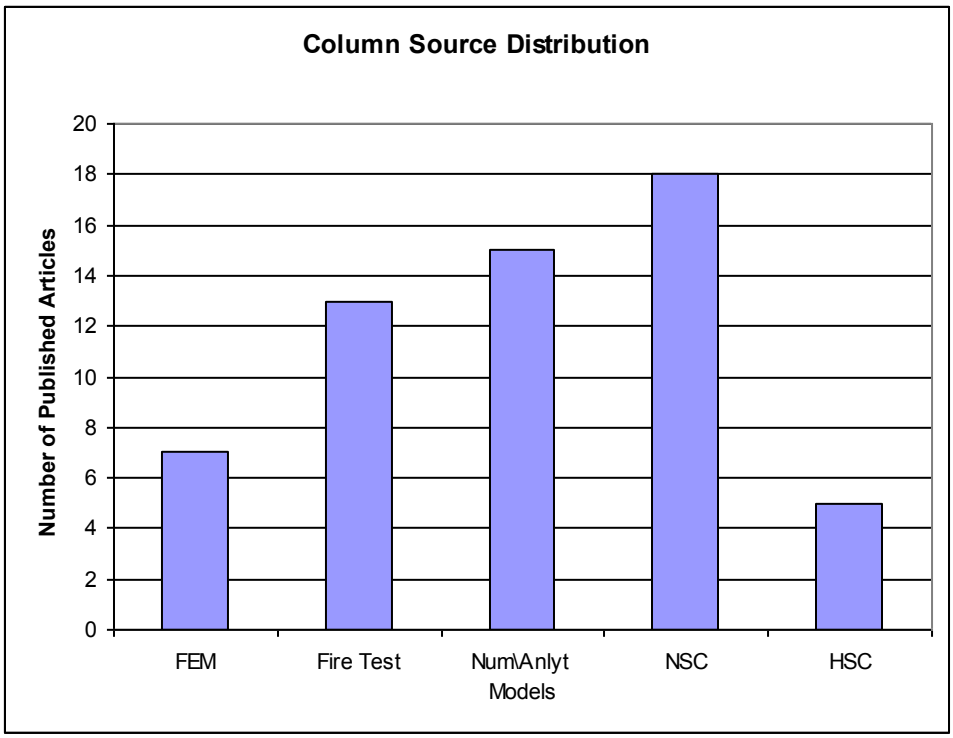

Figure 2.6: Source Distribution for Reinforced Concrete Beams (n = 26)

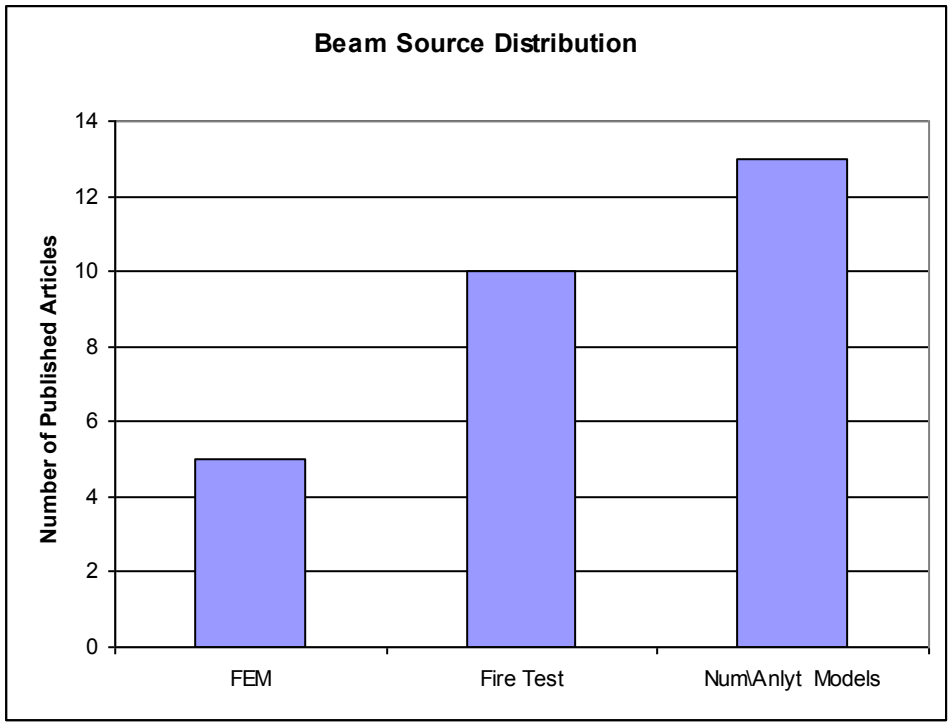

Figure 2.7: Source Distribution for Reinforced Concrete Columns (n = 26)

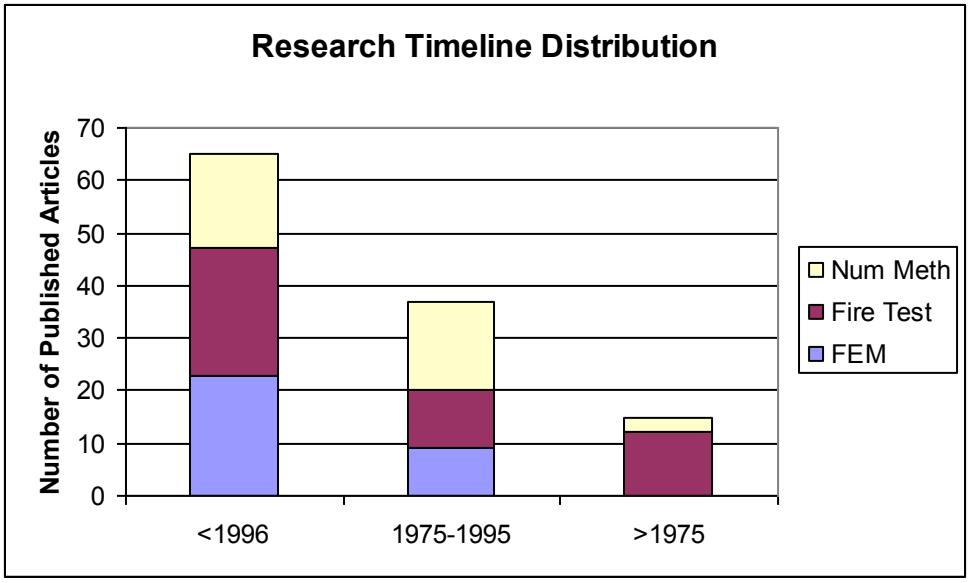

Figure 2.8: Research Timeline

2.3 Pertinent Works

This section provides an overview of published research work that contributed to the development of this thesis. An annotated bibliography of works reviewed on the topic of the fire performance of concrete can be found in Appendix A.

2.3.1 Bushev et al., 1972

This text presents methods for testing and calculating the fire resistance of various structural elements. The fire resistance of concrete structures is examined using a numerical method based on the ISO 834 time-temperature curve. Time-dependent material properties for concrete established during testing in the late 1960s are presented for different aggregates. When examining the literature it was found the time-dependent properties were not accurate when compared with more recently established data (Lie 1992; Malhotra 1982).

2.3.2 Lie, 1972

Lie's book published in 1972 discusses the concept of fire development and severity as well as economic losses due to fire. The behavior of concrete materials in fire conditions is detailed as well as an analytical method for predicting the fire resistance of concrete elements using the ISO 834 fire curve. The concept of applying one-dimensional analysis to predict the behavior of three-dimensional elements is implemented in the analytical procedure.

2.3.3 CRSI, 1980

The Concrete Reinforcing Steel Institute published this text in 1980 to summarize the available technical information covering the fire resistance of reinforced concrete elements. Building code requirements for fire resistance are detailed as well as analytical and rational methods for calculating fire endurance based on ASTM E119 testing. Example problems are presented that illustrate the structural behavior of concrete elements and systems in fire conditions along with design procedures. The empirical design procedures utilizing isotherms from ASTM E119 fire testing provide a more realistic prediction of the performance of a real

structure in an actual fire by detailing the effects fire has on the capacity of concrete elements as opposed to following prescriptive fire resistance ratings.

2.3.4 Malhotra, 1982

This text provides background on fire resistance needs and requirements, methods for determining fire severity, and the material properties of concrete at elevated temperatures. Design methods for the fire performance of reinforced concrete elements are introduced. The proposed design procedure utilizes empirical temperature distribution charts derived from concrete specimens tested according to ISO 834 specifications and data for the strength of concrete and reinforcing steel at elevated temperatures.

2.3.5 Munukutla, 1989

Munukutla's research report in 1989 details numerical simulations of the fire performance of concrete walls. He developed a finite element program to compute temperature profiles within concrete walls for various types of fire conditions. The program performs a one-dimensional heat transfer analysis for a wall exposed to fire on one side. Temperature distributions through the thickness of the wall are calculated using the finite difference method with a correction factor for the unexposed surface. The material properties of concrete are input to the formulation as temperature- dependent values.

2.3.6 Wade, 1991

Similar to Malhotra (1982), Wade presents design methods that assess the fire performance of reinforced concrete elements. There are some differences between the works of Wade and Malhotra. Wade's procedure makes use of updated empirical

temperature distribution charts and data for the strength of concrete and reinforcing steel at elevated temperatures. It also includes alternate design equations for fire conditions that consider building type.

2.3.7 Wade, 1992

In this technical report Wade describes a series of fire tests that were conducted on reinforced concrete slabs composed of different aggregates. Slabs of either 60mm (Alluvial Quartz, Quarried Greywacke, Limestone, and Pumice) or 175mm (Alluvial Quartz and Quarried Greywacke) were prepared, and their mix design and aggregate properties are detailed. Two slabs, each of area 1m by 1m, were cast with reinforcing steel for each aggregate type and thickness. Thermocouples were placed at the following predetermined depths: 60mm slabs (exposed face, 20mm, 40mm, and unexposed face) and 175mm slabs (exposed face, 35mm, 70mm, 105mm, 140mm, and exposed face). The slabs were cured for 28 days in ambient conditions.

A diesel-fired pilot furnace was used to test the concrete slabs at BRANZ laboratories in accordance with the ISO 834 specifications. The specimens were tested unloaded in a vertical orientation and fastened to a frame using two bolts on each side resulting in partial restraint against thermal expansion, but not to an extent that would significantly affect their fire performance. The fire resistance of each slab was recorded following the failure criteria set forth by the ISO 834 standard fire test.

2.3.8 Lie, 1992

This text explains fire resistance needs and requirements according to the prescriptive methods proposed in building codes in addition to the basic principles of

fire protection. The thermal and mechanical properties of concrete are detailed. Lie describes the application of multiple numerical techniques for calculating temperatures and fire resistance for concrete elements. Numerical methods for a wide variety for concrete structural members are detailed including columns with rectangular, square, or circular cross-sections, floor and roof slabs, and concrete-filled tubular steel columns.

2.3.9 Cooper & Franssen, 1999

This report identifies partition designs for which the use of one-dimensional thermal analysis in fire modeling would lead to a successful evaluation of their thermal fire performance. It was determined that gypsum-panel/steel-stud or wood-stud wall systems, concrete block wall, and poured concrete slabs supported by steel beams have three-dimensional elements that have negligible heat transfer effects so a one-dimensional thermal analysis will produce successful results when applied correctly. The authors conclude that reinforced concrete beam/slab systems require a two-dimensional analysis because of heat transfer in the beams.

2.3.10 Summary

Through review of the literature, it was found that the European, Australian, and New Zealand building codes contain simple analytical procedures for assessing the fire performance of concrete elements. These procedures provide an alternative approach to the prescriptive code methods used in the United States for design for fire safety. Additionally, the information provided in the aforementioned sources was essential to the development of a simplified design tool. The implementation of these sources to the development of this thesis is explained in the following chapter.

3 Methodology

The motivation for this thesis was to increase the awareness of the structural engineering field to the concepts behind structural design for fire safety. Extensive research has been published on the performance of structural steel in fire conditions, and simplified design tools already exist to describe its behavior. Such tools do not exist for reinforced concrete structures. As suggested by the literature review, the research on concrete has been more focused on material properties rather than structural performance.

It was decided that the best approach to increase awareness of the structural fire performance of reinforced concrete in fire conditions would be to either provide a detailed commentary on the current state of concrete design for fire safety or the development of a simplified tool to aid in design. It was deemed that the development of a simplified tool would provide a greater contribution to the structural engineering field than a detailed examination of the literature on the topic. However, an annotated bibliography which summarizes the current state of the literature was created as part of this thesis. This section details the process behind the development of a simplified design tool to evaluate the fire performance of reinforced concrete slabs.

While investigating the literature, graphs were found (Figures 3.1 and 3.2 from Wade 1991) that give temperature distributions for dense and lightweight concrete slabs exposed to the ISO 834 fire. Wade (1991) presented the graphs as part of an analytical procedure to evaluate the capacity of slabs exposed to fire. The drawback of the procedure proposed by Wade is that the temperature distribution

graphs are conservative to account for the performance of all aggregates classified as dense and lightweight. If there were a means to produce such curves for specific aggregates it could be used with the detailed design procedure presented by Wade (1991) to provide more accurate capacity calculations. Also, if fire curves representing actual fires could be included in the analysis, then performance-based design for fire conditions would start to approach current design practices for wind and earthquake loads.

Finite element programs can be used to determine temperature distribution curves for different slab elements; however, these analyses are time consuming, limiting the amount and types of slabs that can be analyzed in the typical design practice. In addition most practicing structural engineers do not have software for transient thermal analyses at their disposal or have sufficient understanding of heat transfer to be proficient with analyses. Hutchens and Gupta (2000) demonstrated that EXCEL could accurately solve two-dimensional steady state heat conduction problems. With this information, efforts went towards the development of a spreadsheet application to perform transient, one-dimensional heat transfer to produce the desired temperature distribution curves.

The literature was then investigated for numerical methods for calculating slab temperature profiles that could be implemented in a spreadsheet application. Bushev et al. (1972) developed one of the earliest of these methods; however, it was empirical and limited to the application of slabs exposed to the ISO 834 fire. In fact, the relevant literature mostly contains methods for calculating temperature distributions that are either analytical or make us of finite element programs.

Since their development in the mid 1970s, finite element programs have relied on a multitude of numerical methods to structure and solve the governing equations, subject to certain boundary conditions. The logic and mathematical coding (numerical methods) behind these programs could be applied to a spreadsheet application. One such program, developed by Munukutla (1989) to predict one-dimensional heat transfer through a concrete wall, was based on a numerical method which lent itself to a spreadsheet application. Using the numerical methods presented in Munukutla (1989), spreadsheet applications for calculating temperatures within steel cross-sections exposed to fire, and the thermal properties of concrete, a simplified design tool for analysis of reinforced concrete slabs was developed. The results produced from tool were verified using experimental data found in the literature and TAS (Thermal Analysis Software).

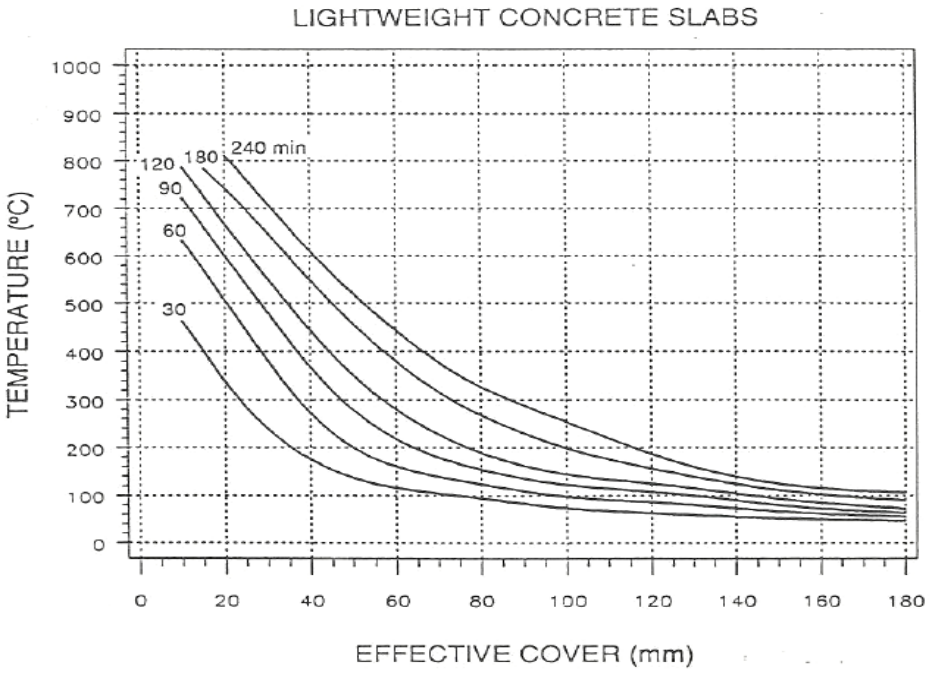

Figure 3.1: Temperature Distribution for Lightweight Concrete Slabs Exposed to the ISO 834 Fire (as taken from Wade 1991)

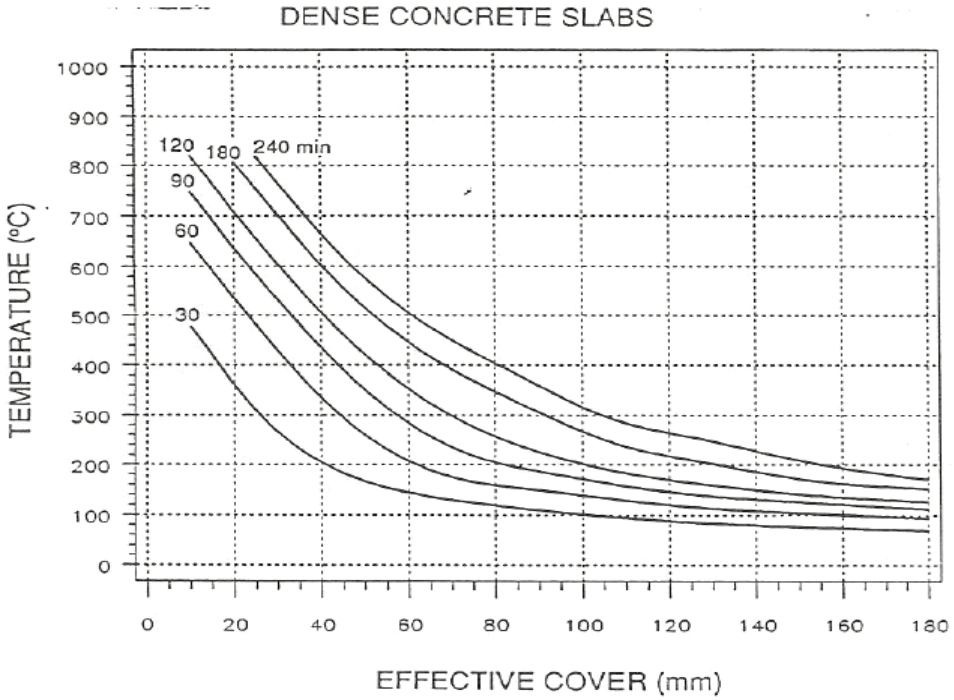

Figure 3.2: Temperature Distribution for Dense Concrete Slabs Exposed to the ISO 834 Fire (as taken from Wade 1991)

4 Development of Excel Calculation Tool

The rate of heat transfer through the cross-section of a concrete slab is dependent on aggregate type and the degree of fire exposure. Eventually the heat reaches the unexposed face of the slab and is released into the atmosphere. Using the investigation done by Cooper and Franssen (1999) and principles of one-dimensional heat transfer, an Excel-based calculation tool was developed to determine temperature distributions in concrete slabs. The model accounts for aggregate type, slab thickness, and fire exposure to predict temperature distributions through the slab cross-section. Separate calculation methods are used to determine the surface temperature at the slab's fire-exposed face, the internal temperature distribution, and temperature at the unexposed face. Verification of the model was done by comparing its temperature distribution analysis of a 175mm alluvial quartz slab exposed to the ISO 834 time-temperature curve with experimental data obtained from BRANZ testing (Wade 1992), which was discussed in the background section. Since the properties of concrete are essential to the accuracy of the model, the reader is referred to Appendices B for background discussion on the thermal properties of concrete.

4.1 Calculation of Slab Temperature Distribution

The proposed calculation tool uses separate calculation methods for determining temperatures at the endpoints (exposed and unexposed faces of the slab) and at internal nodal points (within slab's cross-section). The development and application of these methods are discussed along with the verification of results.

4.1.1 Exposed Surface Temperature Calculation

The temperature of the fire-exposed face of the slab is different than the temperature within the fire environment. The difference is a function of heat transfer by convection and radiation, which are dependent on the emissivity of the flames, the gas temperature, and the properties of the exposed surface of the slab. In determining the surface temperature for concrete walls, the factor 0.85 times the furnace temperature has been found to be adequate (Munukutla 1989). However, this empirical technique cannot be applied to a slab element because according to BRANZ test data (Wade 1992) a slab does not follow the same thermal relationship so a more exact calculation technique is needed.

4.1.1.1 Derivation of Equation

As previously mentioned, spreadsheet applications already exist for determining the fire performance of structural steel elements, and one of these is the lumped parameter method. The lumped parameter method assumes that at every instant in time, temperature is uniformly distributed over the cross-section of the steel member because of steel's relatively high thermal conductivity. For the lumped parameter method, the temperature change in steel over a time increment Δt is governed by the equation (Swedish Institute of Steel Construction 1976):

$$\Delta\theta_s = \frac{\alpha}{\gamma_s C_{ps}} \frac{F_s}{V_s} \left(\theta_g - \theta_s\right) \Delta t \,, \quad \textbf{(Equation 4.1)}$$

where $\Delta\theta_s$ (ºC) is the change in temperature in the section over the time interval Δt (seconds); α (kcal/m^2-ºC-h) is the surface coefficient of heat transfer in the boundary layer between the combustion gases and the steel section; γ_s (kg/m^3) is the density of the steel; C_{ps} (kcal/kg-ºC) is the steel's specific heat capacity; F_s (m^2) is the total

surface area of the section which is exposed to the combustion gases; V_s (m^3) is the volume of the steel section; θ_g (ºC) is the temperature of the combustion gas; θ_s (ºC) is the temperature of the steel section; and Δt (s) is the time interval. Calculations for the lumped parameter method can be easily executed with the use of Excel and the method produces satisfactory results, albeit a bit conservative (Narang 2005).

Concrete is more resistant to heat transfer than steel so the development of a lumped parameter model that assumes a uniform temperature distribution within a concrete section would not be a practical application. However, Equation 4.1 can be modified to predict the surface temperature of concrete slabs exposed to fire assuming the principles of one-dimensional heat transfer.

The equation for one-dimensional heat transfer is:

$$\frac{\delta T}{\delta t} = a\frac{\delta^2 T}{\delta x^2}, \quad \textbf{(Equation 4.2)}$$

where *a* is the thermal diffusivity. Notice that Equation 4.2 for one-dimensional heat transfer contains no lateral dimensions. A one-dimensional model can be used to represent heat transfer within a slab at some distance from the boundaries, assuming that the fire environment is homogeneous and extends for a considerable distance in the two lateral directions. Equation 4.1 can be modified to represent the temperature per unit width of the slab as follows:

$$\Delta\theta_c = \frac{\alpha}{(m)\gamma_c C_{pc}}(\theta_g - \theta_c)\Delta t, \quad \textbf{(Equation 4.3)}$$

where a unit meter is added to the denominator for unit agreement, and the remaining variables represent the properties and temperature of the concrete instead of steel. It is important to note that the specific heat of concrete, C_{pc}, is a temperature-dependent

and aggregate-dependent parameter, and its value can be found in Appendix D based on aggregate type. The heat transfer coefficient for the exposed surface is:

$$\alpha = \alpha_c + \alpha_r, \quad \textbf{(Equation 4.4)}$$

where α_c is the convection transfer coefficient and α_r is the radiative transfer coefficient. From testing, the coefficient of convective transfer has been found to be quite consistent, and the value of 25 W/m^2-ºC is used (Malhotra 1982). Radiative heat transfer is temperature-dependent, and its transfer coefficient is governed by the following equation (Malhotra 1982):

$$\alpha_r = (5.77\varepsilon_r)\frac{\left[\left(\frac{T_t + 273}{100}\right)^4 - \left(\frac{T_0 + 273}{100}\right)^4\right]}{T_t - T_o}, \quad \textbf{(Equation 4.5)}$$

where T_t is the temperature of the gas; T_0 is the temperature of the exposed surface; and ε_r is the emissivity of the boundary surface and combustion gases. The emissivity may be assumed to be 0.5 for furnace tests (Malhotra 1982).

4.1.1.2 Verification

Equation 4.3 was implemented in a spreadsheet application to study heat transfer to an alluvial quartz slab subjected to the ISO 834 fire test. The results for the spreadsheet analysis were compared with data produced from BRANZ testing (Wade 1992). Figure 4.1 displays the ISO 834 time temperature curve, the published BRANZ test data for an alluvial quartz slab exposed to the ISO fire for 4 hours, and the surface temperature predicted using Equation 4.3 for an assumed 4-hour exposure to the ISO 834 fire conditions. The BRANZ fire test data and the results produced using the Excel calculation tool agree up to about a 30-minute exposure. Beyond this

point, the temperatures predicted by the spreadsheet method begin to gravitate towards the ISO 834 time-temperature curve and are up to 8% conservative relative to the BRANZ data. Since the results from Equation 4.3 were encouraging, concrete surface temperatures were additionally calculated for four different types of aggregates. These results are plotted in Figure 4.2. It can be seen that the surface temperature of the lighter shale aggregate increases the fastest due to it lower unit weight value which makes the surface less resistant to heat absorption.

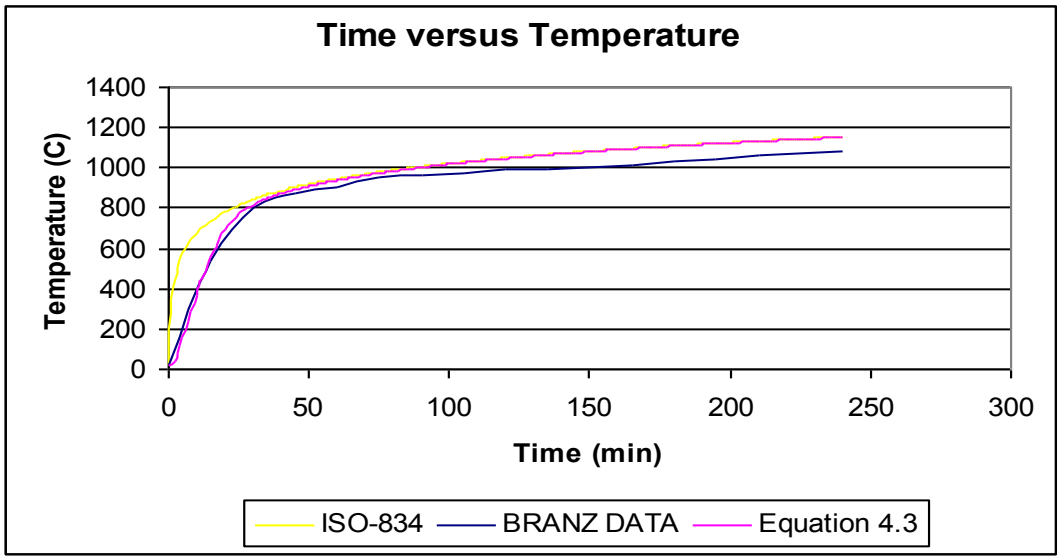

Figure 4.1: Slab Exposed Face Surface Temperature of an Alluvial Quartz Slab

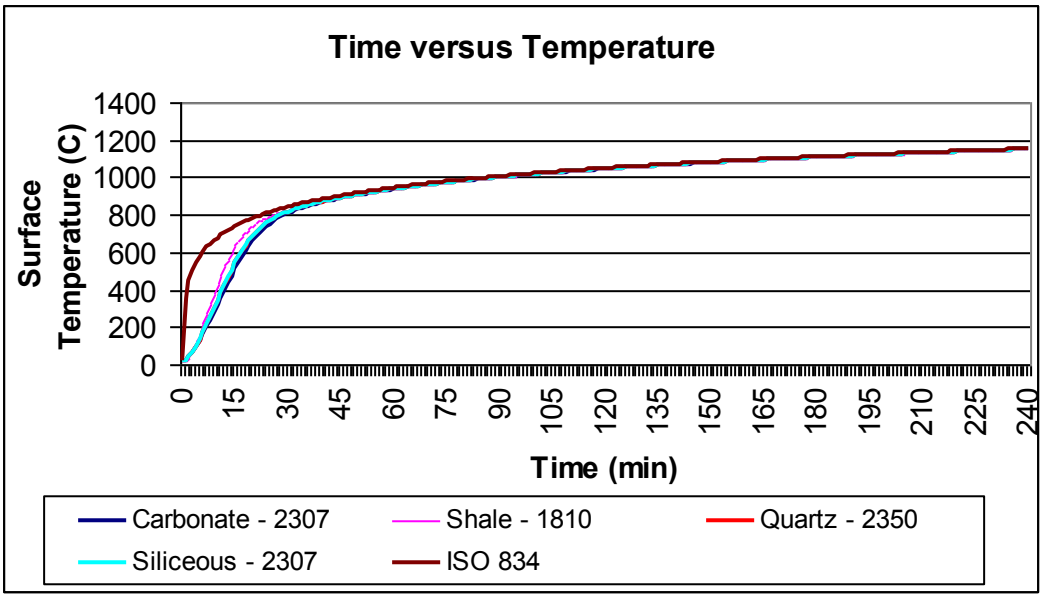

Figure 4.2: Slab Exposed Face Surface Temperature of Various Concrete Aggregates

4.1.2 Internal Temperature Calculation

Heat absorbed by the surface of the slab migrates through its cross-section and forms a temperature distribution profile. Equation 4.3 is limited to calculation of the temperature of the exposed face; another heat transfer model is needed to calculate the slab's internal temperature profile. Since only one face of the exposed slab is subjected to the given fire environment (one-dimension), a finite difference model can be applied to calculate internal temperatures (Munukutla 1989). The finite difference model involves dividing the slab into a number of identical transverse elements across its thickness, and these elements provide a means to determine the variation in temperature through the thickness of the slab. Figure 4.3 shows a slab cut into a number of identical transverse elements. It is assumed that the presence of steel reinforcement has an insignificant effect on the slab's temperature because the steel temperature would just be that of the surrounding concrete due to its lower

resistance to heat transfer than concrete. Thus, the reinforcing steel is not included in the heat transfer model.

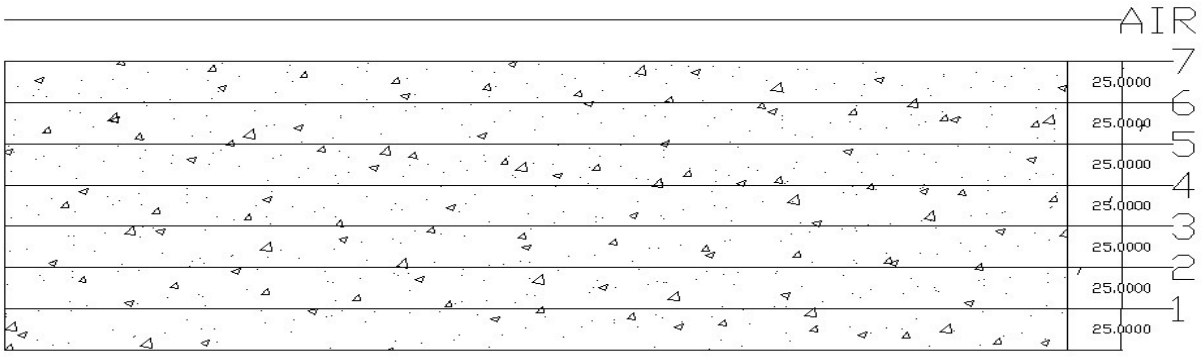

Figure 4.3: Slab Cut into Multiple Increments for Finite Difference Method

4.1.2.1 Finite Difference Method

If a slab is divided into a number of equal elements of thickness Δx, the finite difference equations representing the temperature gradients are:

$$\frac{\delta T}{\delta x} = \frac{T_{m+1} - T_m}{\Delta x}, \quad \textbf{(Equation 4.6)}$$

$$\frac{\delta^2 T}{\delta x^2} = \frac{\left(T_{m+1} - 2T_m + T_{m-1}\right)}{\left(\Delta x\right)^2}, \quad \textbf{(Equation 4.7)}$$

$$\frac{\delta T}{\delta t} = \frac{\left(T_{m}^{'} - T_m\right)}{\Delta t}, \quad \textbf{(Equation 4.8)}$$

where T_{m+1}, T_m, and T_{m-1} are temperatures at the adjacent node points, and $T_{m}^{'}$ is the temperature at node m after time increment Δt. When calculating the temperature at the slab's boundary, an initial value of 20ºC is used for T_{m+1}. Equation 4.3 can be expressed in finite difference notation by substituting Equations 4.7 and 4.8:

$$\frac{\left(T_{m}^{\cdot} - T_m\right)}{\Delta t} = \frac{a\left(T_{m-1} - 2T_m + T_{m+1}\right)}{\left(\Delta x\right)^2}, \quad \textbf{(Equation 4.9)}$$

It is important to note that the thermal diffusivity, *a* (W/m-ºC) is a coefficient that is derived from temperature-dependent properties of concrete, and values are detailed in Appendix B. Solving Equation 4.9 for $T_{m}^{\cdot}$ results in an equation that can be implemented in Excel to compute the temperature of interior nodes at each time interval that describes the fire exposure:

$$T_{m}^{\cdot} = T_m\left[1 - \frac{2a\Delta t}{\left(\Delta x\right)^2}\right] + \left[T_{m-1} + T_{m+1}\right]\frac{a\Delta t}{\left(\Delta x\right)^2}, \quad \textbf{(Equation 4.10)}$$

4.1.2.2 Verification of Finite Difference Method

Equation 4.10 was formulated in a spreadsheet application to study the temperature distribution within a 175mm alluvial quartz slab subjected to the ISO 834 fire test, and the results were compared with data produced from BRANZ testing (Wade 1992). Temperatures were calculated for node spacings of 25mm. Figure 4.4 displays the results from the spreadsheet application while Figure 4.5 compares the BRANZ and spreadsheet data for the same 175mm alluvial quartz slab exposed to the ISO 834 fire curve for four hours. It can be seen that temperatures produced from the proposed calculation method are approximately 12% conservative in comparison with the test data. Also, initially the tool produces temperatures that are less than experimental data. This is most likely due to the size of the time step, a time step of less than one minute would produce higher initial temperatures and is examined in Chapter 5. Figure 4.6 compares the temperature distribution for a 175mm dense and

lightweight aggregate concrete slab. The results display that the tool accounts for the higher thermal resistance exhibited by lightweight concrete slabs exposed to fire conditions. The results produced for the 175mm lightweight (shale aggregate) slab are approximately 15% conservative when compared with the isotherm data in Figure 3.1.

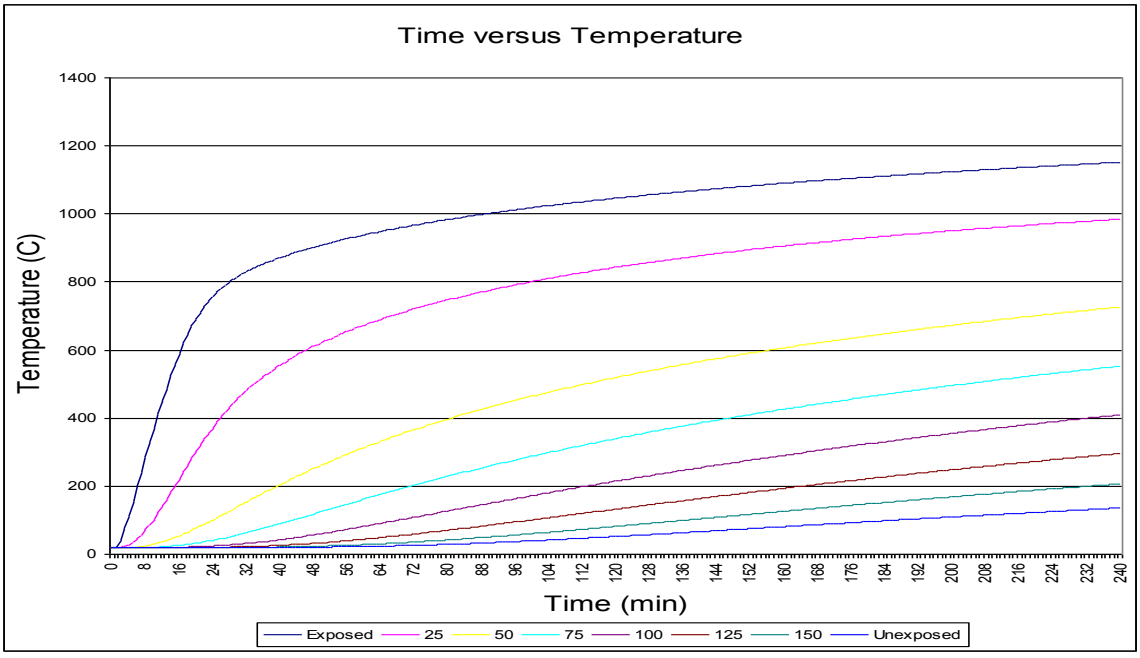

Figure 4.4: Temperature Distribution at 25mm Increments for a 175mm Alluvial Quartz Slab Exposed to ISO 834 Conditions

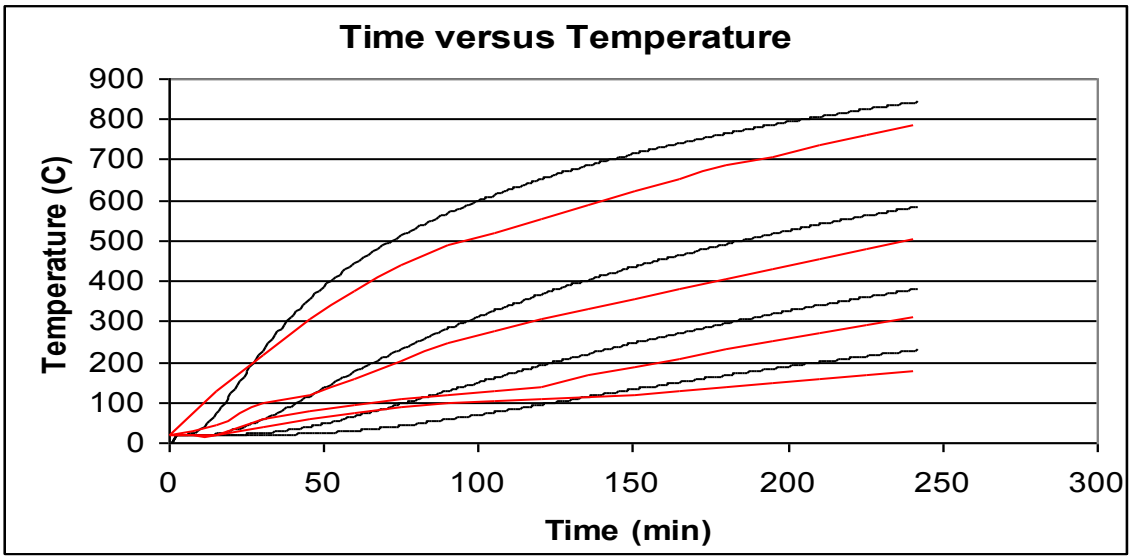

Figure 4.5: Temperature Distribution at 35mm Increments for BRANZ Data (red) and Spreadsheet Application (black) for a 175mm Alluvial Quartz Slab

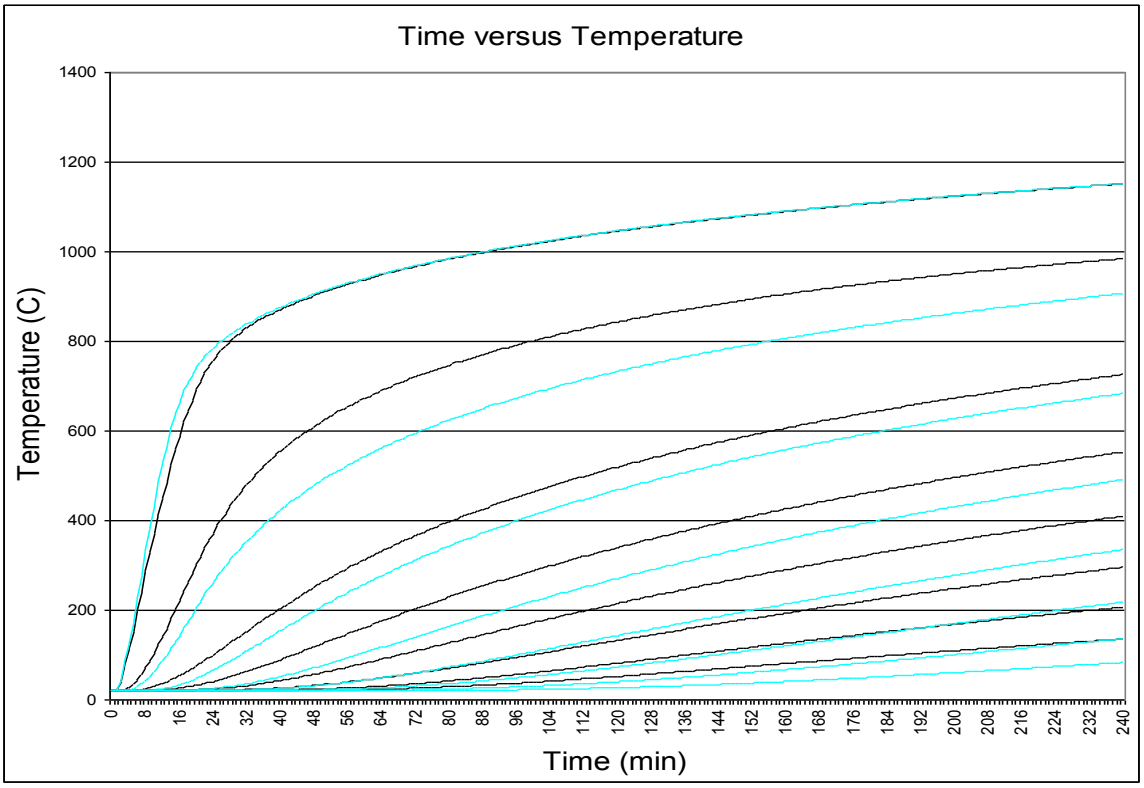

Figure 4.6: Temperature Distribution at 25mm Increments for a 175mm Alluvial Quartz (black) and 175mm Shale (light blue) Slab Exposed to ISO 834 Conditions

4.1.3 Unexposed Face Temperature Calculation

The unexposed face of the slab is that which is not within the fire compartment. As heat passes through the slab's cross-section it eventually reaches the unexposed face where it is released into the atmosphere. The rate of heat release into the atmosphere is dependent on the concrete's surface resistance. Dense concretes are more resistant to heat release than lightweight concretes because they have less pore space through which heat can travel. Since the unexposed face of the slab represents a boundary to the model, the finite difference method cannot be applied directly. When heat reaches the end of the slab's cross-section an alternative

calculation method is needed. Two different techniques for computing the unexposed surface temperature are discussed, and their effectiveness is analyzed.

4.1.3.1 Heat Release Function

Similar to the method used to predict surface temperature, based on the rate of heat absorption, a method can be devised to calculate the rate at which the slab releases heat to the atmosphere. There are a few different techniques that can be used, each of which approaches this phenomenon differently; however, not all can be practically applied within Microsoft Excel because they either involve solving complicated differential equations or long equations that must be reprogrammed each time any variables within the model change. Thus, they are not considered. To calculate the temperature of the unexposed face Equation 4.3 was modified to calculate the temperature change between the concrete surface and the overlying atmosphere:

$$\Delta\theta_c = \frac{\alpha'}{(m)\gamma_c C_{pc}}(\theta_c - \theta_a)\Delta t \text{ , } \textbf{(Equation 4.11)}$$

where θ_c is the temperature of the unexposed surface calculated from Equation 4.10 and θ_a is the atmospheric temperature, which is assumed to be a constant 20ºC. The surface coefficient of heat transfer for the unexposed face (α') is represented by the following equation (Yakovlev 1980):

$$\alpha' = 1.3\sqrt[3]{\theta_o' - \theta_a} + 4.96\varepsilon_r' \frac{\left(\frac{\theta_o' + 273}{100}\right)^4 - \left(\frac{\theta_a + 273}{100}\right)^4}{\theta_o' - \theta_a}, \text{ } \textbf{(Equation 4.12)}$$

where $T_o^{'}$ is the temperature of the exposed face; T_a is the atmospheric temperature; and $\varepsilon_r^{'}$ is the emissivity of the unexposed surface (a value of 0.5 is assumed). Resultant changes in surface temperature predicted by Equation 4.11 are then subtracted from the unexposed face temperature.

The method proposed by Equation 4.11 captures the release of heat into the atmosphere which is a principle of heat transfer; however, it does not consider the increase in atmospheric temperature that occurs as heat from the slab is released. It is difficult to account accurately for the increase in atmospheric temperature because the types of materials, volumetric properties composing the atmosphere, and the type of ventilation bounding the atmosphere above the unexposed face are unknown. Also, an attempt to determine the change in atmospheric temperature would result in a large number of calculations because there is no established boundary. Successive application of Equation 4.11 results in temperatures for the unexposed face that are much lower than established test data (Wade 1992) as can be seen in Figure 4.7. Based on Figure 4.7, it can be assumed that Equation 4.11 overestimates the amount of heat released from the unexposed face.

4.1.3.2 Boundary Layer

Like the proposed heat release function this method provides a limit so calculations need not be extended to a very large distance beyond the slab's surface to garner useful results. The boundary condition that was applied here essentially extends the finite difference method for predicting temperatures within the slab to include an "extra layer." The "extra layer" is assigned the same properties of the concrete slab and a nominal thickness of 10mm. The node to the exterior of this

"extra layer" represents the overlying atmosphere and is assumed to have a constant temperature of 20ºC.

With the establishment of a boundary layer the composition of the atmosphere above the unexposed face of the slab is simplified. Results produced from this method agree closer with BRANZ data (Wade 1992) in comparison with the previously described heat release function as can be seen in Figure 4.7. Using the boundary layer method it takes three hours of exposure to the ISO 834 fire curve for the unexposed face to reach the temperature of the experimental data but once it reaches that point the results are similar. This delay in heat transfer to the unexposed face is due to the large time step of a minute.

If the slab were subjected to an actual fire condition, as opposed to the standard ISO 834 condition, the boundary layer method could possibly have difficulty in predicting temperatures during the "cooling phase" where the fire intensity has been either greatly diminished or extinguished because heat trapped within the slab cannot be released. All further calculations done in this thesis make use of the boundary layer method in predicting the temperature of the unexposed face.

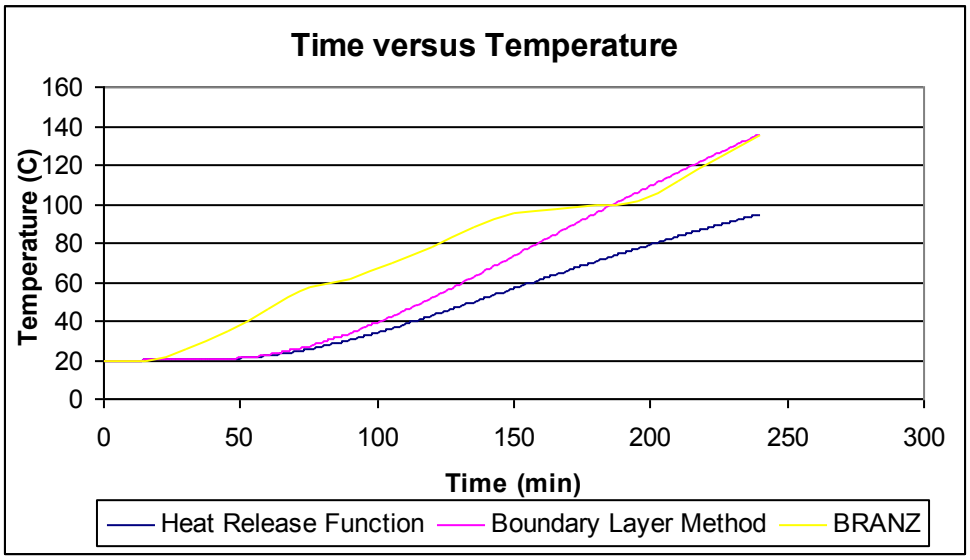

Figure 4.7: Temperature of Unexposed Face of 175mm Alluvial Quartz Slab

4.2 Limitations of Proposed Calculation Model

The proposed model for predicting one-dimensional heat transfer through concrete slabs is a simple spreadsheet application so it allows for calculation ease; however, being a simplified model it cannot account for some complex phenomena that occur when concrete is exposed to fire conditions. Three of these phenomena are discussed below.

First, as previously mentioned, the model does not accurately model heat release on the unexposed surface of the slab. If temperature calculations for a slab exposed to a natural fire are performed, it is probable that temperatures in the vicinity of the unexposed face will be higher than actual conditions because heat is being stored within the concrete slab long after the fire is terminated.

Second, since concrete is composed of water which boils when it reaches 100ºC, concrete experiences phase changes when exposed to fire. These phase changes decrease the rate of temperature increase through the thickness of the slab and in the vicinity of the unexposed face. At the unexposed face, the temperature

tends to increase gradually as the water within the concrete boils and escapes as steam. A phase change function would require an appropriate set of governing equations, and this was deemed beyond the scope of this work.

Lastly, the proposed model cannot directly account for the spalling of concrete. An educated guess could be made on the occurrence if the concrete mix is known and spalling test data are available. The prediction of spalling can be based on comparing the test data with the rate of temperature increase on the fire exposed side generated from the spreadsheet application.

5 Excel Tool Temperature Distribution Analysis

The model developed in this thesis was used to conduct a series of thermal analyses to determine temperature distributions. The objective of the analyses was to explore the effects of slab thickness, aggregate type, and fire exposure on the fire performance of concrete slabs. Temperature distribution calculations were completed for multiple slab thicknesses, four aggregate types (expanded shale, quartz, carbonated, and siliceous), and four different fire exposures (ISO 834, ASTM E119, SDHI-M, and LDMI-M). The ASTM E119 fire condition was used on a limited basis, as an additional means for verifying the calculation tool with experimental data. For ease in comparison, results for the different slabs are mostly summarized in tabular form for a series of discrete points; the complete graphical distributions and summary tables can be seen in Appendix E.

5.1 ASTM E119

Additional verification of the proposed model was completed by applying the ASTM E119 time-temperature curve (Equation 2.2) to the thermal analysis of carbonate, and siliceous aggregate concrete slabs of 4, 5, 6 and 7-inch thickness, and expanded shale slabs of 4, 5, and 6 inches. Results for the temperature of the unexposed face for 4 and 6 inch slabs analyzed can be seen in Figures 5.1 to 5.6. The results are graphed with PCA fire test data (Abrams & Gustaferro 1968) to compare the discrepancies between the test data and Excel tool.

Results produced from the proposed tool lag behind the PCA test data (Abrams & Gustaferro 1968) for the entirety of exposure for the 4-inch slabs. However, after three hours exposure for the 6-inch carbonate and shale slabs, the

Excel tool catches up with the test data, but the siliceous slab still lags behind. The results are similar to those found for the 175mm quartz slab in relation to test data because the unexposed face of the quartz slab lagged the data until approximately three hours of ISO 834 exposure (refer to section 4).

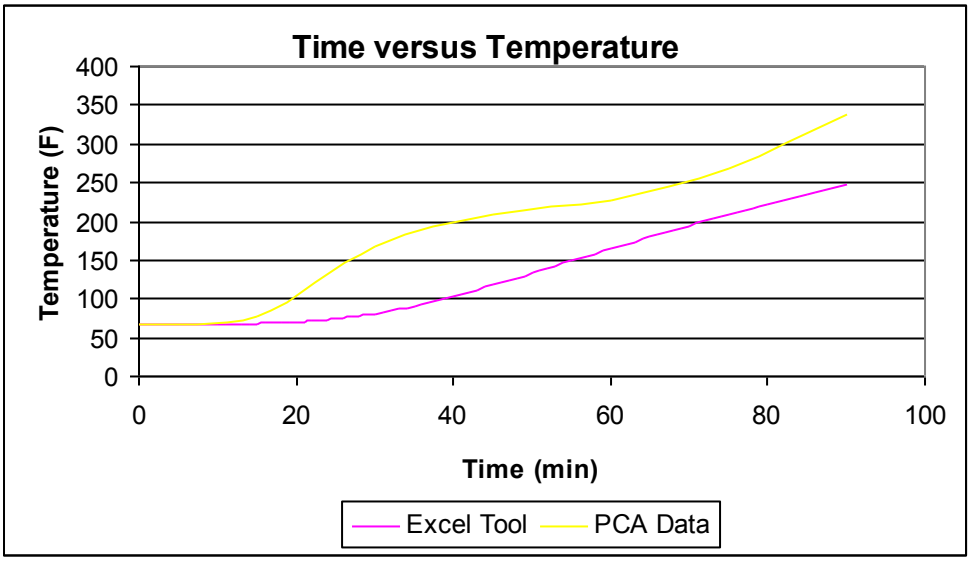

Figure 5.1: Temperature of the Unexposed Face of a 4 inch Carbonate Slab Exposed to ASTM E119 Conditions

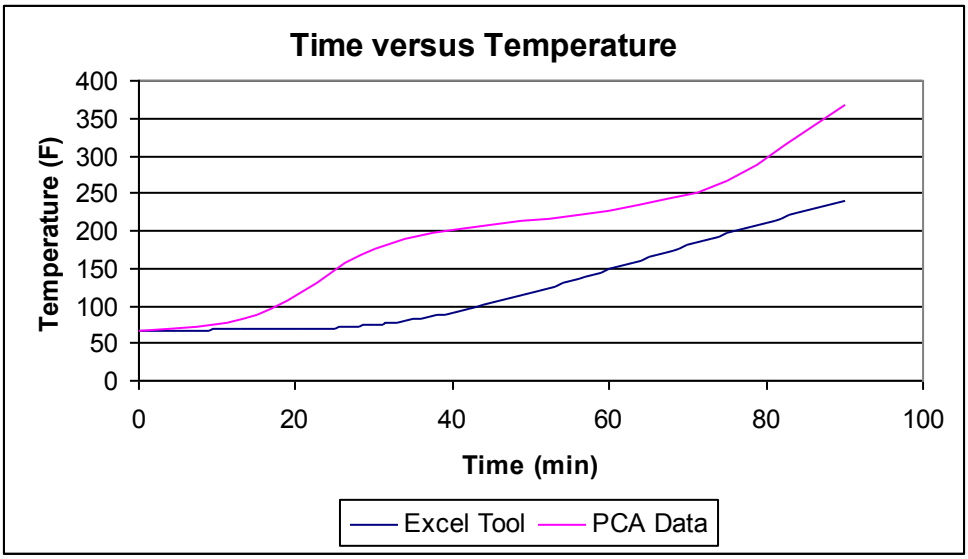

Figure 5.2: Temperature of the Unexposed Face of a 4 inch Siliceous Slab Exposed to ASTM E119 Conditions

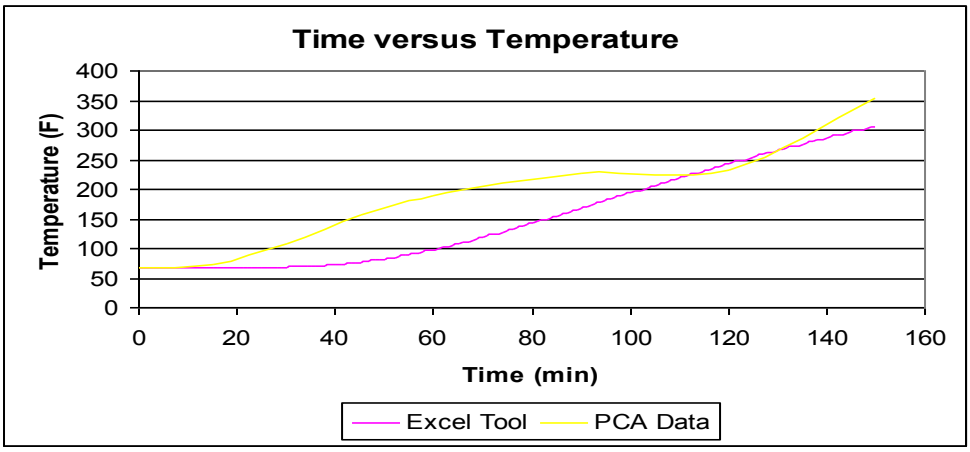

Figure 5.3: Temperature of the Unexposed Face of a 4 inch Shale Slab Exposed to ASTM E119 Conditions

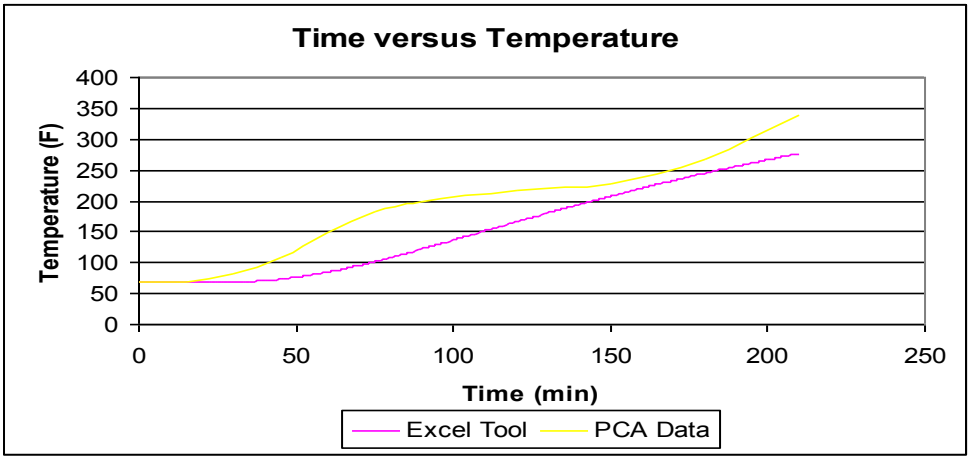

Figure 5.4: Temperature of the Unexposed Face of a 6 inch Carbonate Slab Exposed to ASTM E119 Conditions

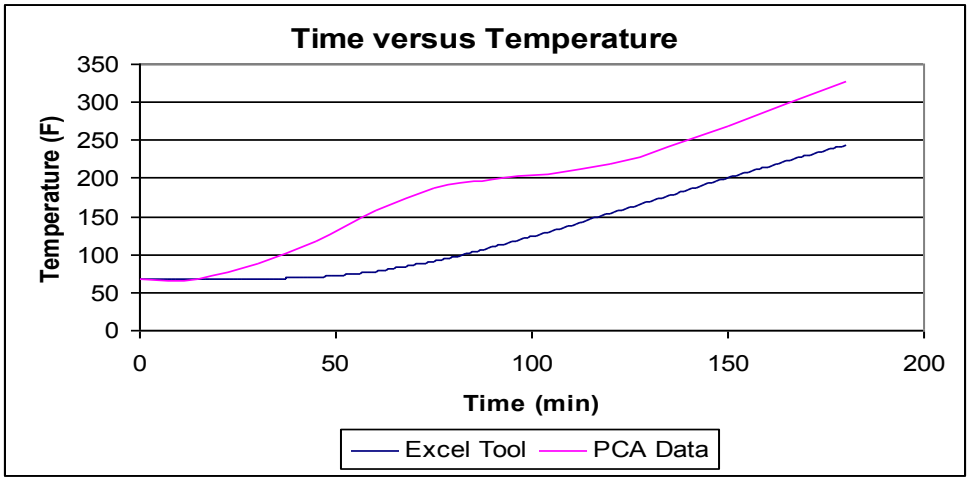

Figure 5.5: Temperature of the Unexposed Face of a 6 inch Siliceous Slab Exposed to ASTM E119 Conditions

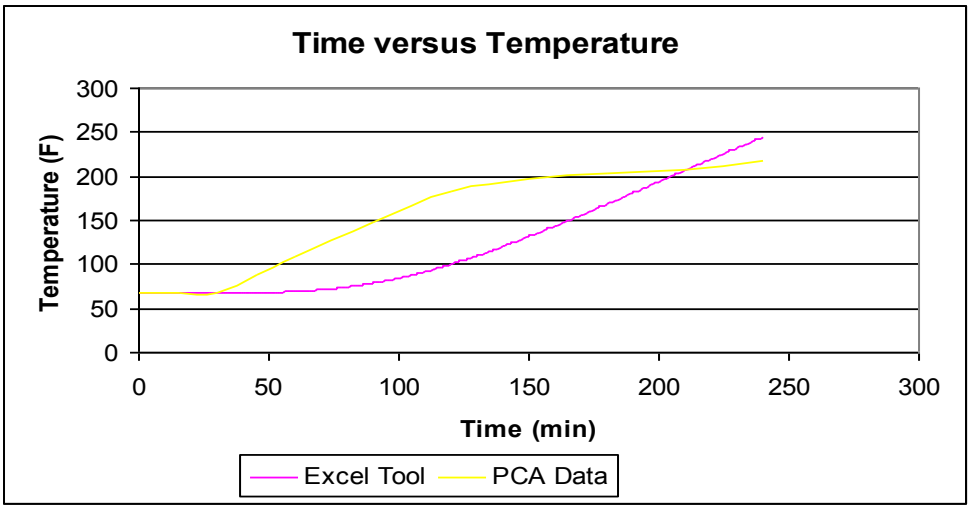

Figure 5.6: Temperature of the Unexposed Face of a 6 inch Shale Slab Exposed to ASTM E119 Conditions

One reason for the lag could be the size of the time step so the 4-inch siliceous and carbonate slabs were analyzed using time steps of 15 and 30 seconds, and the results were compared with those produced from the originally used 60 second time step. Figures 5.7 and 5.8 display these results and it can be seen that the reduction in the time step resulted in the predicting of somewhat higher temperatures during the first two hours of exposure to the ASTM E119 standard fire.

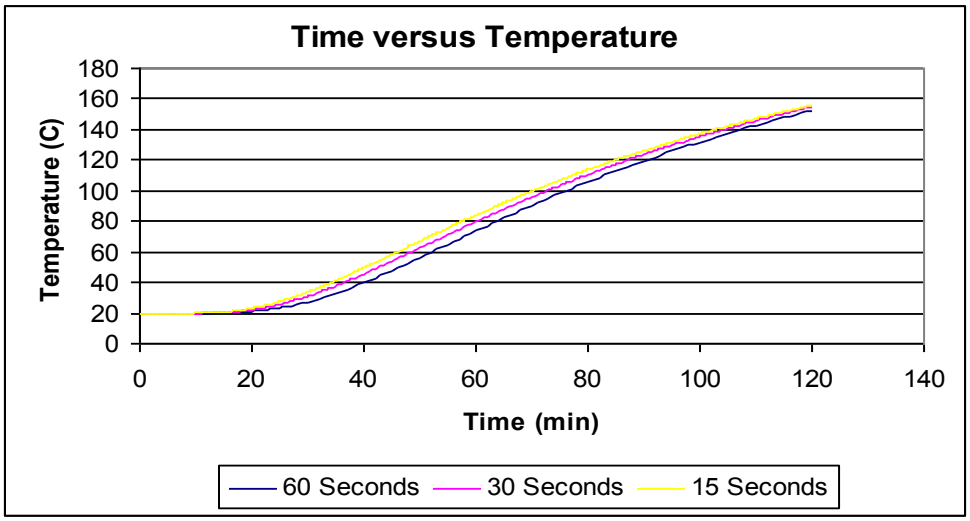

Figure 5.7: Temperature of the Unexposed Face of a 4 inch Carbonate Slab Exposed to ASTM E119 Conditions Based on Various Time Steps

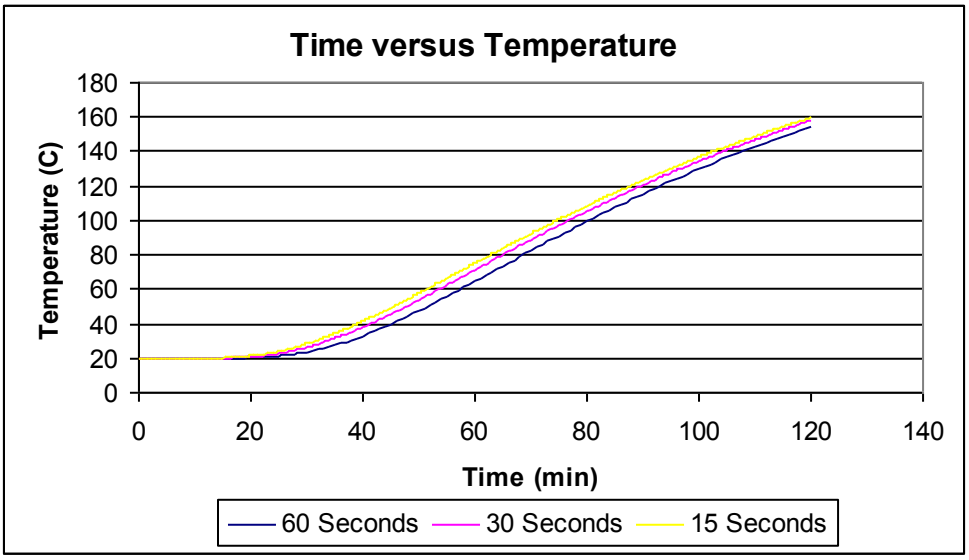

Figure 5.6: Temperature of the Unexposed Face of a 6 inch Siliceous Slab Exposed to ASTM E119 Conditions Based on Various Time Steps

Another reason for the observed temperature lag could be due to the accuracy of the PCA data from Abrams & Gustaferro (1968). Their tests concluded that 63.5mm siliceous and carbonate slabs failed due to the unexposed face reaching temperatures of 140ºC at 35 and 41 minutes of exposure to ASTM E119 conditions, respectively. Consequently, BRANZ tested an alluvial quartz slab of 63.7mm to ISO 834 conditions and the unexposed face reached 140ºC after 44 minutes. Through a series of slab fire tests BRANZ determined that quartz aggregate slabs were most susceptible to fire conditions (Wade 1991). This conclusion from BRANZ contradicts the PCA data which displays siliceous and carbonate slabs as being more susceptible. The ISO 834 and ASTM E119 fire exposures are extremely similar so an error most logically was caused by the testing procedures performed for the two sets of experiments. Also, the document accounting for the work done by Abrams &

Gustaferro does not specify the starting room and concrete temperatures before the fire tests so 68ºF was assumed for both.

Although predicted results for the unexposed face lag the available experimental data, the temperatures produced for the reinforcement region near the bottom of the slab will remain conservative. This is significant because it means the tool conservatively predicts capacities for slabs based on the generated temperature data. However, as can be seen when comparing the Excel tools results with PCA test data, the tool does not accurately predict failure for the condition where the unexposed face reaches 140ºC for slabs less than 6 inches in thickness.

5.2 ISO 834

The time-temperature curve (Equation 2.1) for the ISO 834 standard fire was applied to the thermal analysis of 16 concrete slabs. Since they are based on a standardized test, these analyses can be used to determine fire resistance ratings for the slabs in question. Temperature distribution calculations were completed for five different slab thicknesses (100mm, 125mm, 150mm, 175mm, and 200mm), four aggregate (expanded shale, quartz, carbonated, and siliceous). The analyses are organized by slab thickness so the affects of aggregate type can be seen clearly. Table 5.1 summarizes the fire resistance of the slabs when exposed to ISO 834 conditions. Fire resistance represents the time taken for the unexposed face of the slab to reach 140ºC with 240 minutes signifying that a given configuration survived four hours of exposure. The shale slabs are far more fire resistant than their carbonate and siliceous counterparts which have almost identical resistance ratings.

Table 5.1: Time for Unexposed Face of Slab to Reach 140ºC in ISO 834 Conditions for Various Aggregates and Slab Thicknesses

Aggregate	SlabThickness (mm)	Fire Resistance (min)
Shale	100	132
	125	190
	150	240
	175	240
	200	240
Carbonate	100	101
	125	151
	150	204
	175	240
	200	240
Siliceous	100	103
	125	148
	150	201
	175	240
	200	240

5.3 SDHI-95

To provide a practical design scenario the short duration, high intensity time-temperature curve from Figure 2.1 (SDHI-95), which simulates a ninety-fifth percentile clerical office fire, was used for thermal analysis of five different slab thicknesses (100mm, 125mm, 150mm, 175mm, and 200mm) and four types of aggregates (expanded shale, quartz, carbonated, and siliceous). Since SDHI-95 represents an actual fire, the thermal analyses are representative of a realistic design scenario or design fires for practicing structural engineers. Engineers can apply rational design procedures using these analyses rather than prescriptive code methods that designate fire resistance requirements based on standard furnace testing and are not associated with performance in an actual fire environment. Table 5.2 summarizes the results of these analyses, and it can be seen that shale slabs of all thickness last the duration of the fire while the 100mm carbonate, siliceous, and quartz slabs fail around 100 minutes of exposure.

Table 5.2: Time for Unexposed Face of Slab to Reach 140ºC in SDHI-95 Fire Exposure for Various Aggregates and Slab Thicknesses

Aggregate	Slab Thickness (mm)	Fire Resistance (min)
Shale	100	240
	125	240
	150	240
	175	240
	200	240
Carbonate	100	102
	125	240
	150	240
	175	240
	200	240
Siliceous	100	100
	125	240
	150	240
	175	240
	200	240
Quartz	100	91
	125	240
	150	240
	175	240
	200	240

5.4 LDMI-M

The long duration, medium intensity time-temperature curve from Figure 2.1 (LDMI-M) simulates a fire for storage rooms within office buildings. Its use provides the same advantages as the SDHI-M fire. Thermal analyses for this fire curve were performed for five different slab thicknesses (100mm, 125mm, 150mm, 175mm, and 200mm) and four aggregates (expanded shale, quartz, carbonated, and siliceous). The fire resistance results are summarized in Table 5.3. For shale and siliceous aggregates, only the 100mm slab does not endure the 4-hour fire exposure with the shale slab lasting an hour longer. Both the 100 and 125mm quartz and carbonate slabs fail at approximately the same time during the fire exposure.

Table 5.3: Time for Unexposed Face of Slab to Reach 140ºC in LDMI-M Fire Exposure for Various Aggregates and Slab Thicknesses

Aggregate	Slab Thickness (mm)	Fire Resistance (min)
Shale	100	181
	125	240
	150	240
	175	240
	200	240
Carbonate	100	118
	125	198
	150	240
	175	240
	200	240
Siliceous	100	121
	125	240
	150	240
	175	240
	200	240
Quartz	100	114
	125	187
	150	240
	175	240
	200	240

5.5 Summary

The results for siliceous concrete disagree with test data for durations under three hours of standard fire exposure. Siliceous concretes should be less resistant to heat transfer than carbonate concretes for the entirety of testing; however, the proposed Excel-based tool does not capture this phenomenon for the SDMI-95 and LDMI fire curves. The siliceous slabs temperatures exceeding carbonates is not achieved until after three hours exposure in standard fire conditions. This phenomenon is most likely due to the fact that the specific heat capacity for carbonate concretes is much lower then siliceous concretes at low temperature. Consequently, carbonate concretes would heat up faster initially, and it would take some time for the siliceous concrete to achieve the same temperatures as carbonate concretes. If a

slightly lower value for the specific heat of siliceous concretes is used, then the results would agree with siliceous concretes being less fire resistant than carbonate concretes. Appendix H displays what happens to analysis of different aggregates when certain variables are changed.

6 TAS Analysis

An additional validation of the proposed spreadsheet tool TAS (Thermal Analysis System), a special-purpose finite element software, was used for heat transfer analysis of concrete slabs exposed to the ISO 834, ASTM E119, SDHI-95, and LDMI-M fire conditions. Initially, the model developed in TAS was benchmarked with experimental data (Abrams & Gustaferro 1968; Wade 1992) to validate its effectiveness in analyzing concrete slabs exposed to fire conditions. After the finite element model was validated, it was used to investigate concrete slabs exposed to natural fires. The results from the numerical analyses were compared with those produced from the spreadsheet application, which provided further information on the Excel tools capabilities and limitations.

6.1 General

TAS is a finite element, thermal analysis software capable of performing a wide variety of thermal analyses. Time and temperature-dependent thermal properties can be imported into the software. This leads to simulations accounting for changes in material properties as a function of fire exposure allowing for realistic analyses. Additionally, convection can be applied to both the fire-exposed and unexposed faces of elements. These convection components simulate the increase in an element's surface temperature when exposed to fire and the decrease in temperature caused by heat leaving the element and entering the atmosphere.

6.2 Benchmarking TAS

The first step in the use of TAS for benchmarking the analysis of concrete slabs was the simulation of a 175mm alluvial quartz slab exposed to ISO 834 fire

conditions. The slab was modeled as a 175mm concrete stick broken into 70 bricks, each of which has a nominal thickness of 2.5 mm and a square 1cm by 1cm cross-section. Values for the concrete's specific heat and the thermal conductivity for quartz aggregates were attached to the modeled element as temperature-dependent functions. A convection component simulating the ISO 834 fire was attached to one face of the slab while another convection component was attached to the opposite face to account for heat release. Heat transfer coefficients for both the exposed and unexposed faces were imported as time dependent values as calculated by the Excel model from Equations 4.3 and 4.11.

Results from the first analysis produced surface temperatures that agree with BRANZ test data (Wade 1992) but the temperatures near the unexposed face are rather low, as can be seen in Figure 6.1. It was concluded that the heat release function should be modified to decrease the disparity in the results. The function does not account for the increase in temperature of the surrounding atmosphere as heat is released, so the heat release coefficient was taken as a fraction of the calculated value. Figure 6.2 shows the temperature of the unexposed face versus the BRANZ data and the proposed Excel tool with the heat release coefficient multiplied by values of 0.33 and 1. It can be seen that when the heat release values are multiplied by 0.33 the results agree with BRANZ testing.

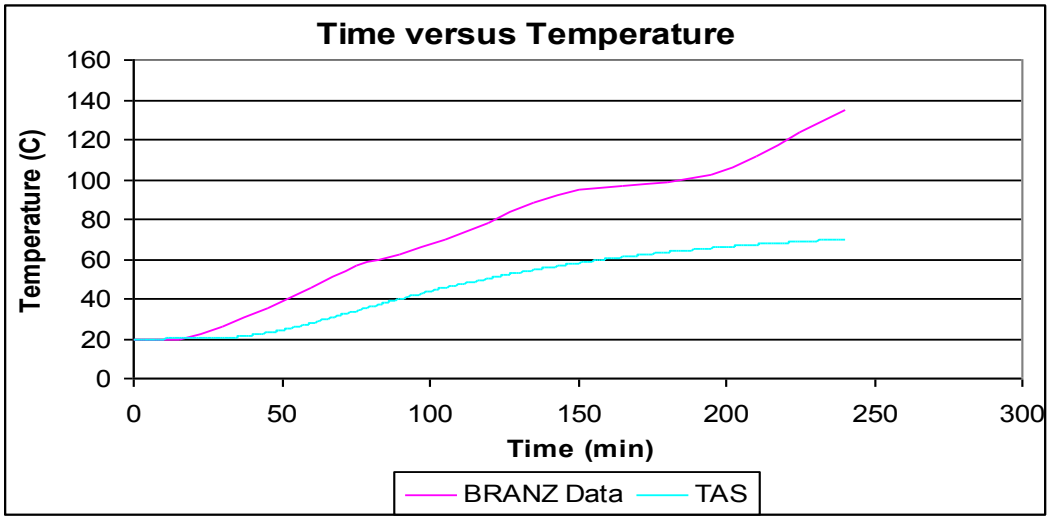

Figure 6.1: BRANZ Experimental Data and TAS Results for Unexposed Face of 175mm Alluvial Quartz Slab

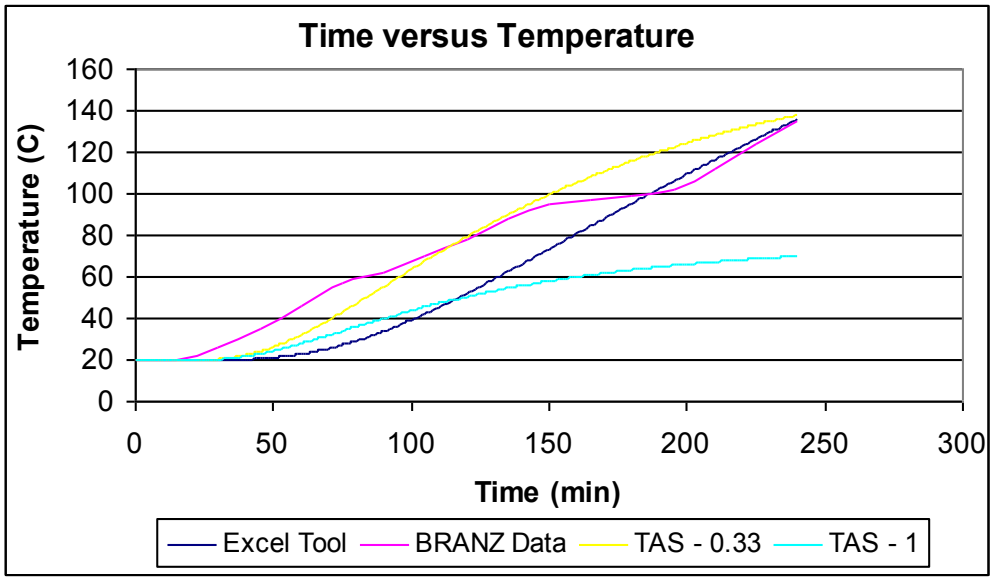

Figure 6.2: BRANZ Experimental Data, TAS, and Excel Results for Unexposed Face of 175mm Alluvial Quartz Slab

Further investigations were done for this slab element using the 0.33 multiple to investigate the effect other variables have on the slab, such as the effect of changing the aspect ratio of the slab element and changing the number of bricks used to model the slab. The slab element was modeled with a square cross-section of 5cm by 5cm (25 times the previous area). Figure 6.3 compares results for the temperature of the unexposed face for the two cross-sections. It can be seen that changing the

exposed surface area has negligible effects on heat transfer because the convection component is applied to the entire exposed face. Additionally, a convergence analysis was performed to see the sensitivity of the results to the number of bricks used. The slab element was modeled using 20 and 150 bricks, and the results are compared with those for the 70 bricks in Figure 6.4. After four hours of exposure to the ISO 834 standard fire, the difference in temperature between the three analyses is approximately two-tenths of a degree. This agreement verified that 70 bricks of 2.5mm are sufficient to model heat transfer through concrete slab elements.

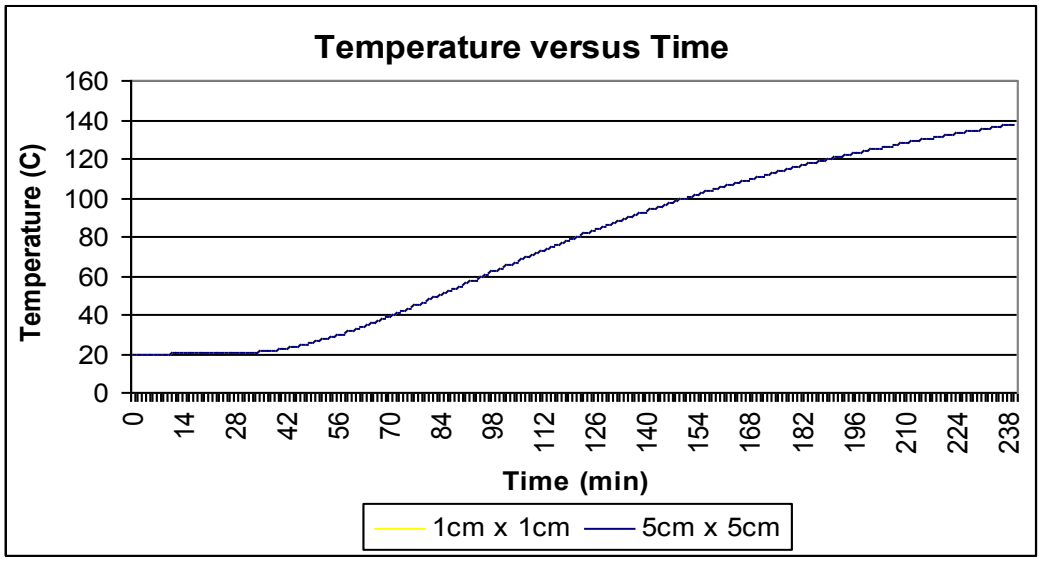

Figure 6.3: Temperature of Unexposed Face of a 175mm Alluvial Quartz Slab with TAS for Slab Elements of Cross-Sectional Areas of 1cm2 and 25cm2

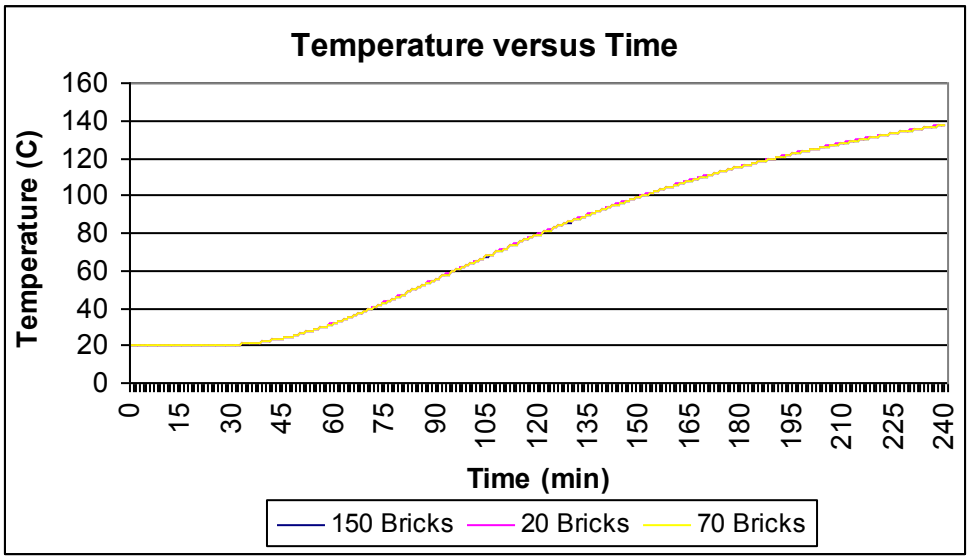

Figure 6.4: Temperature of Unexposed Face of a 175mm Alluvial Quartz Slab with TAS for Slab Elements Modeled with 20, 70, and 150 Bricks

Figure 6.5 displays the temperature distribution through the quartz slab using TAS versus the experimental data from Wade (1992) at 35mm increments. Similar to what was detailed in chapter 5 for the proposed Excel tool, earlier temperatures near the unexposed face predicted by the TAS analyses seem to lag the test data a bit. It can also be seen that like the Excel tool, the TAS analyses are a bit conservative. Figure 6.6 compares the results from TAS versus the Excel tool at 25mm increments. Towards the unexposed face of the slab the temperature results are extremely close to those obtained from the proposed Excel tool. However, the results from TAS for the surface temperature and 25mm from the exposed face are significantly cooler than those acquired through use of the Excel tool. Since reinforcing steel is typically located in this region it is important to note that the proposed tool would be conservative when predicting temperatures here. This is significant because it means that, TAS results, based on the information at hand, should follow this trend for other types of slabs analyzed in various fire conditions.

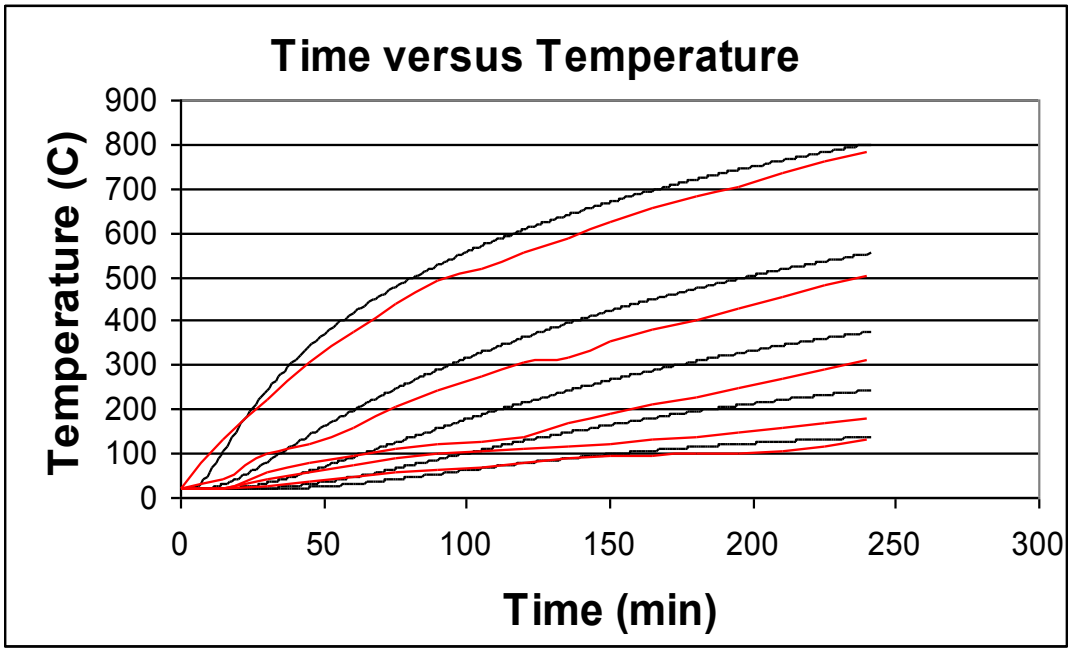

Figure 6.5: Temperature Distribution for a 175mm Alluvial Quartz Slab at 35mm Increments Using TAS (black) and BRANZ (red)

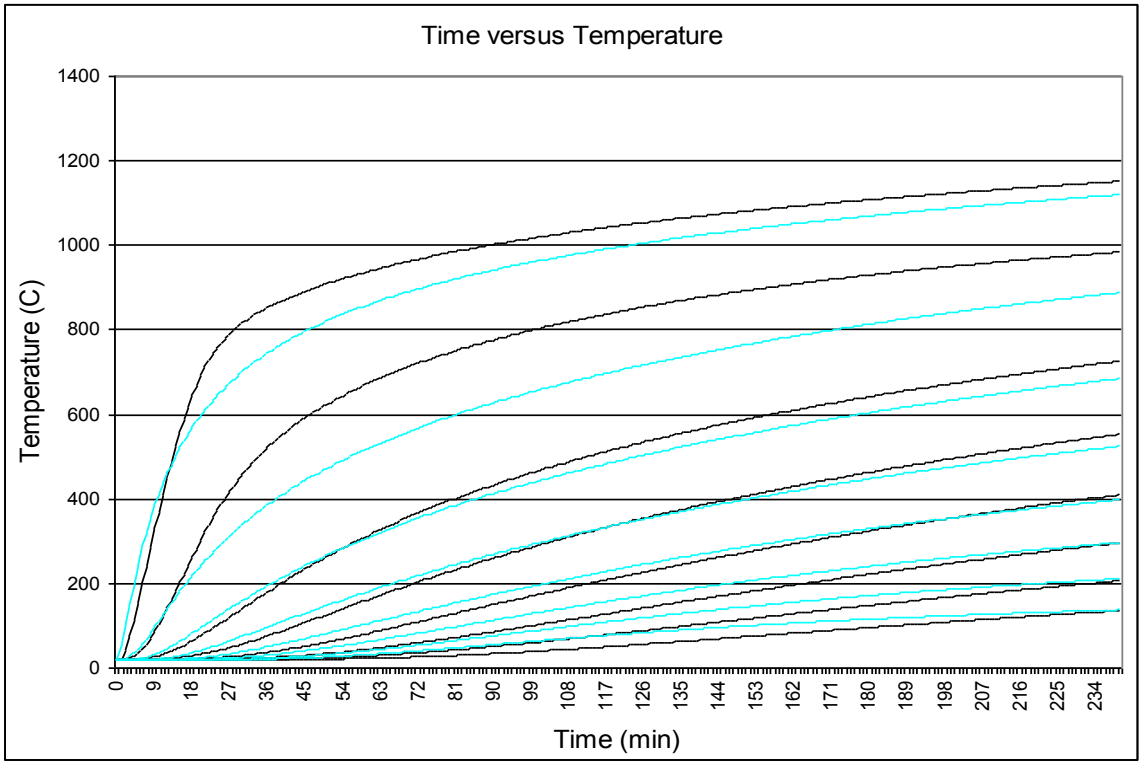

Figure 6.6: Temperature Distribution for a 175mm Alluvial Quartz Slab at 25mm Increments Using the Excel Tool (black) and TAS (light blue)

Next, a 60mm, alluvial quartz slab exposed to ISO 834 conditions was analyzed. It was modeled as 24 bricks of 2.5mm nominal thickness with the same 1cm x 1cm cross section using the 0.33 multiplier for the heat transfer coefficient on the unexposed side. Figure 6.7 displays the results for the TAS analysis and the BRANZ data. It can be seen that the temperatures produced by TAS lag behind those of the test data, which suggests that TAS does not transfer heat through the concrete cross section quickly enough for smaller elements.

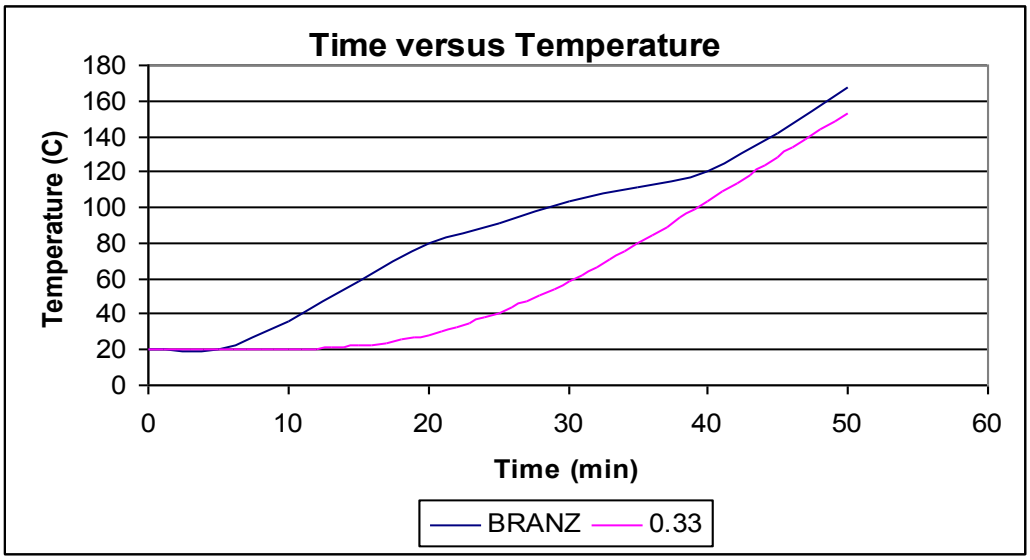

Figure 6.7: Temperature of Unexposed Face for a 60mm Alluvial Quartz Slab for BRANZ and TAS Data

6.3 Analyses using ASTM E119 Conditions

To further explore the use of TAS, slab elements composed of shale and carbonate aggregates were analyzed and compared with established PCA test data from Figure G.7 (Abrams & Gustaferro 1968). TAS simulations were completed for four carbonate (4, 5, 6, and 7 inches) and two shale (4 and 6 inches) slab elements exposed to ASTM E119 conditions. The 7-inch slab was modeled using 70 bricks because it is approximately the same thickness as 175mm. The remaining slab

elements were modeled using 40 bricks (4 inch), 50 bricks (5 inch), and 60 bricks (6 inch).

The results from using the 0.33 coefficient on the unexposed face for all the slab thickness were not promising. It was decided through trial and error that the heat release coefficients should form a linear relationship that is a function of slab thickness. A different type of relationship was needed for both the carbonate and shale aggregate to produce results that agree with the BRANZ data. Using information provided from a few trial analyses it was determined that the carbonate aggregate should have a value of 0.245 for 7 inches and increase by 0.085 for every 1-inch increment the slab thickness decreases.

Using these new multiples for the heat release coefficients simulations were run for each of the slabs again. Figure 6.8 displays the results for the carbonate slabs and when compared with PCA data the resultant temperatures for the unexposed face agree throughout the fire exposure. Figures 6.9 to 6.12 compare the temperature data for the unexposed face produced from the proposed Excel tool with those obtained from TAS and the PCA data for the carbonate slabs. Temperatures were graphed until the time they reached failure in accordance with the PCA test data. It can be seen that like the proposed Excel tool the TAS data also lags behind the ASTM E119 data although not as much. The results for the carbonate slabs maintained a consistent relationship with the proposed Excel tool.

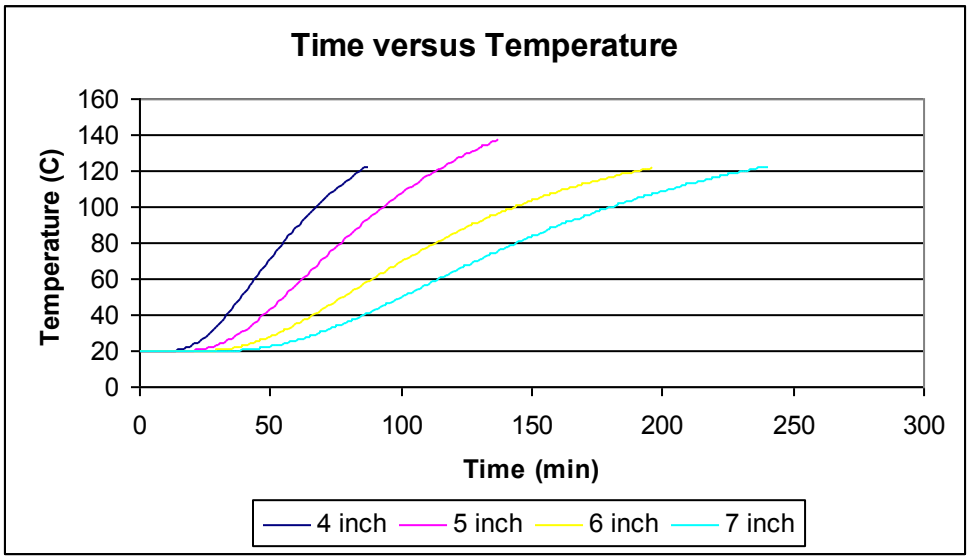

Figure 6.8: Temperature of Unexposed Face for Carbonate Slabs of Various Thicknesses Exposed to ASTM E 119 Conditions

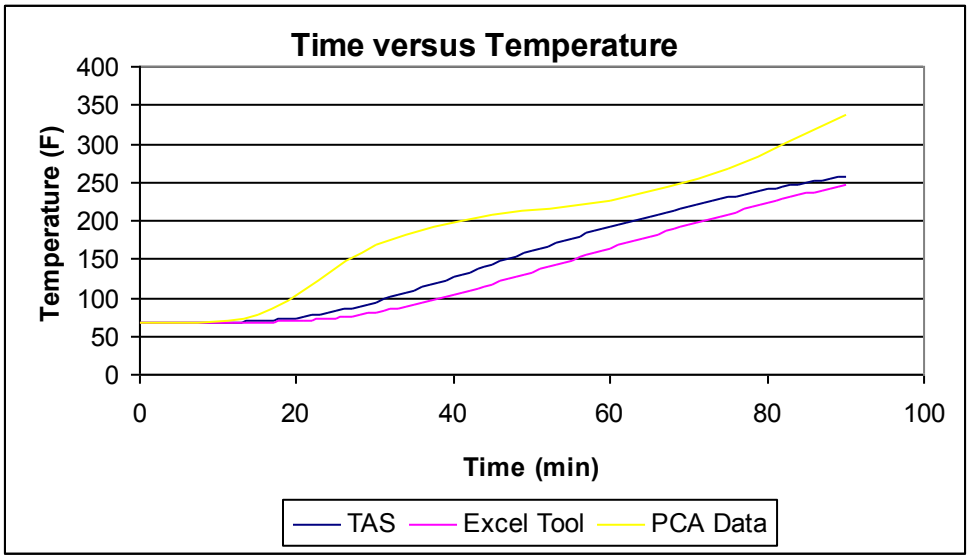

Figure 6.9: Temperature of Unexposed Face for Carbonate 4-Inch Slabs Exposed to ASTM E 119 Conditions

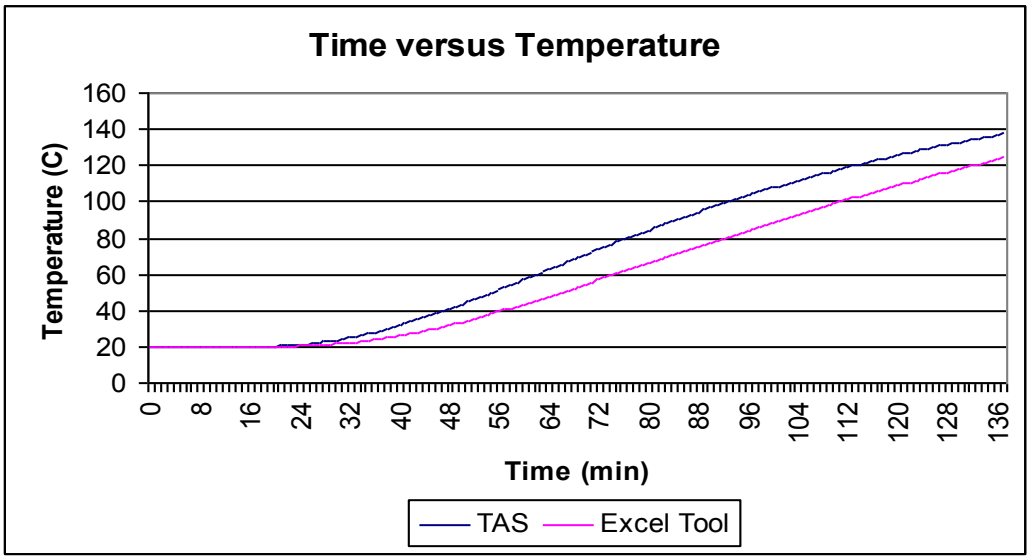

Figure 6.10: Temperature of Unexposed Face for Carbonate 5-Inch Slabs Exposed to ASTM E 119 Conditions

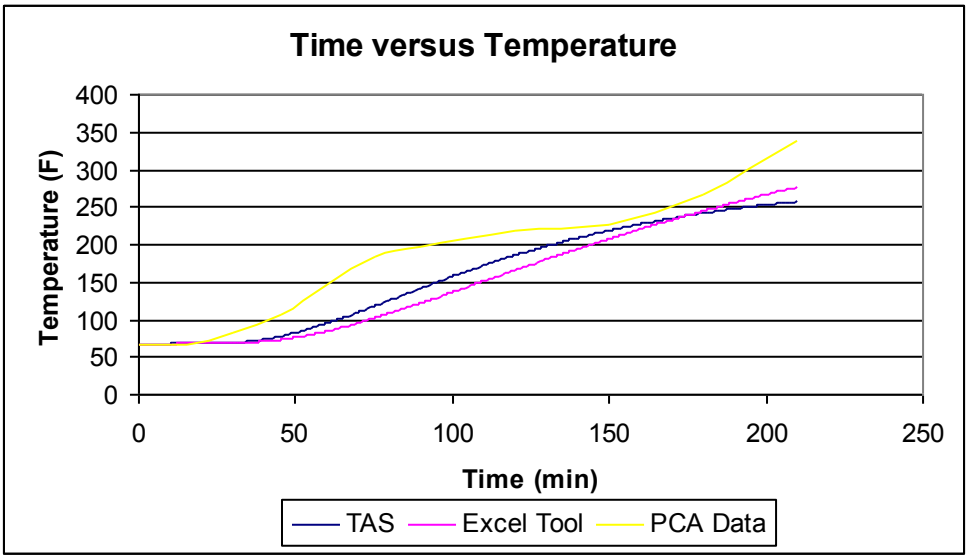

Figure 6.11: Temperature of Unexposed Face for Carbonate 6-Inch Slabs Exposed to ASTM E 119 Conditions

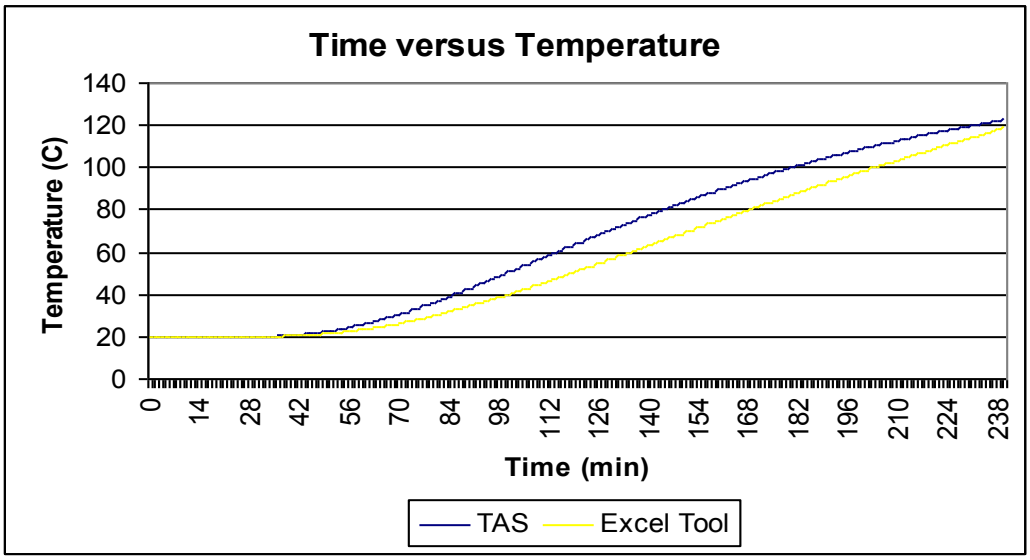

Figure 6.12: Temperature of Unexposed Face for Carbonate 7-Inch Slabs Exposed to ASTM E 119 Conditions

The numerical results obtained from simulations of the shale slabs were more inconsistent with the PCA data and can be seen in Figures 6.13 and 6.14. By investigating the results it was found that the shale slab elements are extremely resistant to heat transfer using TAS and published data for thermal properties. It took a considerable amount of time for heat to pass through the slab element to the unexposed face. Another set of simulations were run using an upper bound (0.9), average (0.775), and lower bound (0.5) value for thermal conductivity and results are displayed in Figure 6.15. The average and upper bound values produced temperatures that were greater than those for a variable thermal conductivity, although they still lag behind the PCA data. The increase in thermal conductivity values causes heat to travel through the slab element faster.

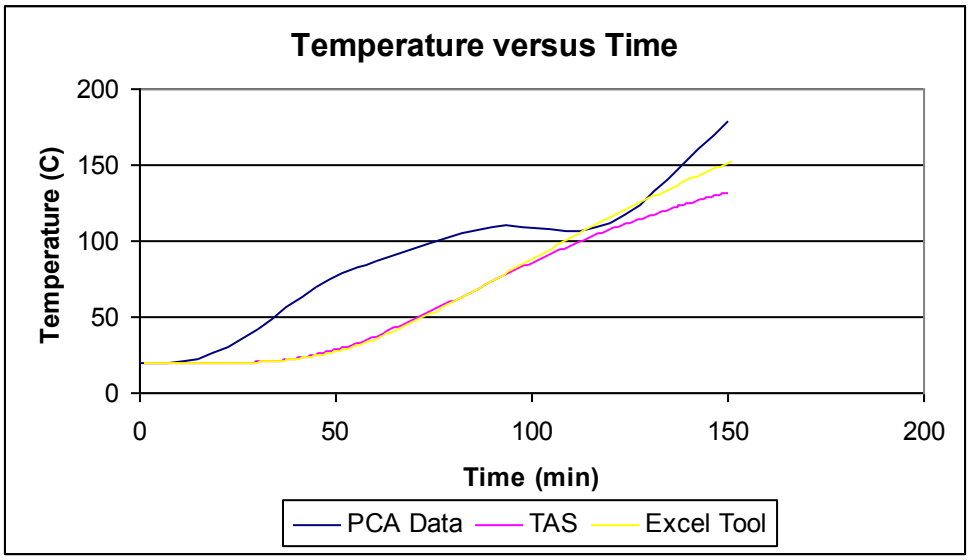

Figure 6.13: Temperature of Unexposed Face for 4 inch Shale Slab Exposed to ASTM E 119 Conditions

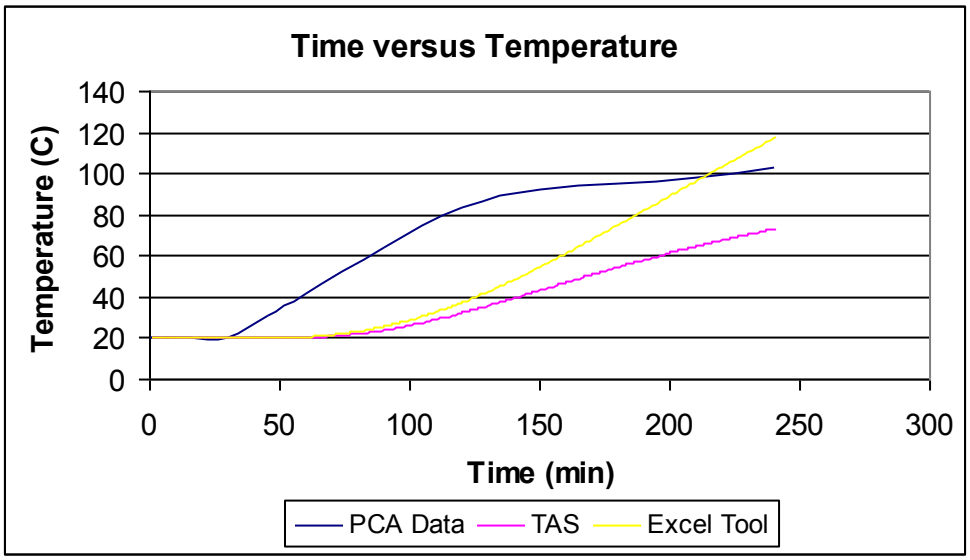

Figure 6.14: Temperature of Unexposed Face for 6 inch Shale Slab Exposed to ASTM E 119 Conditions

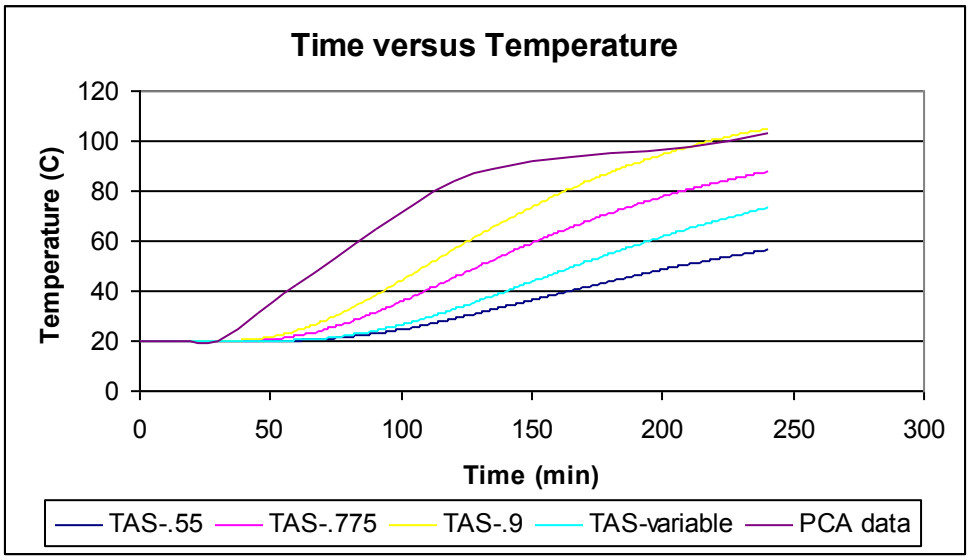

Figure 6.15: Temperature of Unexposed Face for Shale Slabs of Various Thicknesses Exposed to ASTM E 119 Conditions

6.4 Analyses using SDHI-95 and LDMI-M Conditions

Analyses of carbonate and shale slabs were extended to the study of their performance when exposed to the SDHI-95 and LDMI-M fire conditions. A 100mm slab and a 175mm slab were examined for each fire exposure, and the TAS and proposed Excel tool results for 25mm increments can be found in Figures 6.16 to 6.23.

For the carbonate slabs the heat transfer coefficients for both design fires produced from Equations 4.3 and 4.11 were used in place of those from the ASTM E119 fire. However, the use of these coefficients produced results that are extremely impractical. Temperatures for the unexposed face for the slabs generated from TAS were over two times the values produced from the proposed Excel tool. According to the TAS results the design fires are more severe than the ISO 834 standard fire test which is not possible because the time-temperature curve for the standard test is substantially more severe as can be seen by examining the time-temperature curves. Since the design fires are less severe, the heat transfer coefficients for the unexposed

face are lower because there is less heat being released into the atmosphere. When these coefficients with lower values are used for TAS simulations, far too little heat is being released from the slab, which is the reason why the temperatures near the unexposed face are rather high.

The carbonate slab simulations were run again using the heat transfer coefficients for the ASTM E119 fire test to see what affect they would have on the results. It can be seen from Figures 6.16 to 6.19 that these results better reflect the temperature distributions that one would expect to occur during exposure to the design fires. From the graphs it still seems that the cooling period, which takes place after the fire intensity begins to decrease, is not being fully captured.

The shale slab simulations were run using the heat transfer coefficients for the ASTM E119 fire test with both a variable and upper bound values for thermal conductivity. The results are displayed in Figures 6.20 to 6.23, and it can be seen that the upper bound value for thermal conductivity produces temperature distributions that are nearly as severe as those for carbonate. Since the shale slab is lightweight, it has considerably more fire resistance than the carbonate slab so these results do not reflect a simulation that accurately accounts for the fire performance of a shale slab. For the variable thermal conductivity the values near the unexposed face are actually lower than those produced from the proposed Excel tool. This could be a possibility since the TAS model captures heat release while the proposed Excel tool ignores it

It was demonstrated in the previous chapter that the proposed Excel tool is capable of assessing the temperature on the unexposed face after three hours exposure, so it can be assumed that the temperature distributions from the TAS

analyses are conservative near the unexposed face. Also, for a design fire the proposed Excel tool would be more conservative than it is for a standard fire test because it does not account for heat release and the heat will remain inside the slab.

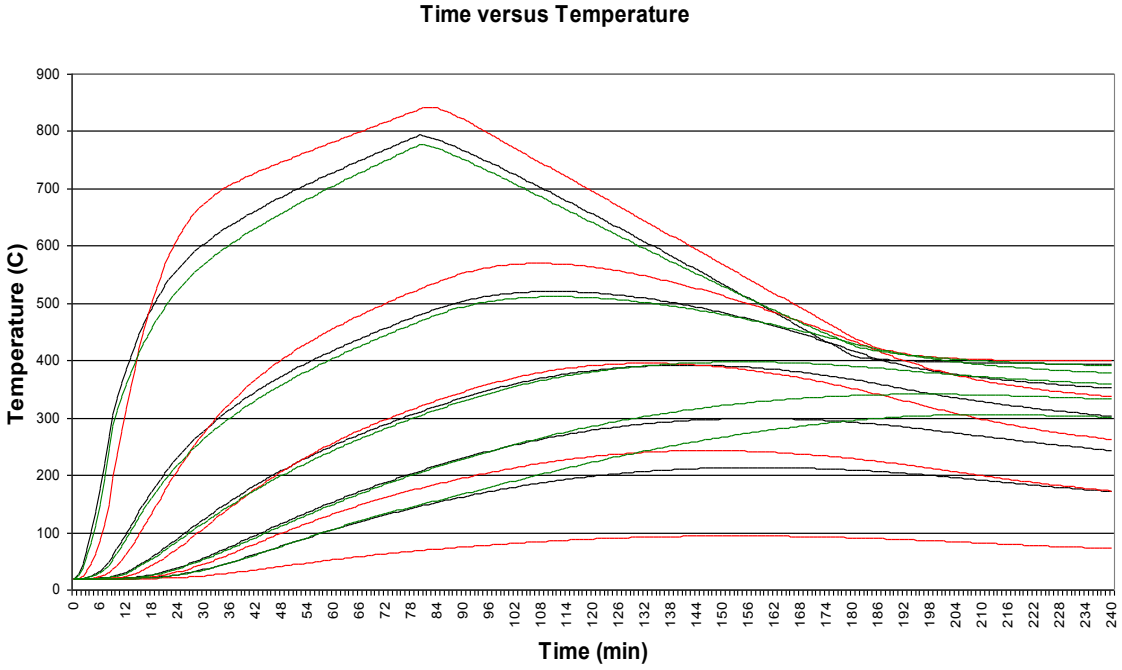

Figure 6.16: Temperature Distribution Analysis for a 100mm Carbonate Slab Exposed to LDMI-M Conditions for the Excel Tool (Red), TAS with ASTM E119 coefficients (Black), and TAS with LDMI-M coefficients (Green)

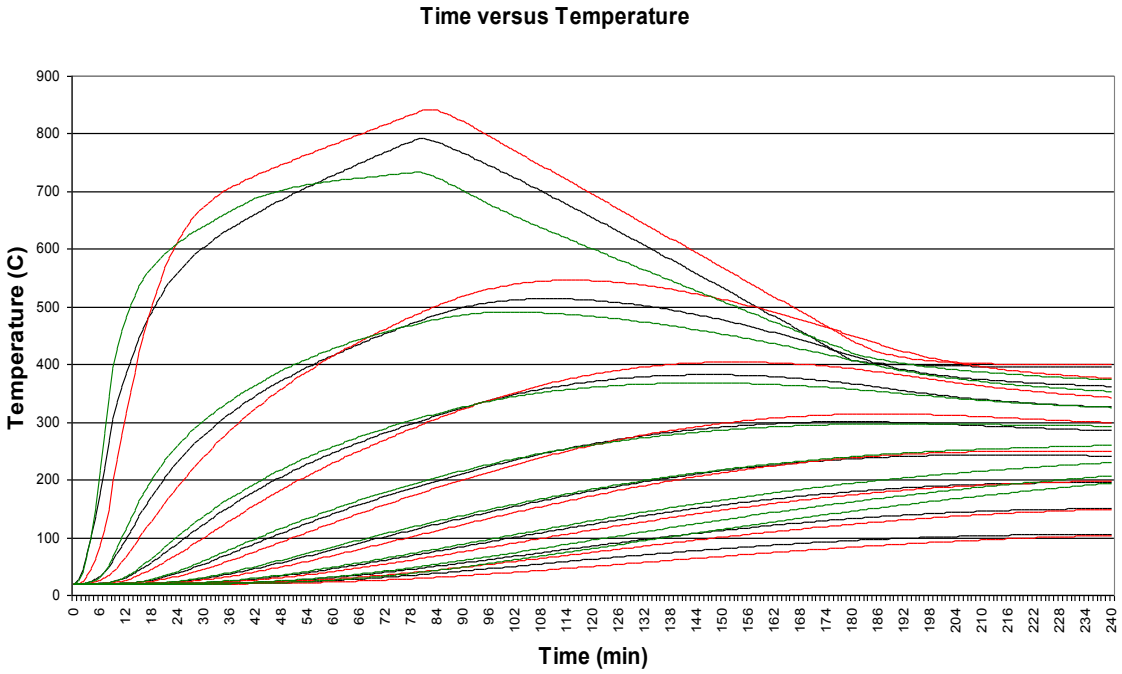

Figure 6.17: Temperature Distribution Analysis for a 175mm Carbonate Slab Exposed to LDMI-M Conditions for the Excel Tool (Red), TAS with ASTM E119 coefficients (Black), and TAS with LDMI-M coefficients (Green)

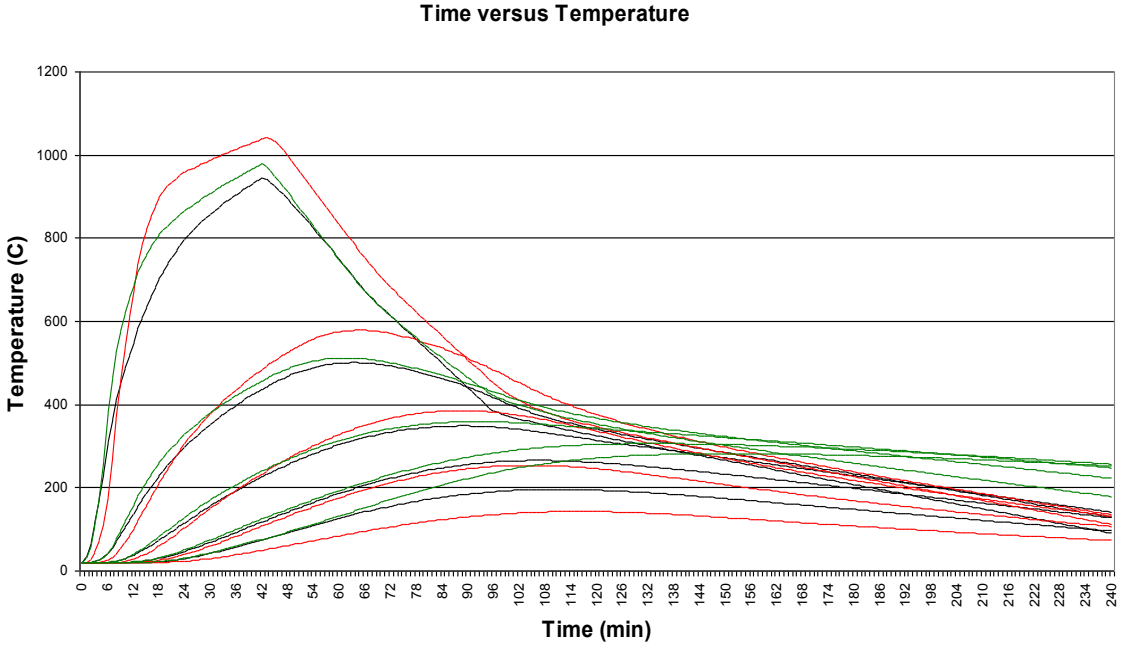

Figure 6.18: Temperature Distribution Analysis for a 100mm Carbonate Slab Exposed to SDHI-95 Conditions for the Excel Tool (Red), TAS with ASTM E119 coefficients (Black), and TAS with SDHI-95 coefficients (Green)

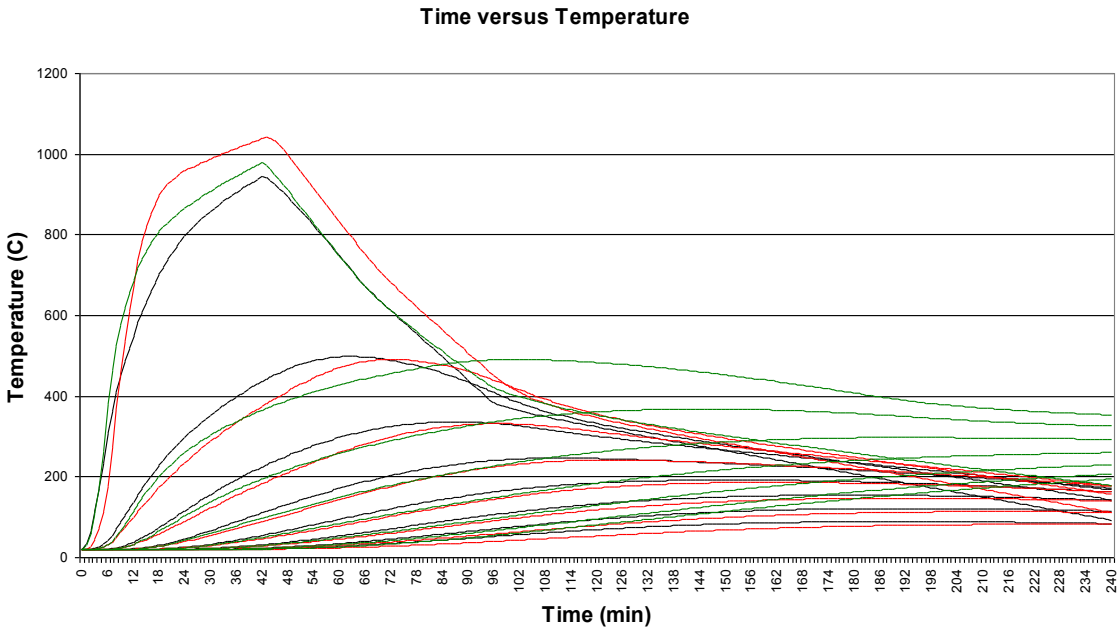

Figure 6.19: Temperature Distribution Analysis for a 175mm Carbonate Slab Exposed to SDHI-95 Conditions for the Excel Tool (Red), TAS with ASTM E119 coefficients (Black), and TAS with SDHI-95 coefficients (Green)

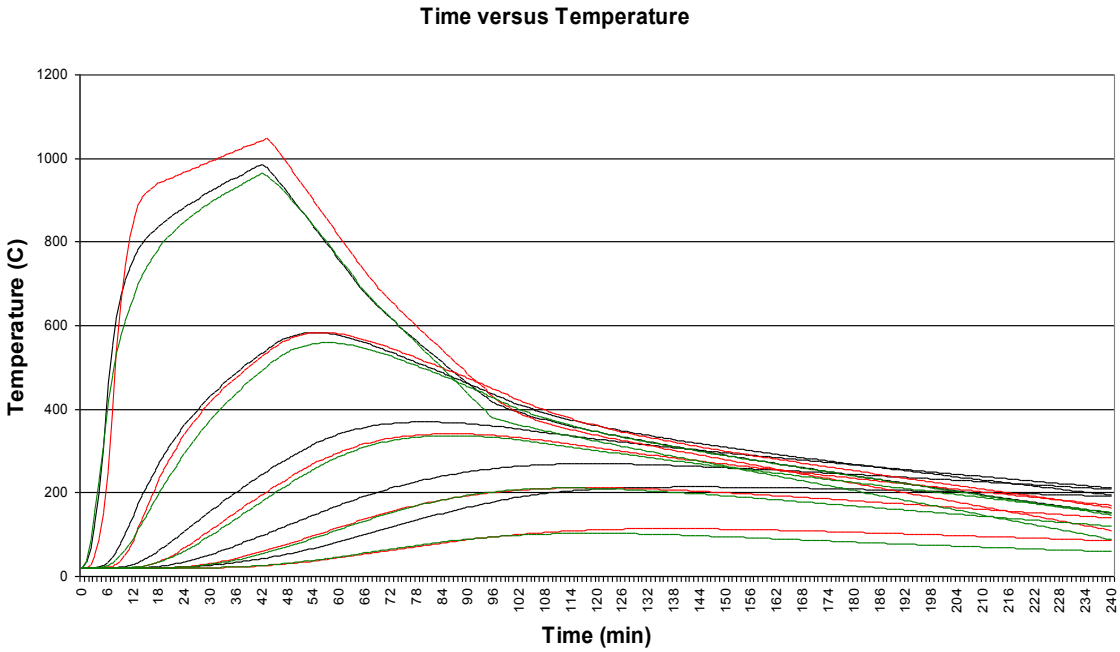

Figure 6.20: Temperature Distribution Analysis for a 100mm Shale Slab Exposed to SDHI-95 Conditions for the Excel Tool (Red), TAS with Upper Bound Thermal Conductivity (Black), and TAS with Variable Thermal Conductivity (Green)

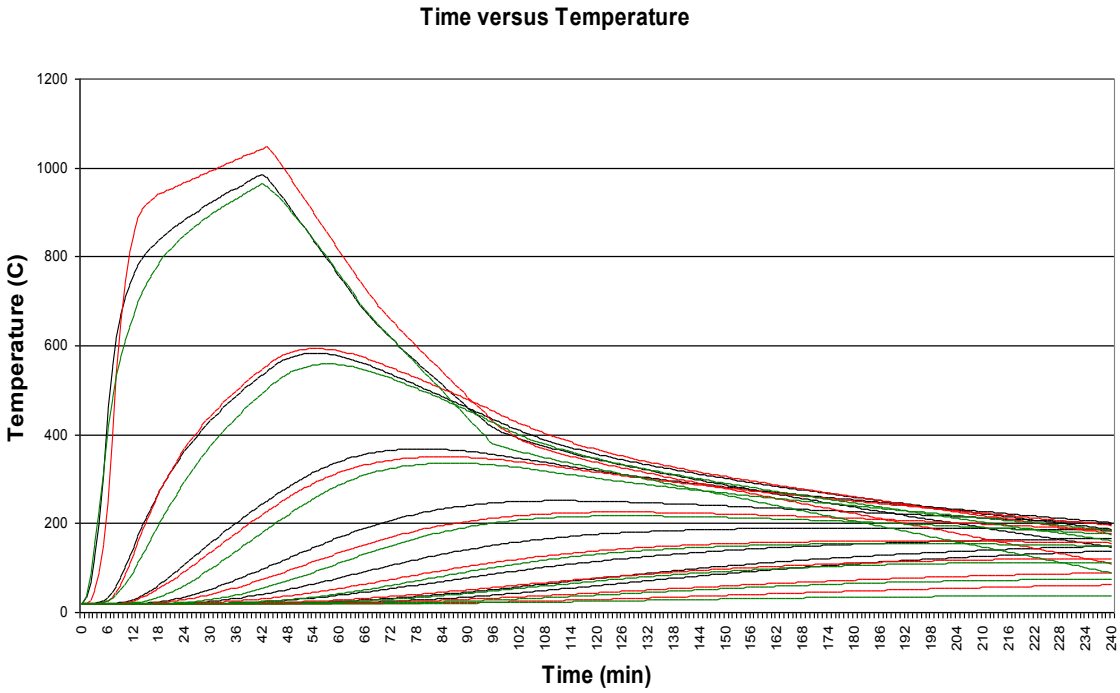

Figure 6.21: Temperature Distribution Analysis for a 175mm Shale Slab Exposed to SDHI-95 Conditions for the Excel Tool (Red), TAS with Upper Bound Thermal Conductivity (Black), and TAS with Variable Thermal Conductivity (Green)

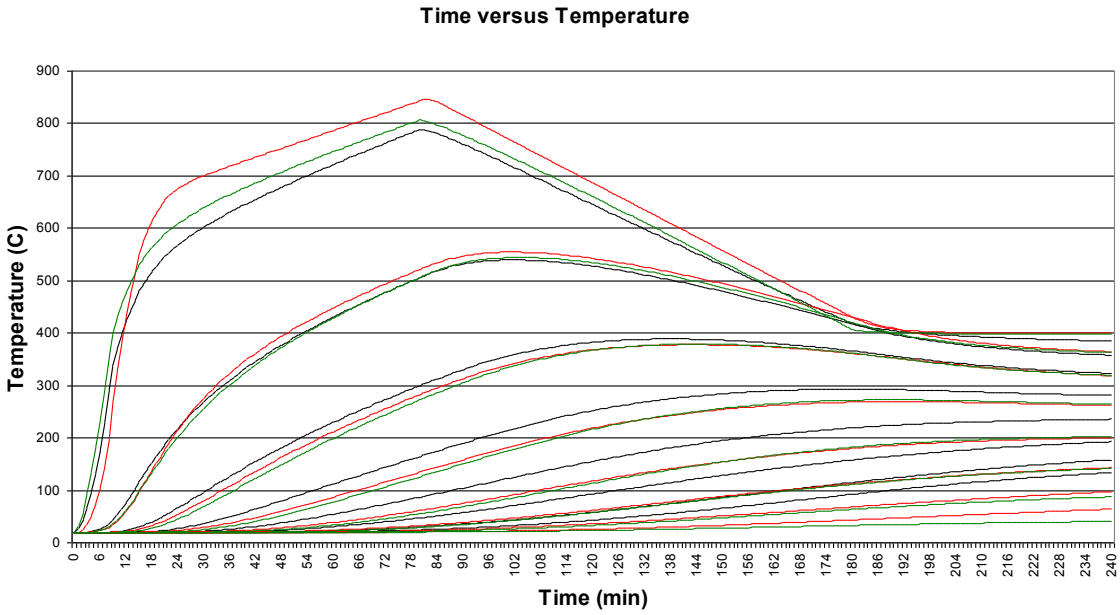

Figure 6.22: Temperature Distribution Analysis for a 100mm Shale Slab Exposed to LDMI-M Conditions for the Excel Tool (Red), TAS with Upper Bound Thermal Conductivity (Black), and TAS with Variable Thermal Conductivity (Green)

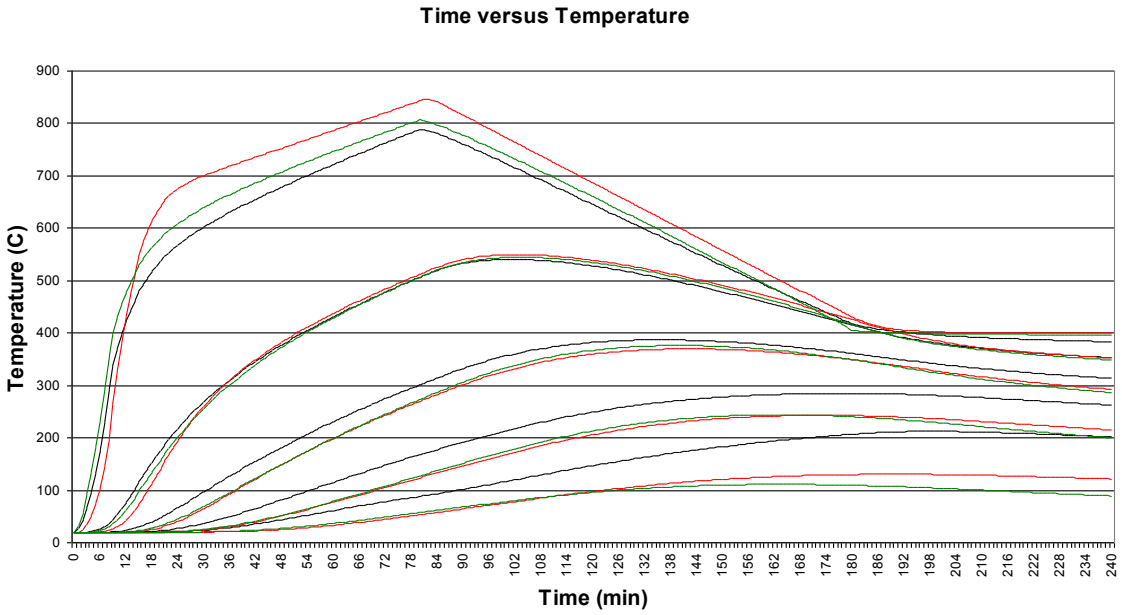

Figure 6.23: Temperature Distribution Analysis for a 175mm Shale Slab Exposed to LDMI-M Conditions for the Excel Tool (Red), TAS with Upper Bound Thermal Conductivity (Black), and TAS with Variable Thermal Conductivity (Green)

6.5 Summary

The modeling of concrete in fire conditions with TAS produced mixed results. Temperatures for the unexposed face of slabs were not able to be reproduced in accordance with published test data; however, they did show a consistent relationship with results from the Excel tool for standard fires. Also temperatures near the exposed face were consistent with the Excel tool which means both conservatively predict temperatures in that region. The trouble is that each type of aggregate for a particular fire condition requires its own individual analysis with coefficients and variables being adjusted accordingly. This leads to results which can not be replicated and serve more as analysis on a case by case basis. Little further verification was obtained for the Excel tool through the use of TAS due to it

ineffectiveness in determining the fire performance of concrete in different design fires.

It is believed that the major issue in TAS's inability to produce consistent results for different types of aggregates, slab thicknesses, and fire exposures is that the heat transfer coefficients on each side are not temperature dependent. These values could not be imported as temperature dependent because they are functions of the temperature of the exposed face, gas temperature, and unexposed face. TAS does not allow for the equation for the heat transfer coefficient to be imported into the program so TAS would calculate the value at every time step. Instead, values had to be imported from those produced from the proposed Excel tool. Since those values were generated from the proposed Excel model it can not be assumed they can be directly applied to TAS analyses. TAS is performing analyses which are separate from the proposed Excel tool so TAS would need its own coefficients for its simulations.

7 Design of Fire Exposed Slabs

The rational design procedure examined in this chapter applies structural engineering principles and material properties at elevated temperatures to analyze the performance of reinforced concrete floor slabs during fire conditions. Modes of failure for this procedure include collapse by flexure and exceeding insulation limits (unexposed face of the slab reaches 140ºC). Shear failure can also be checked similar to its treatment at normal temperatures by taking into account material properties at elevated temperatures (Figures 7.1 and 7.2). It is not typical for shear failures to occur because of the reduced live loads used in fire design (Malhotra 1982) so it is not included as a failure criterion for the procedure.

ISO 834 fire conditions were used as the design fire to evaluate slab capacity in this section. Analysis of slab capacities for actual fire conditions (SDHI-95, SDHI-M, and LDMI-M) can be completed following the same procedure. The design method and theory described is similar to the analytical procedures presented by Malhotra (1982) and Wade (1991). In this case temperature distributions for shale and carbonate determined from the proposed Excel calculation tool for the ISO 834 fire (Figures 7.3 to 7.7) are utilized as opposed to the generalized isotherms (Figures 3.1 and 3.2). By using temperature distribution data for slabs in design fire conditions a structural engineer has the ability to integrate structural fire safety within the structural design process, which avoids the limitations of code-based requirements.

The procedure discussed by both Malhotra (1982) and Wade (1991) uses live load reduction to determine the slab design load for fire conditions. The design load is checked against the allowable capacity of slabs during fire conditions, making use of

the properties of concrete and reinforcing steel at elevated temperatures. If the allowable capacity at temperature exceeds the design load through the duration of the design fire event, then the design is considered satisfactory for a particular fire condition.

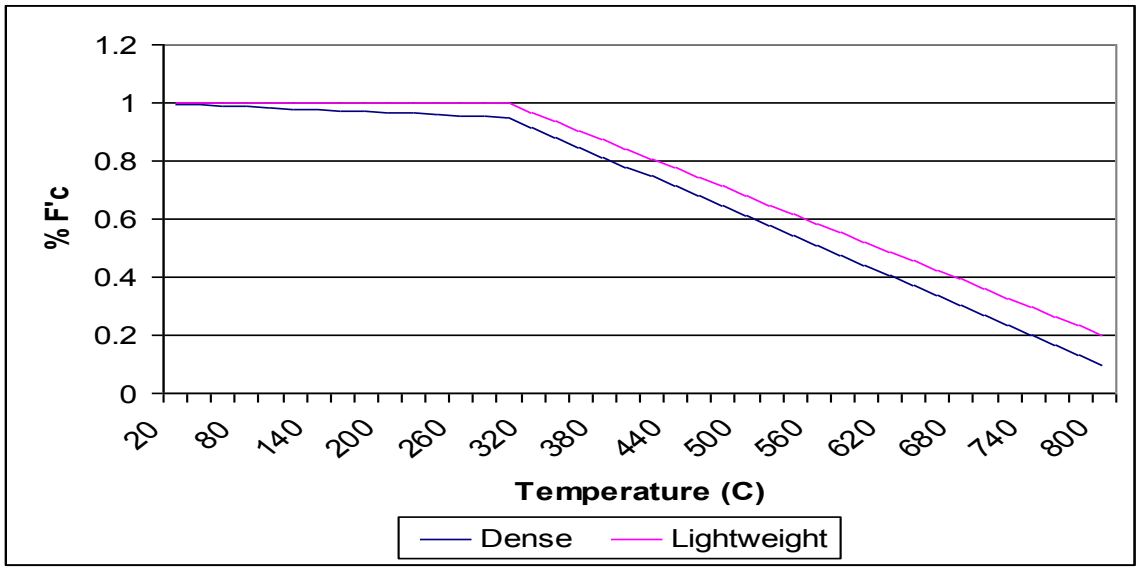

Figure 7.1: Strength of Dense and Lightweight Concrete versus Temperature (from Malhotra 1982)

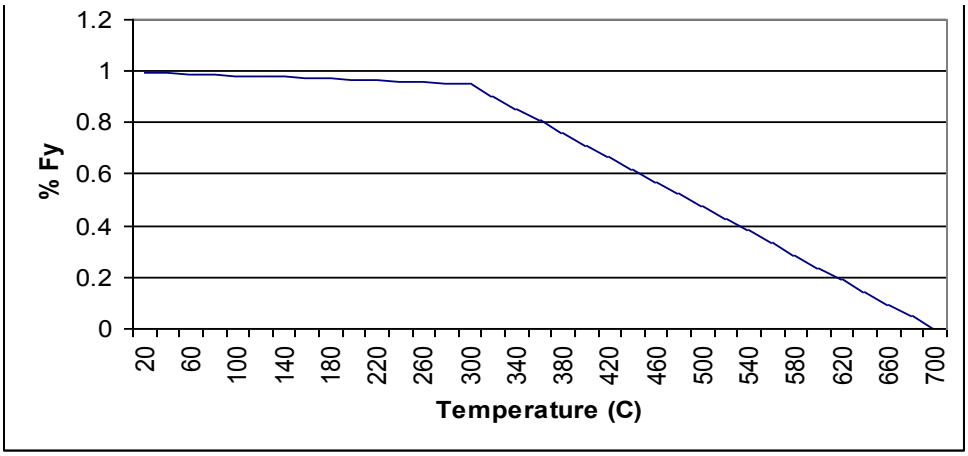

Figure 7.2: Strength of Reinforcing Steel versus Temperature (from Malhotra 1982)

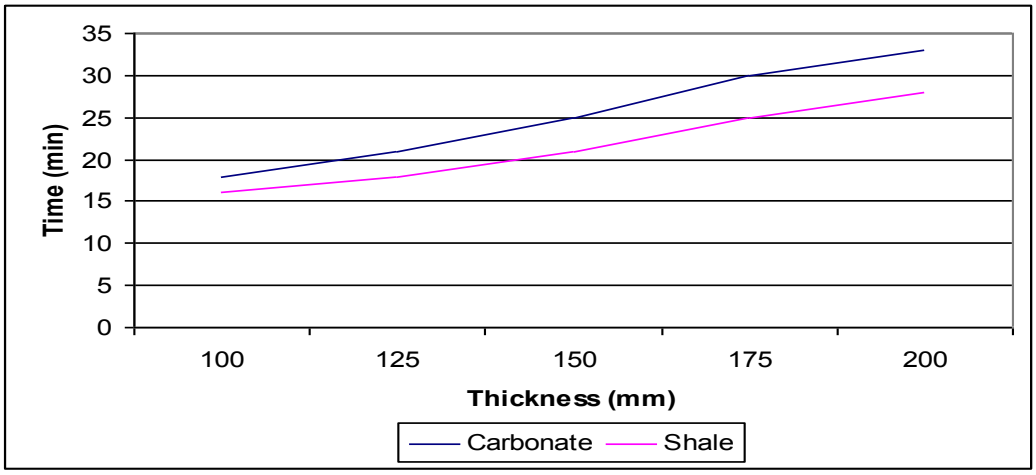

Figure 7.3: Time for Steel Centroid of Varying Thicknesses of Shale and Carbonate Aggregate Slabs to Reach 200ºC

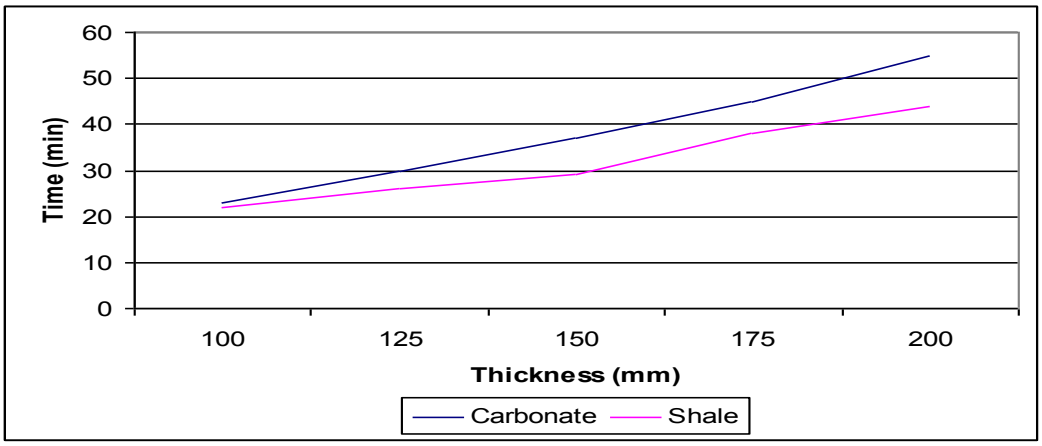

Figure 7.4: Time for Steel Centroid of Varying Thicknesses of Shale and Carbonate Aggregate Slabs to Reach 300ºC

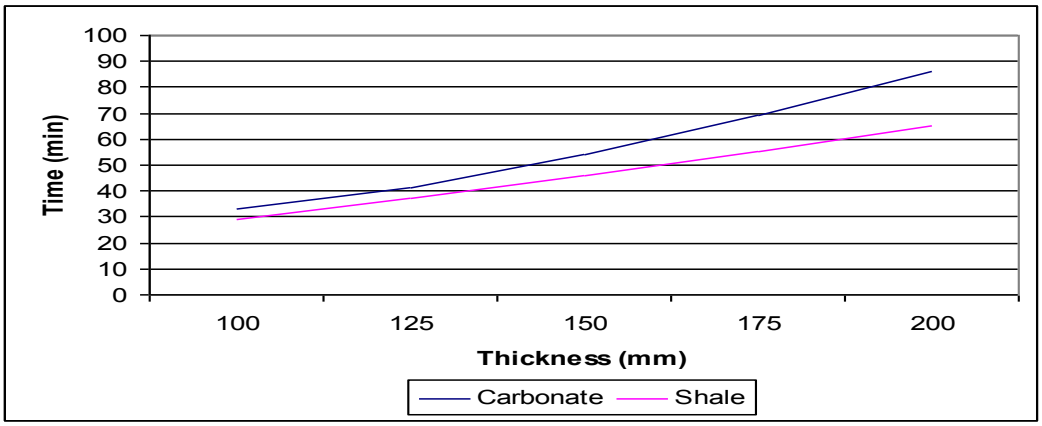

Figure 7.5: Time for Steel Centroid of Varying Thicknesses of Shale and Carbonate Aggregate Slabs to Reach 400ºC

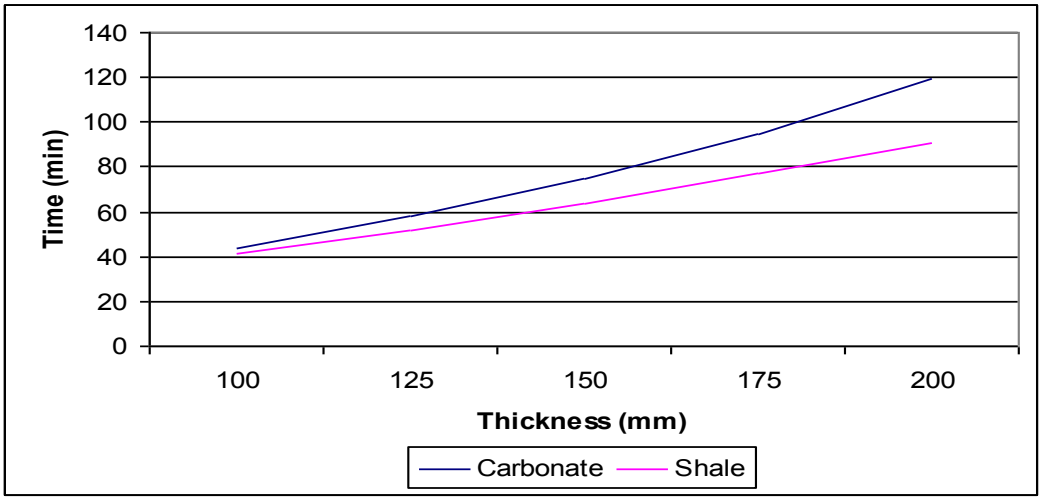

Figure 7.6: Time for Steel Centroid of Varying Thicknesses of Shale and Carbonate Aggregate Slabs to Reach 500ºC

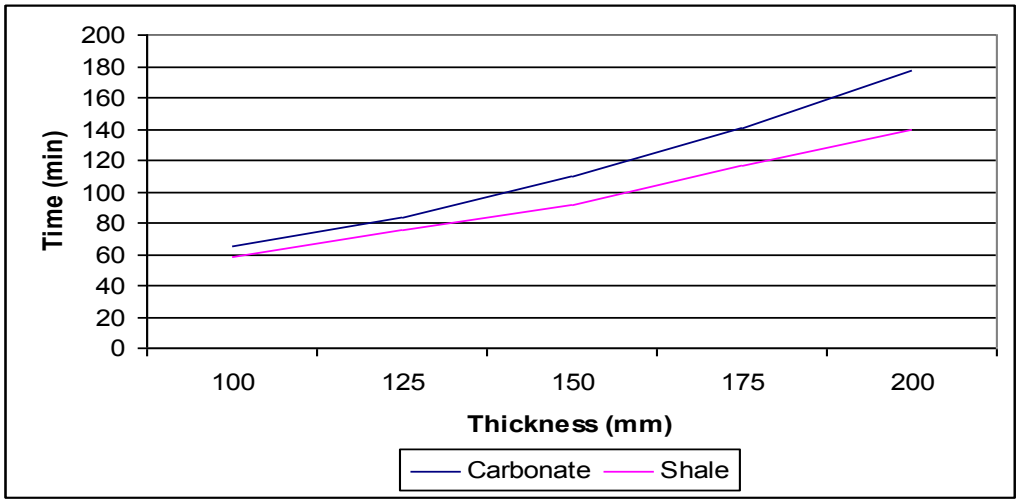

Figure 7.7: Time for Steel Centroid of Varying Thicknesses of Shale and Carbonate Aggregate Slabs to Reach 600ºC

7.1 Unrestrained Slabs

During fire conditions the moment capacity of unrestrained simply supported elements slabs due to the reduction in concrete and steel strength at elevated temperatures. The design procedure for unrestrained simply supported concrete slabs is described, and a capacity analysis of lightweight and dense concretes in fire conditions is performed using the temperature distribution curves presented above in Figures 7.3 through 7.7.

7.1.1 Design Criteria

The first step to design a simply supported concrete slab for fire conditions is to perform a thermal analysis of the slab in question using the spreadsheet application developed in this thesis. The temperature at the steel centroid and at the centroid of the concrete compressive block is obtained, and the strengths of these materials at elevated temperatures are determined. The required design moment capacity for fire conditions M_{uf} (kN-m) is computed by the equation:

$$M_{uf} = \frac{w_{uf} l^2}{8}, \quad \textbf{(Equation 7.1)}$$

where l (m) is the span length and w_{uf} (kN/m) is the fire design load obtained from the equation (Malhotra 1982):

$$w_{uf} = 1.05D + 1.0L, \quad \textbf{(Equation 7.2)}$$

where D is the dead load and L is the live load. Next, the slab's ultimate moment capacity, ϕM_n, at temperature is calculated by first determining the tensile strength, F_{st} (kN), of the steel at temperature:

$$F_{st} = \frac{F_y * \sigma_{st} * A_s}{1000}, \quad \textbf{(Equation 7.3)}$$

where F_y (N/mm^2) is the strength of the reinforcing steel in ambient conditions, σ_{st} is the percentage of steel strength remaining at the subject temperature, and A_s (mm^2) is the area of steel. The compressive strength, F_{ct} (kN), of the concrete slab at temperature is calculated in terms of the depth of the compressive block, d_c (mm) (Malhotra 1982):

$$F_{ct} = \frac{.67 * f'c * \sigma_{ct} * d_c}{\gamma_{mc}}, \quad \textbf{(Equation 7.4)}$$

where $f'c$ (kN/mm^2) is the strength of concrete in ambient conditions, σ_{ct} is the percentage of concrete remaining at temperature, and γ_{mc} is a correction factor for concrete that has a value of 1.3. The depth of the compression block is determined by setting $F_{ct} = F_{st}$ and solving for d_c. The distance, z (mm), from the centroid of the steel to the centroid of the newly established compressive block is determined by taking the lesser value computed from the following equations:

$$z = .95d \text{ or } z = d - \frac{d_c}{2}, \quad \textbf{(Equation 7.5 and 7.6)}$$

where d (mm) is the depth to the steel centroid. The nominal capacity ϕM_n at temperature of the concrete slab is given by:

$$\phi M_n = F_{st} * z, \quad \textbf{(Equation 7.7)}$$

and compared with the design moment M_{uf}. If $M_{uf} < \phi M_n$ slab has sufficient capacity but if $M_{uf} > \phi M_n$ the slab fails and an increase in steel area or cover is needed.

Wade (1991) uses alternative equations for calculating the design loading for fire condtions:

$$w_{uf} = 1.0D + \varphi L \text{ or } w_{uf} = 1.0D + 0.25W, \quad \textbf{(Equation 7.8 and 7.9)}$$

where W is the wind load and φ is a live load reduction factor. Suggested values for φ are 0.4 for domestic office, and parking floors as well as for trafficable roofs; 0.6 for storage and other floor types; and 0.0 for non-trafficable roofs.

The following is a worked example for the design of a slab exposed to fire conditions following the procedure of Equation 7.1 to 7.7.

- Worked Example: Determine the capacity of a 3m carbonate slab with 35mm of steel cover for 1.5 hours of ISO 834 exposure. The slab is 175mm thick, has a density of 2350 kg/m^3, F_y = 460N/mm^2, f'c = 25N/mm^2, and A_s = 420mm^2.

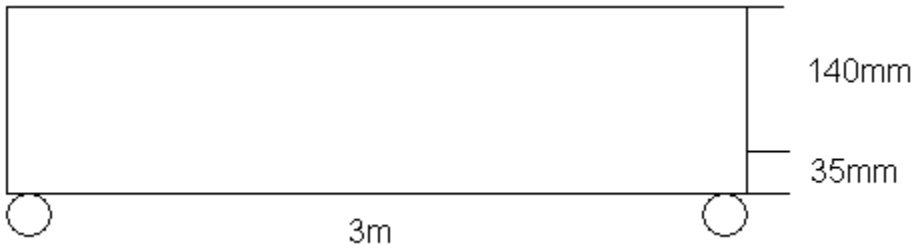

$$DL = .175*23.6 = 4.18kN/m$$

$$w_{uf} = 1.05*4.18 = 4.39kN/m$$

$$M_{uf} = \frac{4.39*(3)^2}{8} = 4.93kN-m$$

$$@35mm, \quad T_s = 500, \quad T_c = 500 \quad (from\ thermal\ analysis)$$

$$\sigma_{st} = .47, \quad \sigma_c = .67 \quad (from\ Figures\ F.1\ and\ F.2)$$

$$F_{st} = F_y \sigma_{st} A_s = .460*.47*420 = 90.8kN$$

$$@z, \quad T_s = 125, \quad T_c = 125 \quad (from\ thermal\ analysis)$$

$$\sigma_{st} = 1, \quad \sigma_c = 1 \quad (from\ Figures\ F.1\ and\ F.2)$$

$$F_{ct} = \frac{.67*25*1*d_c}{1.3} = 12.88d_c$$

$$F_{st} = F_{ct}$$

$$12.88d_c = 90.8$$

$$d_c = 7.05mm$$

$$z = \underline{.95d = 133}, \ or \ z = d - \frac{d_c}{2} \approx 136$$

$$\phi M_n = \frac{90.8*133}{1000} = 12.08kN-m$$

$$M_{uf} = 4.93kN-m < \phi M_n = 12.08kN-m \quad \therefore OK$$

7.1.2 Extension of Capacity Analyses to Other Designs

The fire design procedure for simply supported slabs was extended to the study of expanded shale and carbonated aggregate slabs with thicknesses of 100, 125, 150, 175, and 200mm. The temperature distribution data are presented in the beginning of this chapter (Figures 7.3 to 7.7). The steel cover for the 100mm slab was assumed to be 20mm, and cover was assumed to increases by 5mm for every 25mm increase in thickness. For simplification purposes the area of required steel was determined by CP 110 as presented in Malhotra (1982); the values are summarized in Table 7.1 for the different slab thicknesses. Slab span lengths of 1.5 and 3m were analyzed, and the results are plotted in Figures 7.8 through 12 as the ratio of the nominal capacity at temperature (ϕM_n) to the design moment (M_{uf}) during fire conditions. The objective of this study was to investigate the capacity of unloaded slabs until flexural failure so the only loads considered were the slabs self-weight. It can be seen that the lightweight aggregate slabs have higher capacity ratios as expected because they are less dense although lightweight slabs are not capable of achieving the same concrete strength as normal weight due to the aggregates.

Table 7.1: Area of Reinforcing Steel Used for each Slab Thickness

Slab Thickness (mm)	Area of Steel (mm^2)
100	240
125	300
150	360
175	420
200	480

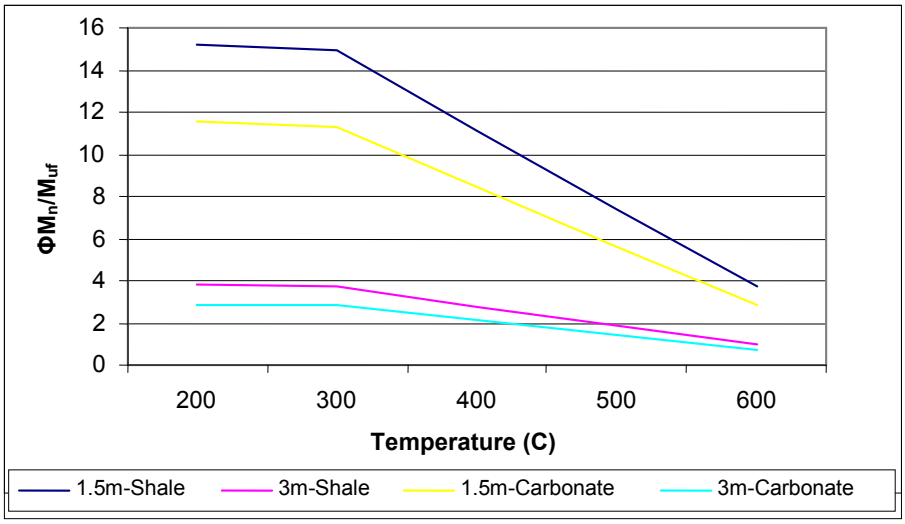

Figure 7.8: Ratio of ϕM_n to M_{uf} for 100mm Unrestrained Slabs

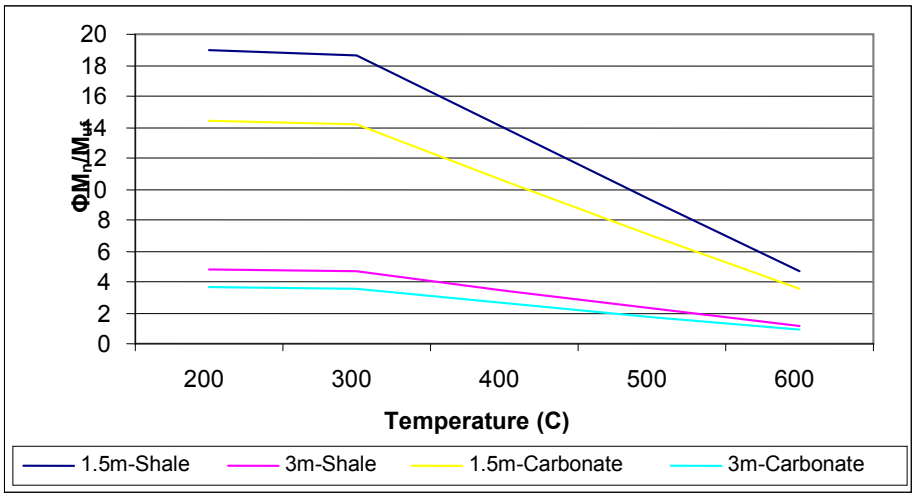

Figure 7.9: Ratio of ϕM_n to M_{uf} for 125mm Unrestrained Slabs

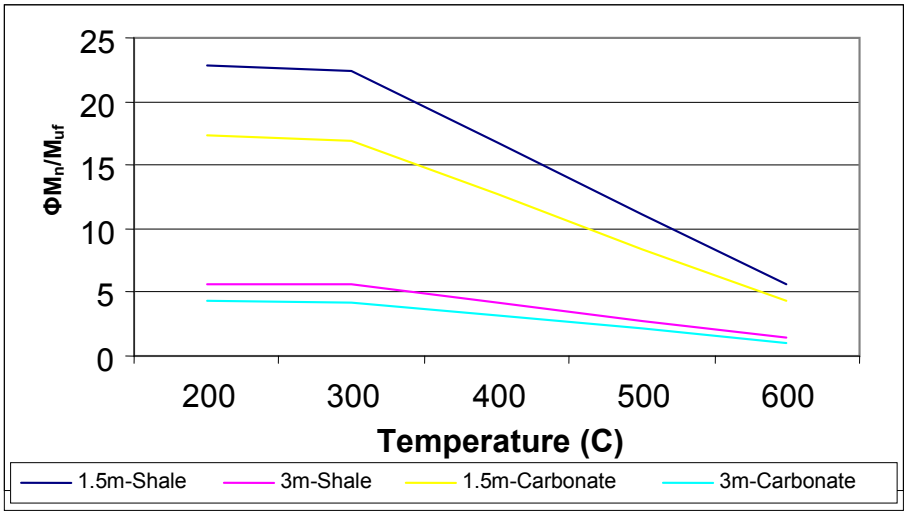

Figure 7.10: Ratio of ϕM_n to M_{uf} for 150mm Unrestrained Slabs

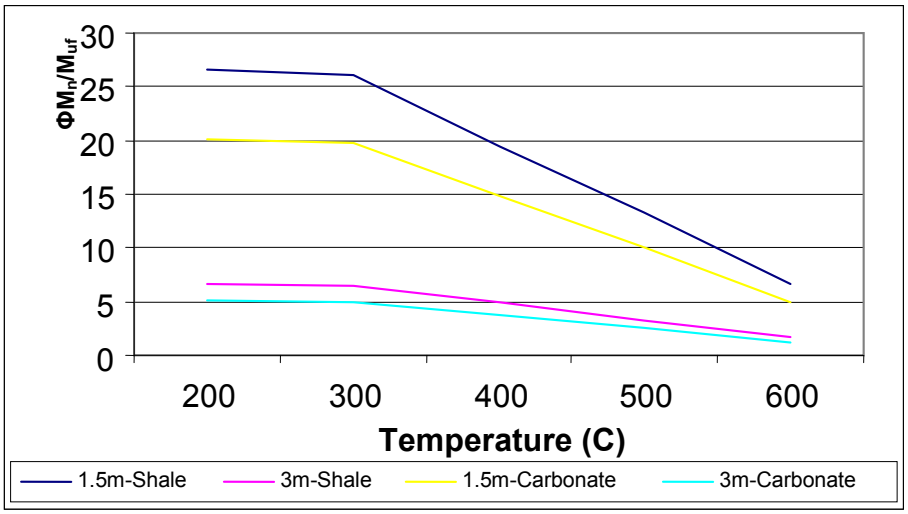

Figure 7.11: Ratio of ϕM_n to M_{uf} for 175mm Unrestrained Slabs

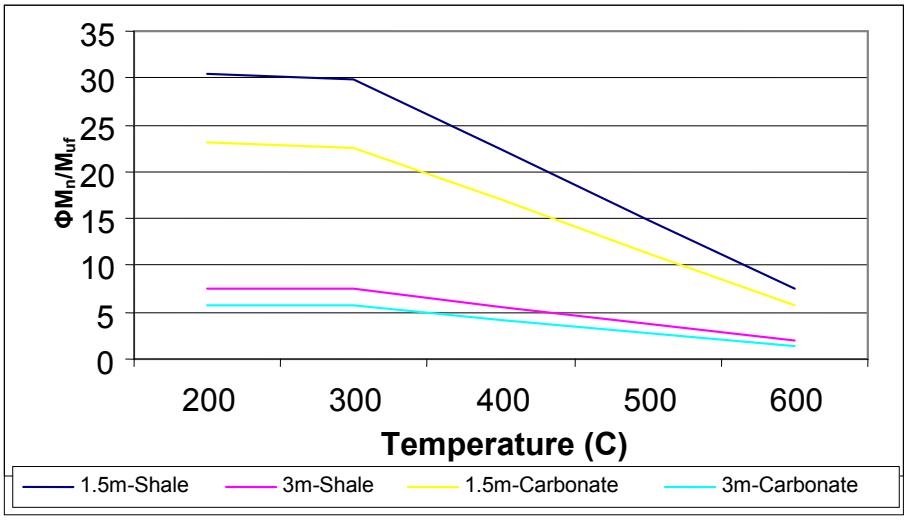

Figure 7.12: Ratio of ϕM_n to M_{uf} for 200mm Unrestrained Slabs

7.2 Restrained Against Thermal Expansion

When fire occurs in a building it will heat the underside of slabs, and that part of the cross-section will want to expand. This expansion will be resisted by the surrounding cooler structure by a force known as thermal thrust. As long as the resultant line of action for thrust is within the element's compressive stress block, this thrust factor will increase the moment capacity of the slab and enhance its fire performance.

7.2.1 Design Criteria

To design a restrained slab for fire conditions one must first perform the procedure for computing the fire performance of an unrestrained, simply supported slab as was previously detailed. Then the temperature at the line of action of the thermal force and steel centroid for the negative reinforcement, located at the top of the slab cross-section, must be obtained (Figures 7.1 and 7.2) to determine the percentage of concrete and steel strength for calculation purposes. The area of negative reinforcement, A'_s (mm^2), is calculated as 15% of the slabs cross-section

according to CP 110. This value is used to calculate F'_{st} for the negative reinforcement using Equation 7.3. F'_{ct} for the line of action of the thermal force is calculated in terms of dc using Equation 7.4. Solving for $F'_{ct} = F'_{st}$ yields d_c which is used to calculate z in Equations 7.5 and 7.6. Finally, the moment capacity produced from restraining thermal expansion, M_r, is computed using Equation 7.7 and is added to the ultimate fire capacity calculated for the slab at temperature assuming unrestrained, simple supports. The total capacity of the restrained slab is given by:

$$M_r + \Phi M_n = M_t, \quad \textbf{(Equation 7.10)}$$

If $M_{uf} < M_t$ slab has sufficient capacity but if $M_{uf} > M_t$ the slab fails and the positive steel area or cover must be increased. The following is a worked example for the effects of thermal thrust.

- Worked Example: Determine the new capacity of the 3m carbonate slab above if measures to restrain thermal expansion are taken.

$$T = 470, T = 210 \quad (from\ thermal\ analysis)$$

$$\sigma_c = .64 \quad , \quad \sigma_s = 1 \quad (from\ Figures\ F.1\ and\ F.2)$$

$$F'_s = .210 * 460 = 96.6kN$$

$$F'_c = \frac{.67 * d_c * .64 * 25 * d_c}{1.3} = 8.25 d_c$$

$$d_c = \frac{96.6}{8.25} = 11.71mm$$

$$z = 105 - \frac{11.71}{2} = 99.14mm$$

$$M_r = 96.6 * .09914 = 9.58kN - m$$

$$M_t = 9.58 + 12.08 = 21.66kN - m$$

7.2.2 Capacity Analysis

The previously analyzed simply supported slabs in Figures 7.8 through 12 were considered to be restrained against thermal expansion and their capacities were then recomputed to observe the effects of thermal thrust from a design standpoint. The results are plotted in Figures 7.13 through 22 as the ratio of the design moment (M_{uf}) durimg fire conditions to the total moment capacity at temperature (M_t). Comparison of the capacity ratios depicted in Figures 7.13 through 7.22 versus those in Figures 7.8 through 7.12 indicates that the effect of thrust contributes significantly to the capacity of the slabs at temperature.

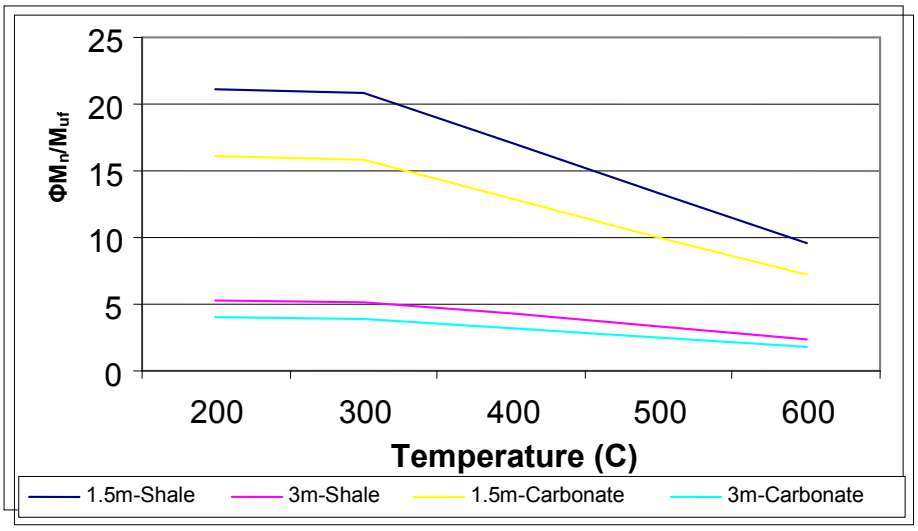

Figure 7.13: Ratio of ϕM_n to M_{uf} for 100mm Restrained Slabs

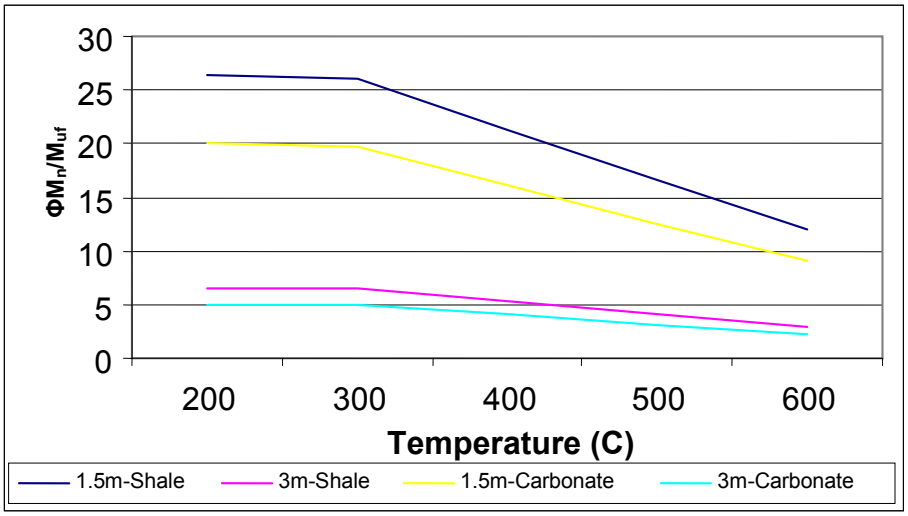

Figure 7.14: Ratio of ϕM_n to M_{uf} for 125mm Restrained Slabs

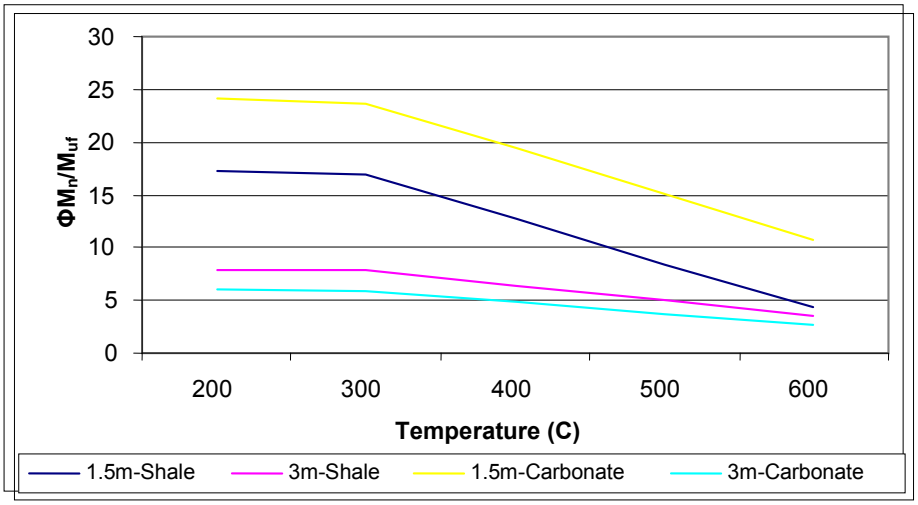

Figure 7.15: Ratio of ϕM_n to M_{uf} for 150mm Restrained Slabs

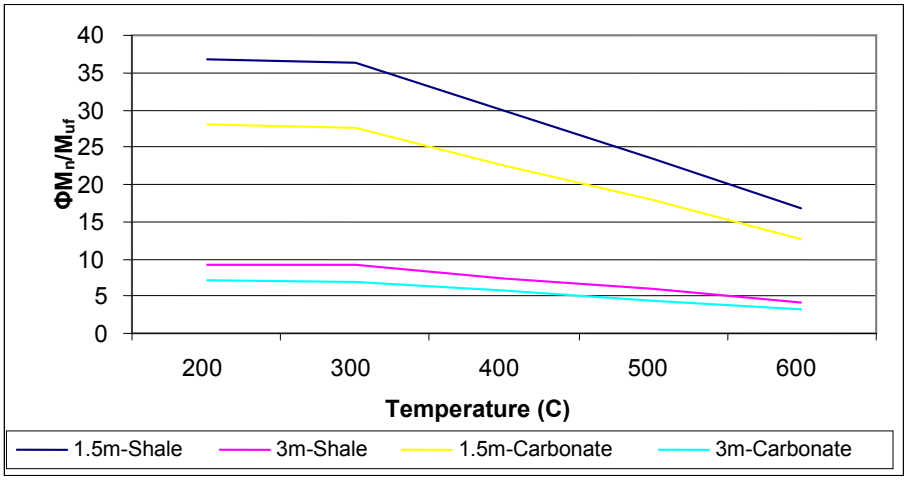

Figure 7.16: Ratio of ϕM_n to M_{uf} for 175mm Restrained Slabs

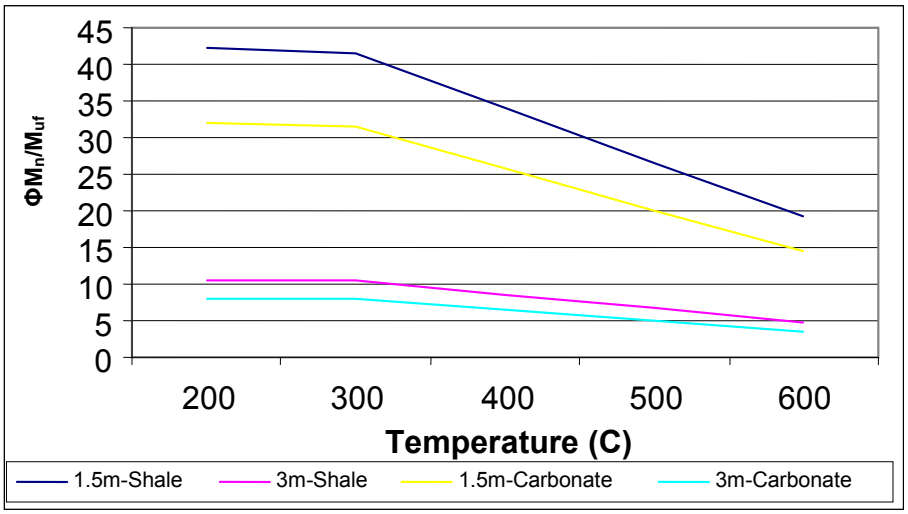

Figure 7.17: Ratio of ϕM_n to M_{uf} for 200mm Restrained Slabs

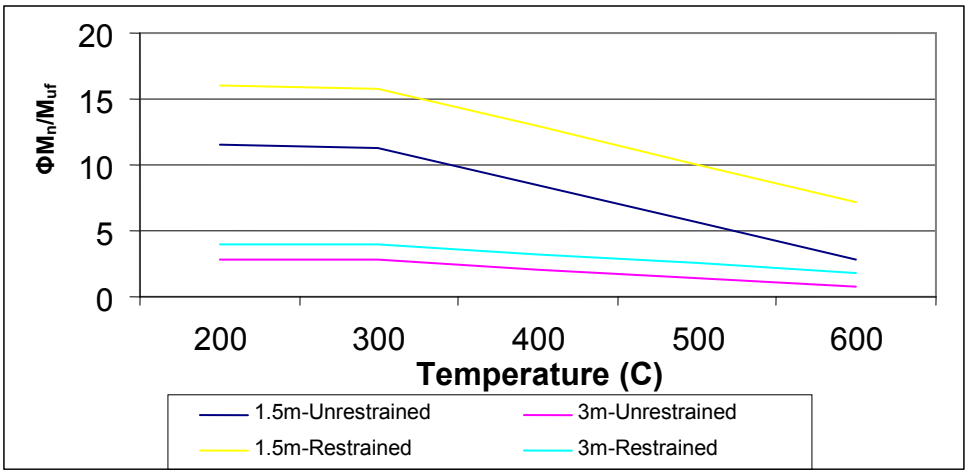

Figure 7.18: Ratio of ϕM_n to M_{uf} for 100mm Carbonate Slabs

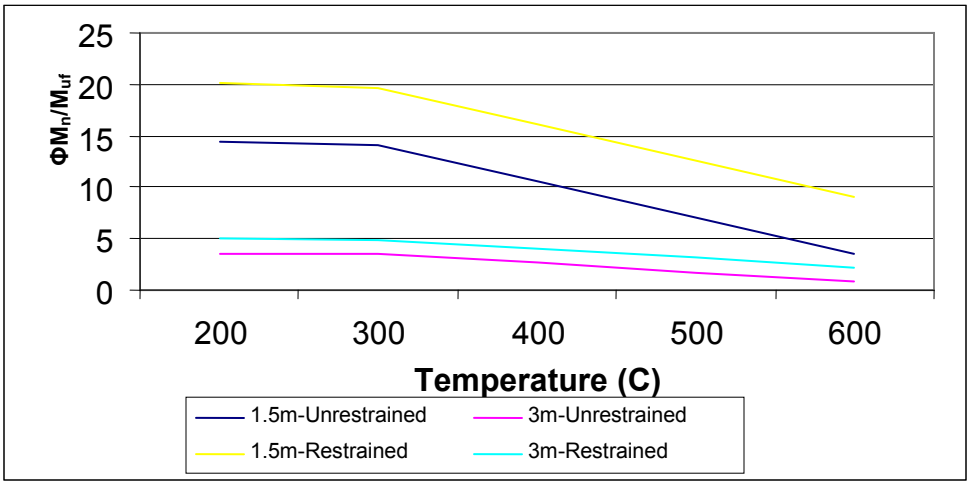

Figure 7.19: Ratio of ϕM_n to M_{uf} for 125mm Carbonate Slabs

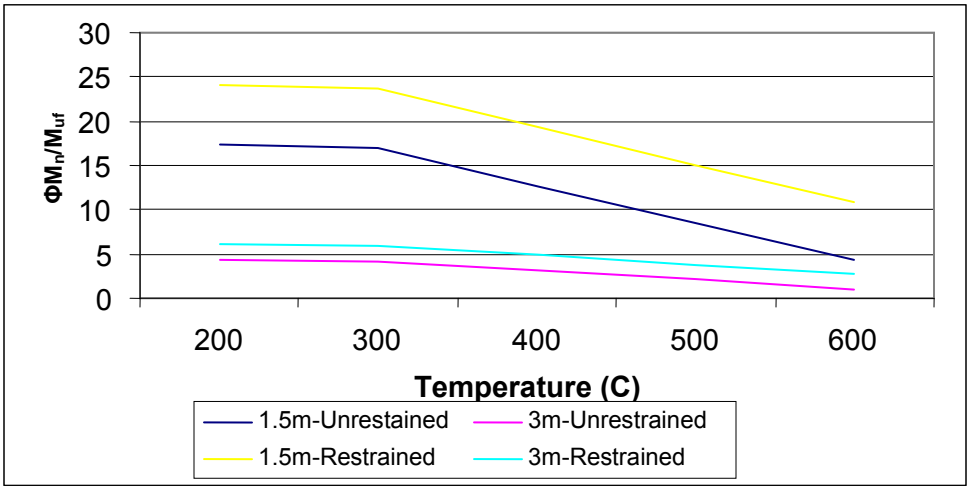

Figure 7.20: Ratio of ϕM_n to M_{uf} for 150mm Carbonate Slabs

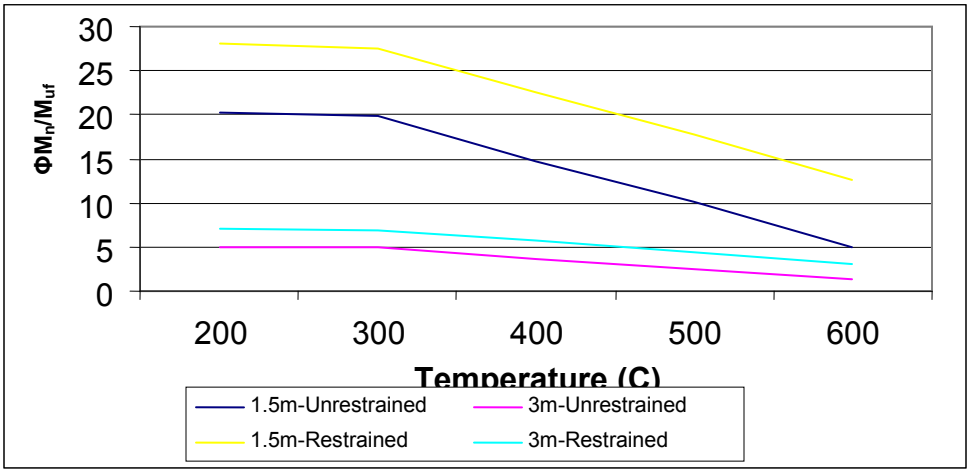

Figure 7.21: Ratio of ϕM_n to M_{uf} for 175mm Carbonate Slabs

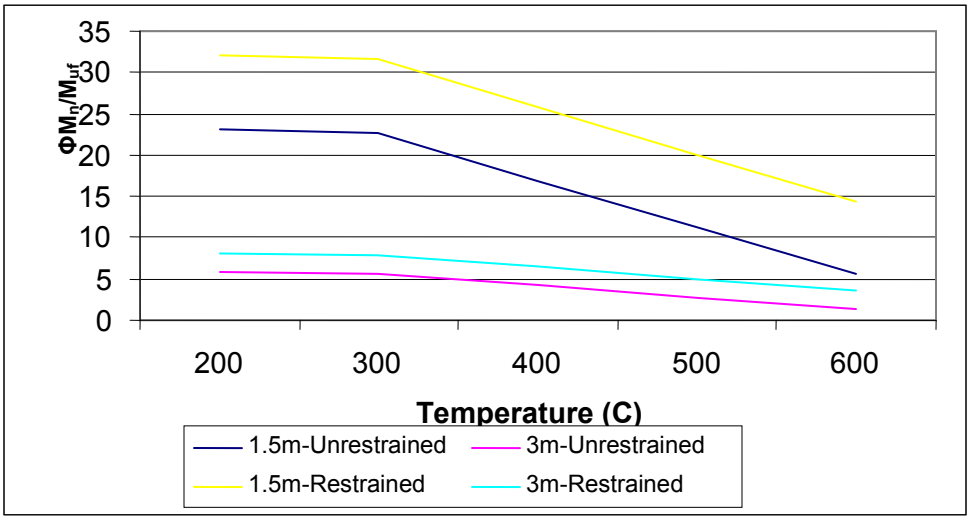

Figure 7.22: Ratio of ϕM_n to M_{uf} for 200mm Carbonate Slabs

8 Conclusions

In the United States design for fire safety follows a prescriptive code-based approach. Building codes detail the types of construction materials, assemblies, and fire suppression systems that are required for various building types. This prescriptive method has prevented structural engineers from exposure to performance-based design approaches for fire safety.

The goal of this thesis is to contribute to bridging the gap between the fire and structural engineering communities by providing structural engineers with a simplified design tool to assess the performance of reinforced concrete slabs during fire conditions. Several analyses were performed using the Excel spreadsheet application developed in this thesis. The results were compared with published test data and finite element software simulations to determine the tools accuracy in assessing the fire performance of reinforced concrete slabs. The overall conclusions are discussed as well as other observations made during the development of the model.

8.1 State of the Literature

From a thorough investigation of the literature it was determined that in addressing the issue of structural design for fire safety the United States is well behind many parts of the world. In the United States the PCA conducted a series of tests in the mid-50's to early-70's on the fire performance of concrete; however, research on concrete performance has been nearly at a standstill since the 1970's. Many countries are conducting state-of-the-art research on concrete fire performance while the United States seems to be falling farther behind. In Canada the fire

performance of high-strength concrete is being vigorously explored. Researches in the United Kingdom are continuing to work on the fire performance of composite structures while making use of data and information obtained from the Cardington tests. Many universities across the world are addressing the issue of concrete performance during fire conditions, where it appears from the literature that none are in the United States. A more conscious effort needs to be made in the United States for establishing methods of structural design for fire conditions.

8.2 Capabilities of Spreadsheet Application

The spreadsheet application was found to produce conservative temperature values in the positive reinforcement section of slabs for all types of aggregates when exposed to ISO 834 conditions based on comparison with published test data. It should be no different for the design fires especially since the TAS analyses agreed with the proposed Excel tool when evaluating the temperature in the reinforcing region. This means the tool would conservatively predict the capacities of slabs in fire conditions. It can be safely utilized as a design aid for a performance-based method for structural design of reinforced concrete slabs in fire conditions.

For the unexposed face, the predicted slab temperatures did not coincide with test data until 3 hours of exposure to standard fire conditions. When the time step for the analyses was reduced the temperatures on the unexposed face were somewhat closer to those of the test data but there still existed a large discrepancy during the initial stages of fire exposure. It was concluded that the proposed Excel tool does not accurately calculate temperatures for the unexposed face of slabs so it cannot be used to assess the failure condition for when the unexposed face reaches 140ºC.

Temperature distribution obtained from the use of various aggregates all demonstrated agreement with published test data with the exception of siliceous. It was found that temperatures for the unexposed face of siliceous slabs were not higher than those for carbonate until about two hours of exposure. According to test data siliceous slabs should remain at higher temperatures than those for carbonate for the entirety of any particular fire exposure. Alternative data for the thermal properties of siliceous concrete can produce desired results because if the specific heat capacity is slightly reduced the results resemble those of published data in terms of its performance in relation to carbonate.

8.3 Modeling Concrete in Fire Conditions with TAS

The modeling of concrete in fire conditions with TAS produced mixed results. Temperatures for the unexposed face of slabs presented in published test data could not be reproduced; however, the TAS results did show a consistent relationship with results from the proposed Excel tool for standard fires. Also temperatures near the exposed face were consistent with the Excel tool which means it also conservatively predicts temperatures in that region. The trouble is that each type of aggregate for a particular fire condition requires a unique analysis with coefficients and variables being adjusted accordingly. This leads to results that cannot be replicated and serve more as analysis on a case by case basis.

8.4 Recommendations for Future Work

- Concrete undergoes a phase change once it reaches 100C because it is composed of water which begins to boil. The effects of this occurrence on temperature distributions is not captured in the model proposed in this thesis. If a phase change function were incorporated the model would better simulate the fire performance of concrete.

- One limitation of the proposed model is its accuracy in predicting temperatures for the unexposed face. If analyses were done using extremely small time steps, the predicted temperature distributions may no longer lag behind the test data and results for the unexposed face may be accurate. Also, the effects of alternative boundary conditions on he unexposed face temperature could be examined.

- It would be interesting to see if the one dimensional model could be applied to the two- and three-dimensional study of concrete elements. If the temperature distributions were applied to multiple sides of an element exposed to fire such as a column it would be interesting to explore the fit of predicted temperature distributions with test data.

- A detailed capacity analysis of concrete slabs in fire conditions could be performed by investigating the effects of different live loads. This would provide information on the time to collapse for a particular slab design and design fire

- In Lie (1992) various numerical methods for assessing the fire performance of reinforced concrete elements are presented. These numerical procedures are similar to those applied in the spreadsheet application proposed in this thesis. It may be possible for these equations to be implemented in Excel so the fire performance of different types of concrete elements could be examined in a similar fashion to that presented for slabs.

.

9 Bibliography

Abrams, M. S. (1973). Compressive strength of concrete at temperatures to 1,600 F (RD016.01T), Portland Cement Association. Authorized reprint from copyrighted American Concrete Institute Special Publication SP-25.

Abrams, M. S., & Gustaferro, A. H. (1968). Fire endurance of concrete slabs as influenced by thickness, aggregate type, and moisture: Journal of the PCA Research and Development Laboratories. 10(2), 9-24.

American Society of Civil Engineers. (2006). Civil Engineering Database.

Anderberg, A. (1972). Fire-exposed hyperstatic concrete structures: an experimental and theoretical study. (Technical Report LUND. SP: 55-17). Sweden: LUND Institute of Technology.

Anderberg, Y., & Nils, E. F. (1982) Fire resistance of concrete structures (Technical Report LUTVDG/(TVBB-3009)). Sweden: LUND Institute of Technology.

Associated Factory Mutual Fire Insurance Companies, The National Board of Fire Underwriters, & Bureau of Standard, Department of Commerce. (1918). Fire Tests of Building Columns. Chicago, Illinois: Underwriters' Laboratories.

Benedetti, A. (1998). On the ultrasonic pulse propagation into fire damaged concrete. ACI Structural Journal. 95(3), 259-271.

Buchanan, A. H. (2001). Structural Design for Fire Safety. Chichester: John Wiley & Sons Ltd.

Bushev, V. P., Pchelintsev, V. A., Fedorenko, V. S., & Yakovlev, A. I. (1970). Fire Resistance of Buildings. Moscow: Construction Literature Publishers

Concrete Reinforcing Steel Institute. (1980). Reinforced Concrete Fire Resistance. Chicago, IL: Concrete Reinforcing Steel Institute

Cooper, L. Y., Franssen, J-M.. (1999). A basis for using fire modeling with 1-D thermal analyses of partitions to simulate 2-D and 3-D structural performance in real fires. Fire Safety Journal. 33, 115-128.

Cruz, C. R. (1962). Elastic properties of concrete at high temperatures. Reprinted from the: Journal of the PCA Research and Development Laboratories. 4(2), 24-32.

Cruz, C. R. (1966). An optical method for determining the elastic constants of concrete. Reprinted from the: Journal of the PCA Research and Development Laboratories. 8(1), 37-45.

Ellingwood, B., & Shaver, J. (1979). Fire effects on reinforced concrete members (Technical Note 985). Washington, D. C.: National Bureau of Standards.

Elsevier B.V. (2006). ScienceDirect.

Harmathy, T. Z. (1979). Design to cope with fully developed fires (DBR Paper No. 854). Ottawa: National Research Council of Canada.

Hutchens, G. J., & Gupta, N. K. (2000). A spreadsheet program for steady-state temperature distributions (Report WSRC-TR-2000-00132). Aiken, South Carolina: Westinghouse Savannah River Company.

Lie, T. T. (1972). Fire and Buildings. London: Applied Science Publishers Ltd.

Lie, T. T. (Eds.) (1992). Structural Fire Protection. (Technical Report No. 78). New York: American Society of Civil Engineers.

Malhotra, H. L. (1982). Design of Fire-Resisting Structures. Bishopbriggs and Glasgow: Surrey University Press.

Munukutla, V. R., Buchanan, A. H., & Carr, A. J. (1989). Modelling fire performance of concrete walls (Research Report No. 89/5). Christchurch, New Zealand: Department of Civil Engineering, University of Canterbury.

Narang, V. A. (2005). Heat Transfer in Steel Structures. (Masters Thesis). Worcester, Massachusetts: Department of Civil Engineering, Worcester Polytechnic Institute.

Swedish Institute of Steel Construction. (1976). Fire Engineering Design of Steel Construction. Publication 50, Stockholm, Sweden.

Wade, C. (1991). Fire engineering design of reinforced and prestressed concrete elements (Study Report No. 33). Judgeford: BRANZ, The Resource Centre for Building Excellence.

Wade, C. (1992). Fire resistance of New Zealand concretes (Study Report No. 40). Judgeford: BRANZ, The Resource Centre for Building Excellence.

Wade, C. (1991). Method for fire engineering design of structural concrete beams and floor systems (Technical Recommendation No. 8). Judgeford: BRANZ, The Resource Centre for Building Excellence.

Wang Y.C. Steel And Composite Structures – Behavior and Design for Fire Safety. Spon Press, 2002.

www.harvardthermal.com - TAS (Thermal Analysis Software)

Yakovlev, A. I. (1980). Basic Principles of Calculations of Building Structures' Fire Resistance Limits. (Final Report). U.S. Department of Commerce: National Bureau of Standards.

Appendices

A. Annotated Bibliography

1. Cooke, G. M. E. (2001). Behaviour of precast concrete floor slabs exposed to standardised fires. Fire Safety Journal. 36, 459-475.

Examines the fire behavior of axially unrestrained, simply supported, precast concrete floor slabs. Seven fire tests on pairs of precast concrete slabs were made in a standard fire resistance floor test furnace and were designed to determine the unrestrained mid-span deflection and axial deflections of the slab ends at mid depth.

2. Gillie, M., Usmani, A., & Rotter, M. (2004). Bending membrane action in concrete slabs. Fire and Materials. 28, 139-157.

Uses the computer program FEAST to obtain a detailed understanding of the strength of composite floor slabs in fire conditions. The Cardington slab will be presented in two ways. Firstly, the slab will be analyzed under conditions of pure membrane strain and of pure bending. Subsequently, the force-moment interaction diagrams of the slab will be presented. Explores
the effects of heating the slab uniformly, heating it with a linear thermal gradient, and heating it with the non-linear thermal gradients observed during the Cardington tests. Then the implications of the results for structures designed to resist fire will be considered.

3. Huang, Z., Burgess, I., Plank, R., & Bailey, C. (2004). Comparison of BRE simple design method for composite floor slabs in fire with non-linear FE modeling. Fire and Materials. 28, 127-138.

The computer software VULCAN is used to model the behavior of composite floor slabs in fire in order to check the applicability and conservatism of the simple design method developed by the BRE tests to calculate the enhanced load capacity due to membrane action of composite flooring systems subject to fire. Different temperature distributions are used across the thickness of the slab to investigate the influence of thermal curvature on structural behavior. The effect of edge support conditions is also analyzed. A series of analyses has been performed, based on different patterns of fire protection to the downstand steel beams. The influence of the steel reinforcement on the structural behavior has been investigated.

4. Huang, Z., Burgess, I. W., & Plank, R. J. (2000). Effective stiffness modeling of composite concrete slabs in fire. Engineering Structures. 22, 1133-1144.

An effective-stiffness concept is used for the modeling of the intact plain concrete of metal-deck composite slabs, including the ribbed lower part. Three Standard Fire tests on composite slabs and one full-scale natural fire test at Cardington are modeled in this paper to validate the formulation. Comparisons have been made with the previous layered procedure to investigate the influence of the ribs on the structural behavior.

5. Lim, L., & Wade, C. (2002, September). Experimental fire tests of two-way concrete slabs. (Fire Engineering Research Report 02/12). Porirua City, New Zealand: BRANZ Limited, University of Canterbury.

Describes the fire resistance tests of six concrete slabs using the BRANZ fire resistance furnace. The verification of the current analytical design methods by Bailey (2001) and Clifton et al (2001) and the SAFIR finite element program are presented by Lim (2003). The slabs were simply supported on all four sides above the furnace and were horizontally unrestrained. The slabs were heated on the underside with the furnace gas time temperature following the prescribed in AS/NZS1530.4 (similar to ISO 834), while subjected to a constant uniformly distributed load. The floor slabs consisted of three reinforced concrete plain flat slabs and three different proprietary composite steel-concrete slabs. The opening of the

furnace measured 3.0m by 4.0m and the slabs were constructed as 3.3m wide by 4.3m long to allow the edges of the slab to be supported over the furnace opening.
Different types of reinforcing mesh were used in the different slabs to determine the steel content required for crack control to prevent integrity failure. The performance of hard-drawn reinforcing mesh at elevated temperatures and the effect of the bar spacing of the mesh on the deformation capacity of the slabs were assessed.

6. Kodur, V. K. R., Williams, B. K., Green, M. F., & Bisby, L. A. (2005, March). Fire endurance experiments on FRP-strengthened reinforced concrete slabs and beam-slabs assemblies. (Research Report No. 175). Canada: Fire Research Program: Institute for Research in Construction, National Research Council Canada.

As part of this effort, fire endurance experiments were carried out on two full-scale FRP-strengthened reinforced concrete beam-slab assemblies and two mini FRP-strengthened reinforced concrete slabs. The results of these experiments are presented in this report. The main objective of the experiments was to investigate the behavior of FRP-strengthened reinforced concrete slabs and beam-slab assemblies under exposure to the standard fire.

7. Lamont, S., Usmani, A. S., & Drysdale, D. D. (2001). Heat transfer analysis of the composite slab in the Cardington frame fire tests. Fire Safety Journal. 36, 815-839.

HADAPT is used to model the temperature rise in the slab for Tests 1–3 of the British Steel Cardington Tests. The temperature profiles through the slab, measured in these tests, have been used to substantiate the heat transfer model. This improved our understanding of the process, and the verified model was then applied to the fourth test.

8. Lim, L., Buchanan, A., Moss, P. J., & Franssen, J. M. (2004). Numerical modeling of two-way reinforced concrete slabs in fire. Engineering Structures. 26, 1081-1091.

Describes the computer analysis of simply supported two-way slabs in fire conditions using a special purpose finite-element program, SAFIR. The analysis was carried out to validate the performance of the concrete shell element in the SAFIR program by comparing the output with the results on several fire tests of two-way slabs.

9. Lim, L., Buchanan, A. H., & Moss, P. J. (2004). Restraint of fire-exposed concrete floor systems. Fire and Materials. 28, 95-125.

Describes the numerical analysis of single span one-way concrete floor slabs exposed to fire, with varying levels of axial restraint at the supports. Analysis of the slabs was carried out with the SAFIR.

10. Sanad, A.M., Lamont, S., Usmani, A. S., & Rotter, J. M. (2000). Structural behavior in fire compartment under different heating regimes - Part 1 (slab thermal gradients). Fire Safety Journal. 35, 99-116.

Presents details of the model used before presenting the results and their interpretation for the case of applying different thermal gradients to the concrete slab while maintaining the average temperature increase over the slab depth equal to a fixed reference value. The second part presents the results and interpretations of applying different average temperature increases and maintaining the gradients at reference value.

11. Bailey, C. G., White, D. S., & Moore, D. B. (2000). The tensile membrane action of unrestrained composite slabs simulated under fire conditions. Engineering Structures. 22, 1583-1595.

Test on a 9.5 m x 6.5 m composite slab to investigate if tensile membrane action can occur at both elevated temperatures and large displacements by conducting a test at ambient temperature. Steel decking was removed from slab and loaded till failure.

12. Kodur, V. K .R., Wang, T. C., Cheng, F. P., & Sultan, M. A. (2002, June). A model for evaluating the fire resistance of high performance concrete columns. Paper presented at the Seventh International Association of Fire Safety Science Symposium, Worcester, MA.

A numerical model in the form of a computer program, for evaluating the fire resistance of high performance concrete (HPC) columns, is presented. Results of experiments are used to trace the structural behavior of HPC concrete columns at elevated temperatures. The validity of the numerical model used in the program is established by comparing the predictions from the computer program with results from full-scale fire resistance tests.

13. Wade, C. A., Cowles, G. S., Potter, R. J., Sanders, P. (1997, May). Concrete blade columns in fire. Paper presented at the Concrete 97 Conference, Adelaide, Australia.

Use of a computer model to calculate the thermal and structural response of reinforced concrete columns under simulated standard fire conditions. Results were analyzed by attempting to fit a conservative equation to the computer simulation results using a multiple linear regression technique. The equation was intended to be suitable for inclusion in a building control document for determining the fire resistance of reinforced concrete columns.

14. Aldea, C. M., Franssen, J. M., & Dotreppe, J. C. (1997, February). Fire test on normal and high-strength reinforced concrete columns. Paper presented at the International Workshop on Fire Performance of High-Strength Concrete, Gaithersburg, MD.

Quantify the parameters influencing fire spalling of normal and high-strength concrete in order to provide recommendations for fire safe constructions. Experiments were performed and numerical simulations were planned to compare results. Six short reinforced concrete columns were studied in fire conditions.

15. Bisby, L, Kodur, V, and Green, M. (2004, May). Modelling the fire behaviour of frp-strengthened reinforced concrete columns. Paper presented at the meeting of the Third International Workshop: Structures in Fire, Ottawa.

Full-scale fire tests have been conducted on loaded FRP-wrapped and insulated circular RC columns, and numerical models have been developed to simulate their behavior in fire. This paper presents details of the numerical models that have been developed to date, and verifies these models against test data.

16. Ali, F., Nadjai, A., Silcock, G., & Abu-Tair, A. (2004). Outcomes of a major research on fire resistance of concrete columns. Fire Safety Journal. 39, 433-445.

Discusses the outcomes of a major research program that investigated the performance of high and normal strength concrete columns under fire. The research focused on the explosive spalling of concrete during fire. The recorded measurements of axial displacements, heating rates, and generated restraint forces are presented and a parametric analysis of interaction between the factors is also included.

17. Abbasi, H., & Hogg, P. J. A model for predicting the properties of the constituents of a glass fibre rebar reinforced concrete beam at elevated temperatures simulating a fire test (Paper). England: Queen Mary University of London, Department of Materials.

Develop a general method of predicting the properties of the constituent elements of a composite rebar reinforced concrete beam during a fire test. The constituents in question are the FRP rebar and the concrete itself.

18. Moss, P. J., Buchanan, A. H., Seputro, J., Wastney, C., & Welsh, R. (2004). Effect of support conditions on the fire behaviour of steel and composite beams. Fire and Materials. 28, 159-175.

Describes the structural performance of unprotected single span steel and composite steel-concrete beams exposed to uniformly increasing temperatures on three sides, as well as the ISO 834 fire. The beams were analyzed using SAFIR with four different support conditions: simply-supported (pin-roller supported), pin supported at each end, fixed and slide supported, or fixed at each end.

19. Abbasi, A., & Hogg, P. J. Fire testing of concrete beams with fibre reinforced plastic rebar (Paper). England: Queen Mary University of London, Department of Materials.

Glass fiber reinforced concrete beams using continuous fiber bars as main reinforcements were subjected to heating under load tests. The evaluation of flexural behavior and to choose a sustained load for the fire test were examined. The objective of the study was to determine the fire resistance of GFRP reinforced concrete beams experimentally and to validate the predictive models for fire resistance.

20. Ongah, R., Mendis, P. A., & Sanjayan, J. G. Fire performance of high strength concrete walls (Paper). Victoria, Australia: The University of Melbourne & Monash University.

Numerical procedure for simulating the thermal and structural behavior of concrete walls in fire with the incorporation of HSC.

21. Lim, L., Buchanan, A., Moss, P., & Franssen, J. M. (2004). Computer modeling of restrained reinforced concrete slabs in fire conditions. Journal of Structural Engineering. 130(12), 1964-1971.

The objective of this research was to investigate the effects of axial restraint on the behavior of single span one-way flat slabs in fire conditions. The scope of this study covers the behavior of pin-supported slabs and slabs with rotational restraint at the end supports. This study was carried out using *SAFIR*.

22. Bailey, C. G., & Moore, D. B. (2000). The structural behaviour of steel frames with composite floorslabs subject to fire: part 1: theory. The Structural Engineer. 78(11), 19-27.

Develops a new design method for calculating the performance of steel framed buildings with composite flooring subject to fire (based off of Cardington work).

23. Bailey, C. G., & Moore, D. B. (2000). The structural behaviour of steel frames with composite floorslabs subject to fire: part 2: design. The Structural Engineer. 78(11), 28-33.

Comparison is made between amount of fire protection required using a new approach and predictions according to current UK design methods for composite floor slabs. New approach is less conservative leaving many beams unprotected due to the recognitions of a complete flooring system and other design options.

24. Talamona, D., Nadjai, A., & Ali, F. (2003). Determination of the bending moment capacity of rc beams at ambient and elevated temperatures. Journal of Applied Fire Science. 11(1), 75-90.

A program using Visual Basic and the method of slices has been developed to calculate the ultimate bending capacity of reinforced concrete beams and slabs subjected to high and ambient temperature. The material properties used in this model are defined in the Eurocode 2: concrete and steel at room temperature and under fire conditions

25. Frannsen, J. M., & Dotreppe, J. C. (2003). Fire tests and calculation methods for circular concrete columns. Fire Technology. 39, 89-97.

Circular columns were subjected to the standard ISO 834 fire in a test furnace to examine their behavior at elevated temperatures. Two alternative simple design methods were developed.

26. Bratina, S., Cas, B., Saje, M., & Planinc, I. (2005). Numerical modeling of behavior of reinforced concrete columns in fire and comparison with Eurocode 2. International Journal of Solids and Structures. 42, 5715-5733.

Describes a two-step finite element formulation for the thermo-mechanical non-linear analysis of the behavior of reinforced concrete columns in fire. In the first step, the distributions of the temperature over the cross-section during fire are determined. In the next step, the mechanical analysis is made in which these distributions are used as the temperature loads. The results are compared with the measurements of the full-scale test on columns in fire and with the results of the European building code EC 2.

27. El-Hawary, M. M., Ragab, A. M., El-Azim, A. A., & Elibiari, S. (1997). Effect of fire on shear behaviour of r.c. beams. Computers & Structures. 65(2), 281-287.

Examines the effect of fire exposure time and concrete cover thickness on the behaviour of R.C. beams subjected to fire in shear zone and cooled by water. Eight reinforced concrete beams were subjected to a fire of 650°C for different periods of time. Beams were tested by applying two transverse loads incrementally and Strains and deformations were measured at each load increment.

28. Tan, K. H., & Yao. Y. (2003). Fire resistance of four-face heated reinforced concrete columns. Journal of Structural Enfineering. 129(9), 1220-1229.

Develops a simple and rational method to predict the fire resistance of RC columns subjected to four-face heating. The effects of elevated temperature on material deterioration with regard to the strength and stability of the columns are quantified. Both uniaxial and biaxial bending of columns is considered. The computer code *SAFIR* was used to analyze reported experimental results and to simulate the deformation response.

29. Ahmed, G. N., & Hurst, J. P. (1999). Modeling pore pressure, moisture, and temperature in high-strength concrete columns exposed to fire. Fire Technology. 35(3), 232-262.

Presents a mathematical and computational model which simulates the two-dimensional thermal response of high-strength concrete columns subjected to fire. Models predictions are validated against ASTM-E199 fire test data.

30. Tan, K. H., & Yao, Y. (2004). Fire resistance of reinforced concrete columns subjected to 1-, 2-, and 3-face heating. Journal of Structural Engineering. 130(11), 1820-1828.

Develops a simple and rational method to predict the fire resistance of RC columns subjected to 1-, 2-, and 3-face heating. The effects of elevated temperature on material deterioration with regard to the strength and stability of columns are quantified. Furthermore, the shift of neutral axis due to nonsymmetric heating is predicted in the proposed method. For columns under 1- or 3-face heating, only uniaxial bending needs to be considered, but for 2-face heating, the

effect of biaxial bending is taken into account. *SAFIR* was used to benchmark the proposed simplified calculation method.

31. Kodur, V. K. R., & Bisby, L. A. (2005). Evaluation of fire endurance of concrete slabs reinforced with fiber-reinforced polymer bars. Journal of Structural Engineering. 131(1), 34-43.

Discusses the various factors that differentiate the performance of FRP-reinforced concrete slabs at elevated temperatures with steel reinforced slabs. Numerical model for evaluating the fire resistance of FRP-reinforced concrete slabs based on a thermal analysis, is presented and validated against test data, and the application of the numerical procedure for modeling the fire behavior of FRP–RC slabs is illustrated through parametric studies.

32. Cai, J., Burgess, I., & Plank, R. A (2002). Generalised steel/reinforced concrete beam-column element model for fire conditions (Research Report DCSE/02/F/2). University of Sheffield, United Kingdom.

Presents a beam-column element, which can model reinforced concrete sections and steel sections of different shapes for three-dimensional composite structures at ambient and high temperatures. Method includes both geometrical and material non-linearities and considers unloading for steel, cracking and crushing for concrete, and thermal expansion and degradation of material for both with elevated temperatures. Formulation of the method has been validated by VULCAN in comparison with existing theoretical and experimental results.

33. Khoury, G. A. (2000). Effect of fire on concrete and concrete structures. Progress in Structural Engineering and Materials. 2, 429-447.

Presents a brief outline of the effect of fire on both concrete material and concrete structures with emphasis being placed upon; deterioration in mechanical properties of concrete and especially of high performance and ultra-high-performance concretes in fire; (b) explosive spalling and the use of polypropylene fibres; (c) the development of finite element structural analysis models capable of predicting pore pressures and spalling; and (d) fires in tunnels. The basic principles of fire engineering are also presented.

34. Shi, X., Tan, T. H., Tan, K. H., & Guo, Z. (2002). Effect of force-temperature paths on behaviors of reinforced concrete flexural members. Journal of Structural Engineering. 128(3), 365-373

Force-temperature paths are expressed simply by the path of constant forces but subjected to elevated temperature FT path, and the path of constant temperature but subjected to applying forces TF path. A total of 13 beam specimens subjected to two such basic paths using a closed-loop servo-controlled 2000kN hydraulic test machine equipped with an electric furnace. The results show that the fire resistance for the FT path is different from that for the TF path.

35. Elghazouli, A. Y., & Izzuddin, B. A. (2004). Failure of lightly reinforced concrete members under fire. II: parametric studies and design considerations. Journal of Structural Engineering. 130(1), 18-31.

Deals with the behavior of lightly reinforced concrete members under fire conditions, focusing on the failure state associated with rupture of the reinforcement The analytical model proposed in the companion paper is utilized to perform a parametric investigation into the salient factors influencing the failure of lightly reinforced restrained members. A detailed account of the analytical results is given, and the relative importance of the main material and geometric parameters is illustrated. It is shown that in addition to temperature effects, the bond characteristics, member length, and the steel material response have a direct and significant influence on failure.

36. Elghazouli, A. Y., & Izzuddin, B. A. (2004). Failure of lightly reinforced concrete members under fire. I: analytical modeling. Journal of Structural Engineering. 130(1), 3-17.

Deals with the failure of lightly reinforced concrete members under fire conditions, with particular emphasis given to the catenary action arising from axial restraint at the supports and the ensuing rupture of the reinforcement. A new analytical model is proposed for lightly reinforced members subject to axial restraint, which accounts for the compressive arch and tensile catenary stages, bond-slip, yielding, and rupture of the steel reinforcement as well as the effect of elevated temperature.

37. Concrete Reinforcing Steel Institute. Fire resistance of reinforced concrete buildings (Engineering Data Report Number 52).

General description of reinforced concrete fire resistance

38. Elghazouli, A. Y., Izzuddin, B. A., & Richardson, A. J. (2000). Numerical modelling of the structural fire behaviour of composite buildings. Fire Safety Journal 35, 279-297.

Describes numerical models constructed to simulate the response of composite steel/concrete building floors under fire conditions. Deals with two of the fire tests recently undertaken on a full-scale multi-storey building at Cardington, UK. The analysis is carried out using a structural analysis program, ADAPTIC, which accounts for both geometric and material nonlinearities, and which includes temperature-dependent constitutive models for steel and concrete materials. The approaches used to represent the various structural details are discussed, and the procedure employed for incorporating the experimentally measured temperature profiles and histories is outlined.

39. Wang, Y. C. (2005). Performance of steel–concrete composite structures in fire. Progress in Structural Engineering and Materials. 7, 86-102.

Review recent studies on the behaviour of steel–concrete composite structures in fire, including an assessment of research investigations and their implications on fire-resistant design of composite structures. The paper focuses on the three main parts of composite structure: floor systems, columns and joints.

40. Rigberth, J. (2000). Simplified design of fire exposed concrete beams and columns (Report 5063). Sweden: LUND, Lunds University.

The 500 degree Celsius (BKR) and Herts's (Eurocode) method for calculating strength reduction of fire-exposed concrete were evaluated against a finite element model (CONFIRE) to evaluate the bending capacity of beams and load-bearing capacity of columns.

41. Sanad, A. M., Lamont, S., Usmani, A. S., & Rotter, J. M. (2000). Structural behaviour in fire compartment under different heating regimes - Part 1 (slab thermal gradients). Fire Safety Journal 35, 99-116.

Discusses the structural response when subjected to different heating regimes obtained by changing the mean temperature and temperature gradient applied in the concrete slab of the composite floor slab system to a computer model (ABAQUS) of the British Steel restrained beam test.

42. Zha, X. X. (2003). Three-dimensional non-linear analysis of reinforced concrete members in fire. Building and Environment. 38, 297-307.

The behavior of reinforced concrete members such as columns and beams subjected to a fire are investigated by three-dimensional non-linear finite elements. The temperature distribution in the section of concrete member is calculated by Hertz's simplified method, which is then

input into the FE program (DYNA3D) for doing the time-dependent thermal stress analysis. The influence of main parameters on the behavior of concrete members subjected to a fire is analyzed.

43. Shi, X., Tan, T. H., Tan, K. H., & Guo, Z. (2004). Influence of concrete cover on fire resistance of reinforced concrete flexural members. Journal of Structural Engineering. 130(8), 1225-1232.

Six specimens with different concrete cover thickness were tested to investigate the influence of cover on the properties of reinforced concrete flexural members exposed to fire. The specimens were heated on their bottom and two lateral surfaces.

44. Sanders, P. T. Advances in fire design for reinforced concrete structures - moving to more rational design methods. Steel Reinforcement Institute of Australia.

Examines research work and development of design methods for the fire performance of reinforced concrete structures in the past five years (93-98)

45. Kodur, V., McGrath, R. (2003). Fire endurance of high strength concrete columns. Fire Technology. 39, 73-87.

Determine the behavior of HSC structural columns under standard building fire exposures, and to evaluate its fire endurance. Full scale fire endurance tests on HSC columns were conducted, and the results from these experiments are presented in this paper. The experimental program consisted of conducting fire resistance tests on six reinforced concrete column in furnace design for testing loaded columns

46. Cameron. N. J. K. (2003). The behaviour and design of composite floor systems in fire. Published doctoral dissertation, University of Edinburgh, Edinburgh.

Three-stage design method was developed to determine the load capacity of concrete floor slabs in fire. First the temperature distribution through the slab was calculated for the design fire. Then the deflection of the slab and resulting stress strain distributions in the steel reinforcement due to the thermal loads were calculated.

47. Ellingwood, B., & Lin, T. D. (1991). Flexure and shear behavior of concrete beams during fires. Journal of Structural Engineering. 117(2), 440-458.

Describes the results of six full-scale reinforced concrete beams exposed to fire tests. Four beams were exposed to the standard ASTM E119 fire and two to a short-duration high-intensity (SDHI). Mathematical models to predict thermal and structural response of concrete beams exposed to fires were developed.

48. Crozier, D. A., & Sanjayan, J. G. (2000). Tests on load-bearing slender reinforced concrete walls in fire. ACI Structural Journal. 97(2), 243-251.

Eighteen large-scale slender reinforced concrete walls were tested under standard fire conditions (furnace). The conditions included different height-to-thickness ratios, reinforcement covers, concrete strengths and mixture proportions, and varying levels of eccentric inplane load.

49. Sidibé, K., Duprat, F., Pinglot, M., & Bourret, B. (2000). Fire safety of reinforced concrete columns. ACI Structural Journal. 97(4), 642-647.

Involves the fire safety of reinforced concrete columns designed for stability. A Monte Carlo simulation technique assesses the probability of failure by accounting for the effect of temperature on statistical distributions. Model is based on the segment method, uses CESAR-LCPC finite element program for the thermal study and a specific program (Monte Carlo) for the structural behavior computing the instability load.

50. Dotreppe, J. C., Franssen, J. M., & Vanderzeypen, Y. (1999). Calculation method for design of reinforced concrete columns under fire conditions. ACI Structural Journal. 96(1), 9-18.

Develops a three-step formula for the design of reinforced concrete columns under fire conditions which has been validated using SAFIR. The first step consists of determining the plastic crushing load of the column at elevated temperature on the basis of numerical simulations. Second is determining the buckling coefficient for centrically loaded columns. The final step is the development of a nonlinear amplification term for eccentric loads.

51. Huang, Z., Burgess, I. W., & Plank, R. J. (1999). Nonlinear analysis of reinforced concrete slabs subjected to fire. ACI Structural Journal. 96(1), 127-135.

Describes a nonlinear layered finite element procedure for predicting the structural response of reinforced concrete slabs (composite) subject to fire. Procedure is based on the Mindlin/Reissner theory and an iterative, tangent stiffness method is employed and has now been programmed into VULCAN now that it has been verified versus a fire test.

52. Huang, Z. & Platten, A. (1997). Nonlinear finite element analysis of planar reinforced members subjected to fires. ACI Structural Journal. 94(3), 272-282.

Describes a nonlinear finite-element procedure (based on an iterative, secant stiffness formulation) for predicting the structural behavior of planar-reinforced concrete members subjected to fire. Considers the dimensional changes caused by temperature differentials, changes in mechanical properties of material with change in temperature, degradation of the element by cracking or crushing, and shrinkage and creep.

53. Terro, M. J. (1998). Numerical modeling of the behavior of concrete structures in fire. ACI Structural Journal. 95(2), 183-193.

Finite element thermal (TEMP) l and structural (STRUCT) computer programs were developed to predict the behavior of three-dimensional reinforced concrete structures in fire. First a nonlinear thermal analysis determines the temperature distribution history. Next the variations in the stiffness matrix due to changes in the material properties are calculated, and a static analysis is performed in time-steps until failure.

54. Benedetti, A. (1998). On the ultrasonic pulse propagation into fire damaged concrete. ACI Structural Journal. 95(3), 259-271.

Describes an identification technique (ultrasonic pulse propagation) capable of reconstructing the residual elastic modulus distribution in fire damaged concrete.

55. Meda, A., Gambarova, P. G., & Bonomi, M. (2002). High-performance concrete in fire-exposed reinforced concrete sections. ACI Structural Journal. 99(3), 277-287.

The behavior of eight HSC square sections subjected to an eccentric axial force are tested using different fire durations (Norm ISO 834). Thermal maps were evaluated by integrating the Fourier equation numerically by making use of FE code MAPPTEMP.

56. Tan, K. H., & Tang, C. Y. (2004). Interaction formula for reinforced concrete columns in fire conditions. ACI Structural Journal. 101(1), 19-28.

Uses the Rankine method to predict the fire resistance of reinforced concrete columns under fire conditions. Theoretical model is derived for both axially and eccentrically loaded columns and is validated against experimental test results.

57. Tsai, C. L., Chiang, C. H., Yang, C. C., & Chen, C. M. (2005). Tracking concrete strength under variable high temperature. ACI Structural Journal. 102(5), 322-329.

An algorithm based on the damage accumulation of concrete exposed to fire is developed to analyze concrete mechanical decay in a variable-temperature environment. It is validated against experimental testing.

58. Lie, T. T., & Celikkol, B. (1991). Method to calculate the fire resistance of circular reinforced concrete columns. ACI Materials Journal. 88(1), 84-91.

Describes a mathematical model to calculate the fire resistance of circular reinforced concrete columns (validated with experimental results). Model can be used for various parameters; load, column section, column length, concrete strength, percentage of reinforcing steel, and concrete types.

59. Haksever, A. (1981). Fire response of total systems in a local fire. Fire Safety Journal. 4(3), 141-146.

Presents a finite element technique (computer model) for the elastic-plastic analysis of two dimensional reinforced concrete structures and frame systems subjected to non-steady temperature conditions. The frame forces due to a local fire in a multistory framework have been studied.

60. Morley, P. D., & Royles, R. (1980). The influence of high temperature on the bond in reinforced concrete. Fire Safety Journal. 2(4), 243-255.

A summary of the strength of concrete and steel during and after exposure to elevated temperatures is made. Reviews procedures for testing bond at ambient temperatures. Discusses work that has been done on bond at high temperature and suggests its relevance to structural performance.

61. Purkiss, J. A., Claridge, S. L., & Durkin, P. S. (1989). Calibration of simple methods of calculating the fire safety of flexural reinforced concrete members. Fire Safety Journal.
15(3), 245-263.

Compares tabular methods of determining fire resistance and calculation methods for flexural members (one-way slabs) (BS 8110). Variation of temperature in the slab is taken from the FIP/CEB report

62. Kang, S., & Hong, S. (2004). Analytical method for the behaviour of a reinforced concrete flexural member at elevated temperatures. Fire and Materials. 28, 227-235.

An analytical method is proposed for the thermal behavior of a reinforced concrete flexural member (beam) subjected to fire. Analysis procedure is subdivided into two different steps; sectional analysis and member solution. Uniform sectional properties and temperature distribution through the longitudinal axis of the member are assumed. The proposed method takes into account the material deterioration, the material nonlinearity and nonlinear strain changes of concrete with temperature increase.

63. Ellingwood, B., & Shaver, J. R. (1980). Effects of fire on reinforced concrete members. Journal of the Structural Division. 106(11), 2151-2166.

Describes the application of an improved analysis procedure for reinforced concrete members in relation to the use of the ASTM E119 fire test. Develops fire exposure curves from fire load survey data and uses them to examine the structural behavior of various reinforced concrete members (beams and beam-slab) and compares them with ASTM E119 data. Analytical and numerical methods are used with the developed fire curves to predict the structural response of members.

64. Iwankiw, N. R. (1979). Thermal effects on load capacity of concrete slabs. Journal of the Structural Division. 105(7), 1417-1433.

Investigates the effects of high temperature on the ultimate strength capacity of two-way reinforced concrete rectangular slabs containing fully fixed edges along four sides. Yield line theory for determining the ultimate load-carrying capacity of reinforced concrete slabs was extended to account for high temperature effects. A finite element program (FASBUS) based on the analysis was written and validated.

65. Nizamudding, Z. (1979). Fire response of reinforced concrete slabs. Journal of the Structural Division. 105(8), 1653-1671.

Uses a nonlinear finite element method coupled with time-step integration to analyze the structural response of reinforced concrete slabs to fire. The slab is divided into triangular or rectangular finite elements, and each element is divided into several layers. A finite element program (FIRES-T3) was used to calculate temperature distribution histories and (FIRES-SL) is used to determine the structural response history.

66. Becker, J. M., & Bresler, B. (1977). Reinforced concrete frames in fire environments. Journal of the Structural Division. 103(1), 211-224.

Predicts the history of structural response in reinforced concrete elements (structures) exposed to fire. Deformations, stresses, cracking, crushing, and reductions in stiffness and strength in reinforced concrete elements are determined at small time intervals. Uses finite element software to do a two phase analysis; first thermal effects are calculated and then structural response. The software is based on numerical procedures.

67. Ellingwood, B., & Shaver, R. (1977). Reliability of rc beams subjected to fire. Journal of the Structural Division. 103(5), 1047-1059.

Describes the behavior of a simply supported reinforced concrete beam based on uncertain criteria that effect thermomechanical predictions and observations. Beam behavior based on deterministic parameters is outlined and is credibly is established. The variability in the observed behavior that can arise from uncertain criteria is illustrated and methods to implement them in design methods are examined based on the furnace testing of a beam.

68. Salse, E., & Lin, T. D. (1976). Structural fire resistance of concrete. Journal of the Structural Division. 102(1), 51-63.

Discusses the progress which has been made in calculating temperatures within concrete beams. Also, analyzes the conditions at failure during fire of continuous beams subjected to axial restraint (numerical methods).

69. Lin, T. D., & Abrams, M. S. (1983). Simulation of realistic thermal restraint during fire tests of floors and roofs. In M. Abrams (Eds.), Fire Safety of Concrete Structures (pp. 1-68). Detroit, MI: ACI.

Describes a multiple phase furnace test of concrete roof and floor systems (slabs). In phase the first phase a combination of 13 flat plates, flat plate with edge beams, and ribbed slabs were tested. The second phase made use of computer programs for heat flow calculations and stress analysis. These programs were used in conjunction with six floor slabs which were tested in a furnace. Results were compared. Finally four more slabs were tested to verify the results of the study and to develop methods of simulating realistic restraints in a fixed frame surface.

70. Dougill, J. W. (1983). Materials dominated aspects of design for structural fire resistance of concrete structures. In M. Abrams (Eds.), Fire Safety of Concrete Structures (pp. 151-176). Detroit, MI: ACI.

Rational design for fire resistance by examining the material behavior of concrete and reinforced concrete exposed to fire.

71. Copier, W. J. (1983). The spalling of normal weight and lightweight concrete exposed to fire. In M. Abrams (Eds.), Fire Safety of Concrete (pp. 219-236). Detroit, MI: ACI.

Investigates the influence of spalling on fire resistance.

72. Gustaferro, A. (1983) Experiences from evaluating fire-damaged concrete structures. In M. Abrams (Eds.), Fire Safety of Concrete (pp. 269-278). Detroit, MI: ACI.

Describes the evaluation (techniques) of structural damage caused by fires to reinforced, cast-in-place post tensioned and precast prestressed concrete.

73. Smith, L., & Placido, F. (1983). Thermoluminescence: A comparison with the residual strength of various concretes. In M. Abrams (Eds.), Fire Safety of Concrete (pp. 293-304). Detroit, MI: ACI.

Describes the thermoluminescence test and its success in examining post-fire damage to concrete.

74. Wade, C. (1991). Method for fire engineering design of structural concrete beams and floor systems (Technical Recommendation No. 8). Judgeford: BRANZ, The Resource Centre for Building Excellence.

Describes a design procedure for the calculation of fire resistance for reinforced or prestressed concrete beams and floor slabs.

75. Wade, C. (1991). Fire engineering design of reinforced and prestressed concrete elements (Study Report No. 33). Judgeford: BRANZ, The Resource Centre for Building Excellence.

Discusses design procedures such as selecting an appropriate design fire and predicting the thermal and structural response of a member. Explains design procedures for concrete slabs, beams, columns, and walls.

76. Ellingwood, B., & Shaver, J. (1979). Fire effects on reinforced concrete members (Technical Note 985). Washington, D. C.: National Bureau of Standards.

Thermal and structural response of reinforced concrete members with an analytical model are validated using experimental data. Conducts a thermal analysis on a concrete section using various fire curves and compares it with ASTM fire test data. Continues on to validate use of different fire curve by comparing results of a 40 foot beam and beam slab interaction with the ASTM E199 fire curve.

77. IBBC, Instituut TNO voor Bouwmaterialen en Bouwconstructies (1985). Numerical analyses of steel and concrete structures in fire conditions (Report no. BI-85-23/68.8.2002). Rijswijk.

Fire test on a concrete column with different end-restraints and loading conditions. Compares results with a finite element program.

78. Anderberg, Y., & Nils, E. F. (1982) Fire resistance of concrete structures (Technical Report LUTVDG/(TVBB-3009)). Sweden: LUND Institute of Technology.

Predicts structural behavior and fire resistance of a plate strip. Uses two computer programs to calculate the thermal and structural response.

79. Lin, T. D., Zwiers, R. I., Shirley, S. T., & Burg, R. G. (1989). Fire test of slab with epoxy-coated bars. ACI Structural Journal. 86(2), 156-162.

Presents results of a fire test conducted on a two way reinforced concrete flat slab with epoxy-coated bars. The slab was subjected to a uniform load and the ASTM E119 fire test.

80. Lie, T. T., & Irwin, R. J. (1993). Method to calculate the fire resistance of reinforced concrete columns with rectangular cross section. ACI Structural Journal. 90(1), 52-60.

Describes a method for the calculation of fire resistance for reinforced concrete columns with rectangular cross sections. Method is based on three furnace tests which were conducted on concrete columns and are explained in the paper.

81. Lin, C., Chen, S., & Yang, C. (1995). Repair of fire-damaged reinforced concrete columns. ACI Structural Journal. 92(4), 406-411.

Analytical and experimental methods were used to investigate the behavior of reinforced concrete columns repaired after fire exposure. Eleven columns were exposed to fire and repaired using results from a thermal analysis. The columns were then loaded to determine their strength.

82. Ng, A. B., Mirza, M. S., & Lie, T. T. (1990). Response of direct models of reinforced concrete columns subjected to fire. ACI Structural Journal. 87(3), 313-325.

Experimental study of the complete response of scale sized reinforced concrete columns subjected to fire (furnace test) and axial loads.

83. Anderberg, A. (1972). Fire-exposed hyperstatic concrete structures: an experimental and theoretical study. (Technical Report LUND. SP: 55-17). Sweden: LUND Institute of Technology.

Presents analytical predictions for the thermal and mechanical behavior of reinforced concrete structures (plate strip) exposed to differentiated complete fire processes. The modeling of the fire response is done in two steps; the first is a heat flow analysis of the structure, the second is a structural analysis using two computer programs and the previously obtained heat flow analysis data. Model is compared with experimental data from various tests.

84. Concrete Reinforcing Steel Institute. (1980). Reinforced Concrete Fire Resistance. Chicago, IL: Concrete Reinforcing Steel Institute.

Analytical and rational methods for calculating the structural fire endurance of reinforced concrete elements are presented in detail along with example problems. Provides a more realistic prediction of the performance of a real structure in an actual fire than traditional fire ratings.

85. Cooper, L. Y., Franssen, J-M., & Lie, T. T. (1999). A basis for using fire modeling with 1-D thermal analyses of partitions to simulate 2-D and 3-D structural performance in real fires. Fire Safety Journal. 33, 115-128.

This report identifies partition designs for which the use of one-dimensional thermal analysis in fire modeling would lead to a successful evaluation of their thermal fire performance. It was determined that gypsum-panel/steel-stud or wood-stud wall systems, concrete block wall, and poured concrete slabs supported by steel beams have three-dimensional elements that have negligible heat transfer effects so a one-dimensional thermal analysis will produce

successful results when applied. Reinforced concrete beam/slab systems require a two-dimensional analysis because of heat transfer in the beams.

86. Wade, C. (1992). Fire resistance of New Zealand concretes (Study Report No. 40). Judgeford: BRANZ, The Resource Centre for Building Excellence.

Displays fire test (furnace) data for various concrete slabs. Shows mix designs and aggregate properties for the different slabs tested. .

87. Wade, C. (1993). Summary report on a finite element program for modeling the thermal response of building components exposed to fire (Study Report No. 51). Judgeford: BRANZ, The Resource Centre for Building Excellence.

Explains the finite element program NISA which can be used to model the temperatures of building components exposed to fire. Gives some examples of slabs and steel columns which were analyzed using the program. Contains excellent references.

88. Munukutla, V. R., Buchanan, A. H., & Carr, A. J. (1989). Modelling fire performance of concrete walls (Research Report No. 89/5). Christchurch, New Zealand: Department of Civil Engineering, University of Canterbury.

Develops a finite element program which displays the temperature distribution through a concrete wall. Program uses one-dimensional heat transfer. Surface temperatures on the exposed face were determined by 85% of the furnace temperature and the interior distributions were calculated using the finite difference method with a correction factor for the unexposed surface.

89. Lie, T. T. (1972). Fire and Buildings. London: Applied Science Publishers Ltd.

Discussion of fire development, fire severity, behavior of materials, economic aspects of fire, and building fires. Discusses thermal, strength, and deformation properties of building materials at elevated temperatures. Develops a method to predict the fire resistance of structural elements. Contains excellent references.

90. Bushev, V. P., Pchelintsev, V. A., Fedorenko, V. S., & Yakovlev, A. I. (1970). Fire Resistance of Buildings. Moscow: Construction Literature Publishers.

Presents methods for testing and calculating the fire resistance of common (concrete and steel) structural elements. Contains some analytical procedures.

91. Malhotra, H. L. (1982). Design of Fire-Resisting Structures. Bishopbriggs and Glasgow: Surrey University Press.

Discusses fire resistance, properties of materials, design of concrete, steel, timber, and masonry elements for fire conditions, and repair of fire-damaged structures. Contains excellent references.

92. Wickström, U. (1985). Application of the standard fire curve for expressing natural fires for design purposes. In T. Z. Harmathy (Eds.), Fire Safety: Science and Engineering (pp. 145-159). Philadelphia, PA: ASTM

Presents a method suitable for design purposes whish allows postflashover compartment fires to be expressed in a single curve which modifies time based on ventilation conditions and wall properties. Shows results using TASEF-2 and compares with those from the standard ISO 834 curve.

93. Lie, T. T., & Lin, T. D. (1985). Fire performance of reinforced concrete columns. In T. Z. Harmathy (Eds.), Fire Safety: Science and Engineering (pp. 176-205). Philadelphia, PA: ASTM

Experimental and theoretical studies were carried out for the development of general methods which predict the fire resistance of reinforced concrete columns. Twelve columns were tested in a furnace and then calculation methods were developed to describe their temperature distributions.

94. Bresler, B., & Iding, R. H. (1985). Effect of fire exposure on structural response and fireproofing requirements of structural steel frame assemblies. In T. Z. Harmathy (Eds.), Fire Safety: Science and Engineering (pp. 206-222). Philadelphia, PA: ASTM

Examines the effects two fire exposures (SDHI and LDLI) have on a typical steel deck floor assembly specimen. Response of the system is determined analytically. Application to concrete because the flooring systems consist of concrete and the two fire curves can be applied to the analysis of concrete structures in fire conditions.

95. Harmathy, T. Z. (1979). Design to cope with fully developed fires (DBR Paper No. 854). Ottawa: National Research Council of Canada.

Discusses fire development and the design of steel and reinforced concrete structures exposed to fire. Shows temperature distribution curves for fire tests of concrete slabs and beams with various aggregates.

96. Harmathy, T. Z., & Sultan, M. A. (1987). Correlation between the severities of the ASTM E119 and ISO 834 fire exposure (Technical Report). Ottawa: National Research Council Canada.

Compared the severities of the ASTM E119 and ISO 834 fire tests. It was found that the ISO fire is slightly less severe and results in the need for less fire endurance. Displays a method to calculate the temperature distribution within a concrete slab (including exposed surface temperature).

97. Hertz, K. (1980). Reference list on concrete constructions exposed to high temperatures (Report No. 141). Lyngby, Denmark: Technical University of Denmark.

List of approximately 500 sources from before 1980 on the effects fire has on concrete constructions.

98. Buchanan, A. H. (2001). Structural Design for Fire Safety. England: John Wiley & Sons Ltd.

Presents criteria on structural design for fire safety in discussion format. Gives generalities for structural fire design but does not get into specific design calculations. Excellent text if used to gain a general understanding of the topic of fire safety and its effect on structural design

99. Hertz, K. (1981). Design of fire exposed concrete structures (Report No. 160). Lyngby, Denmark: Technical University of Denmark.

Discusses the material properties of concrete at elevated temperatures. Develops equations to express the ultimate limit state analysis of rectangular beams, slabs, t-shaped cross-sections, wall, and rectangular columns at any time of any fire. The procedure described is for designing a structure for any type of fire exposure.

100. Hertz, K. (1981). Microwave heating for fire material testing of concrete – a theoretical study (Report No. 144). Lyngby, Denmark: Technical University of Denmark.

A theoretical study is performed to analyze the effects microwave energy has on the elimination of temperature gradients in concrete specimens during fire tests.

101. Hertz, K. (1981). Simple temperature calculations of fire exposed concrete constructions (Report No. 159). Lyngby, Denmark: Technical University of Denmark.

Discusses the thermal properties of concrete and presents a method which determines the temperature distribution in fire exposed concrete constructions. The calculation method is extremely mathematically intensive. The method calculates both surface and internal temperatures.

102. Hertz, K. (1983). Equivalent time of fire exposure for concrete structures (Report No. 163). Lyngby, Denmark: Technical University of Denmark.

The equivalent time (based on standard fire curve – ISO 834) concept is described and analyzed as an application to fire safety design. It was found that it has a limited application due to an extreme sensitivity to parameters for an accurate calculation.

103. Hertz, K. (1985). Design philosophy for fire exposed concrete structures (Report No. 169). Lyngby, Denmark: Technical University of Denmark.

Details the requirements for a procedure to design concrete structures for fire safety. The fire exposure for design should be related to the potential of a real fire. Concludes that plastic design procedures are suitable for design of concrete structures for fire conditions. Also, recommends that the industry uses furnaces which better simulate actual fire conditions.

104. Abrams, M. S. (1973). Compressive strength of concrete at temperatures to 1,600 F (RD016.01T), Portland Cement Association. Authorized reprint from copyrighted American Concrete Institute Special Publication SP-25.

The compressive strength of three different types of concrete at various elevated temperatures is examined. Each type of concrete is tested with a f'c around 4,000 psi and another around 5,500 psi. Strength retained after heating is also measured.

105. Cruz, C. R. (1966). Elastic properties of concrete at high temperatures. Reprinted from the: Journal of the PCA Research and Development Laboratories. 8(1), 37-45.

The elasticity and shear strength of four different types of concrete at various elevated temperatures are examined. Each type of concrete is tested with a f'c around 4,250 psi and another around 6,000 psi. Elasticity and shear strength retained after heating is also measured.

106. Lie, T. T. (Eds.) (1992). Structural Fire Protection. (Technical Report No. 78). New York: American Society of Civil Engineers.

This text explains fire resistance needs and requirements according to building codes in addition to the basic principles of fire protection. The thermal and mechanical properties of concrete are detailed. Lie describes the application of multiple numerical methods for calculating temperatures and fire resistance for concrete elements. Numerical methods for a wide variety for concrete structural members are detailed including columns with rectangular, square, or circular cross-sections, floor and roof slabs, and concrete filled tubular columns.

107. Yakovlev, A. I. (1980). Basic Principles of Calculations of Building Structures' Fire Resistance Limits. (Final Report). U.S. Department of Commerce: National Bureau of Standards.

Presents methods of calculation for determining the fire resistance of structures based on ISO 834 testing. Contains equations for surface temperature heat transfer coefficient on the exposed and unexposed faces.

108. Abrams, M. S., & Gustaferro, A. H. (1968). Fire endurance of concrete slabs as influenced by thickness, aggregate type, and moisture: Journal of the PCA Research and Development Laboratories. 10(2), 9-24.

Shows fire test performed on concrete slabs of varying thickness and aggregate type exposed to the ASTM E119 curve.

109. Associated Factory Mutual Fire Insurance Companies, The National Board of Fire Underwriters, & Bureau of Standard, Department of Commerce. (1918). Fire Tests of Building Columns. Chicago, Illinois: Underwriters' Laboratories.

Details a series of fire tests on reinforced concrete columns. One of the earliest works on the subject of structural fire performance.

110. Hutchens, G. J., & Gupta, N. K. (2000). A spreadsheet program for steady-state temperature distributions (Report WSRC-TR-2000-00132). Aiken, South Carolina: Westinghouse Savannah River Company.

Describes the use of Excel in calculating a two-dimensional steady state heat conduction problem.

B. Material Properties of Concrete

Concrete is non-combustible and has a low thermal conductivity. Also, the cement paste in concrete undertakes an endothermic reaction when heated which assists in the reduction of temperature rises in concrete elements. When those factors are combined with concrete's large member sizes, the result is that concrete structures perform relatively well in fire conditions in comparison with other construction types. Since concrete is a composition of other elements there are many factors which affect its performance at elevated temperatures.

During a fire, heat is absorbed by concrete leading to an increase in its temperature. When a concrete element is at elevated temperatures its resultant strength and deformations are highly dependent on its thermal and mechanical properties. These properties determine the temperature rise in concrete so knowing and understanding their function is critical in determining the behavior of concrete elements in fire conditions.

B.1 Density

The density of concrete depends primarily upon the type of aggregate. Concretes made of dense aggregates have densities ranging from 2000 kg/m^3 to 2400 kg/m^3. Lightweight aggregate concretes have densities ranging from 1000kg/m^3 to 1500kg/m^3.

B.2 Moisture Content

When concrete is heated free moisture is driven away once the temperature in the section exceeds 100ºC. Vapor migrates through the capillaries and forces the moisture to the outer surfaces of the concrete element. On an exposed side of an element it will turn into steam but an unexposed side it will condense. Losses in

moisture reduce the density of concrete by a small amount but for practical purposes it is commonly neglected.

B.3 Thermal Conductivity

The thermal conductivity of concrete, k, is the rate of heat transferred through a unit thickness of the material per unit temperature difference, with common units W/m-ºC and kcal/m-h-ºC. It is dependent upon the type of aggregate, porosity of the concrete, and the moisture content. Also, thermal conductivity values for concrete elements are dependent on the temperature of the concrete as is shown in figure B.1 and as defined for a few aggregates in the following equations (Lie 1992).

- **Siliceous Aggregate Concrete**

For $0 \leq T \leq 800$ºC; $k_c = -0.000625T + 1.5$ W/m-ºC

For $T > 800$ºC; $k_c = 1.0$ W/m-ºC

- **Pure Quartz Concrete Aggregate**

For $0 \leq T \leq 800$ºC; $k_c = -0.00085T + 1.9$ W/m-ºC

For $T > 800$ºC; $k_c = 1.22$ W/m-ºC

- **Carbonate Aggregate Concrete**

For $0 \leq T \leq 293$ºC; $k_c = 1.355$ W/m-ºC

For $T > 293$ºC; $k_c = -0.001241T + 1.762$ W/m-ºC

- **Expanded Shale Aggregate Concrete**

For $0 \leq T \leq 600$ºC; $k_c = -0.00039583T + 0.0925$ W/m-ºC

For $T > 600$ºC; $k_c = 0.6875$ W/m-ºC

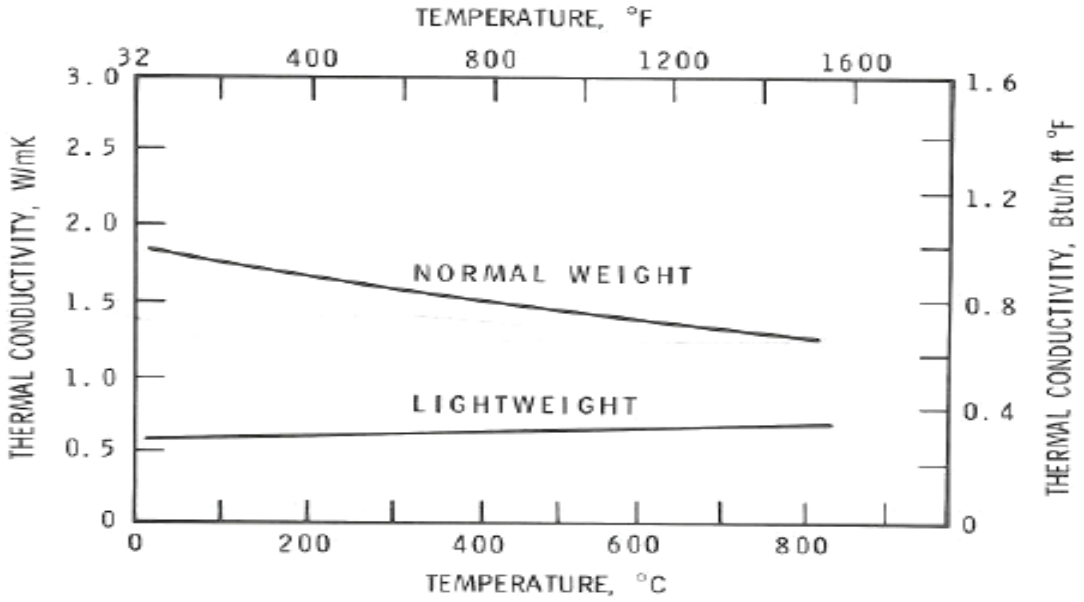

Figure B.1: Thermal Conductivity of Normal and Lightweight Concrete (as taken from Lie 1992)

B.4 Specific Heat

Specific heat, denoted as C_p or c, is the heat required to raise the temperature of a unit mass of material by one degree. The common units for specific heat are kcal/kg-ºC and kJ/kg-ºC. Similarly to thermal conductivity, values for the specific heat of concrete elements are dependent on temperature and typical values are shown in Figure B.2 as extracted from Malhotra (1982) and as defined for a few aggregates in the following equations (Lie 1992).

- **Siliceous Aggregate Concrete**

For $0 \leq T \leq 200$ºC; $\rho_c c_c = (0.005T + 1.7) \times 10^6$ J/m^3-ºC

For 200ºC $< T \leq 400$ºC; $\rho_c c_c = 2.7 \times 10^6$ J/m^3-ºC

For 400ºC $< T \leq 500$ºC; $\rho_c c_c = (0.013T - 2.5) \times 10^6$ J/m^3-ºC

For 500ºC $< T \leq 600$ºC; $\rho_c c_c = (-0.013T + 10.5) \times 10^6$ J/m^3-ºC

For $T > 600$ºC; $\rho_c c_c = 2.7 \times 10^6$ J/m^3-ºC

- **Carbonate Aggregate Concrete**

For $0 \leq T \leq 400$ºC; $\rho_c c_c = 2.566 \times 10^6$ J/m^3-ºC

For 400ºC $< T \leq 410$ºC; $\rho_c c_c = (0.1765T - 68.034) \times 10^6$ J/m^3-ºC

For 410ºC < $T \leq$ 445ºC; $\rho_c c_c = (-0.05043T + 25.00671) \times 10^6$ J/m^3-ºC

For 445ºC < $T \leq$ 500ºC; $\rho_c c_c = (2.566) \times 10^6$ J/m^3-ºC

For 500ºC < $T \leq$ 635ºC; $\rho_c c_c = (0.01603T - 5.44881) \times 10^6$ J/m^3-ºC

For 635ºC < $T \leq$ 715ºC; $\rho_c c_c = (0.16635T - 100.90225) \times 10^6$ J/m^3-ºC

For 715ºC < $T \leq$ 785ºC; $\rho_c c_c = (-0.22103T + 176.07343) \times 10^6$ J/m^3-ºC

For $T >$ 785ºC; $\rho_c c_c = 2.566 \times 10^6$ J/m^3-ºC

- **Expanded Shale Aggregate Concrete**

For $0 \leq T \leq$ 400ºC; $\rho_c c_c = 1.930 \times 10^6$ J/m^3-ºC

For 400ºC < $T \leq$ 420ºC; $\rho_c c_c = (0.0722T - 28.95) \times 10^6$ J/m^3-ºC

For 400ºC < $T \leq$ 500ºC; $\rho_c c_c = (-0.1029T + 46.706) \times 10^6$ J/m^3-ºC

For 500ºC < $T \leq$ 600ºC; $\rho_c c_c = 1.930 \times 10^6$ J/m^3-ºC

For 200ºC < $T \leq$ 400ºC; $\rho_c c_c = (0.03474T - 18.9140) \times 10^6$ J/m^3-ºC

For 400ºC < $T \leq$ 500ºC; $\rho_c c_c = (-0.1737T + 126.994) \times 10^6$ J/m^3-ºC

For $T >$ 600ºC; $\rho_c c_c = 1.930 \times 10^6$ J/m^3-ºC

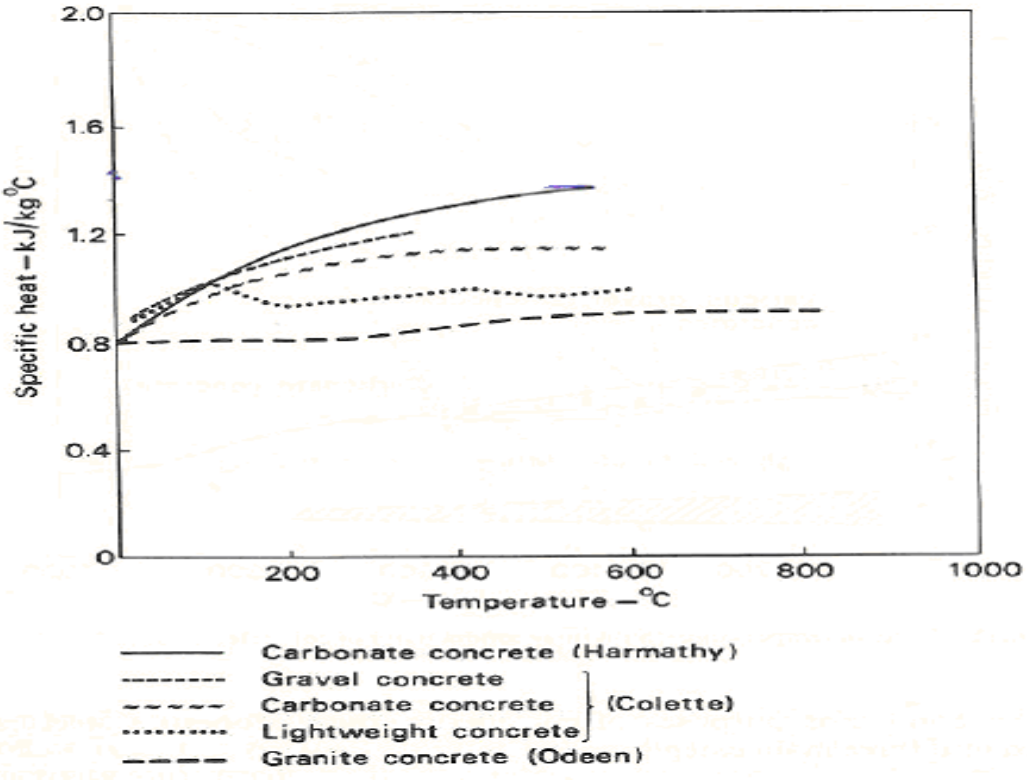

Figure B.2: Specific Heat Values versus Temperature for Various Aggregates (as taken from Malhotra 1982)

B.5 Thermal Capacity

Thermal capacity is the product of the density and specific heat of a material, ρc, and is defined as the heat required to raise the temperature of a material by one degree. Since it is dependent upon specific heat its values are identically dependent upon the temperature of concrete.

B.6 Thermal Diffusivity

The thermal diffusivity of concrete, often denoted as a, is the ratio between its thermal conductivity and thermal capacity ($a = k/\rho c$). It is a measure of the rate of heat transport from the exposed surface of concrete to the inside and its typical units are m^2/h. Thus it is a measure of the rate of temperature rise at a certain depth of the concrete with large diffusivities leading to faster temperature rises at a given depth. .

B.7 Thermal Deformation

Concrete typically expands as its temperature is raised. The thermal expansion of concrete is affected by cement, water content, aggregate type, age, heating rate, and externally applied forces. Data for the thermal expansion of concrete made with different aggregates is illustrated in Figure B.3 and the equations below calculate the coefficients of thermal expansion for some concretes (Lie 1992).

- Siliceous and Carbonate Aggregates

$\alpha = (0.008T + 6) \times 10^{-6}$

- Expanded Shale Aggregate Concrete

$\alpha = 7.5 \times 10^{-6}$

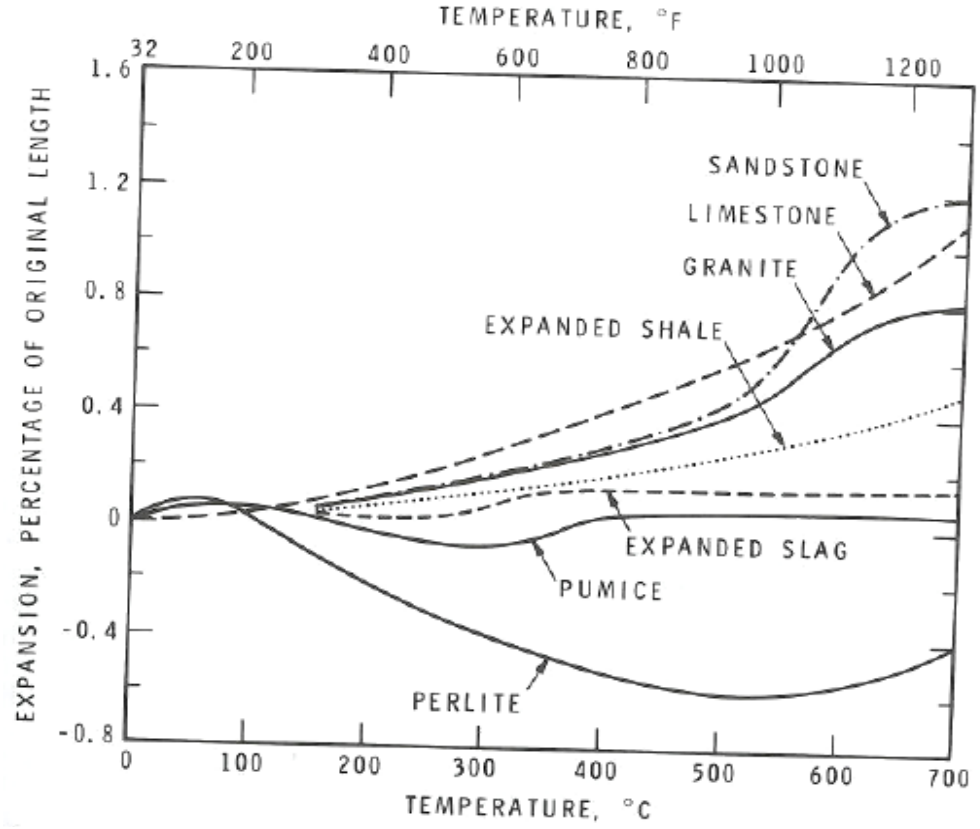

Figure B.3: Thermal Expansion of Various Concrete Aggregates (as taken from Lie 1992)

It is shown in Figure B.4 (Anderberg 1972) that the total thermal strain displayed by heated concrete consists of four components,

$$\varepsilon = \varepsilon_{th} + \varepsilon_{\sigma} + \varepsilon_{c} + \varepsilon_{tr},$$

where ε_{th} is the thermal expansion undergone by concrete without external loads including drying shrinkage, ε_{σ} is the elastic and plastic deformation caused by externally applied forces, ε_{c} is creep strain which is dependent on temperature, time, and stress, and ε_{tr} is the transient strain caused by heating while loaded due to the chemical transformation in the cement paste.

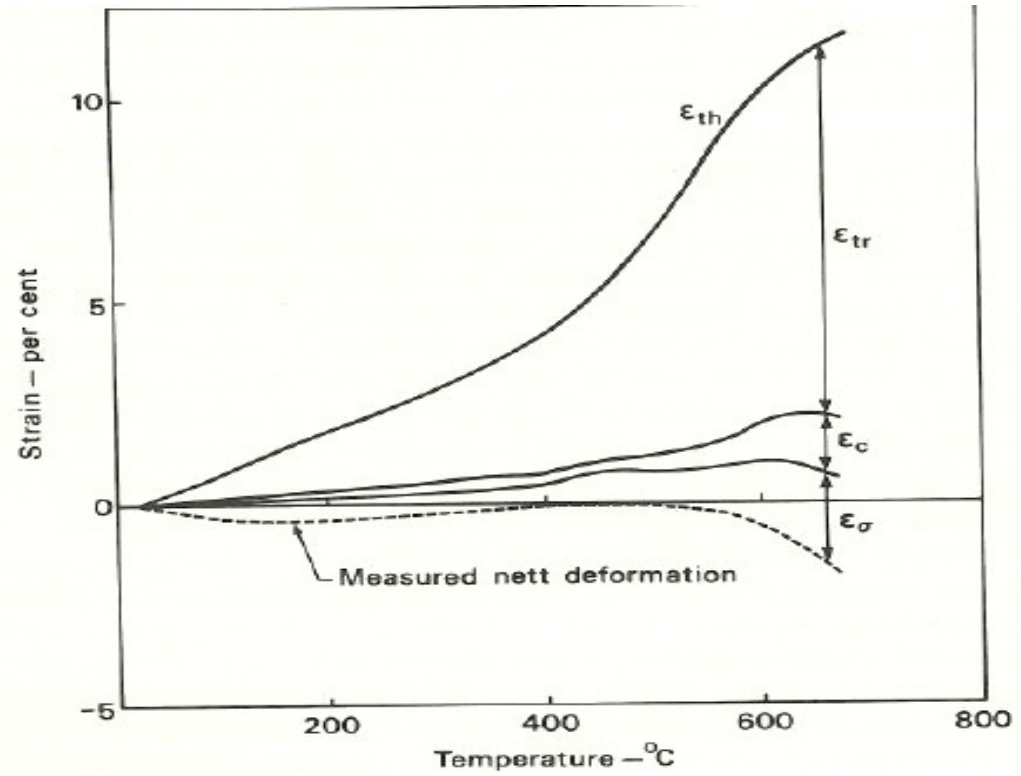

Figure B.4: Components of Strain in Heated and Loaded Concrete (as taken from Anderberg 1972)

The effects different load levels have on the thermal expansion of siliceous-aggregate concrete heated at 5Cº/min are illustrated in Figure B.5 (Anderberg 1982). As can be seen, increasing levels of loading greatly reduces the thermal expansion of concrete.

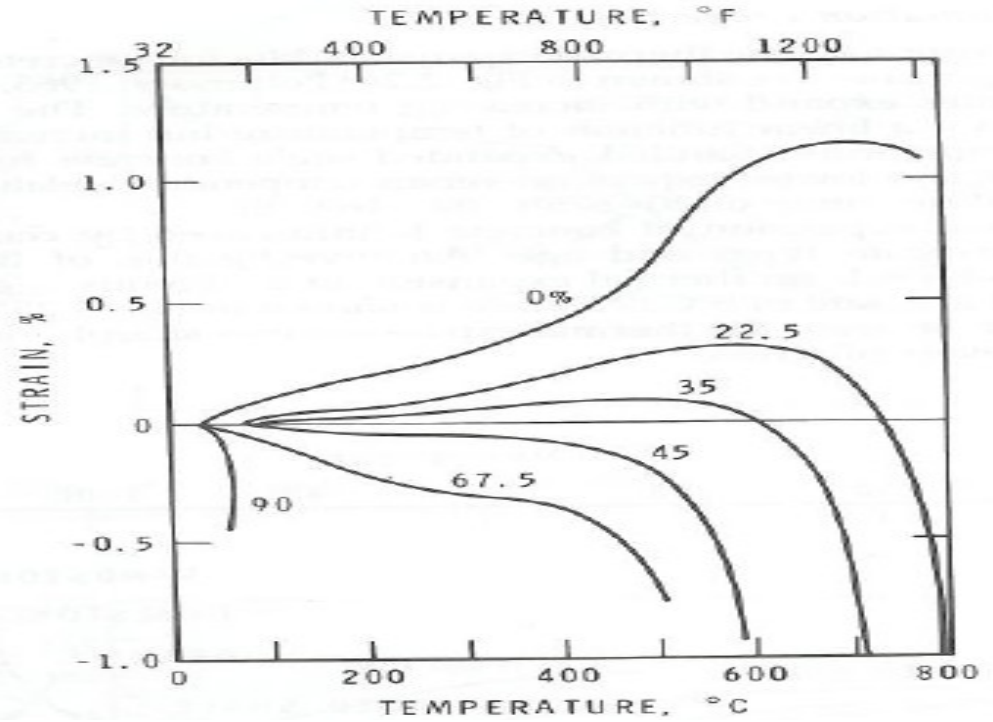

Figure B.5: Strain of Concrete versus Different Loadings (as taken from Anderberg 1982)

B.8 Strength

Concrete primary use in structures is to reduce compressive stresses, thus much research has been done on the compressive strength of concrete at elevated temperatures. The compressive strength of concrete varies primarily by the type of aggregate, cement to aggregate ratio, and degree of loading. Malhotra (1989) examined the compressive strength of concrete with varying cement to aggregate ratios and 20% loading and the results are shown in Figure B.6. Figures B.7, B.8, and B.9 show the compressive strength of concretes composed of different aggregates (Abrams 1973). When concrete cools it loses a percentage of its original strength depending upon the exposure and time since exposure. Abrams (1973) investigated these effects and his results are illustrated in Figure B.10.

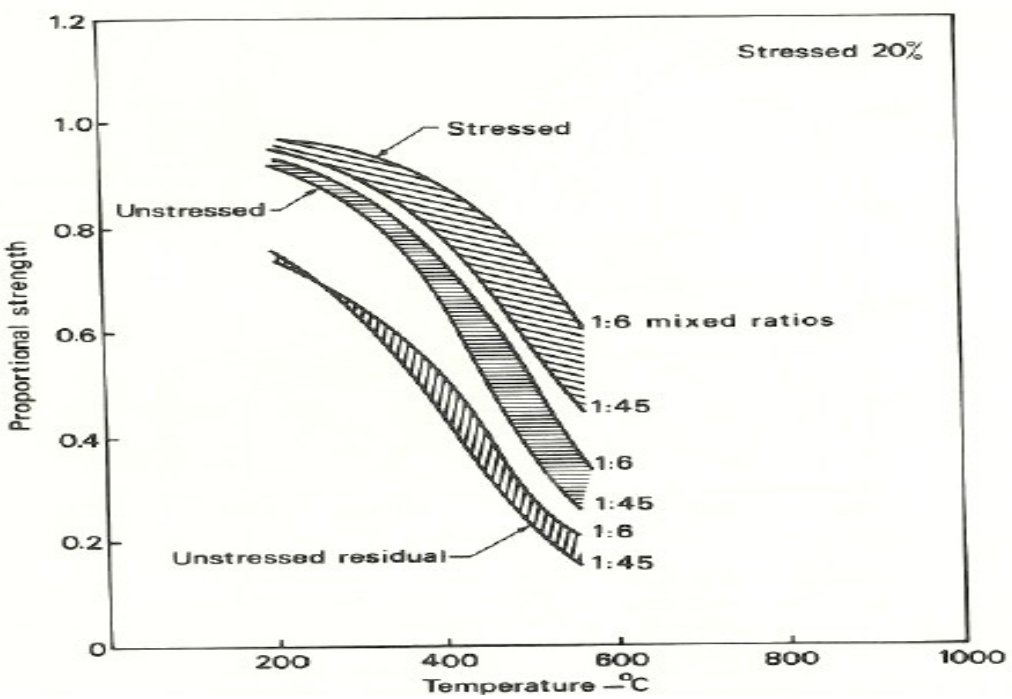

Figure B.6: Concrete Compressive Strength with Varying Cement/Aggregate Ratios (as taken from Malhotra 1989)

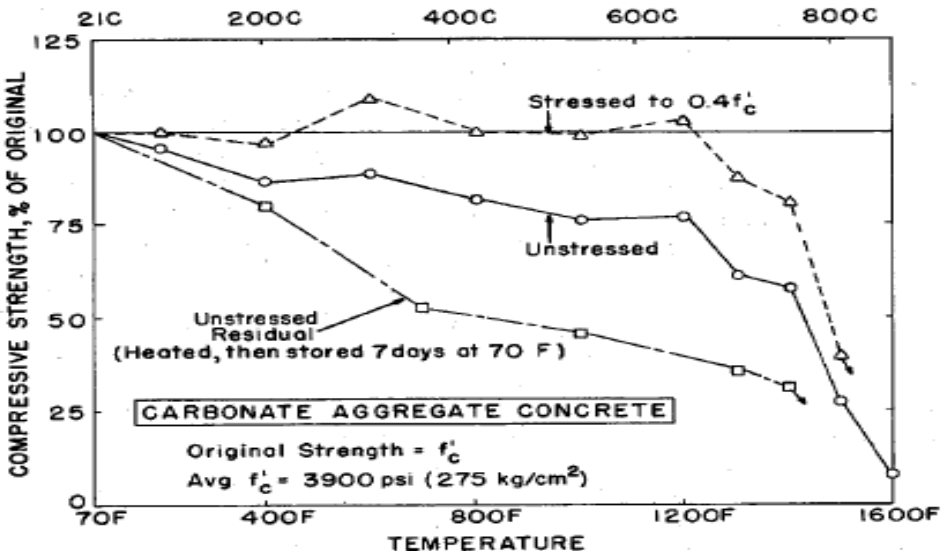

Figure B.7: Compressive Strength of Carbonate Aggregate Concrete versus Temperature (as taken from Abrams 1973)

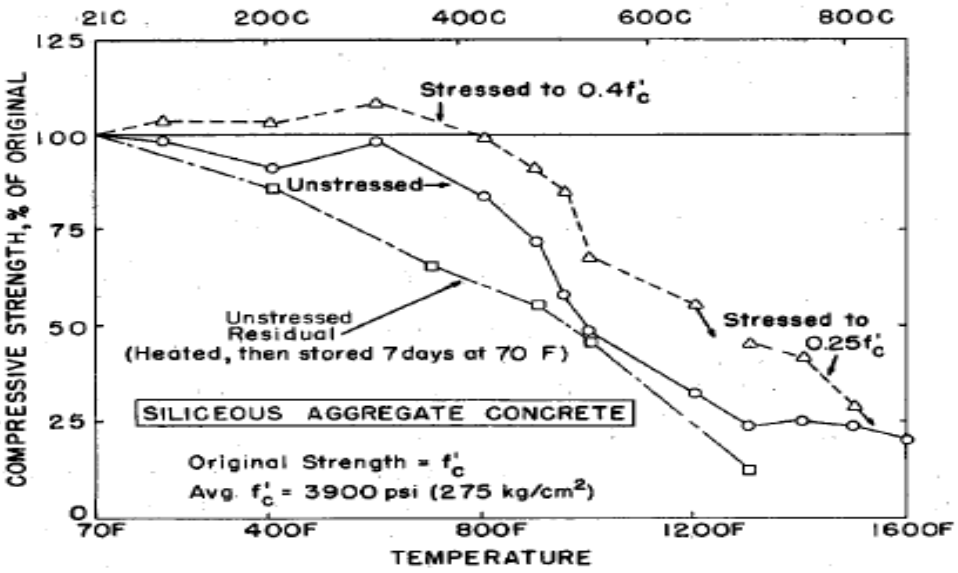

Figure B.8: Compressive Strength of Siliceous Aggregate Concrete versus Temperature (as taken from Abrams 1973)

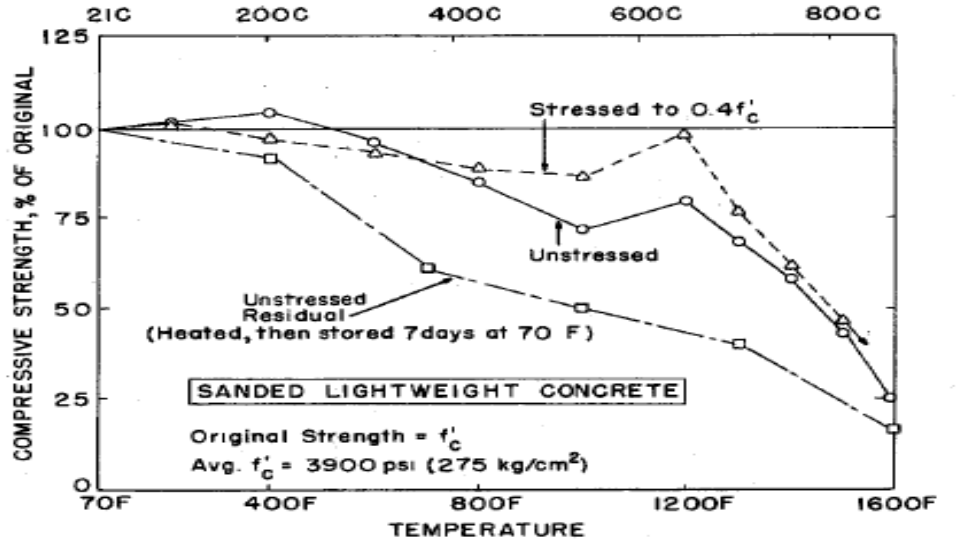

Figure B.9: Compressive Strength of Sanded Lightweight Concrete versus Temperature (as taken from Abrams 1973)

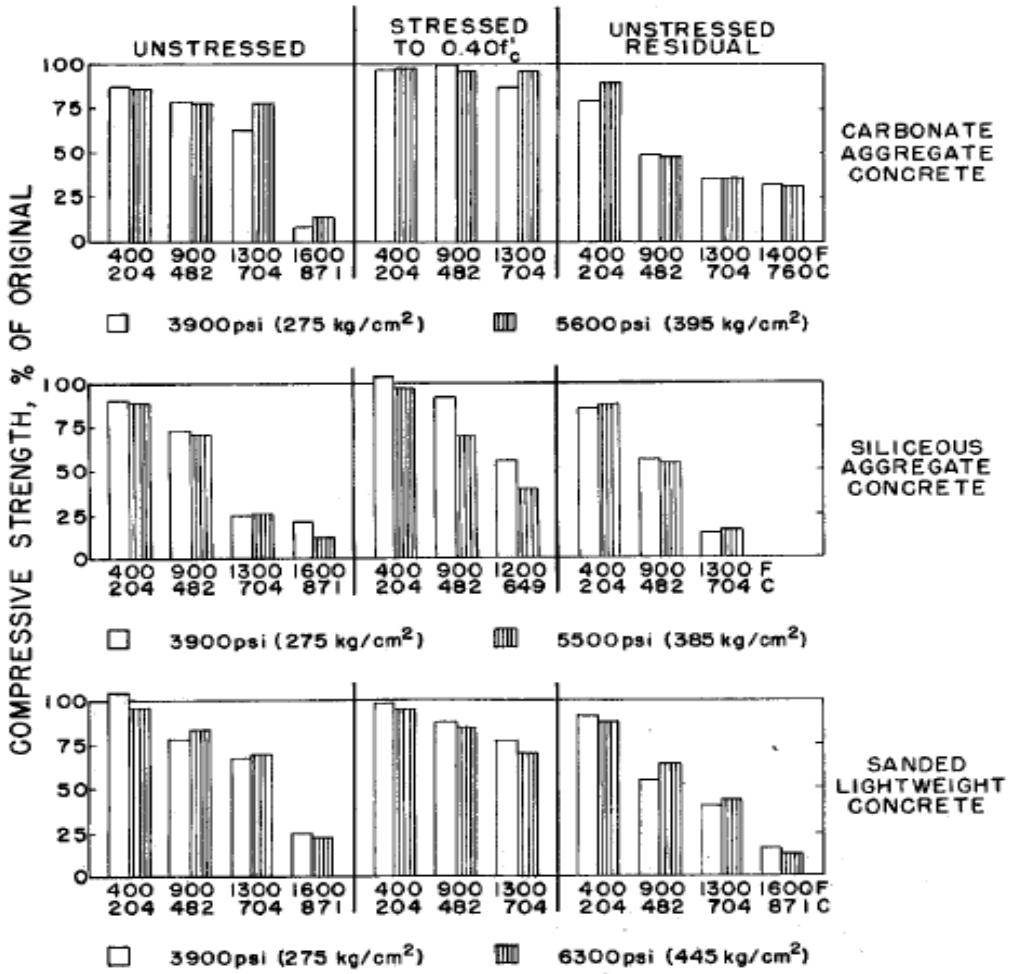

Figure B.10: Percent of Compressive Strength Recovered for Various Aggregates versus Different Heating Regimes (as taken from Abrams 1973)

B.9 Elasticity

Similarly to compressive strength the elasticity of concrete decreases rapidly when heated as illustrated in Figure B.11 (Cruz 1966). It can be seen that the aggregate type has little effect on elasticity of concrete at elevated temperatures. Also, when concrete cools only a percentage of its original elasticity is restored.

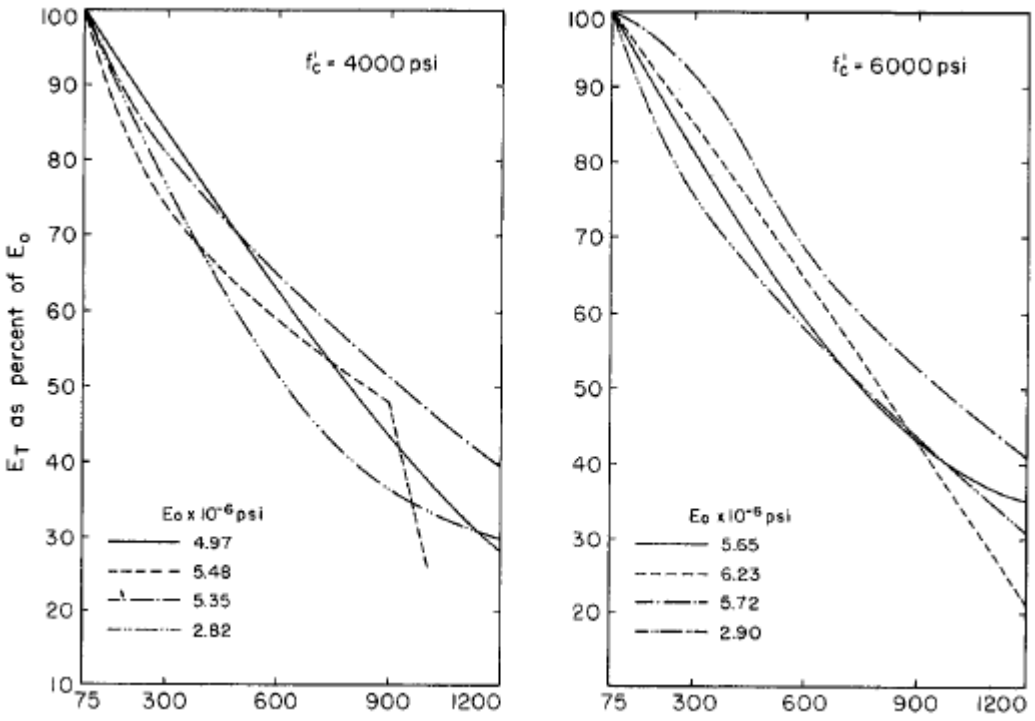

Figure B.11: Elasticity of Concrete versus Temperature (as taken from Cruz 1966)

B.10 Creep

The important factors affecting the creep of concrete at high temperatures are age, moisture conditioning, type of concrete, strength, and stress-strength ratio. Cruz investigated the creep of a carbonate aggregate concrete by heating specimens to a test temperature and then applying a 45% room temperature load for 5 hours. The results of his tests are illustrated in figure B.12 as extracted from Lie (1992). Creep increased slightly until a temperature of 320ºC where it begins to increase significantly.

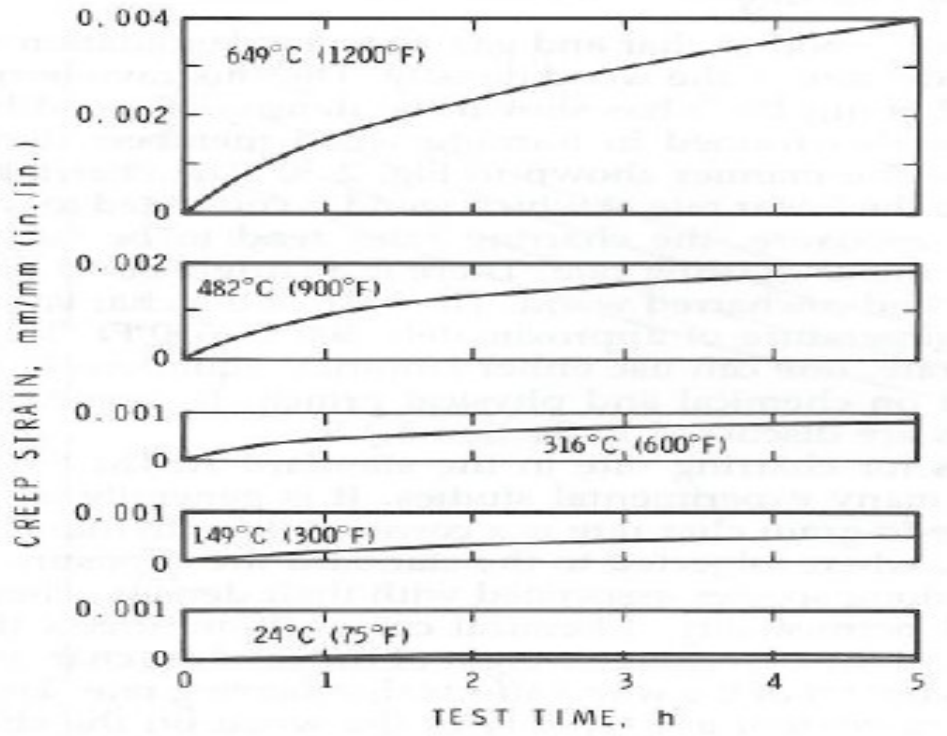

Figure B.12: Creep of Loaded Concrete versus Temperature (as taken from Lie 1992)

B.11 Bond Strength

The critical factor affecting the bond strength of concrete is the surface of the bars with deformed bars or rusted plain bars having higher bond strength at high temperatures than smooth bars. Also, the type of concrete has an influence on bond strength with concretes having lower thermal strains retaining higher bond strength values.

C. Types of Concrete

The thermal properties of concrete vary significantly with the type and quantity of aggregate present. The material properties of concrete vary significantly depending on mix design. Important factors effecting mix design include the cement to water ratio, aggregate type, and the percentage of aggregate used in the total mix. Since concrete mixes vary considerably different types of concrete react differently to fire conditions.

C.1 Lightweight

Lightweight concrete is usually made with standard cement and a lightweight aggregate such as pumice and typical densities range from 1000 kg/m^3 to 1500 kg/m^3. It has excellent fire resistance because of its low thermal conductivity in contrast to normal weight concrete and its low density allows for a higher rate of heat release on unexposed surfaces during fire conditions. Additionally, lightweight concrete is less susceptible to spalling.

C.2 High-strength

Recently the construction industry has been utilizing high-strength concrete (HSC) for column design in numerous high-rise buildings because it contains additives which increase its compressive strength and durability in relation to normal concrete. Typical compressive strengths for high strength concrete range from 50 to 120 MPa. Studies have shown HSC to be quite sensitive to elevated temperatures, especially if highly siliceous aggregates are used, with strength decreasing at a higher rate than normal concrete at temperatures up to 400ºC and increased susceptibility to spalling. HSC is more vulnerable to spalling due to lower water-cement ratios which decrease its permeability and lead to increased pore pressures.

D. Phenomena

D.1 Spalling

Spalling of concrete exposed to fire is the explosive detachment of large or small pieces of concrete from the concrete surface subjected to heating due to built up pore pressure. It typically occurs when there are steep temperature gradients across the concrete section and causes damage in the early stages of a fire which significantly increases the total damage to a concrete structure in fire conditions. The critical factors affecting concrete spalling are moisture content and aggregate type. There are three types of spalling which can occur and they are aggregate splitting, explosive spalling, and sloughing off.

Aggregate splitting is the bursting and splitting of silica containing aggregates due to physical changes in their crystalline structure at high temperatures. This type of spalling occurs at the surface of dense concrete elements and its effect on structural performance is extremely minor and often ignored.

Explosive spalling occurs when pieces of concrete are violently pushed off the surface and it is accompanied by loud noises. It typically transpires during the early stages of fire exposure and its occurrence is related to the type of aggregate, porosity of the concrete, moisture content, and subjected stress level.

Sloughing off takes place when the surface layer of concrete becomes weak after extended exposure to high temperatures and is unable to recover from the development of cracks. Dense concretes are more susceptible to its occurrence. This phenomenon typically occurs in beams and columns and prolonged heating causes outer layers to become detached.

There are a few measures for preventing the spalling of concrete. The use of limestone or lightweight aggregates and aerating agents reduces the chances of spalling. Insertion of anti-spalling reinforcement and the elimination of sharp corners and sudden changes in the cross-section help in the avoidance of spalling issues. Also, plaster and other finishes assist in the prevention of steep temperature gradients across the section.

D.2 Effects of Restraint

The expansion of structural elements in buildings due to heating is commonly restricted by other building components which are either fixed or part of the exposed element. This is especially true in concrete construction where the joints are moment resisting. For example, if a continuous concrete beam is heated its expansion is restricted by cooler parts of the beam as well as the attached columns and slabs.

The two types of restraint are axial and angular. Axial restraint restricts elongation while angular restraint resists the bending or rotation of an element. Both types of restraint can be partial or complete (concrete construction) and can be applied either internally (concrete construction) or externally to an element.

It is difficult to assess the magnitude of restraint quantitatively especially when elements are exposed to fire conditions. Some of the factors complicating its determination include the deformation of the restraining element, range of coefficients for thermal expansion, and change of elastic moduli with temperature, shrinkage due to drying, and creep. Restraint is expressed quantitatively by either expressing the forces acting on the restrained construction when expansion is restricted or by measuring allowed movement (Lie 1972).

Variations in restraint conditions have a significant influence on the fire resistance of structural members. The fire resistance of concrete constructions due to restraint is more commonly reduced than steel because excessive compressive stresses are created which can lead to cracking, spalling, buckling, or collapse. Restraint in horizontal members typically results in increased structural fire performance. For example, an axially or angularly restrained beam exposed to fire will experience an increase in capacity because the underside of the beam remains hotter than the topside resulting in higher restraining forces at the bottom. The increased restraining forces produce a moment that counteracts the applied moment resulting in an increased moment capacity. However, if the topside of a beam is heated the compressive forces in the compression zone will be increased which leads to a reduction in fire resistance. Columns and walls exposed to heating usually experience a reduction in fire resistance due to increased lateral deflection and eccentricity. On the contrary, if an eccentrically loaded column is heated on either its tension or compression side it will experience the same effects mentioned previously for horizontal members with heating on the tension side resulting in increased capacity while heating on the compression side causes a reduction in capacity.

E. Temperature Distributions

This section contains the temperature distribution graphs for all analyses performed for this thesis. Analyses are grouped under aggregate type and fire exposure. All distributions are in millimeters. Also, summary tables which display slab distribution temperatures at discrete points for different aggregates and slab thicknesses appear at the end of the section.

E.1 Quartz

E.1.1 SDHI-95

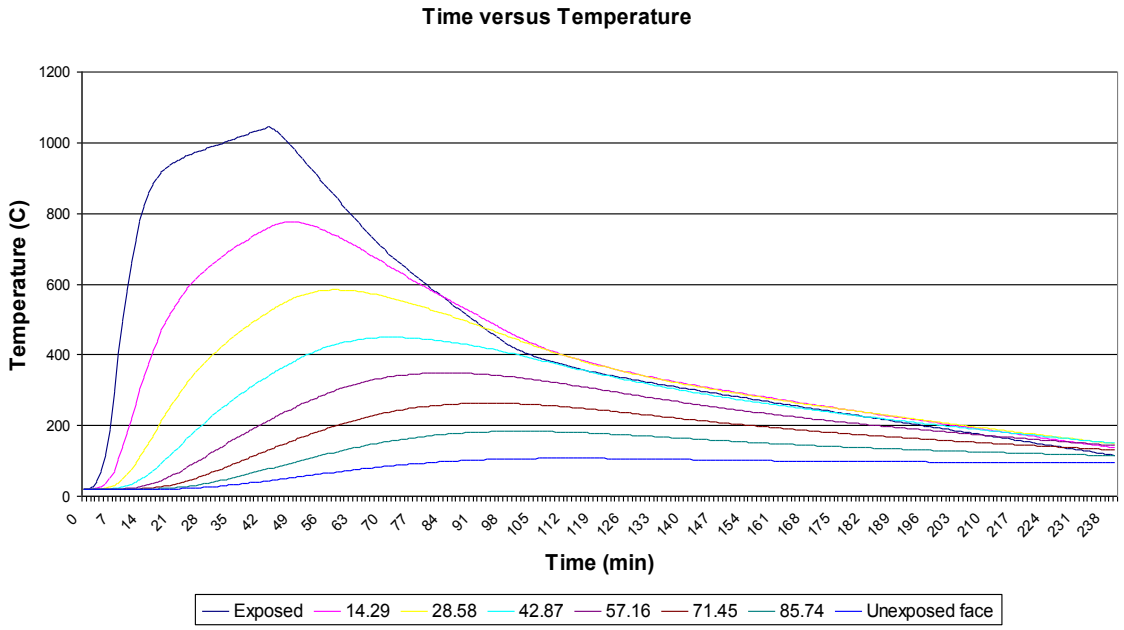

Figure E.1: Temperature Distribution for 100mm Alluvial Quartz Slab

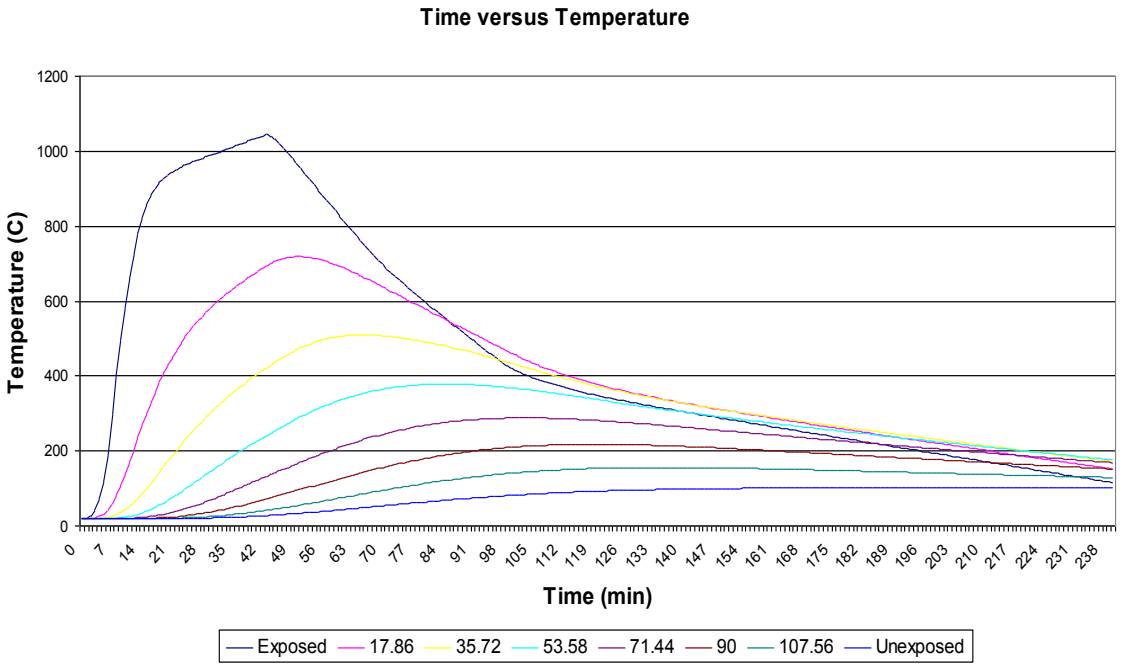

Figure E.2: Temperature Distribution for 125mm Alluvial Quartz Slab

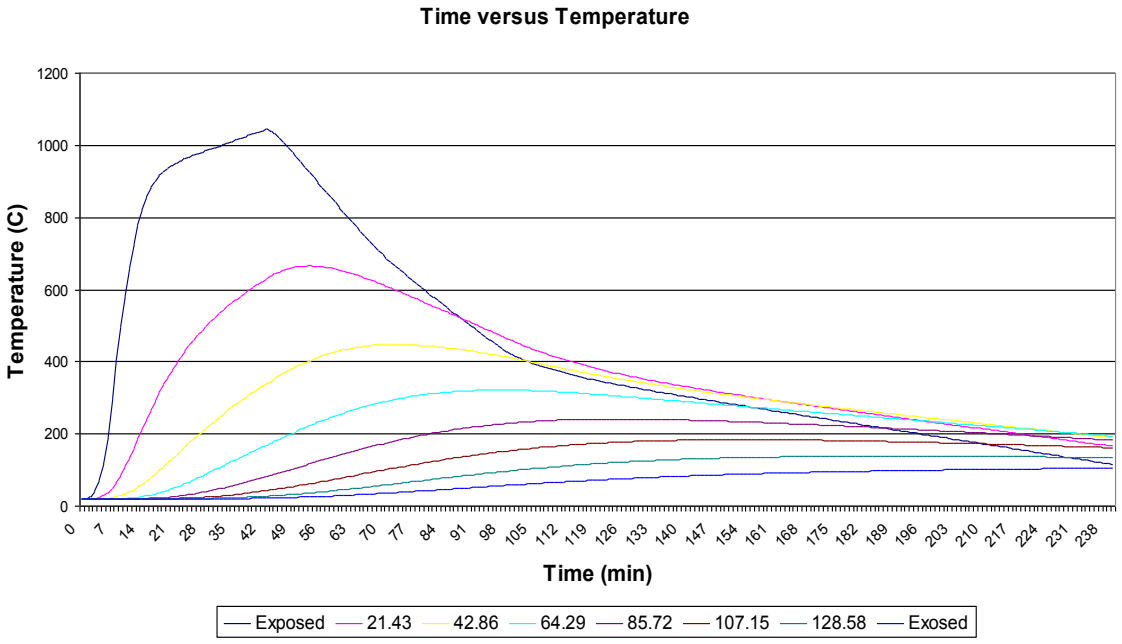

Figure E.3: Temperature Distribution for 150mm Alluvial Quartz Slab

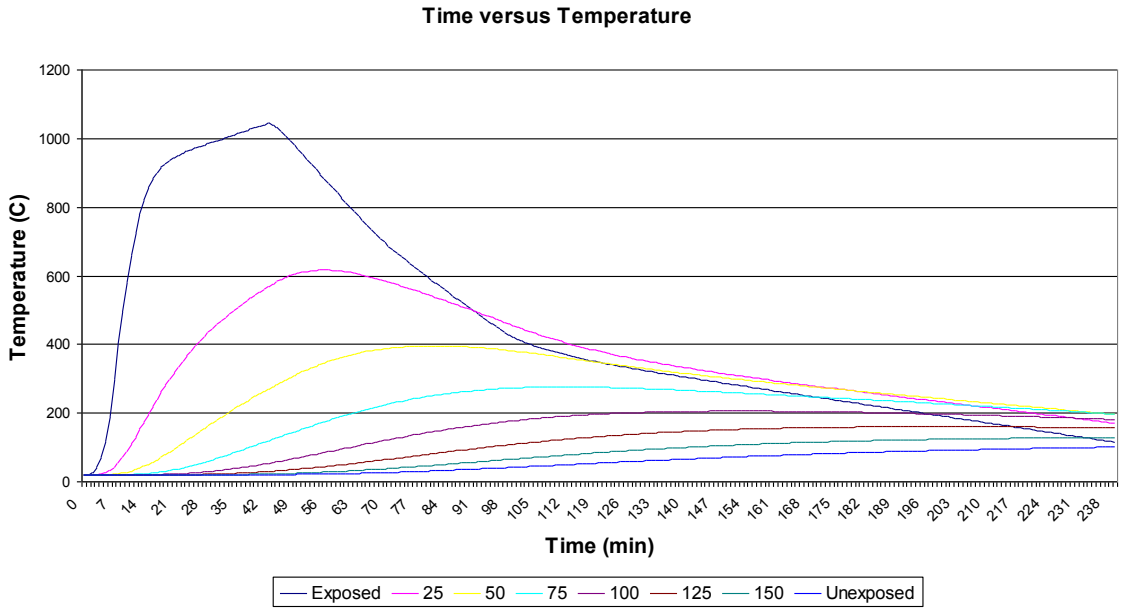

Figure E.4: Temperature Distribution for 175mm Alluvial Quartz Slab

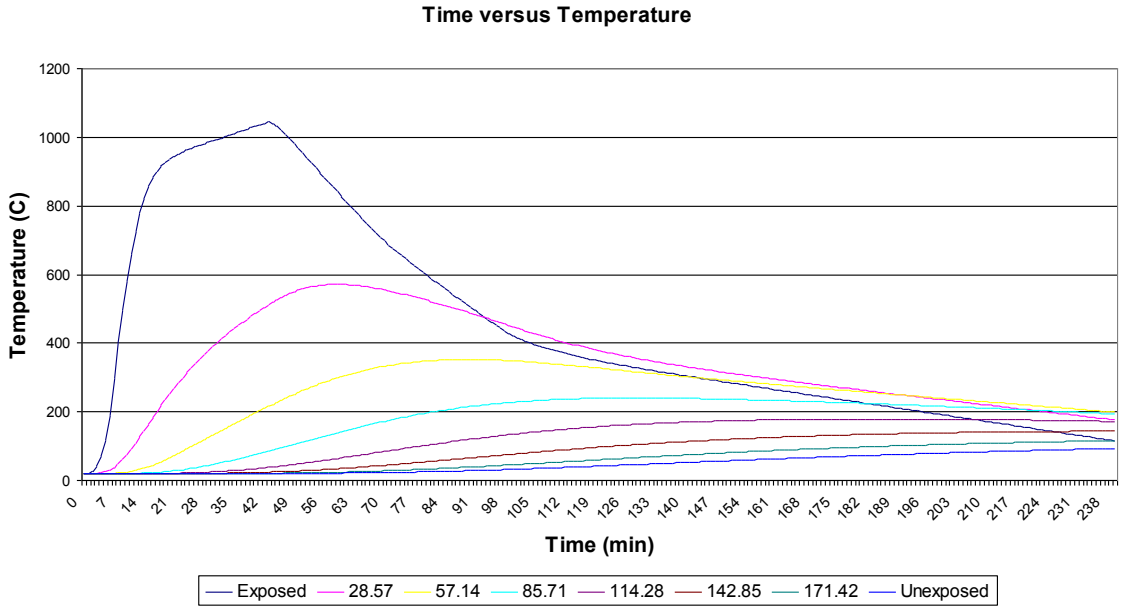

Figure E.5: Temperature Distribution for 200mm Alluvial Quartz Slab

E.1.2 LDMI-M

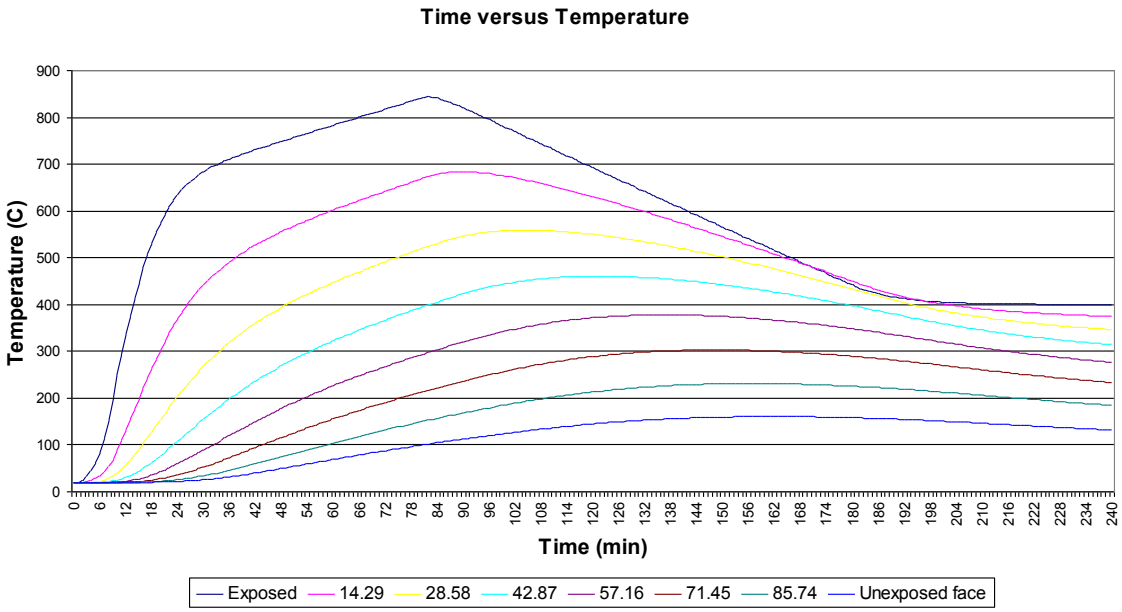

Figure E.6: Temperature Distribution for 100mm Alluvial Quartz Slab

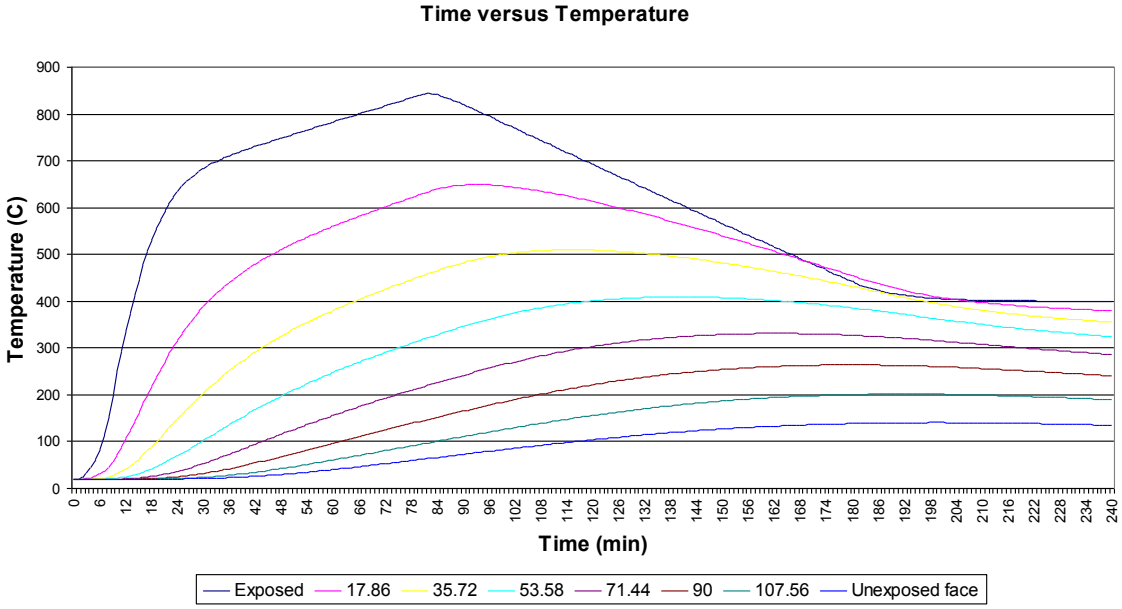

Figure E.7: Temperature Distribution for 125mm Alluvial Quartz Slab

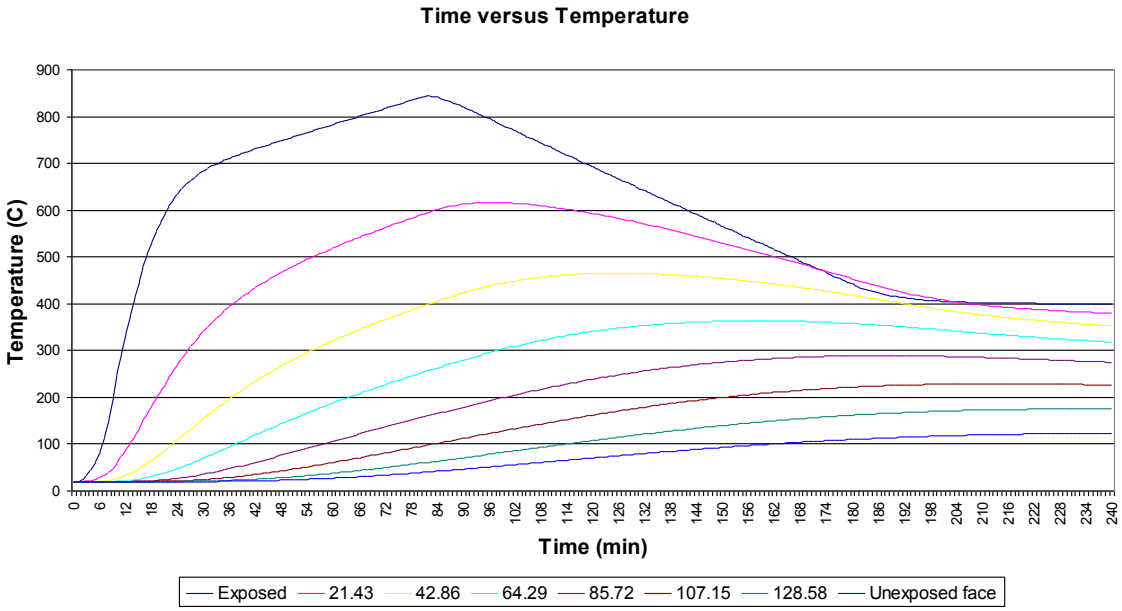

Figure E.8: Temperature Distribution for 150mm Alluvial Quartz Slab

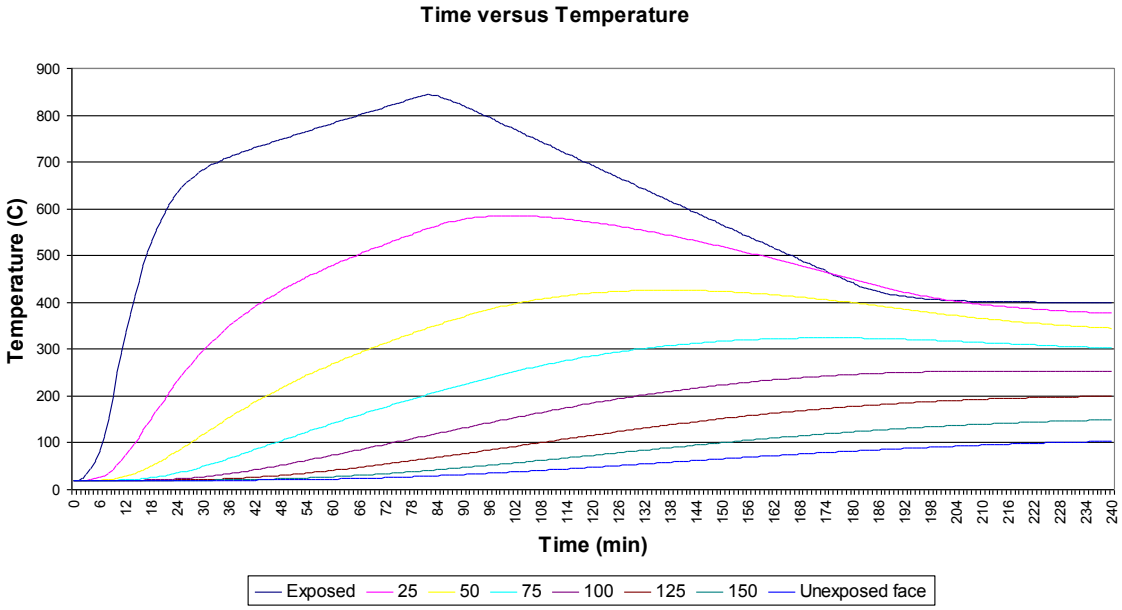

Figure E.9: Temperature Distribution for 175mm Alluvial Quartz Slab

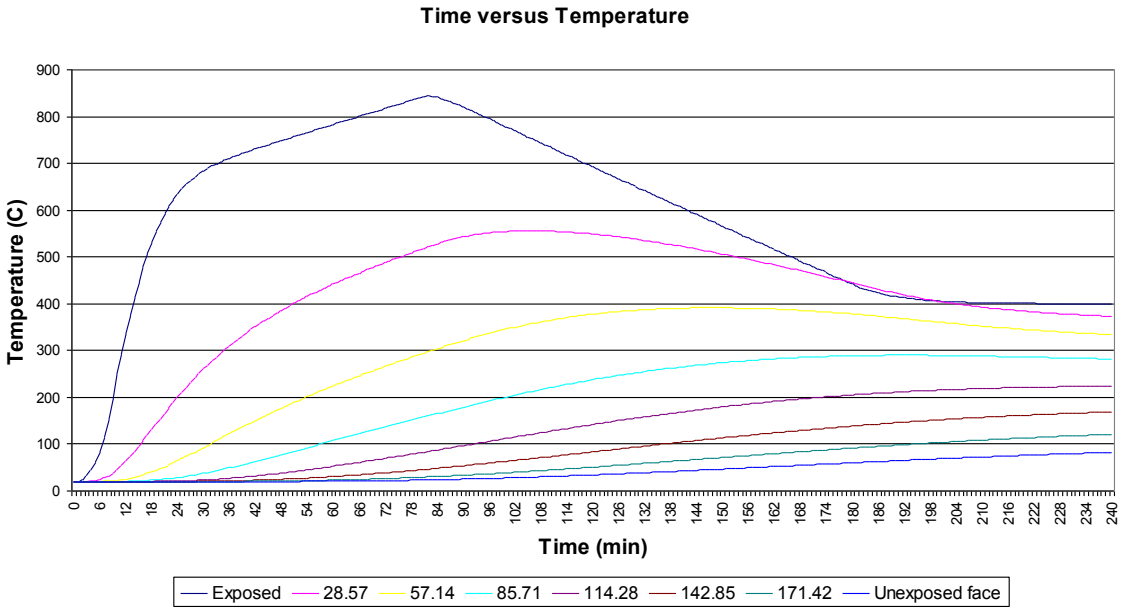

Figure E.10: Temperature Distribution for 200mm Alluvial Quartz Slab

E.2 Carbonate

E.2.1 ISO 834

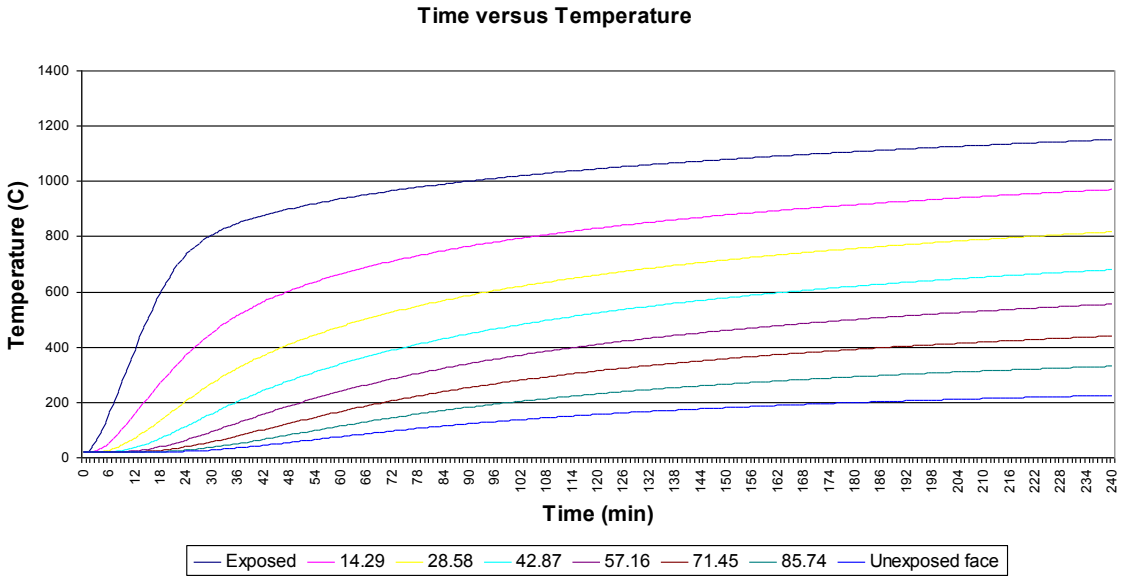

Figure E.11: Temperature Distribution for 100mm Carbonate Slab

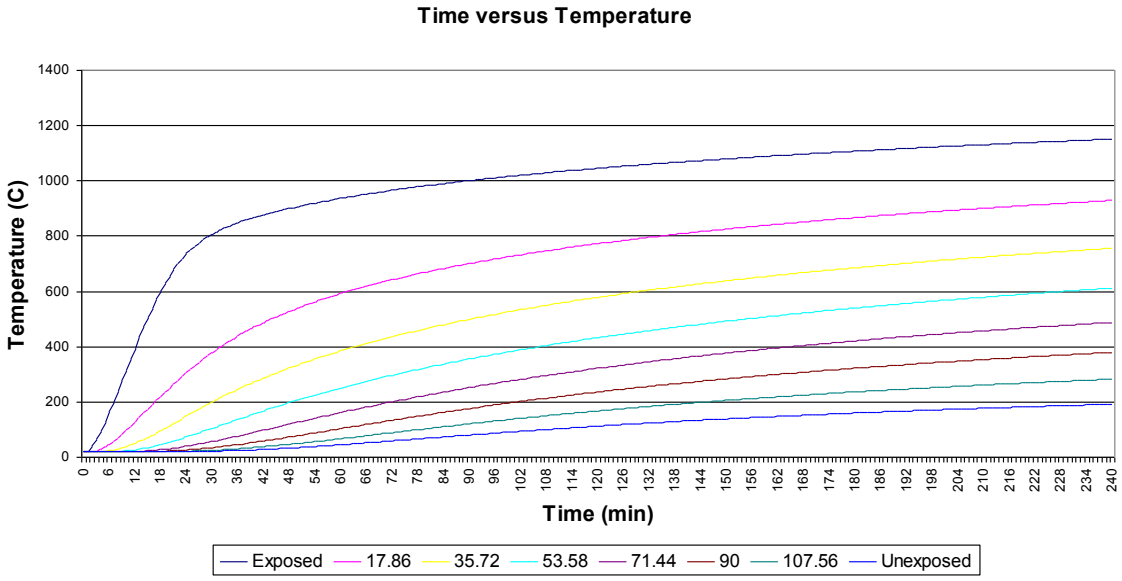

Figure E.12: Temperature Distribution for 125mm Carbonate Slab

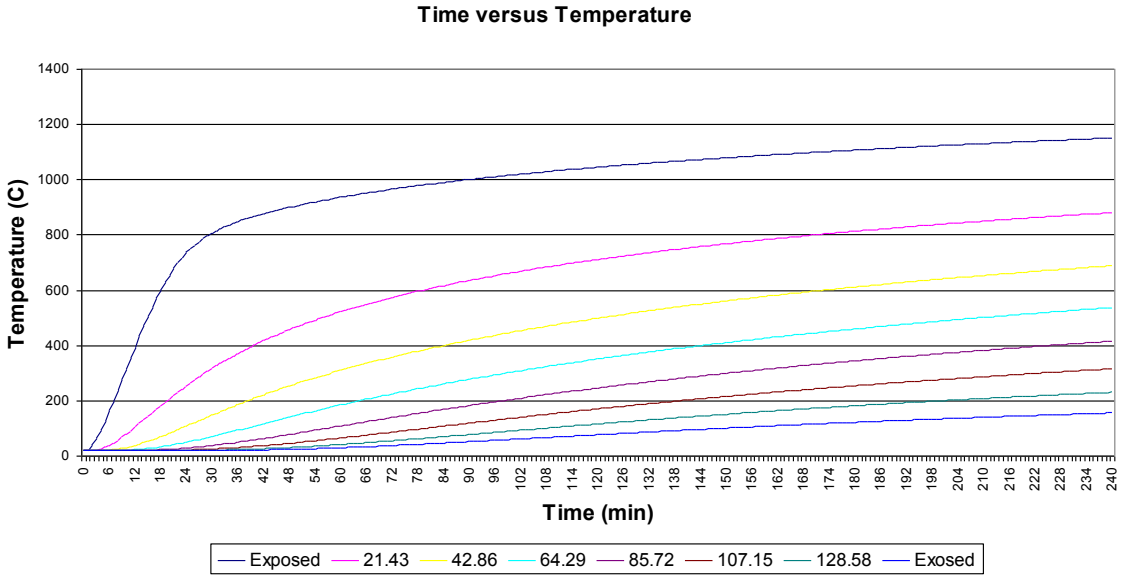

Figure E.13: Temperature Distribution for 150mm Carbonate Slab

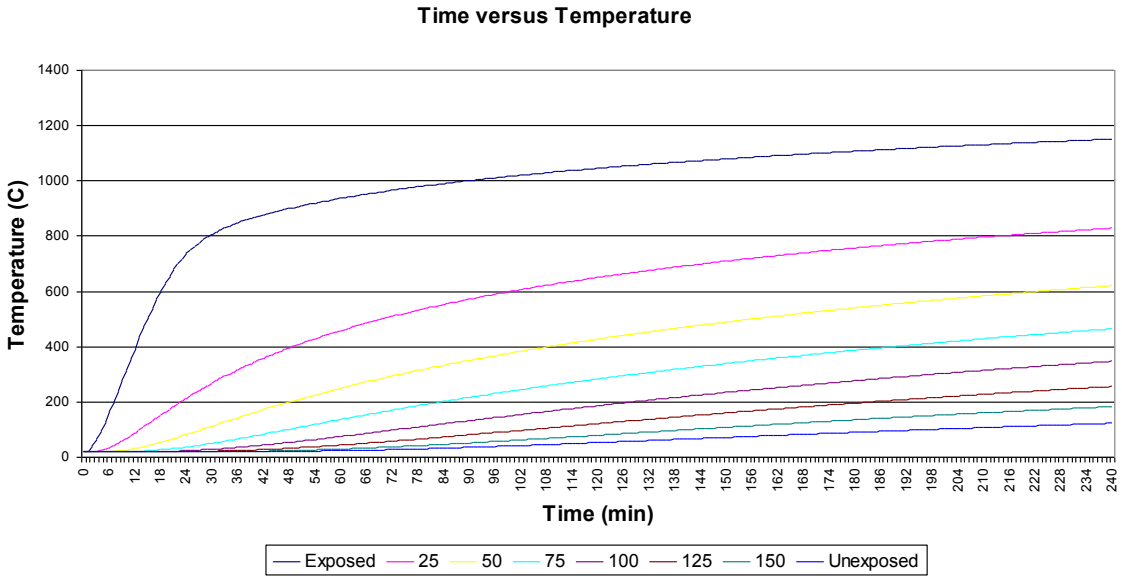

Figure E.14: Temperature Distribution for 175mm Carbonate Slab

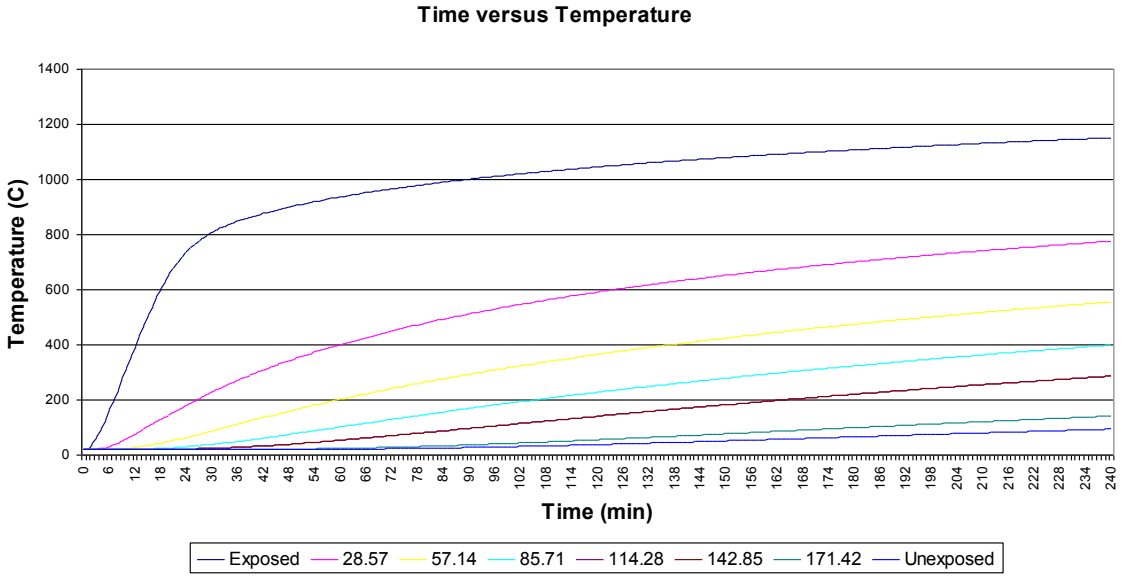

Figure E.15: Temperature Distribution for 200mm Carbonate Slab

E.2.2 ASTM E119

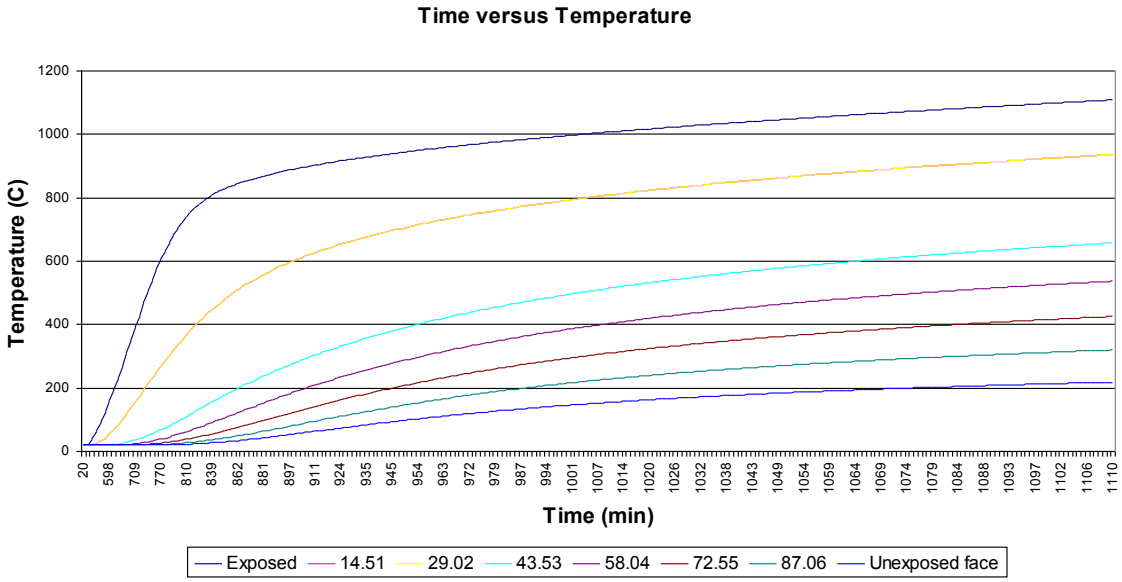

Figure E.16: Temperature Distribution for 4 inch Carbonate Slab

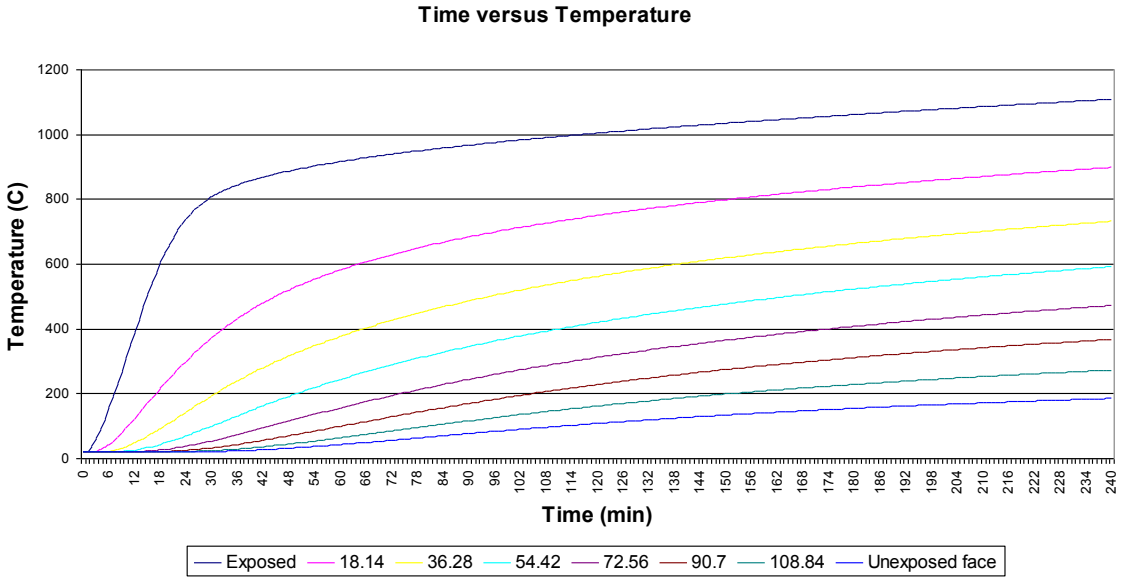

Figure E.17: Temperature Distribution for 5 inch Carbonate Slab

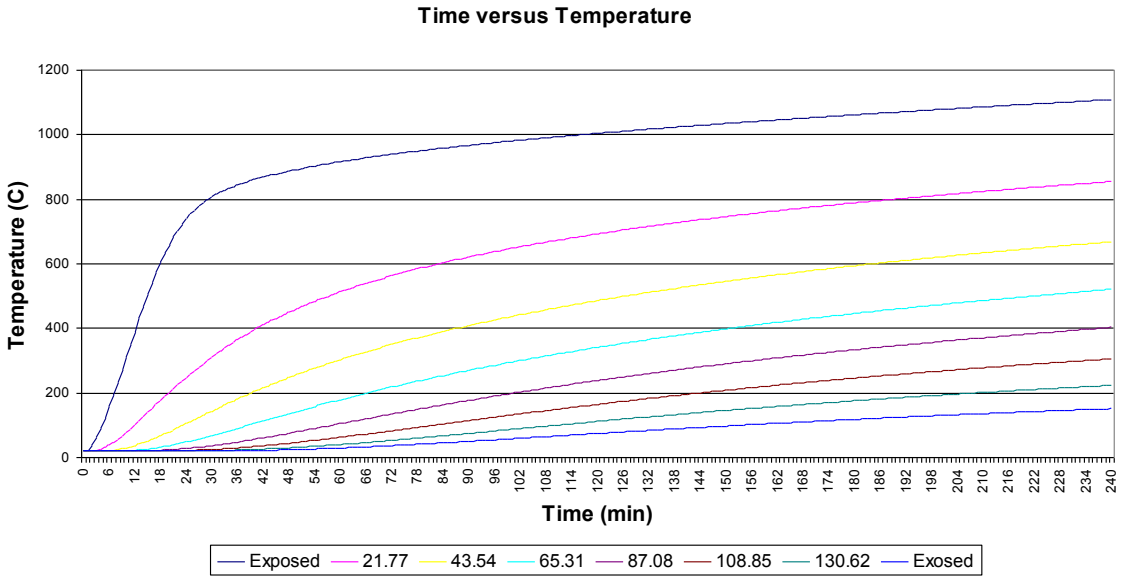

Figure E.18: Temperature Distribution for 6 inch Carbonate Slab

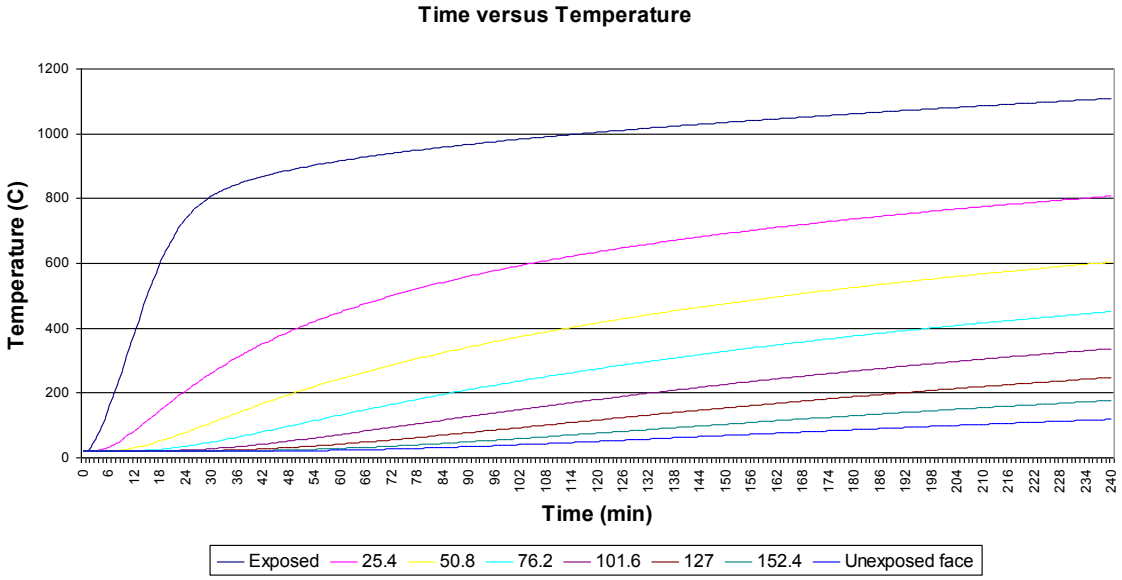

Figure E.19: Temperature Distribution for 7 inch Carbonate Slab

E.2.3 SDHI-95

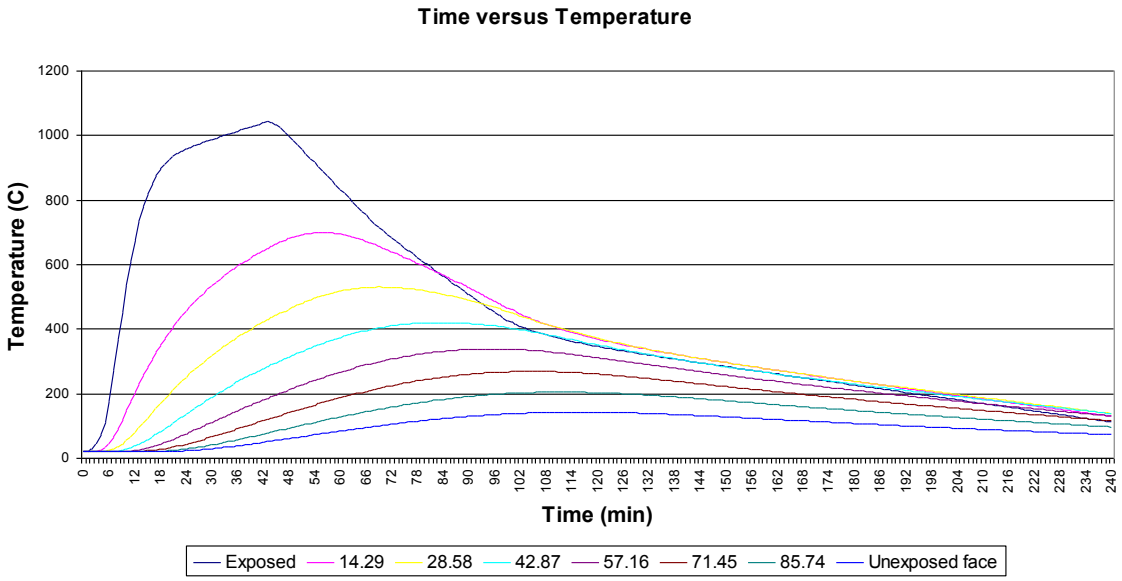

Figure E.20: Temperature Distribution for 100mm Carbonate Slab

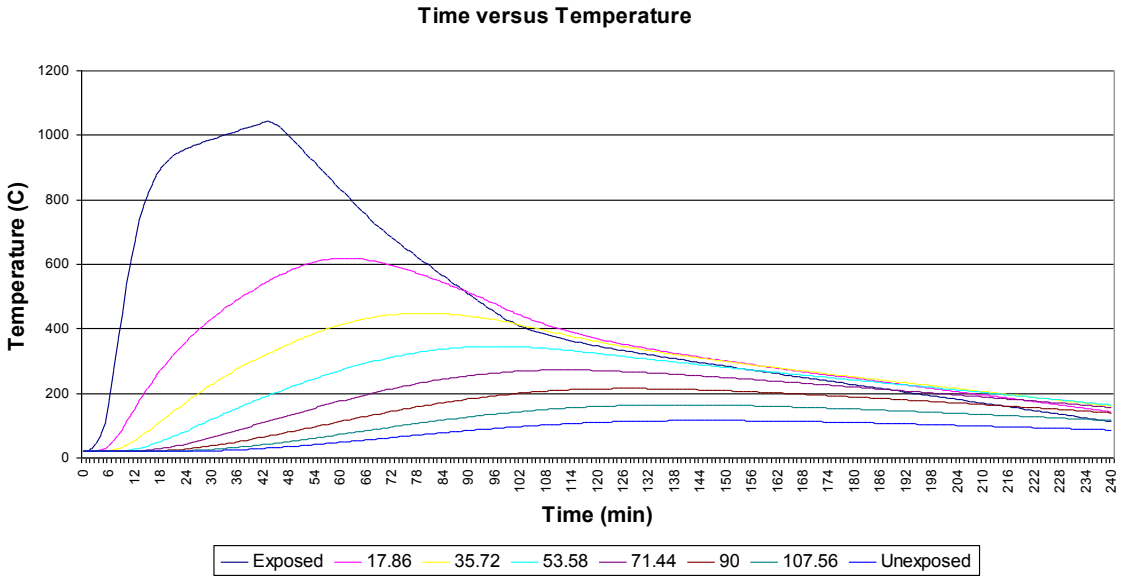

Figure E.21: Temperature Distribution for 125mm Carbonate Slab

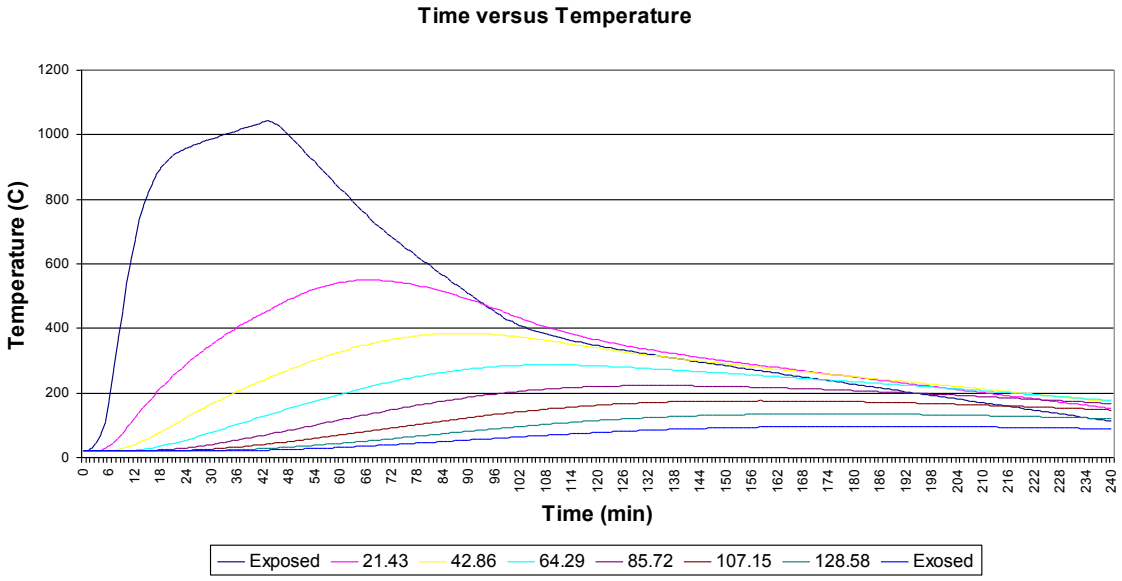

Figure E.22: Temperature Distribution for 150mm Carbonate Slab

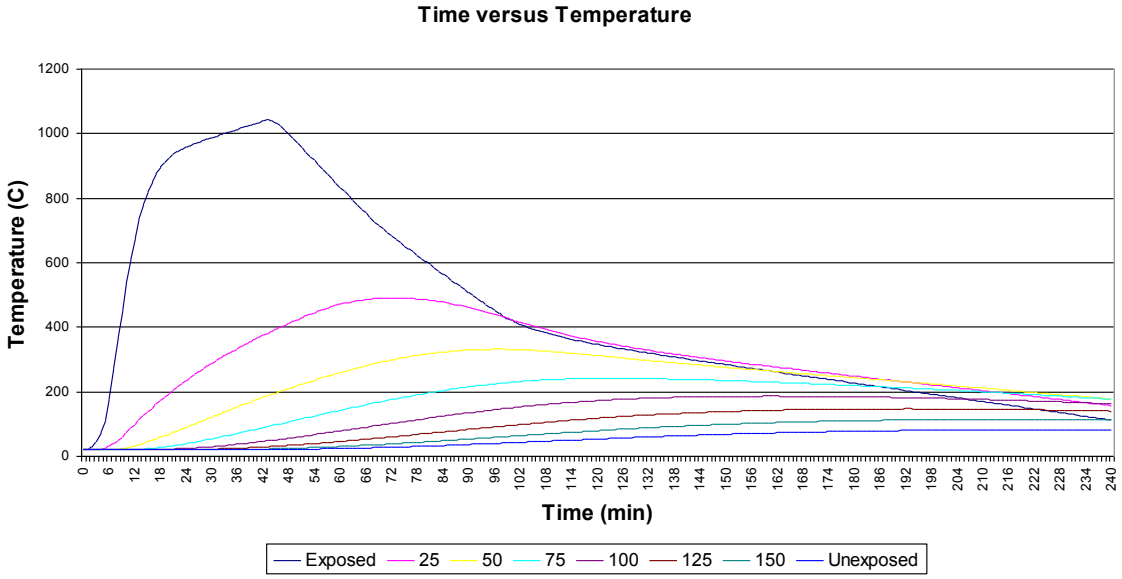

Figure E.23: Temperature Distribution for 175mm Carbonate Slab

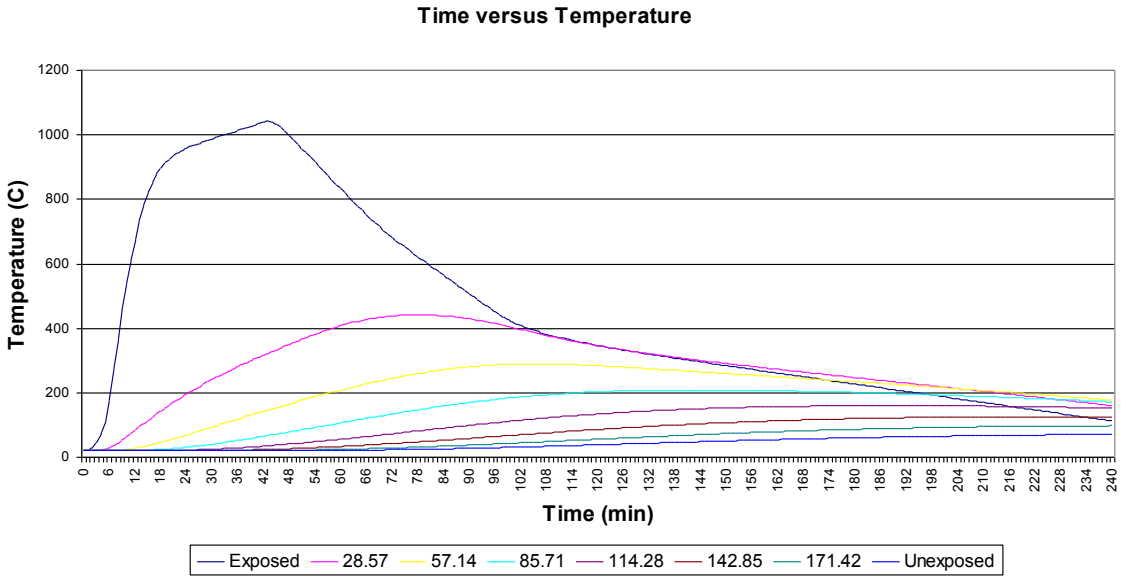

Figure E.24: Temperature Distribution for 200mm Carbonate Slab

E.2.4 LDMI-M

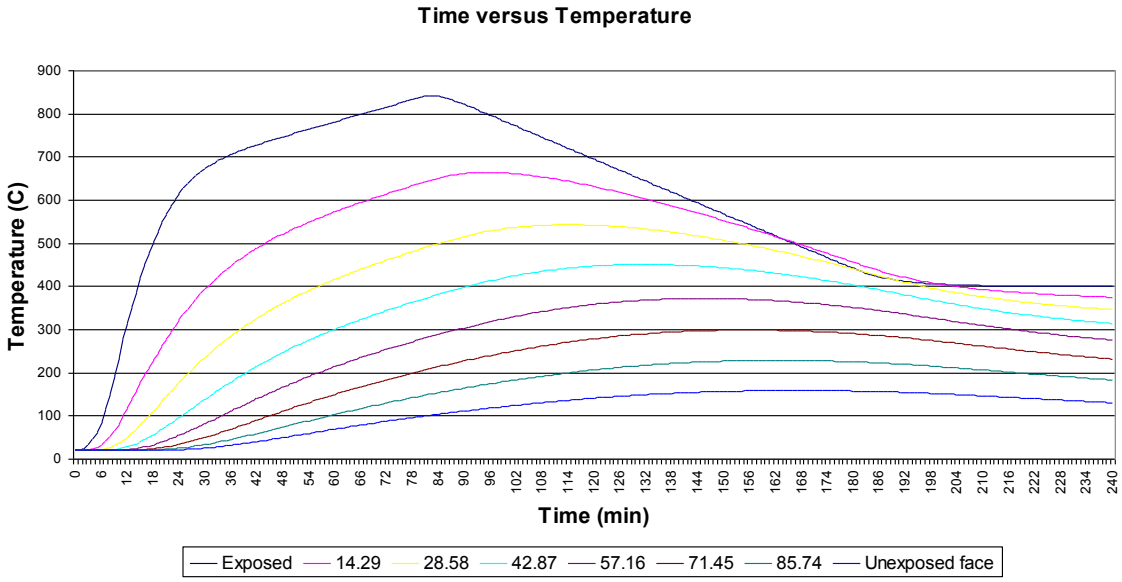

Figure E.25: Temperature Distribution for 100mm Carbonate Slab

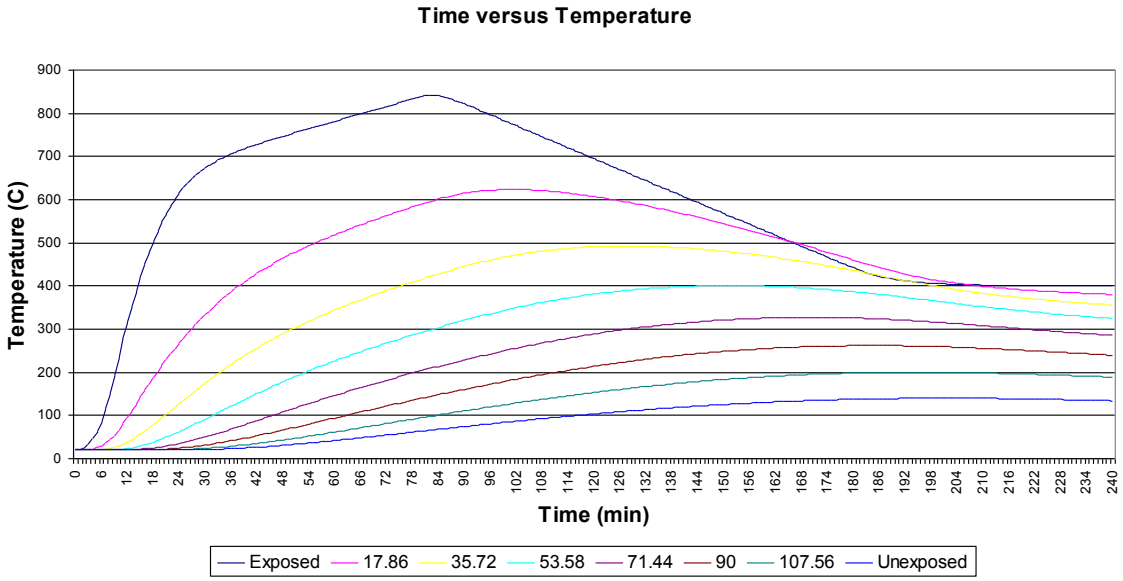

Figure E.26: Temperature Distribution for 125mm Carbonate Slab

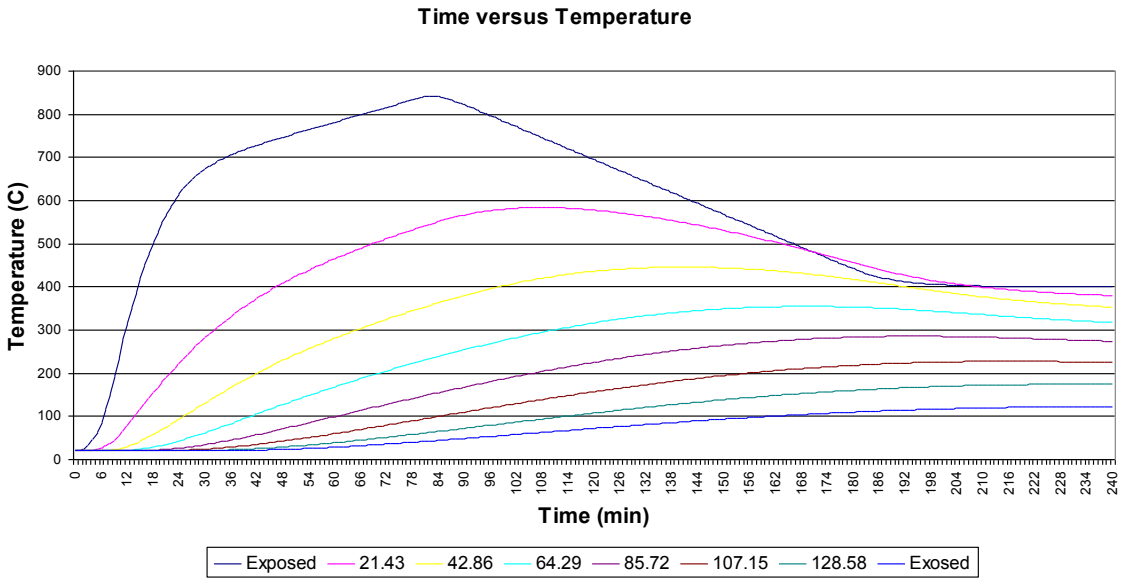

Figure E.27: Temperature Distribution for 150mm Carbonate Slab

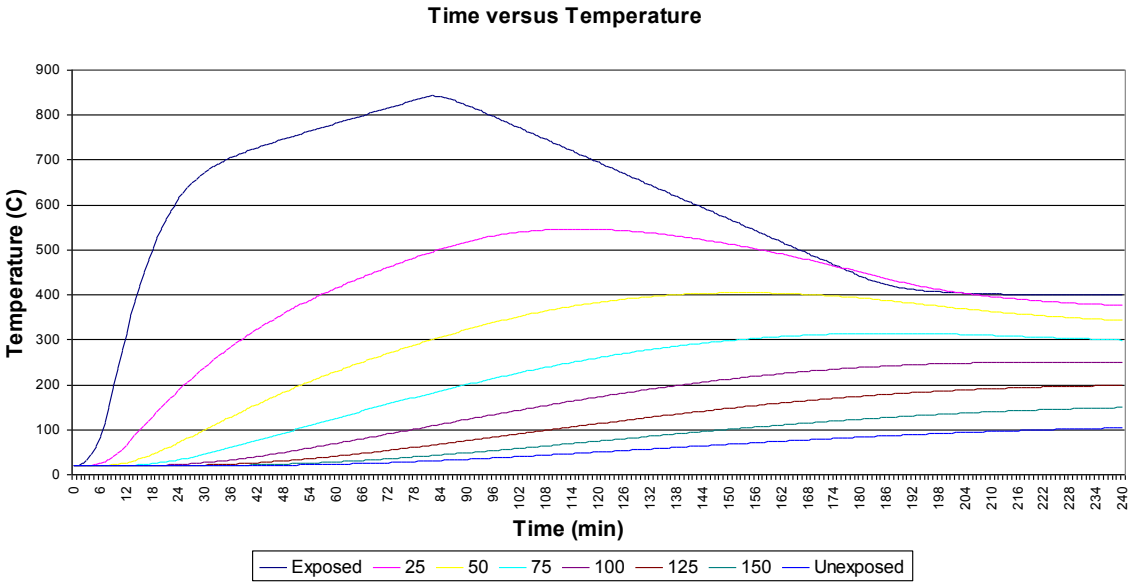

Figure E.28: Temperature Distribution for 175mm Carbonate Slab

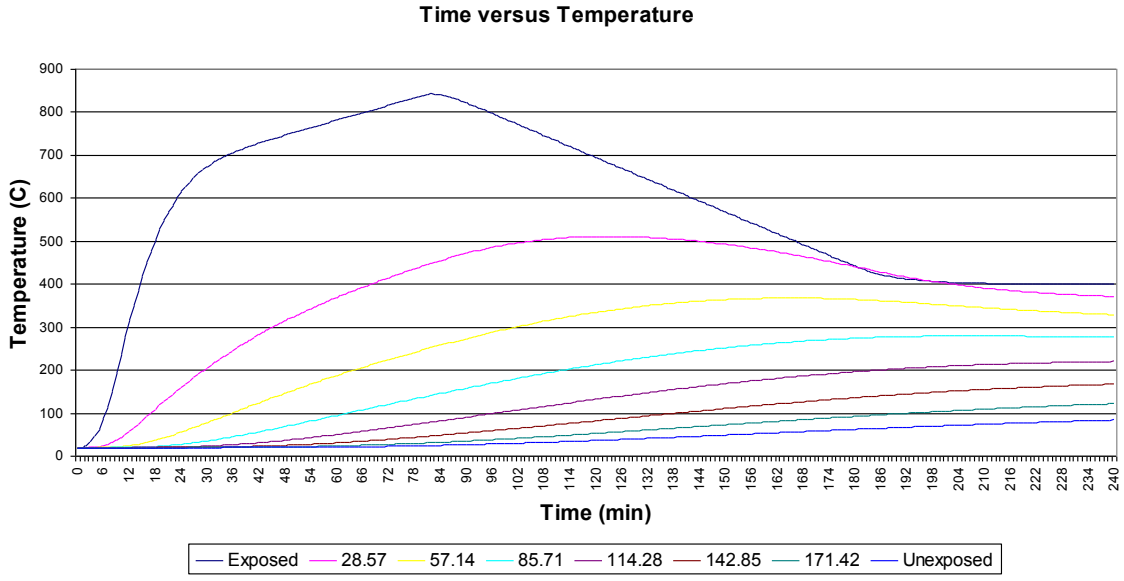

Figure E.29: Temperature Distribution for 200mm Carbonate Slab

E.3 Shale

E.3.1 ISO 834

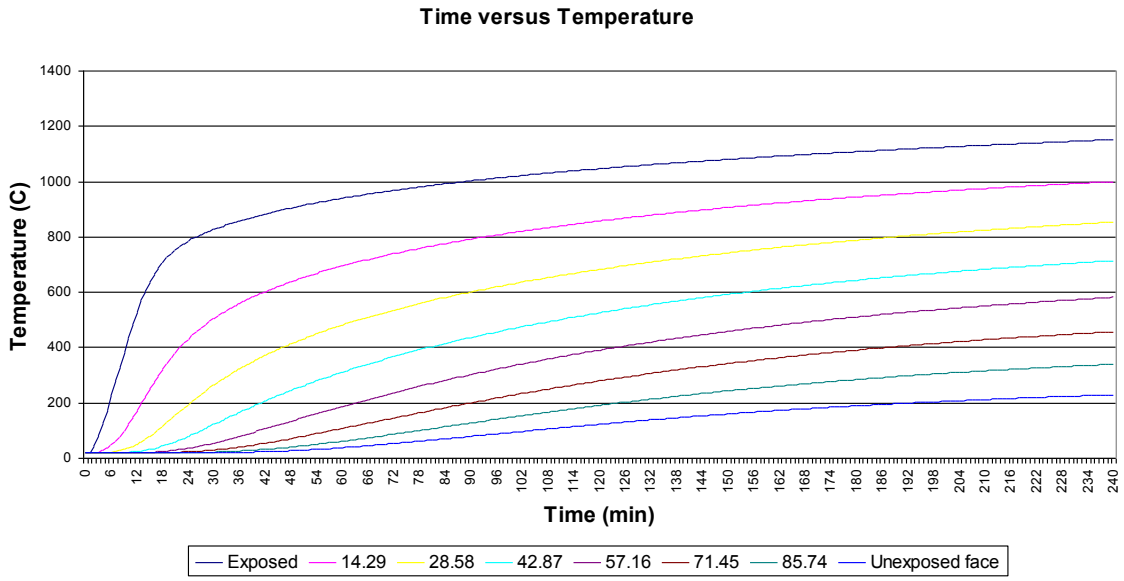

Figure E.30: Temperature Distribution for 100mm Shale Slab

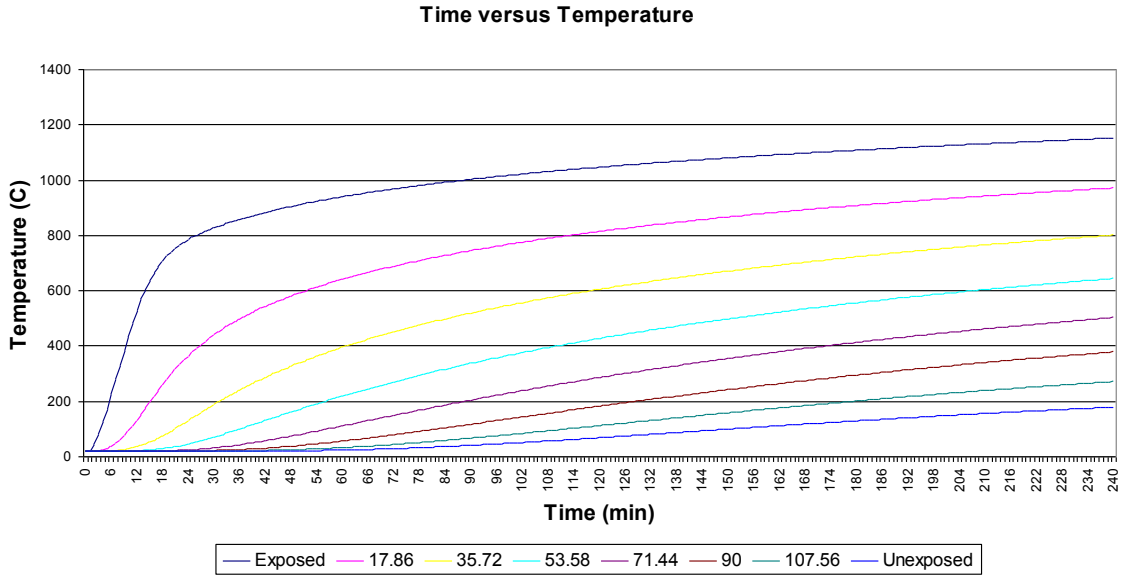

Figure E.31: Temperature Distribution for 125mm Shale Slab

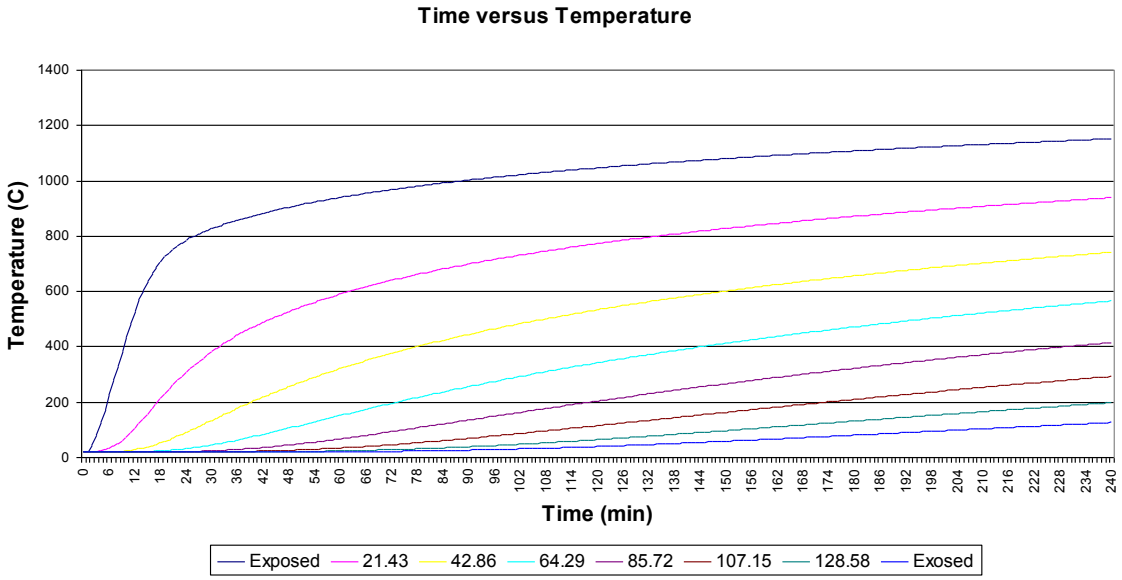

Figure E.32: Temperature Distribution for 150mm Shale Slab

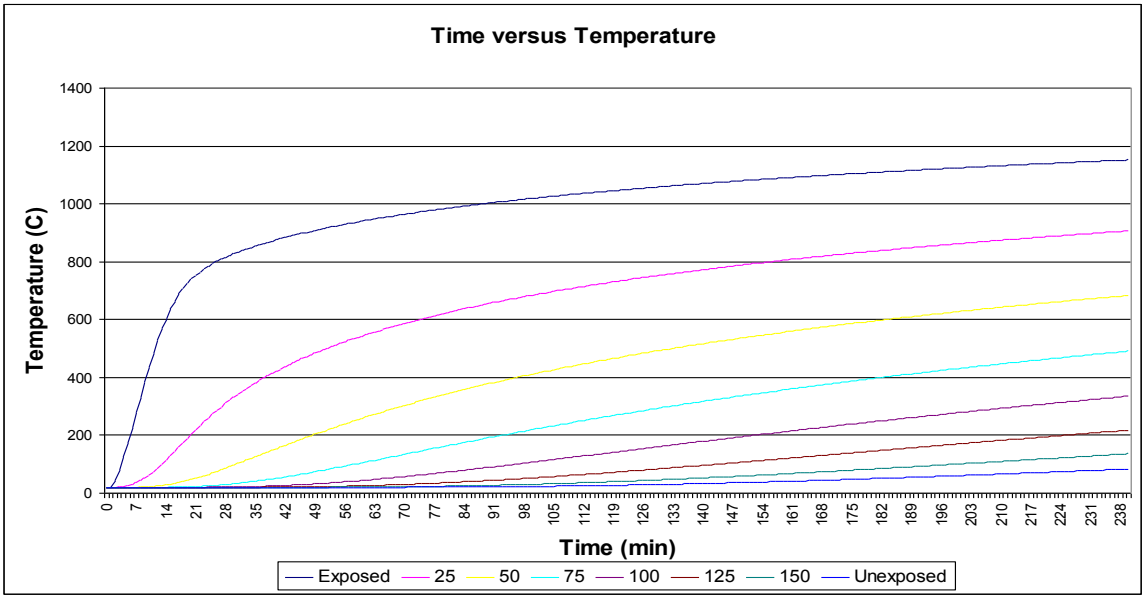

Figure E.33: Temperature Distribution for 175mm Shale Slab

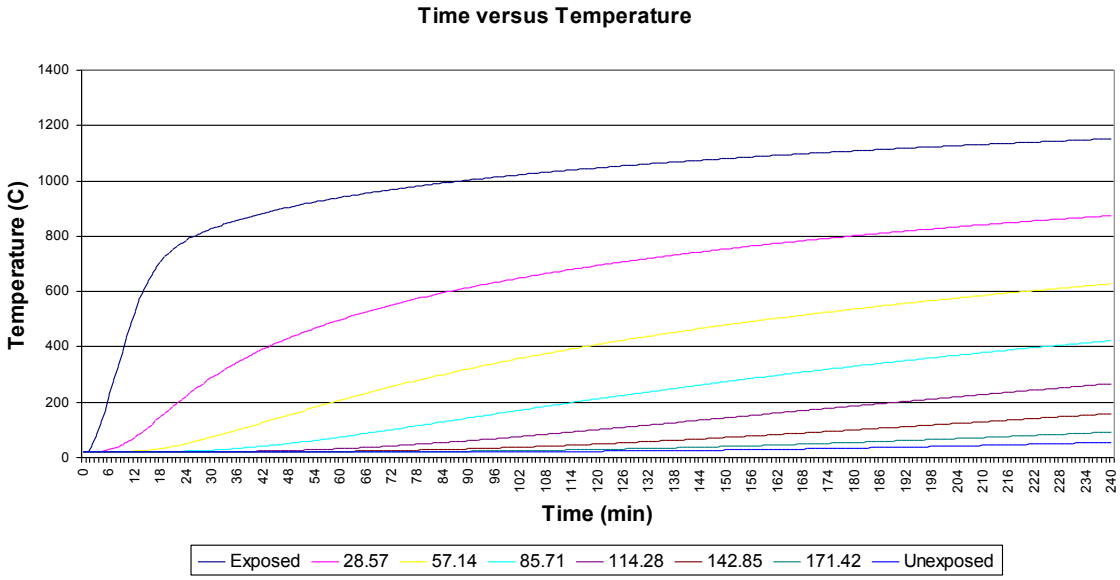

Figure E.34: Temperature Distribution for 200mm Shale Slab

E.3.2 ASTM E119

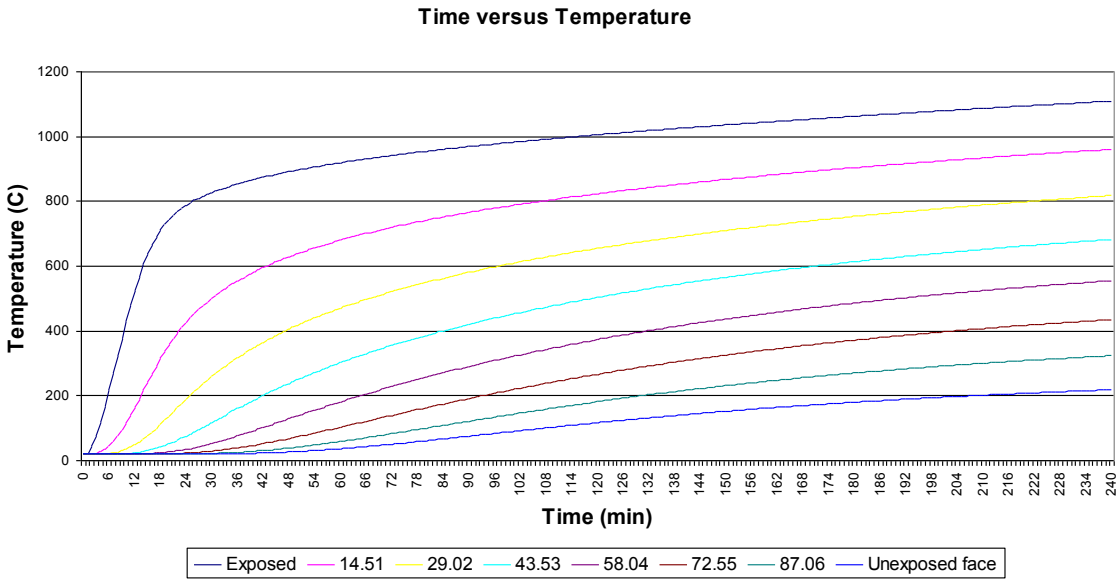

Figure E.35: Temperature Distribution for 4 inch Shale Slab

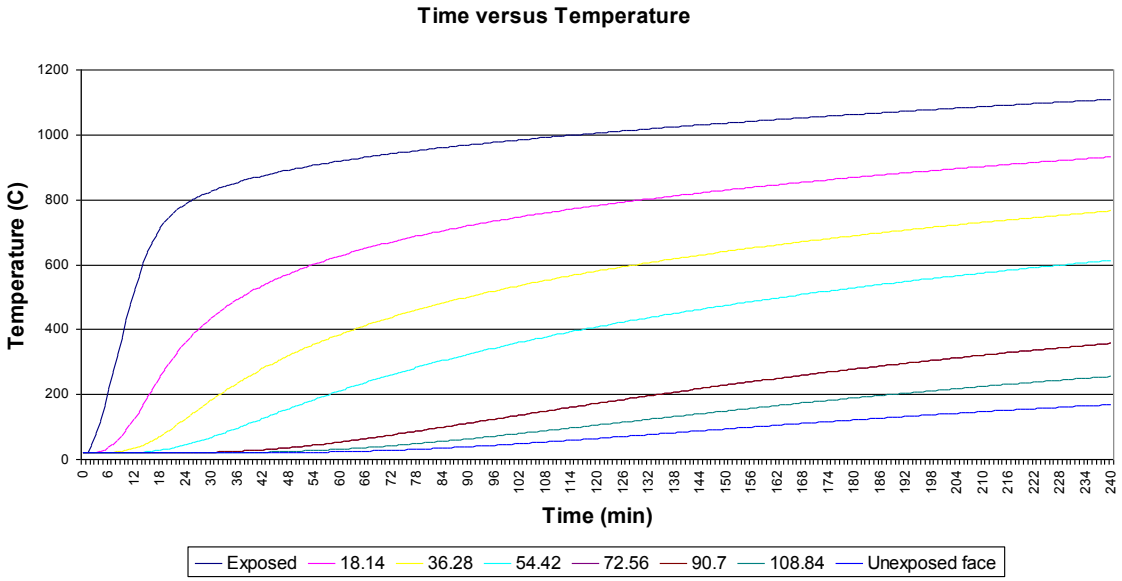

Figure E.36: Temperature Distribution for 5 inch Shale Slab

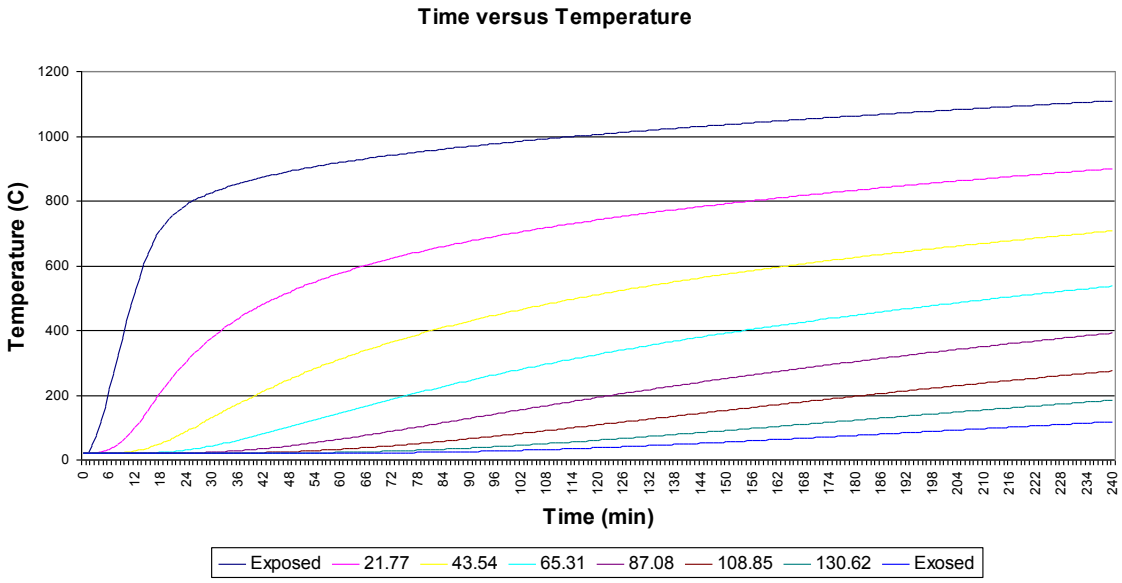

Figure E.37: Temperature Distribution for 6 inch Shale Slab

E.3.3 SDHI-95

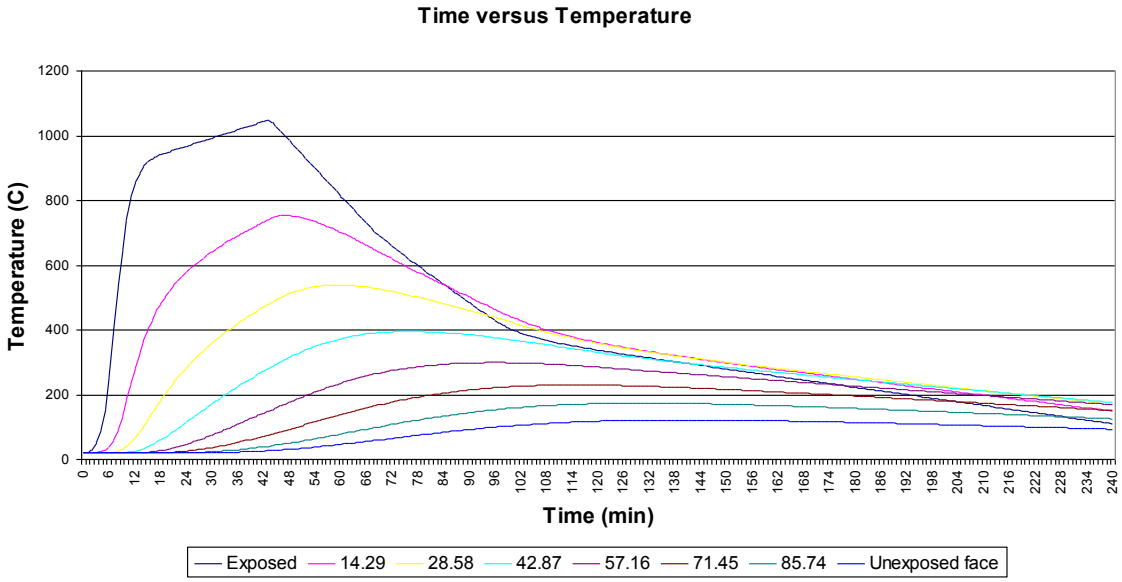

Figure E.38: Temperature Distribution for 100mm Shale Slab

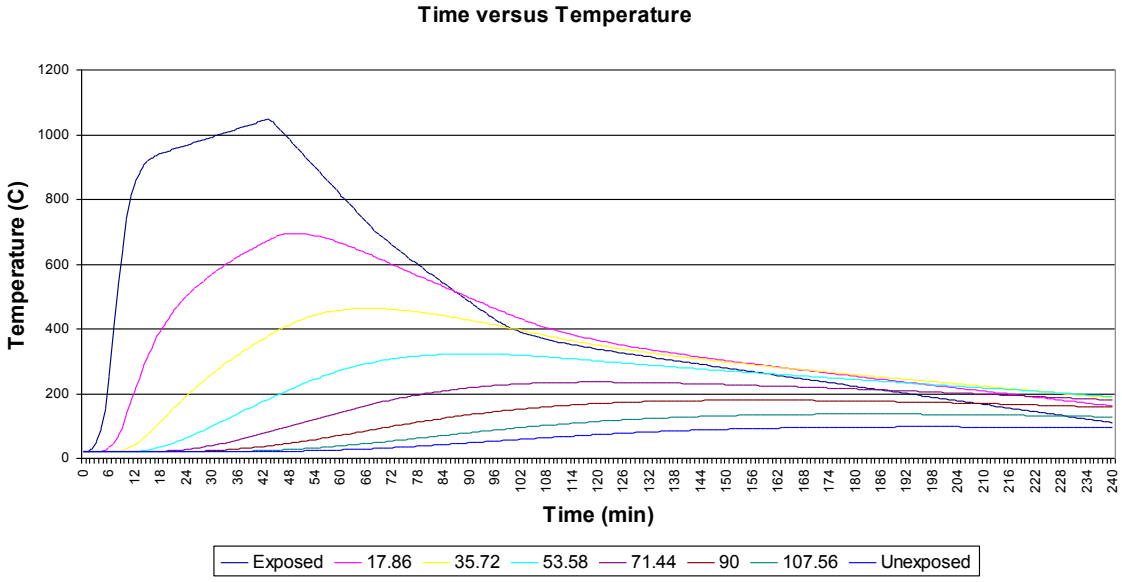

Figure E.39: Temperature Distribution for 125mm Shale Slab

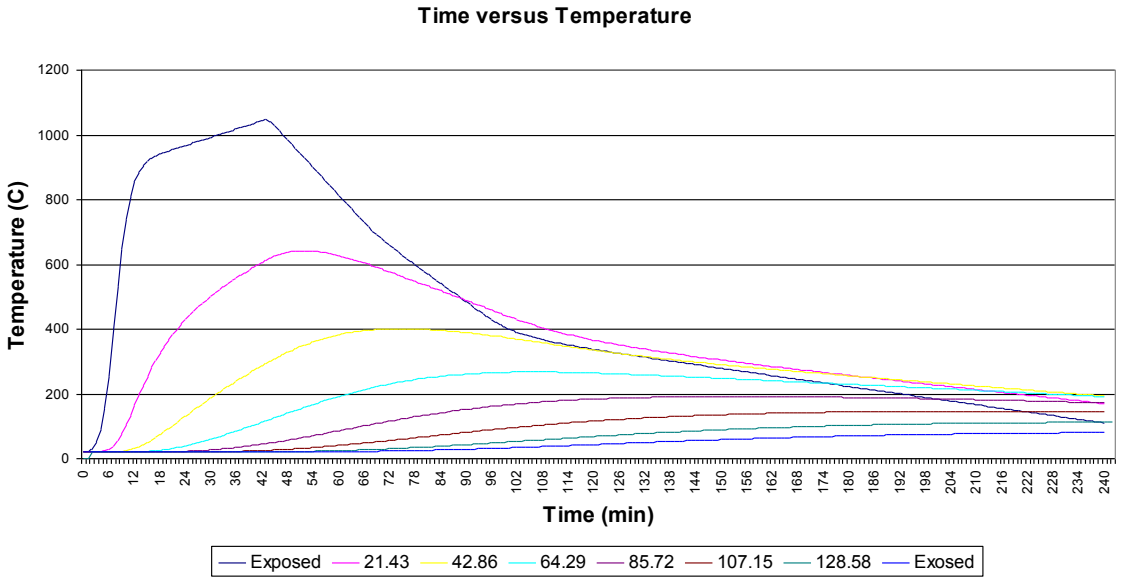

Figure E.40: Temperature Distribution for 150mm Shale Slab

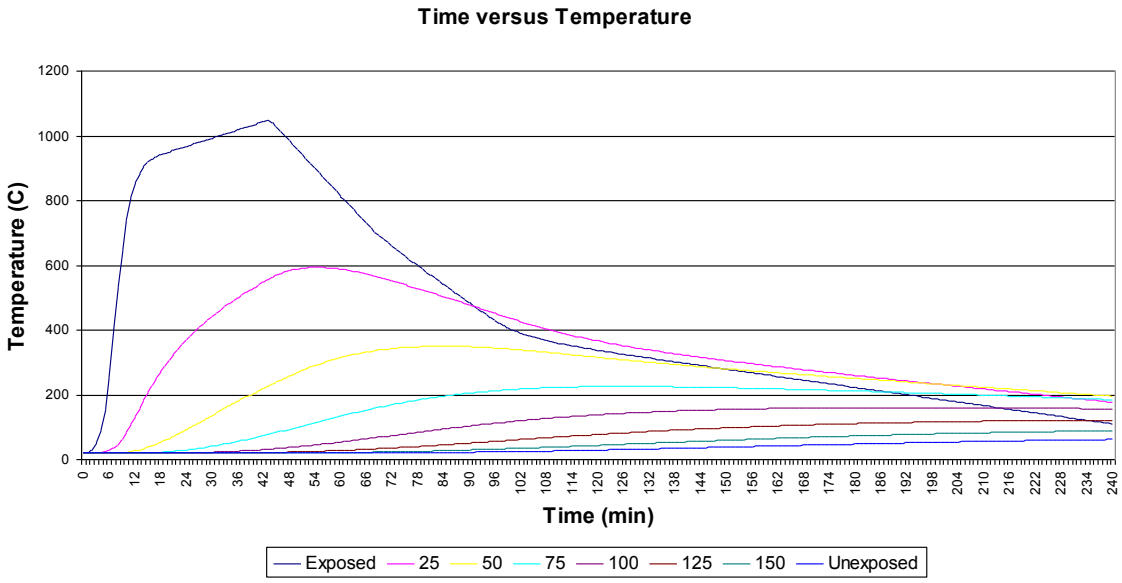

Figure E.41: Temperature Distribution for 175mm Shale Slab

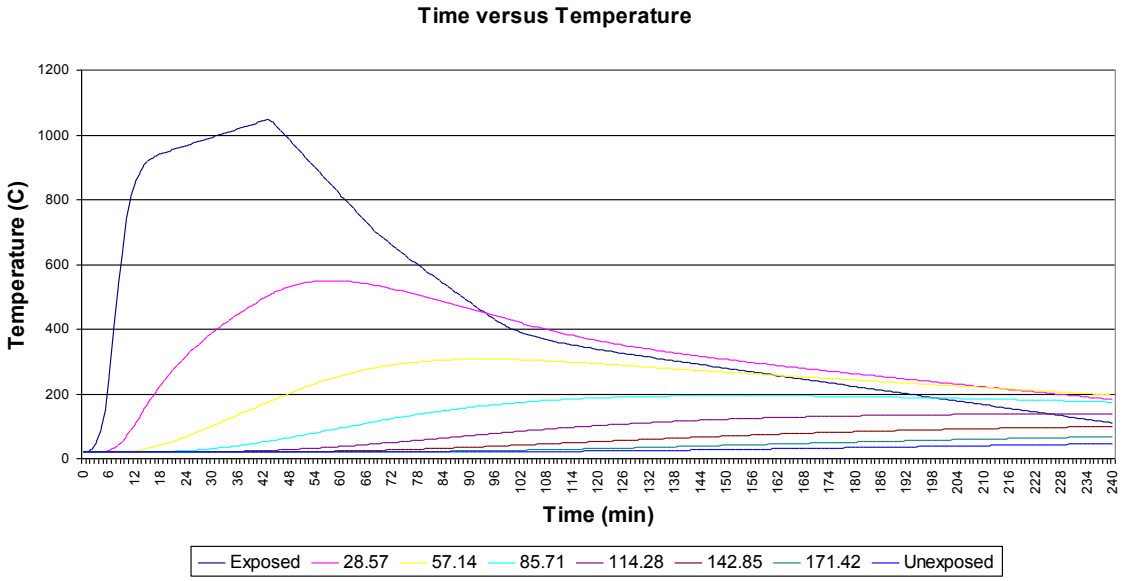

Figure E.42: Temperature Distribution for 200mm Shale Slab

E.3.4 LDMI-M

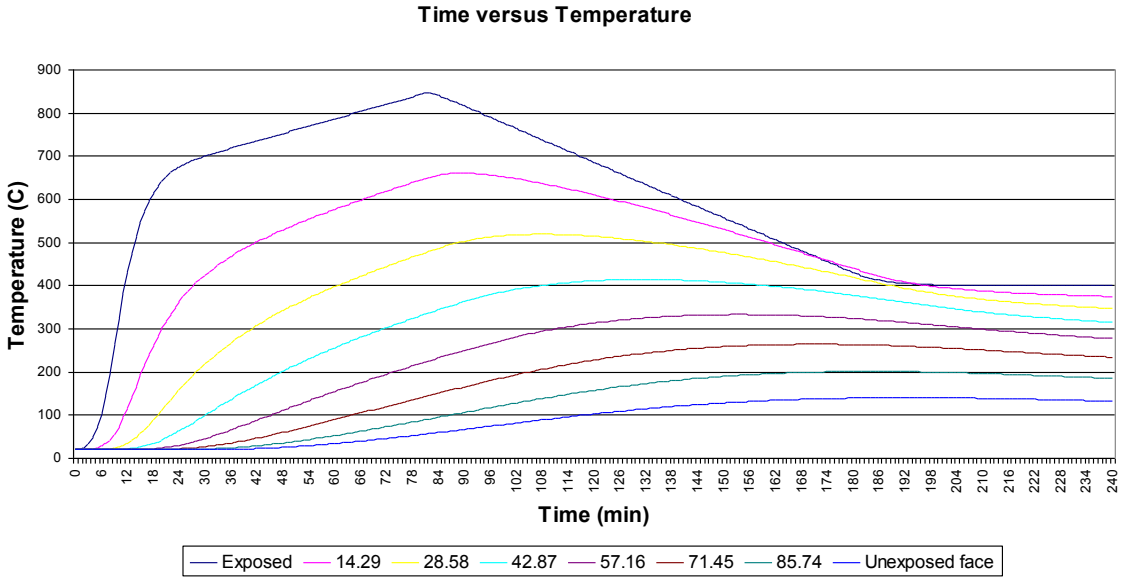

Figure E.43: Temperature Distribution for 100mm Shale Slab

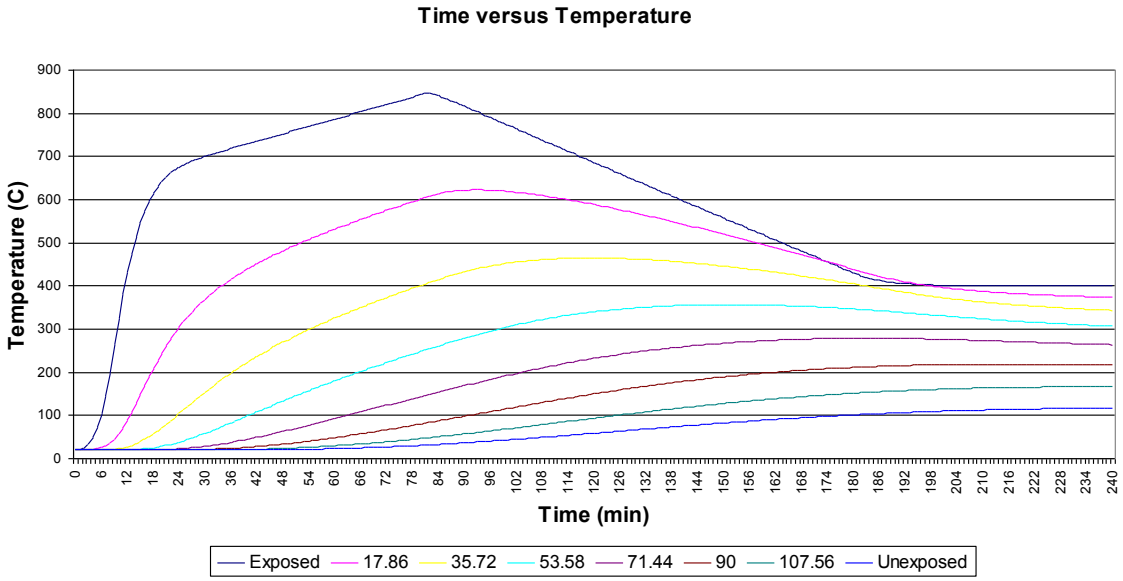

Figure E.44: Temperature Distribution for 125mm Shale Slab

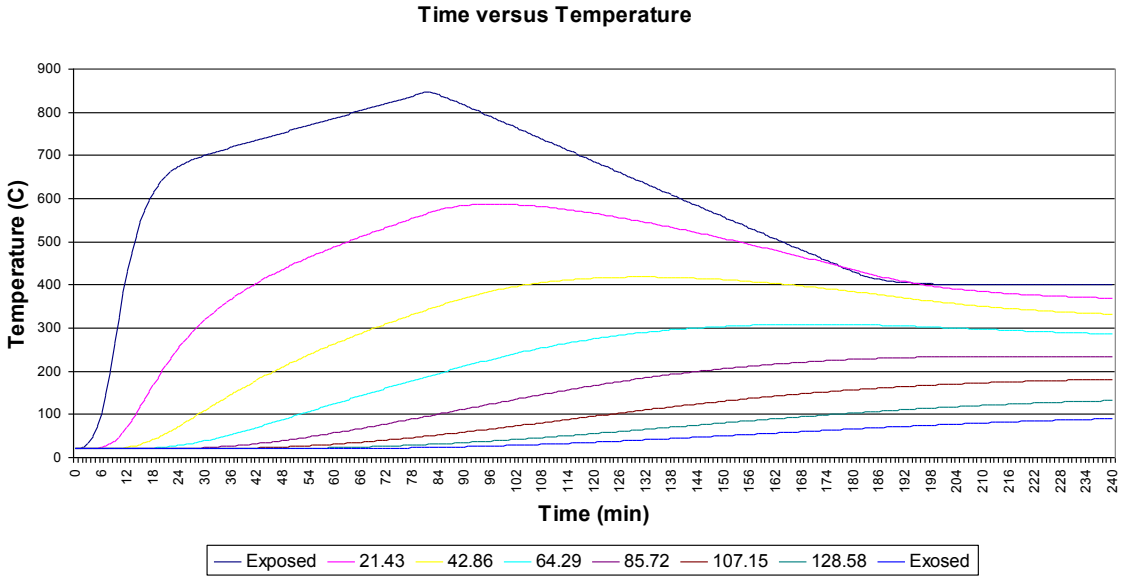

Figure E.45: Temperature Distribution for 150mm Shale Slab

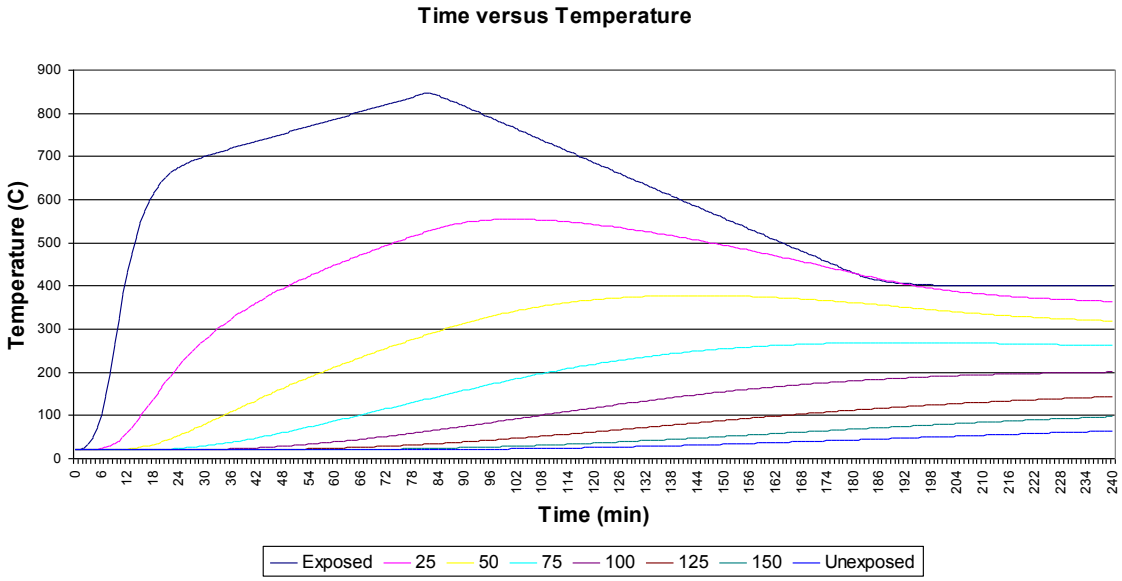

Figure E.46: Temperature Distribution for 175mm Shale Slab

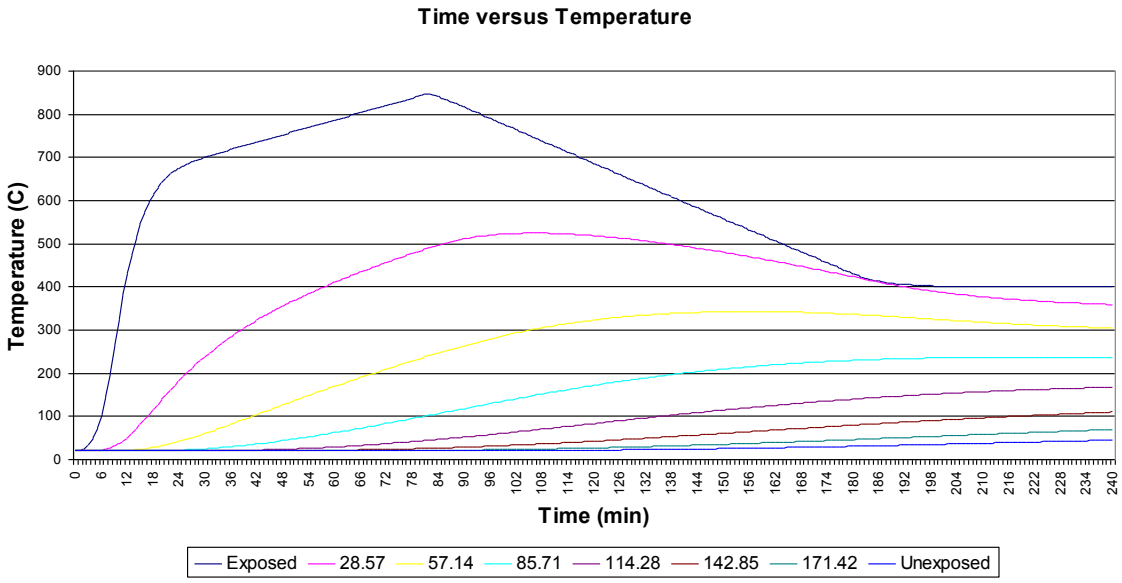

Figure E.47: Temperature Distribution for 200mm Shale Slab

E.4 Siliceous

E.4.1 ISO 834

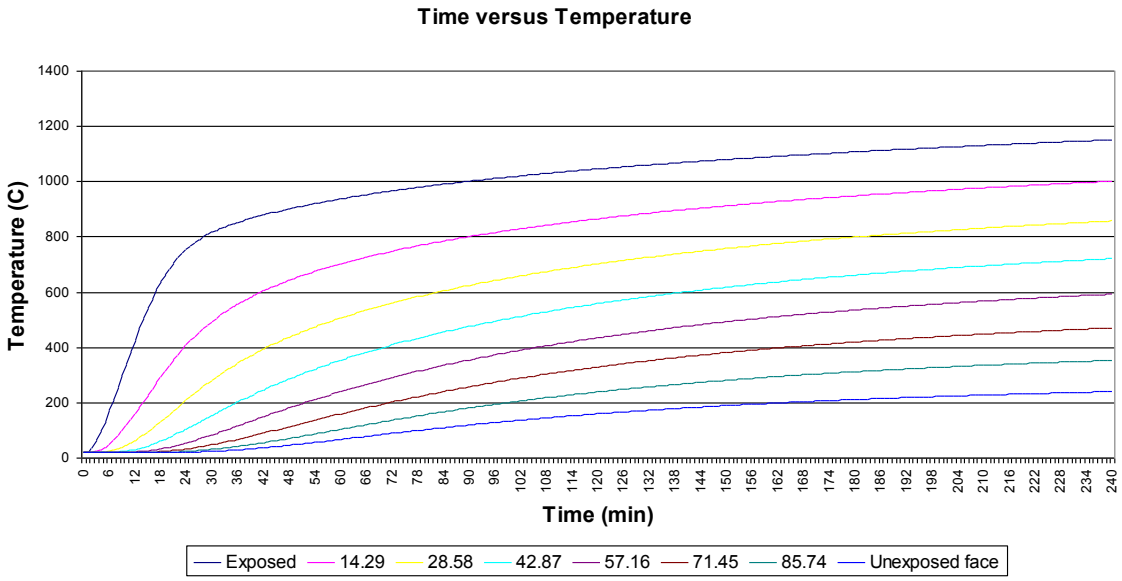

Figure E.48: Temperature Distribution for 100mm Siliceous Slab

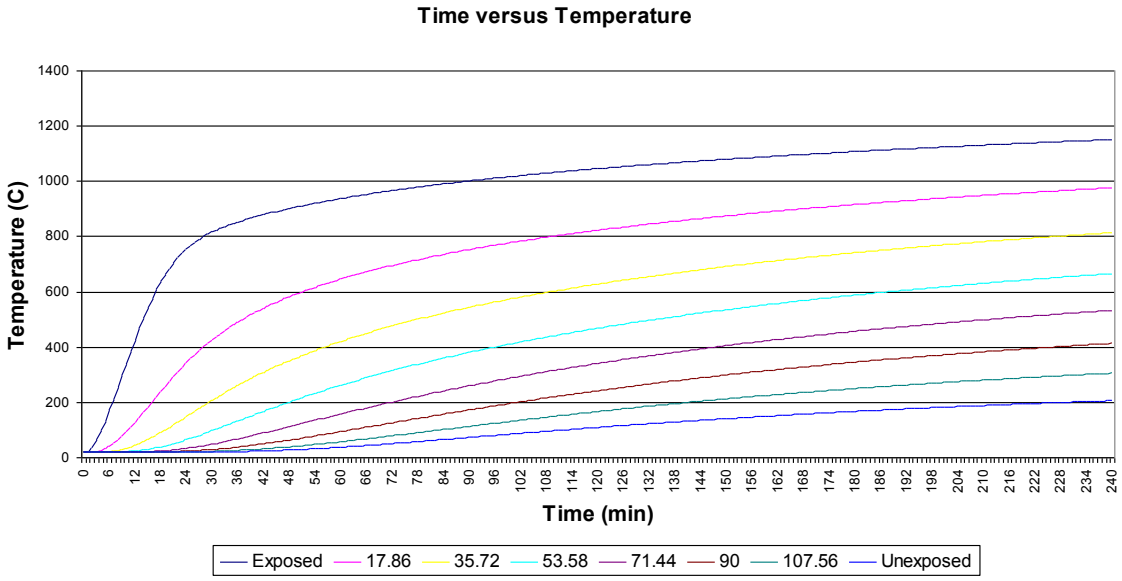

Figure E.49: Temperature Distribution for 125mm Siliceous Slab

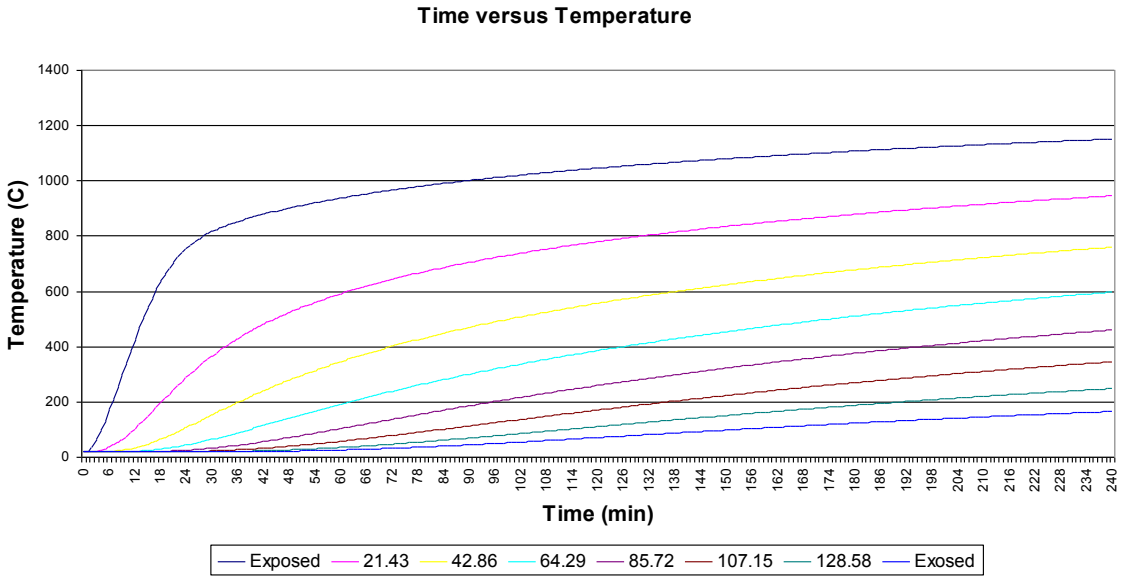

Figure E.50: Temperature Distribution for 150mm Siliceous Slab

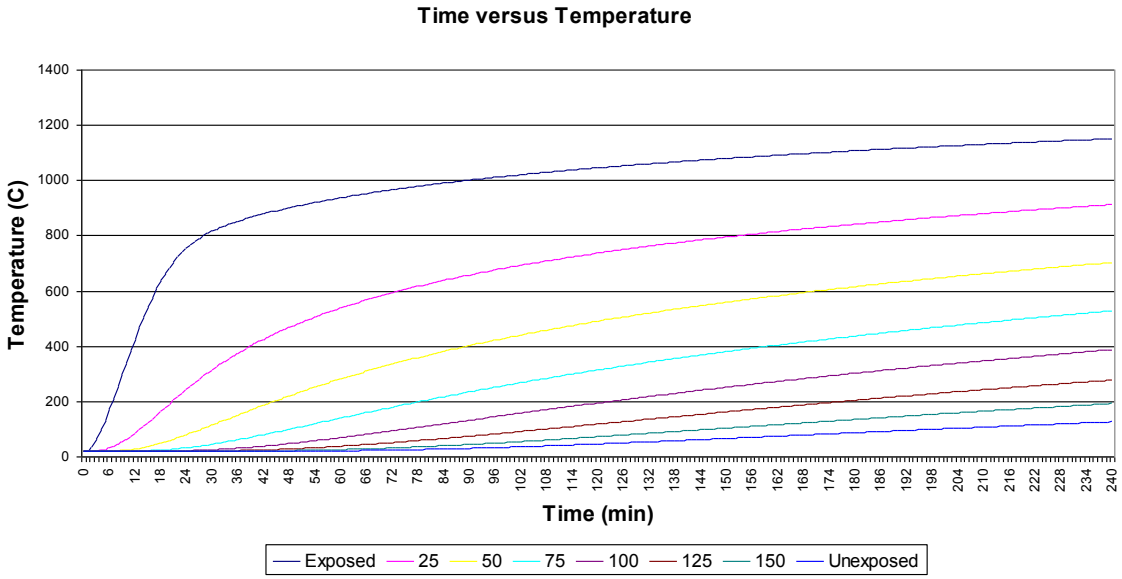

Figure E.51: Temperature Distribution for 175mm Siliceous Slab

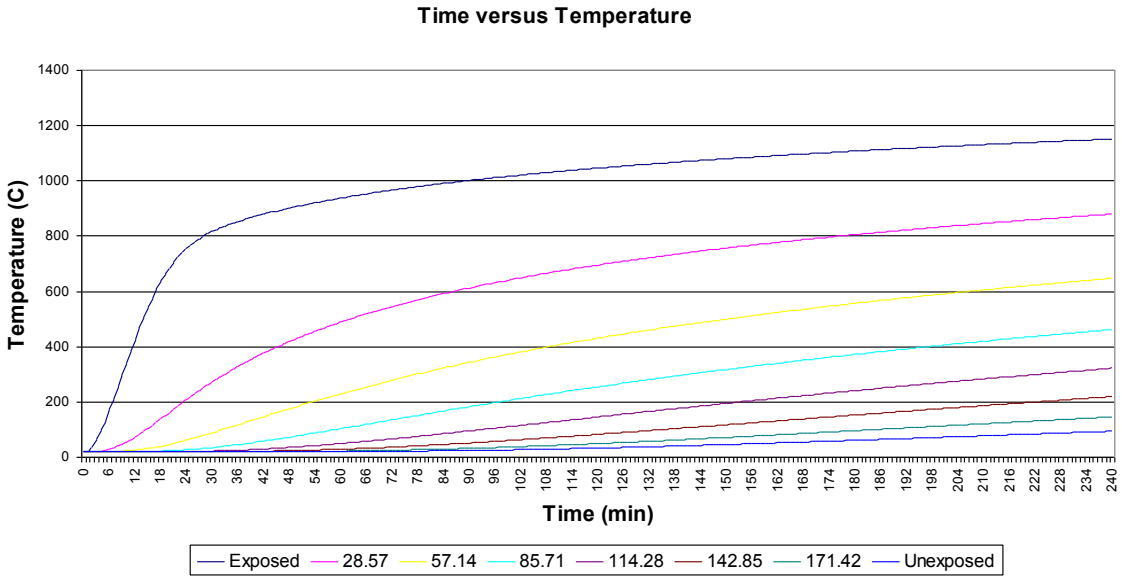

Figure E.52: Temperature Distribution for 200mm Siliceous Slab

E.4.2 ASTM E119

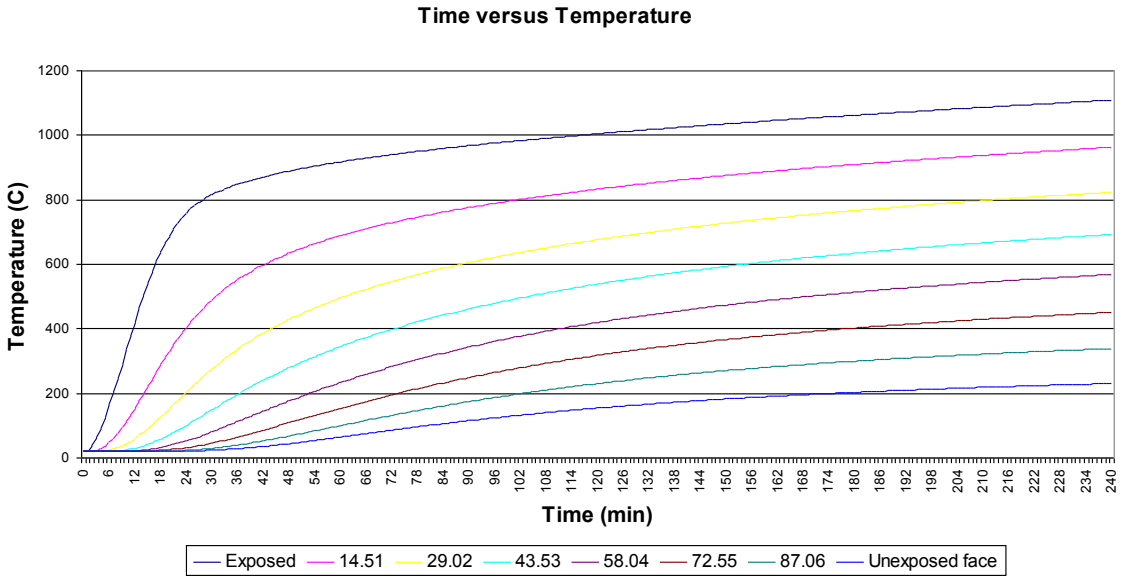

Figure E.53: Temperature Distribution for 4 inch Siliceous Slab

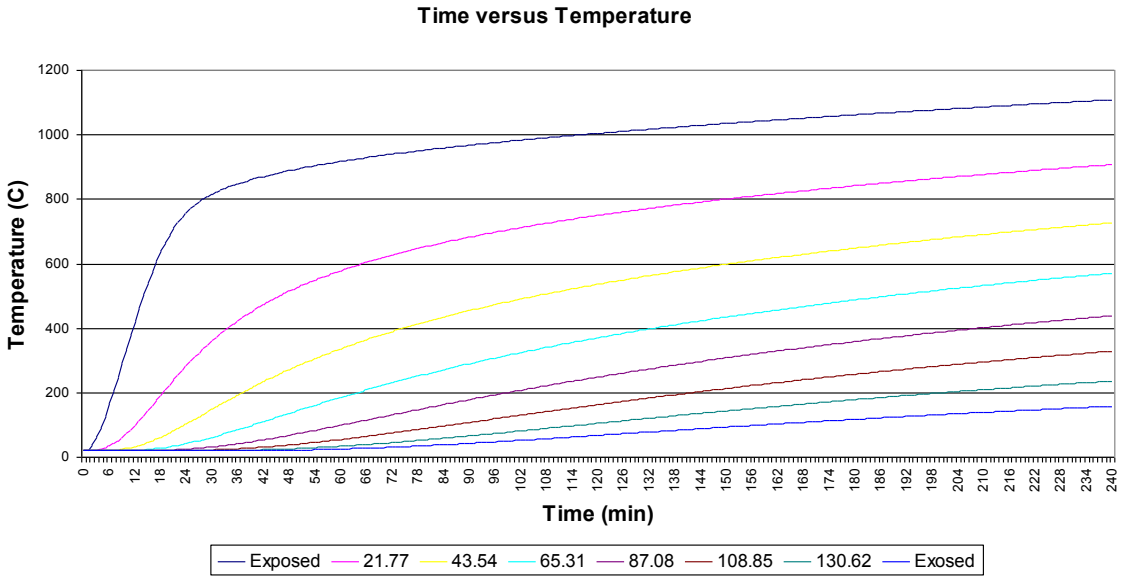

Figure E.54: Temperature Distribution for 6 inch Siliceous Slab

E.4.3 SDHI-95

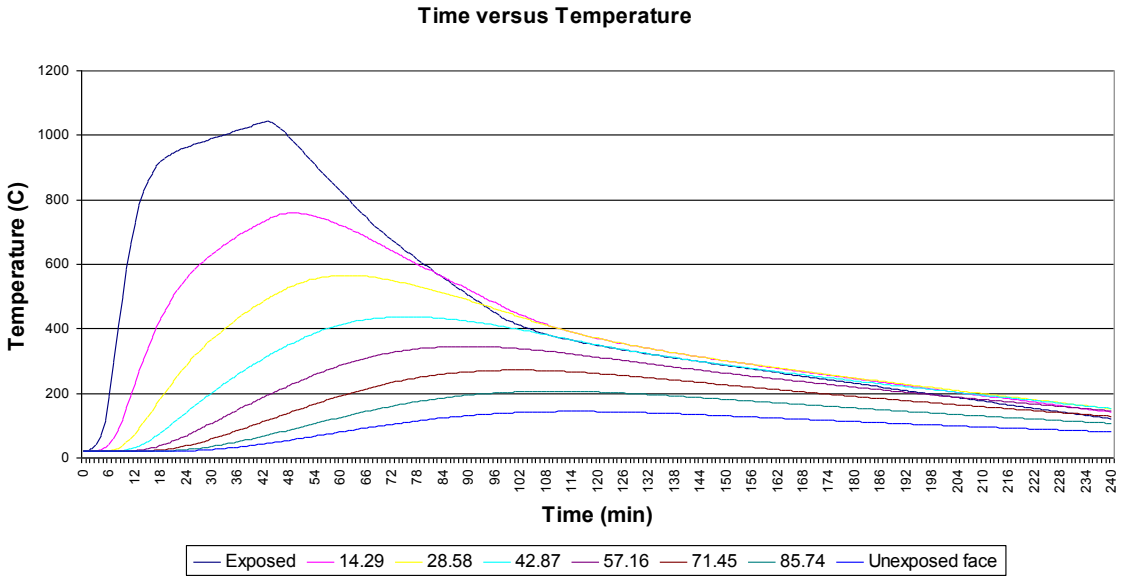

Figure E.55: Temperature Distribution for 100mm Siliceous Slab

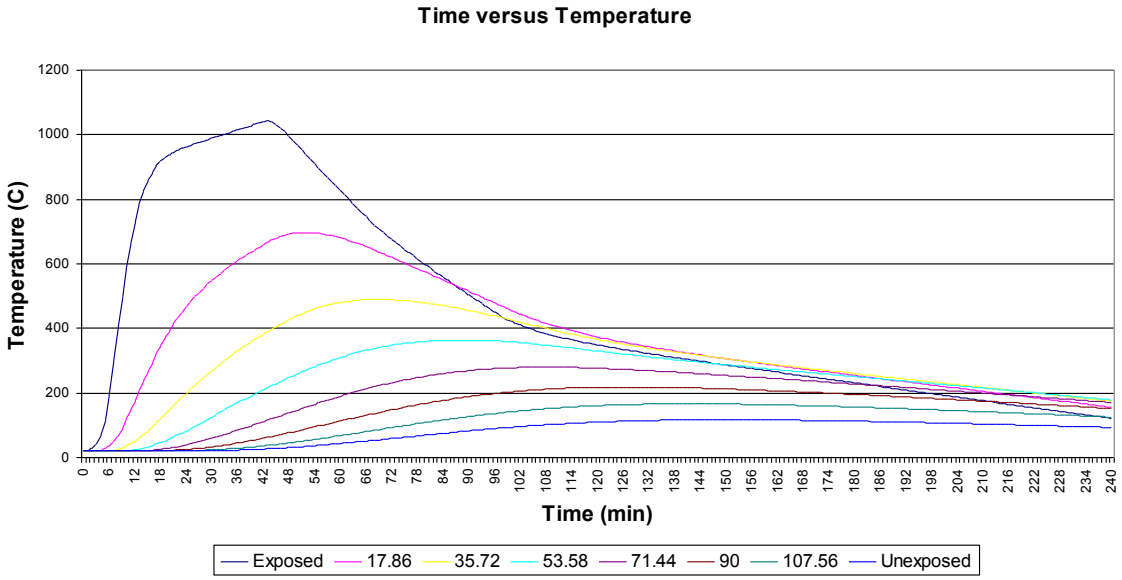

Figure E.56: Temperature Distribution for 125mm Siliceous Slab

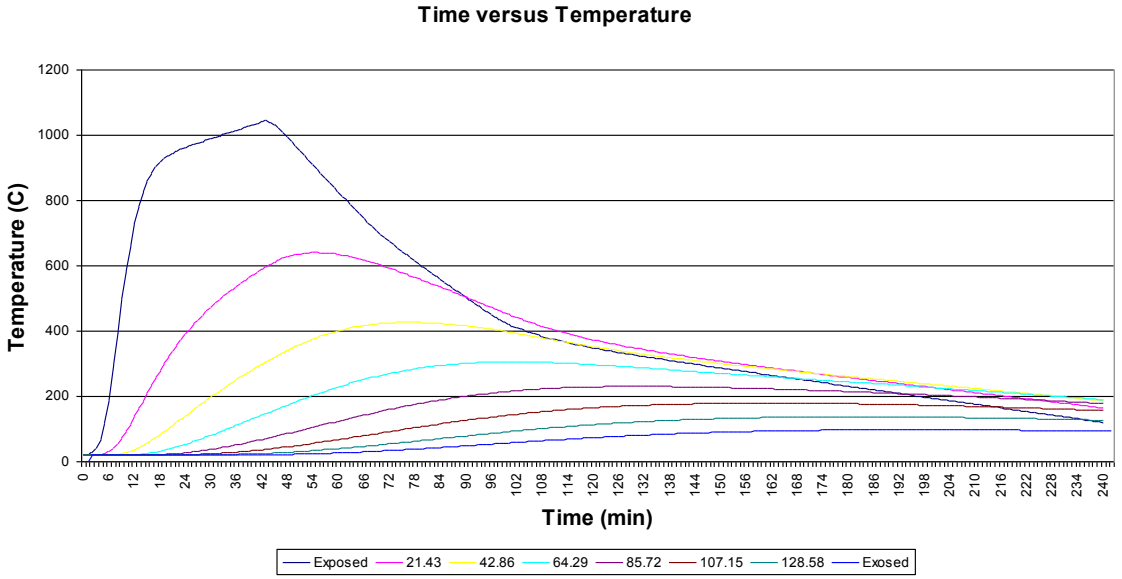

Figure E.57: Temperature Distribution for 150mm Siliceous Slab

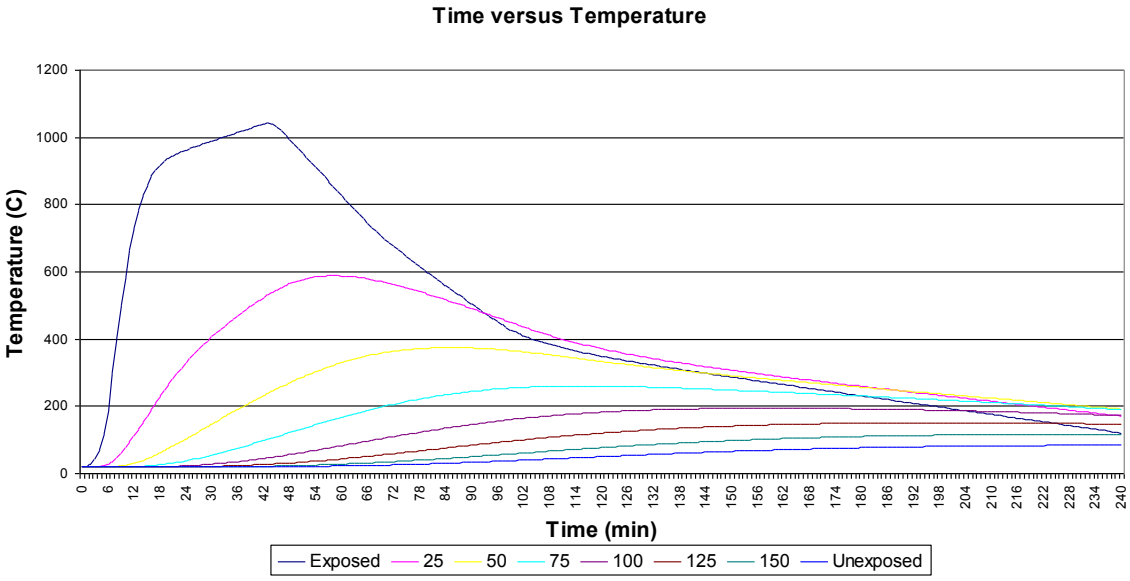

Figure E.58: Temperature Distribution for 175mm Siliceous Slab

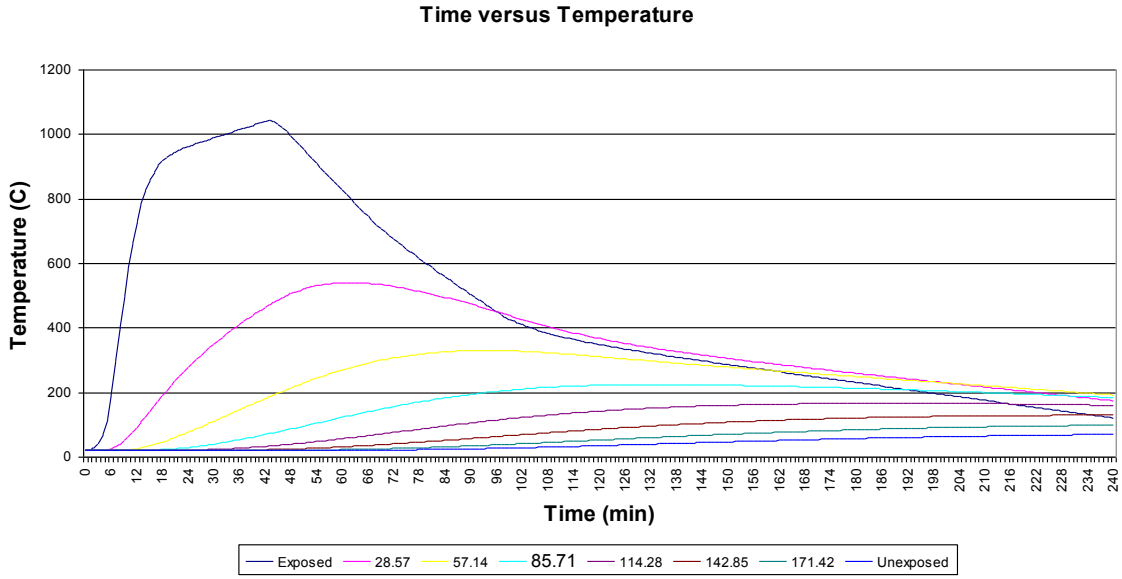

Figure E.59: Temperature Distribution for 200mm Siliceous Slab

E.4.4 LDMI-M

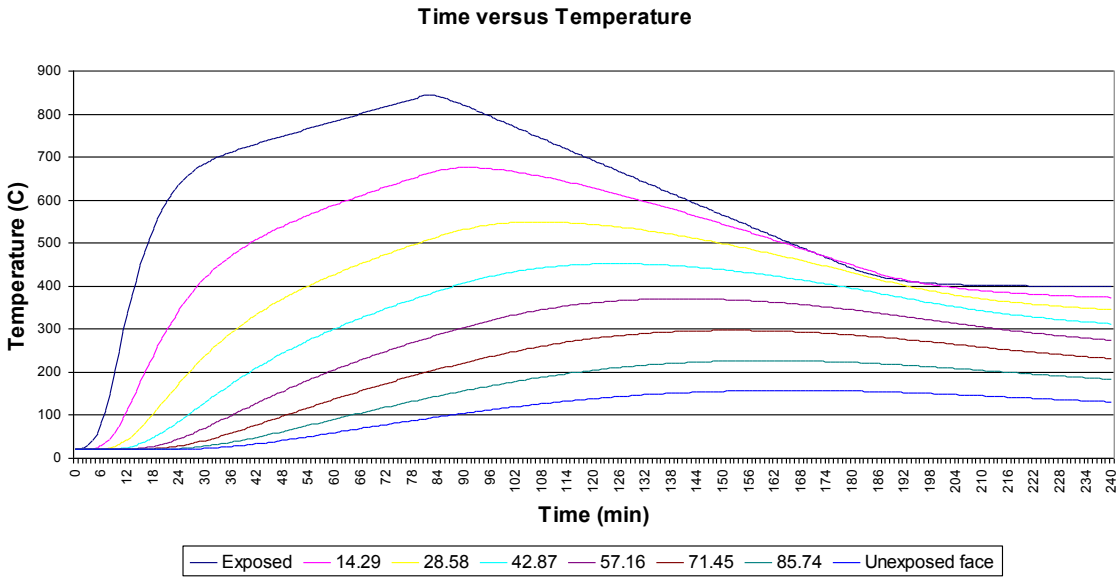

Figure E.60: Temperature Distribution for 100mm Siliceous Slab

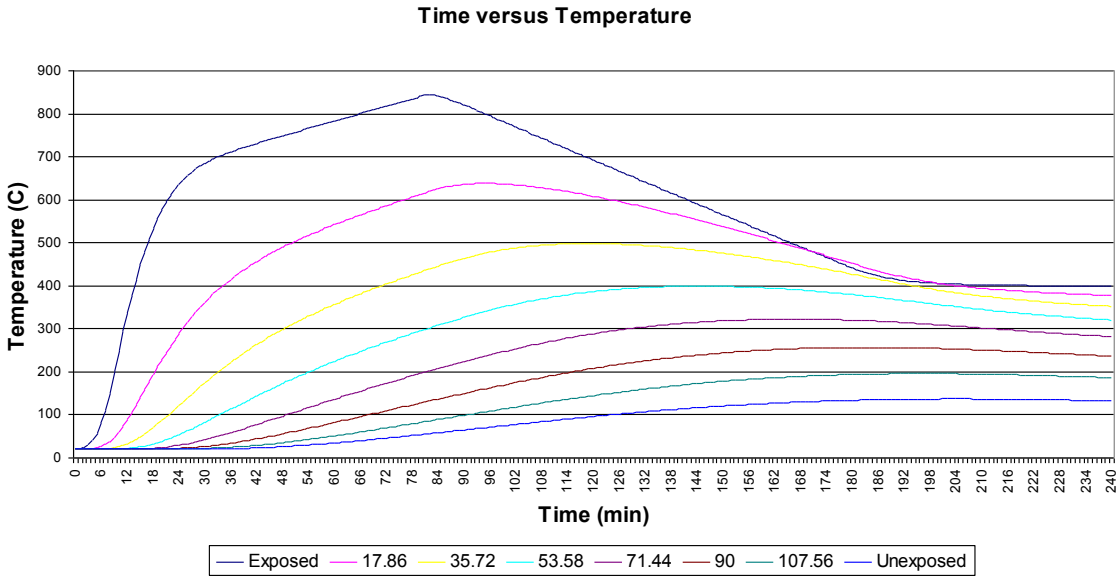

Figure E.61: Temperature Distribution for 125mm Siliceous Slab

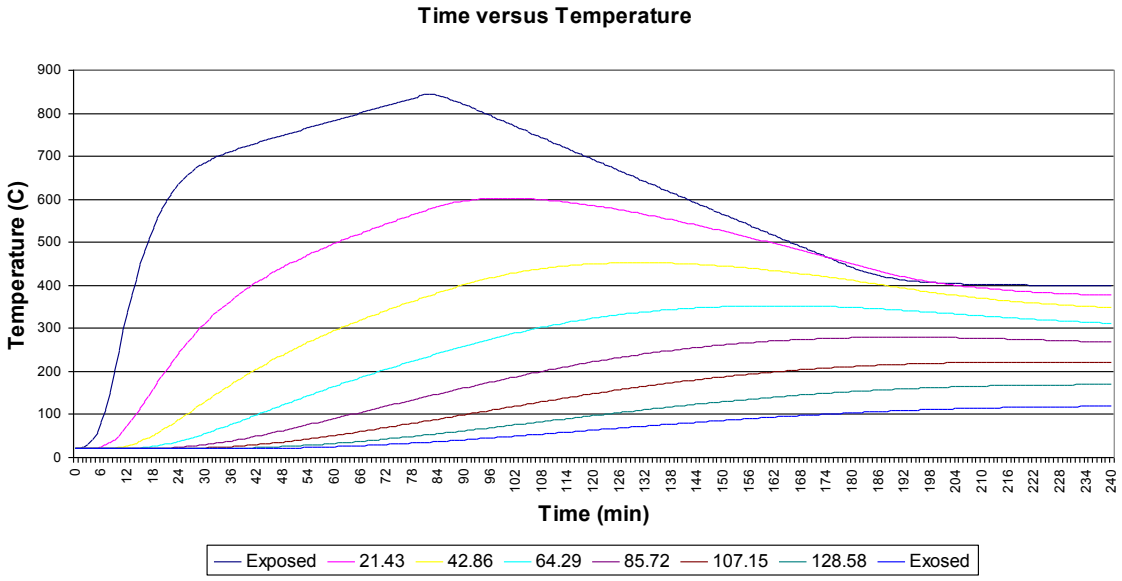

Figure E.62: Temperature Distribution for 150mm Siliceous Slab

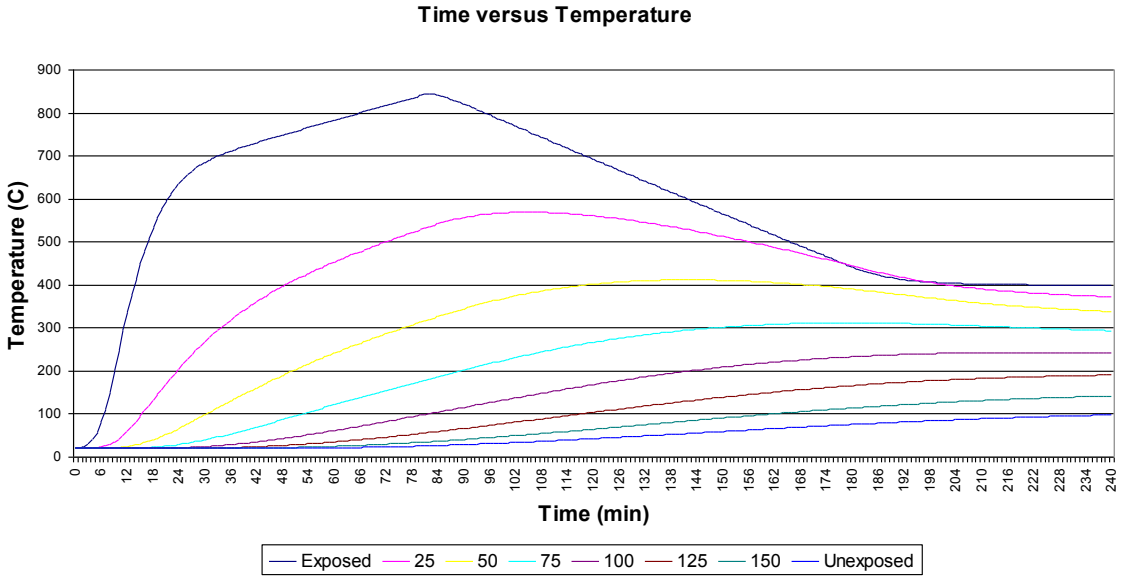

Figure E.63: Temperature Distribution for 175mm Siliceous Slab

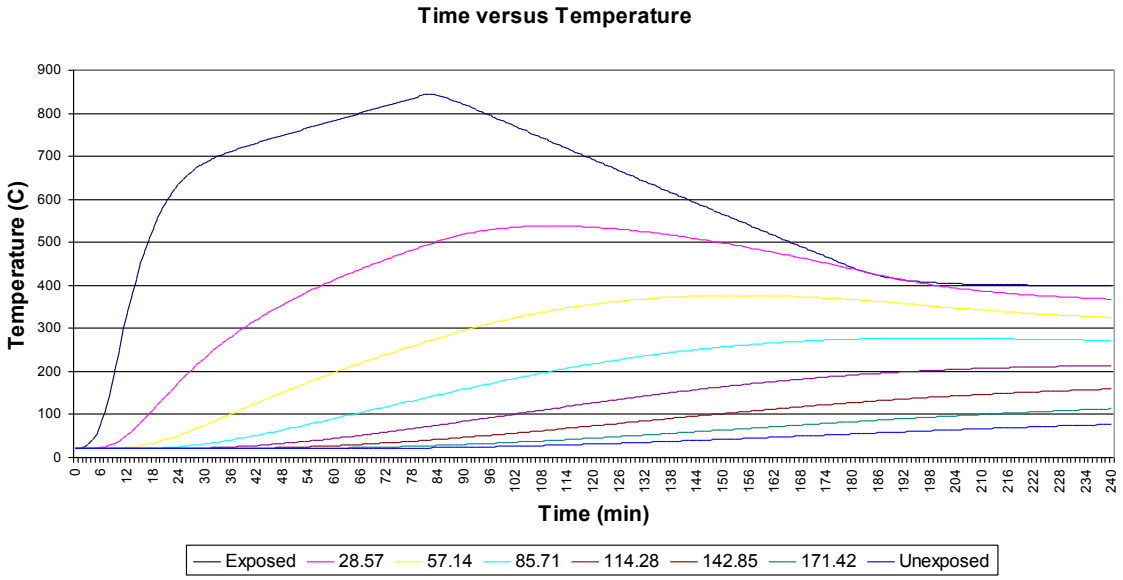

Figure E.64: Temperature Distribution for 200mm Siliceous Slab

E.5 Temperature Distribution Summation Tables

E.5.1 ISO 834

Table E.1: Temperature Distribution for 100mm Concrete Slab Composed of Various Aggregates Exposed to ISO 834 Conditions

Aggregate	Time (min)	Temperature (ºC) Per Total Slab Depth (mm)						
		14.3	28.6	42.9	57.2	71.5	85.7	100
Shale	0	20	20	20	20	20	20	20
Carbonate		20	20	20	20	20	20	20
Siliceous		20	20	20	20	20	20	20
Shale	5	36.1	20.8	20	20	20	20	20
Carbonate		42.3	23	20.2	20	20	20	20
Siliceous		38.5	21.8	20.1	20	20	20	20
Shale	15	251	80.7	31.7	21.8	20.2	20	20
Carbonate		217	103	51.4	30.6	23.1	20.8	20.2
Siliceous		228	94.9	43.6	26.4	21.4	20.3	20
Shale	30	506	266	122	55	30.1	22.5	20.5
Carbonate		453	270	160	94.4	57.5	37.8	28
Siliceous		496	283	155	83.8	47.9	31.2	24.2
Shale	45	621	394	227	120	62.7	36.1	25.5
Carbonate		585	391	261	173	113	74.3	49.7
Siliceous		625	417	267	166	102	63.1	41.4
Shale	60	695	482	311	188	108	61.8	38.3
Carbonate		665	475	339	240	168	115	76.4
Siliceous		703	506	354	240	160	104	67.4

Shale		792	601	437	303	200	128	79.3
Carbonate	90	766	588	449	341	254	183	123
Siliceous		801	625	476	355	258	181	120
Shale		858	683	526	391	280	191	123
Carbonate	120	N/A	N/A	N/A	N/A	N/A	N/A	N/A
Siliceous		N/A	N/A	N/A	N/A	N/A	N/A	N/A

Table E.2: Temperature Distribution for 150mm Concrete Slab Composed of Various Aggregates Exposed to ISO 834 Conditions

Aggregate	Time (min)	Temperature (ºC) Per Total Slab Depth (mm)						
		21.4	42.9	64.3	85.7	107	129	150
Shale		20	20	20	20	20	20	20
Carbonate	0	20	20	20	20	20	20	20
Siliceous		20	20	20	20	20	20	20
Shale		27.6	20.2	20	20	20	20	20
Carbonate	5	31.3	20.7	20	20	20	20	20
Siliceous		29.1	20.4	20	20	20	20	20
Shale		159	38.2	21.7	20.1	20	20	20
Carbonate	15	145	53.1	27.3	21.3	20.2	20	20
Siliceous		150	47.4	24.6	20.6	20.1	20	20
Shale		384	134	45.4	24.3	20.6	20.1	20
Carbonate	30	318	148	70.6	38	25.7	21.6	20.4
Siliceous		367	153	64.6	32.9	23.2	20.7	20.1
Shale		509	237	95	40.4	24.6	20.9	20.1
Carbonate	45	438	238	129	70.8	41.9	28.7	23.3
Siliceous		503	260	128	63.7	35.9	25.2	21.6
Shale		591	321	152	67.5	34.4	23.8	20.9
Carbonate	60	522	310	185	109	65.5	42	30.2
Siliceous		591	345	192	104	57.6	35.6	26.1
Shale		700	445	257	136	69.5	38.8	26.7
Carbonate	90	636	419	278	183	119	78.1	52.1
Siliceous		705	470	301	186	113	69.7	45.1
Shale		773	534	343	204	115	64.9	39.8
Carbonate	120	712	499	351	247	171	116	77.4
Siliceous		780	557	386	260	171	111	71.3
Shale		828	602	413	267	163	97.3	58.9
Carbonate	150	769	562	411	300	216	152	101
Siliceous		836	624	454	323	224	151	98.4
Shale		872	657	472	323	210	132	81.1
Carbonate	180	814	612	460	345	255	182	122
Siliceous		880	678	511	376	270	188	124
Shale		939	742	566	416	293	198	126
Carbonate	240	N/A	N/A	N/A	N/A	N/A	N/A	N/A
Siliceous		N/A	N/A	N/A	N/A	N/A	N/A	N/A

Table E.3: Temperature Distribution for 200mm Concrete Slab Composed of Various Aggregates Exposed to ISO 834 Conditions

Aggregate	Time (min)	Temperature (ºC) Per Total Slab Depth (mm)						
		28.6	57.1	85.7	114	143	171	200
Shale	0	20	20	20	20	20	20	20
Carbonate		20	20	20	20	20	20	20
Siliceous		20	20	20	20	20	20	20
Shale	5	24.4	20.1	20	20	20	20	20
Carbonate		26.7	20.2	20	20	20	20	20
Siliceous		25.3	20.1	20	20	20	20	20
Shale	15	109	26.7	20.3	20	20	20	20
Carbonate		103	34.5	21.9	20.2	20	20	20
Siliceous		105	31.3	21.1	20.1	20	20	20
Shale	30	290	72.8	26.9	20.7	20.1	20	20
Carbonate		228	87.2	38.8	24.5	20.9	20.2	20
Siliceous		272	88.1	35.2	22.8	20.4	20.1	20
Shale	45	413	140	45.7	24.2	20.6	20.1	20
Carbonate		326	148	68.3	36.4	24.9	21.3	20.3
Siliceous		398	161	65.4	32.5	23	20.6	20.1
Shale	60	498	207	74.3	32.2	22.2	20.3	20
Carbonate		401	203	102	54	32.8	24.4	21.4
Siliceous		489	230	103	49.4	29.1	22.5	20.6
Shale	90	615	321	143	61	31.4	22.7	20.6
Carbonate		512	293	169	96.8	57.2	36.9	27.4
Siliceous		613	343	183	95.2	51.7	32.3	24.5
Shale	120	694	409	212	100	48.8	29	22.6
Carbonate		591	365	228	141	87.2	55.7	38.2
Siliceous		696	431	255	146	83	49.6	33.3
Shale	150	754	479	274	144	72.6	39.8	27
Carbonate		652	424	279	183	118	77.3	51.6
Siliceous		757	500	318	195	118	71.8	46.2
Shale	180	802	537	330	187	100	54.6	34.1
Carbonate		701	475	324	221	149	99.6	66.1
Siliceous		806	557	372	241	153	96.3	61.5
Shale	240	875	628	423	267	159	92.2	55.3
Carbonate		776	556	400	287	204	142	94.6
Siliceous		880	647	462	322	219	146	94.2

E.5.2 SDHI-95

Table E.4: Temperature Distribution for 100mm Concrete Slab Composed of Various Aggregates Exposed to SDHI-95 Fire Exposure

Aggregate	Time (min)	Temperature (ºC) Per Total Slab Depth (mm)						
		14.3	28.6	42.9	57.2	71.5	85.7	100
Shale	0	20	20	20	20	20	20	20
Carbonate		20	20	20	20	20	20	20
Siliceous		20	20	20	20	20	20	20
Quartz		20	20	20	20	20	20	20
Shale	5	29.3	20.4	20	20	20	20	20
Carbonate		34.5	21.6	20.1	20	20	20	20
Siliceous		31	20.8	20	20	20	20	20
Quartz		36.1	22	20.1	20	20	20	20
Shale	15	403	123	38.1	22.3	20.2	20	20
Carbonate		283	125	57.9	31.8	23.1	20.7	20.1
Siliceous		342	128	51	27.4	21.4	20.2	20
Quartz		376	152	62	31.5	22.7	20.5	20.1
Shale	30	642	360	173	75.4	36.4	24.1	20.9
Carbonate		536	320	190	111	66.1	41.8	29.7
Siliceous		633	369	203	108	58.7	35.5	25.7
Quartz		659	401	229	125	67.9	40.1	27.8
Shale	45	750	492	293	160	82.3	44.4	28.6
Carbonate		664	442	296	197	129	84.2	55.4
Siliceous		750	508	329	206	126	76.9	48.7
Quartz		770	536	355	227	141	86.9	54.5
Shale	60	702	539	373	235	138	78.3	46.4
Carbonate		694	518	374	267	187	128	84.7
Siliceous		722	566	412	286	192	126	80.1
Quartz		729	584	435	307	209	138	88.4
Shale	90	502	461	385	298	215	145	92.3
Carbonate		528	490	418	337	260	192	130
Siliceous		521	488	424	346	267	195	131
Quartz		531	498	435	357	278	204	138
Shale	120	361	358	331	285	230	173	118
Carbonate		370	372	352	312	261	203	143
Siliceous		371	371	351	312	262	204	144
Quartz		374	377	358	320	269	210	148
Shale	150	299	300	284	255	216	171	121
Carbonate		297	297	284	258	222	178	128
Siliceous		301	301	288	263	226	182	131
Quartz		302	305	293	268	231	186	133
Shale	180	248	255	247	226	196	158	114
Carbonate		239	239	230	211	183	148	108
Siliceous		246	248	239	220	191	155	113
Quartz		246	250	242	223	194	157	114

Shale	240	150	171	176	169	151	125	93.4
Carbonate		130	139	139	131	117	97.1	73.4
Siliceous		142	153	153	145	129	107	80.5
Quartz		139	151	153	145	130	108	80.8

Table E.5: Temperature Distribution for 150mm Concrete Slab Composed of Various Aggregates Exposed to SDHI-95 Fire Exposure

Aggregate	Time (min)	Temperature (ºC) Per Total Slab Depth (mm)						
		21.4	42.9	64.3	85.7	107	129	150
Shale	0	20	20	20	20	20	20	20
Carbonate		20	20	20	20	20	20	20
Siliceous		20	20	20	20	20	20	20
Quartz		20	20	20	20	20	20	20
Shale	5	24.3	20.1	20	20	20	20	20
Carbonate		27.2	20.3	20	20	20	20	20
Siliceous		25.3	20.2	20	20	20	20	20
Quartz		28.1	20.4	20	20	20	20	20
Shale	15	256	50	22.3	20.1	20	20	20
Carbonate		171	58.4	27.9	21.3	20.2	20	20
Siliceous		212	56.9	25.5	20.6	20.1	20	20
Quartz		241	68.1	28.2	21.1	20.1	20	20
Shale	30	503	188	60.2	27	21	20.1	20
Carbonate		352	165	78	40.7	26.5	21.8	20.4
Siliceous		475	199	80.6	37.5	24.3	20.9	20.2
Quartz		512	228	94.7	42.7	25.9	21.3	20.3
Shale	45	625	308	126	50.6	27.1	21.4	20.2
Carbonate		469	256	140	76.4	44.6	29.9	23.8
Siliceous		611	320	158	76.9	41	26.9	22.1
Quartz		644	354	180	88.9	46.4	29	22.9
Shale	60	628	383	192	85.9	40.8	25.6	21.4
Carbonate		543	328	197	116	69.7	44.2	31.3
Siliceous		635	401	229	124	67.6	40	28
Quartz		655	430	254	141	77.2	44.8	30.2
Shale	90	489	390	261	152	81.6	44.9	29.2
Carbonate		490	385	274	187	124	81.5	54.3
Siliceous		505	416	302	201	127	78.8	50.4
Quartz		512	431	320	218	140	87.9	56
Shale	120	366	335	264	184	116	70	43.7
Carbonate		364	339	284	220	162	115	77.6
Siliceous		374	352	297	229	165	114	75.2
Quartz		381	364	310	243	177	123	81.8
Shale	150	305	291	248	192	136	90.4	58.8
Carbonate		299	290	261	220	175	132	92.1
Siliceous		308	301	271	227	179	132	91.2
Quartz		313	310	282	238	189	141	97.3

Shale	180	257	256	230	189	144	103	70.2
Carbonate		249	251	235	207	173	135	96.6
Siliceous		258	261	245	215	178	137	97.5
Quartz		262	268	254	224	186	145	103
Shale	240	170	194	191	172	144	112	80.4
Carbonate		152	172	176	167	147	120	88.8
Siliceous		165	187	190	178	156	127	93.3
Quartz		167	191	196	185	162	132	96.7

Table E.6: Temperature Distribution for 200mm Concrete Slab Composed of Various Aggregates Exposed to SDHI-95 Fire Exposure

Aggregate	Time (min)	Temperature (ºC) Per Total Slab Depth (mm)						
		28.6	57.1	85.7	114	143	171	200
Shale	0	20	20	20	20	20	20	20
Carbonate		20	20	20	20	20	20	20
Siliceous		20	20	20	20	20	20	20
Quartz		20	20	20	20	20	20	20
Shale	5	22.5	20	20	20	20	20	20
Carbonate		24.2	20.1	20	20	20	20	20
Siliceous		23.1	20.1	20	20	20	20	20
Quartz		24.8	20.1	20	20	20	20	20
Shale	15	172	30.9	20.5	20	20	20	20
Carbonate		115	36	22	20.2	20	20	20
Siliceous		142	34.7	21.3	20.1	20	20	20
Quartz		165	39.7	22	20.2	20	20	20
Shale	30	389	100	31	21.1	20.1	20	20
Carbonate		241	93	40.7	24.9	21	20.2	20
Siliceous		352	111	40.4	23.7	20.5	20.1	20
Quartz		391	131	46.2	25	20.8	20.1	20
Shale	45	516	185	57.8	26.4	20.9	20.1	20
Carbonate		333	154	71.7	37.7	25.3	21.4	20.3
Siliceous		487	198	78.5	36.4	23.9	20.8	20.1
Quartz		527	228	91.8	41	25.2	21.1	20.3
Shale	60	549	256	94.3	37.6	23.3	20.5	20.1
Carbonate		408	208	106	55.9	33.6	24.7	21.5
Siliceous		540	271	123	57.1	31.7	23.2	20.8
Quartz		571	303	142	65.8	34.9	24.3	21.4
Shale	90	465	308	158	71.1	35.2	23.8	20.9
Carbonate		430	280	170	99	58.7	37.8	27.9
Siliceous		474	330	195	106	57.8	35	25.7
Quartz		488	352	215	120	65.6	39.1	28.5
Shale	120	365	293	188	102	52.9	31.1	23.4
Carbonate		346	284	203	134	86.3	56.1	38.6
Siliceous		368	311	223	143	86.6	53	35.4
Quartz		378	327	239	157	97.1	60.4	41.9

Shale	150	306	267	194	122	70	41.1	28.1
Carbonate		291	260	208	153	107	73.6	50.6
Siliceous		306	279	223	161	108	70.9	47.2
Quartz		313	291	237	174	120	80.9	57.4
Shale	180	262	243	191	132	83.4	51.3	34.1
Carbonate		247	234	201	160	120	86.7	60.6
Siliceous		260	250	213	167	122	84.8	57.8
Quartz		265	259	225	179	134	96.9	71.7
Shale	240	183	196	175	138	99.2	67.9	46.2
Carbonate		160	177	172	152	126	97.9	71
Siliceous		175	193	184	160	130	98.9	70.5
Quartz		176	199	194	172	144	116	93.2

E.5.3 LDMI-M

Table E.7: Temperature Distribution for 100mm Concrete Slab Composed of Various Aggregates Exposed to LDMI-M Fire Exposure

Aggregate	Time (min)	Temperature (ºC) Per Total Slab Depth (mm)						
		14.3	28.6	42.9	57.2	71.5	85.7	100
Shale	0	20	20	20	20	20	20	20
Carbonate		20	20	20	20	20	20	20
Siliceous		20	20	20	20	20	20	20
Quartz		20	20	20	20	20	20	20
Shale	5	24.1	20.2	20	20	20	20	20
Carbonate		27.6	20.8	20	20	20	20	20
Siliceous		25.1	20.4	20	20	20	20	20
Quartz		28.1	21.1	20.1	20	20	20	20
Shale	15	193	57.6	25.9	20.7	20.1	20	20
Carbonate		177	80.1	40.3	26	21.5	20.3	20.1
Siliceous		178	70.3	33.6	23.1	20.6	20.1	20
Quartz		200	90.4	44.3	27.3	21.9	20.5	20.1
Shale	30	426	220	99.6	45.8	26.9	21.6	20.3
Carbonate		394	236	139	81.9	50.2	33.8	25.9
Siliceous		420	239	130	70.5	41.2	28.1	22.9
Quartz		443	269	156	88.9	52.4	34.2	25.8
Shale	45	515	326	187	99.5	53.1	32.2	24
Carbonate		506	344	232	153	100	66.5	45.2
Siliceous		524	353	227	142	87.5	55.2	37.2
Quartz		542	378	253	164	105	67.2	44.6
Shale	60	577	398	256	155	89.7	52.8	34.2
Carbonate		573	416	300	214	150	103	69.4
Siliceous		588	427	301	205	137	90.7	59.6
Quartz		602	447	323	226	155	105	69
Shale	90	661	503	363	250	166	106	67.2
Carbonate		662	516	398	304	228	165	112
Siliceous		675	532	407	304	222	157	104
Quartz		684	546	423	320	236	168	113

Shale	120	611	515	412	314	228	158	103
Carbonate		632	542	448	359	279	207	141
Siliceous		628	544	451	361	279	205	139
Quartz		631	550	461	372	289	213	145
Shale	150	530	477	408	333	259	190	129
Carbonate		553	507	443	372	299	227	157
Siliceous		545	499	438	369	297	226	156
Quartz		545	502	443	375	303	231	160
Shale	180	440	419	378	324	264	201	140
Carbonate		457	441	404	352	291	226	158
Siliceous		449	431	395	345	287	223	156
Quartz		450	433	398	348	290	226	158
Shale	240	375	347	315	278	234	185	132
Carbonate		375	347	314	276	232	183	131
Siliceous		374	345	313	275	232	183	131
Quartz		375	347	314	277	233	185	132

Table E.8: Temperature Distribution for 150mm Concrete Slab Composed of Various Aggregates Exposed to LDMI-M Fire Exposure

Aggregate	Time (min)	Temperature (ºC) Per Total Slab Depth (mm)						
		21.4	42.9	64.3	85.7	107	129	150
Shale	0	20	20	20	20	20	20	20
Carbonate		20	20	20	20	20	20	20
Siliceous		20	20	20	20	20	20	20
Quartz		20	20	20	20	20	20	20
Shale	5	21.9	20	20	20	20	20	20
Carbonate		23.8	20.2	20	20	20	20	20
Siliceous		22.5	20.1	20	20	20	20	20
Quartz		24.1	20.2	20	20	20	20	20
Shale	15	119	30.5	20.8	20	20	20	20
Carbonate		118	42.7	24.3	20.6	20.1	20	20
Siliceous		115	37	22.4	20.3	20	20	20
Quartz		135	47.2	25.2	20.8	20.1	20	20
Shale	30	320	109	38.7	23	20.4	20	20
Carbonate		283	131	62.3	34.4	24.3	21.1	20.3
Siliceous		312	130	55.1	29.6	22.2	20.4	20.1
Quartz		342	155	69.4	35.7	24.4	21.1	20.2
Shale	45	421	195	78.8	35.6	23.4	20.6	20.1
Carbonate		392	215	116	64.2	38.6	27.2	22.7
Siliceous		425	222	110	55.9	32.7	24	21.2
Quartz		451	251	132	68.4	39	26.7	22.2
Shale	60	488	264	125	57.2	31.1	22.8	20.7
Carbonate		465	281	168	99.5	60.2	39.1	28.7
Siliceous		497	294	165	90.5	51.3	32.8	24.9
Quartz		519	321	188	107	61.1	38.1	27.6

Shale	90	584	369	211	112	59	34.7	25.2
Carbonate		567	380	254	168	110	72.4	48.9
Siliceous		596	401	258	161	99.2	62	41.2
Quartz		613	423	279	179	112	70.9	46.6
Shale	120	566	416	275	167	95.8	55.5	35.6
Carbonate		578	436	317	225	157	108	72.3
Siliceous		585	450	324	222	148	97.4	63.7
Quartz		593	465	341	239	162	108	70.5
Shale	150	508	412	304	206	131	80.4	50.5
Carbonate		531	444	349	265	195	139	93.6
Siliceous		526	445	350	262	188	130	86.2
Quartz		530	454	363	275	200	140	93.2
Shale	180	435	385	308	227	157	103	66.5
Carbonate		457	418	353	284	218	161	110
Siliceous		450	411	349	278	212	153	104
Quartz		453	418	358	289	222	162	110
Shale	240	369	332	286	234	181	132	90.2
Carbonate		380	353	317	274	225	174	123
Siliceous		377	348	312	268	220	169	119
Quartz		380	353	318	275	226	175	123

Table E.9: Temperature Distribution for 200mm Concrete Slab Composed of Various Aggregates Exposed to LDMI-M Fire Exposure

Aggregate	Time (min)	Temperature (ºC) Per Total Slab Depth (mm)						
		28.6	57.1	85.7	114	143	171	200
Shale	0	20	20	20	20	20	20	20
Carbonate		20	20	20	20	20	20	20
Siliceous		20	20	20	20	20	20	20
Quartz		20	20	20	20	20	20	20
Shale	5	21.1	20	20	20	20	20	20
Carbonate		22.2	20.1	20	20	20	20	20
Siliceous		21.4	20	20	20	20	20	20
Quartz		22.4	20.1	20	20	20	20	20
Shale	15	81.9	23.8	20.2	20	20	20	20
Carbonate		84.1	29.6	21.1	20.1	20	20	20
Siliceous		81.1	26.8	20.6	20	20	20	20
Quartz		96.3	31.6	21.3	20.1	20	20	20
Shale	30	240	60.3	24.9	20.5	20	20	20
Carbonate		206	78	35.4	23.4	20.6	20.1	20
Siliceous		233	75.3	31.6	22	20.3	20	20
Quartz		261	92.6	37.8	23.6	20.6	20.1	20
Shale	45	340	115	39.8	23.1	20.4	20	20
Carbonate		299	135	62.7	34	24.1	21	20.2
Siliceous		339	139	57.6	30.1	22.3	20.4	20.1
Quartz		369	164	70.2	35	23.9	20.9	20.2

Shale	60	410	170	62.5	29.4	21.7	20.3	20
Carbonate		369	188	94.8	50.4	31.2	23.7	21.2
Siliceous		413	198	90.5	44.5	27.5	22	20.5
Quartz		442	224	107	52.8	30.9	23.2	20.9
Shale	90	512	264	118	52.2	28.9	22.1	20.5
Carbonate		472	273	158	90.7	54	35.3	26.6
Siliceous		519	295	159	83.9	46.8	30.3	23.8
Quartz		543	321	179	96.7	53.9	33.7	25.3
Shale	120	519	323	172	83.6	42.6	27	22
Carbonate		511	335	213	132	82.2	52.9	36.7
Siliceous		535	357	218	127	73.7	45.2	31.3
Quartz		549	378	238	142	83.6	50.9	34.4
Shale	150	480	342	210	115	60.8	35.5	25.5
Carbonate		493	364	252	169	111	73	49.3
Siliceous		498	376	257	165	102	63.9	42.3
Quartz		506	391	274	180	114	71.5	46.8
Shale	180	424	337	230	140	79.8	46.4	30.9
Carbonate		441	365	275	196	136	92.7	62.5
Siliceous		438	367	275	192	128	83.2	54.8
Quartz		445	378	289	205	139	91.6	60.2
Shale	240	359	305	237	168	110	69.7	45.2
Carbonate		371	329	277	220	168	122	84.2
Siliceous		368	326	272	214	159	113	77
Quartz		373	334	282	224	169	121	82.6

F. Testing of Parameters

This appendix discusses and displays what occurs to analyses using the Excel tool when certain variables are changed. These analyses were critical to the development of the Excel tool by showing the effects different variables have on temperature distribution data. Variables which were examined include specific heat capacity, thermal conductivity, time step, and segmentation of the slab. All analyses in this section assumed ISO 834 conditions.

The first parameter which was evaluated was thermal conductivity. Varying thermal conductivity values were tested for a 175mm alluvial quartz slab and the results can be seen in Figures F.1, F.2, F.3, and F.7. Specific heat remained constant for all of the analysis while the effects of an upper bound, average, lower bound, and variable thermal conductivity value were examined. It can be seen from Figures F.1, F.2, and F.3 that as the value for thermal conductivity decreases so does the temperature distribution for the slab. The temperature-dependent thermal conductivity values produce results which capture the effects of all the thermal conductivity values with the portion of the slab near the exposed face having values close to the upper bound while those near the unexposed side are closer to those for a lower bound thermal conductivity value.

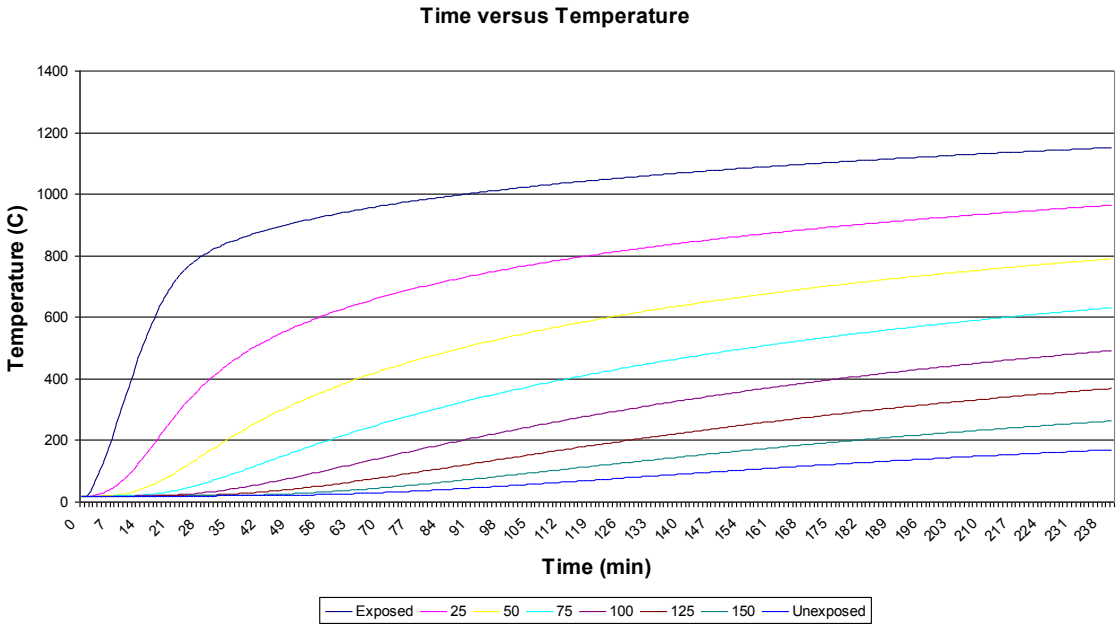

Figure F.1: Temperature Distribution for 175mm Alluvial Quartz Slab with Upper Bound Constant Thermal Conductivity and Constant Upper Bound Specific Heat

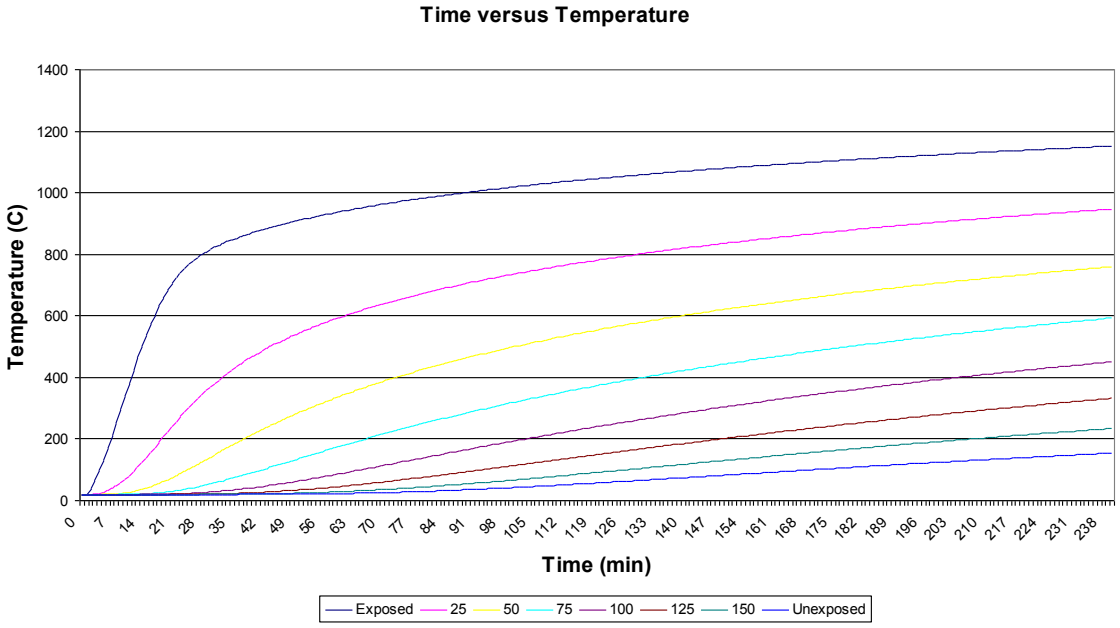

Figure F.2: Temperature Distribution for 175mm Alluvial Quartz Slab with Average Constant Thermal Conductivity and Constant Upper Bound Specific Heat

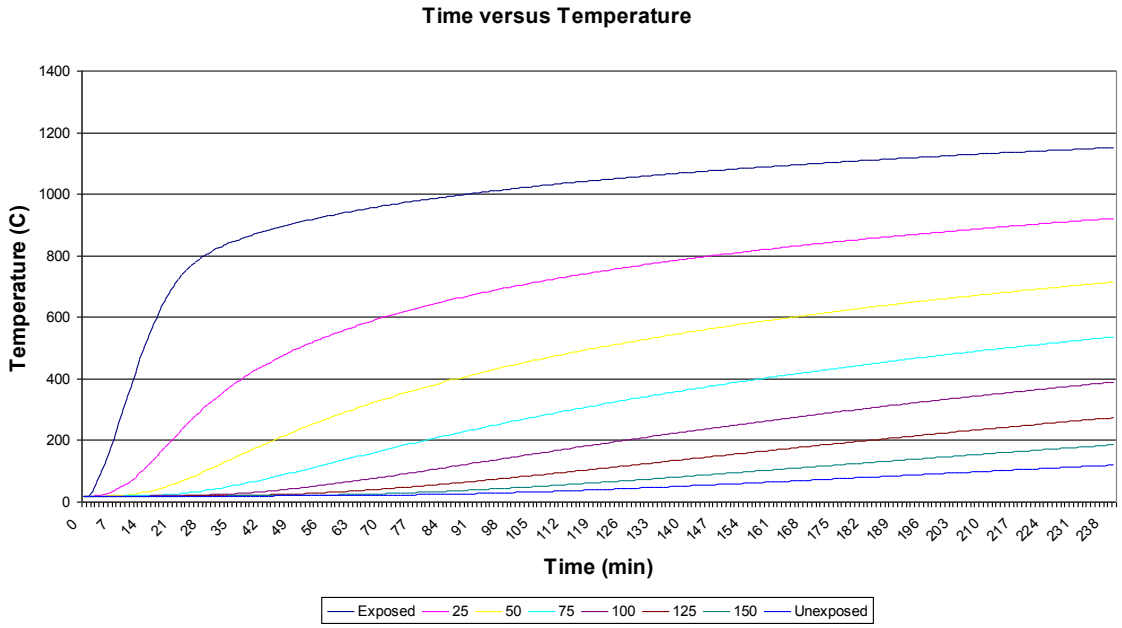

Figure F.3: Temperature Distribution for 175mm Alluvial Quartz Slab with Lower Bound Constant Thermal Conductivity and Constant Upper Bound Specific Heat

Secondly, the effects of specific heat were examined for the same 175mm alluvial quartz slab. Thermal conductivity remained variable for all of the analysis while the effects of an upper bound, average, lower bound, and variable specific heat value were examined. Figures F.4, F.5, and F.6 display that as specific heat decreases the temperature distribution values increase while Figure F.7 shows what occurs when a variable thermal conductivity and specific heat are used for the same slab.

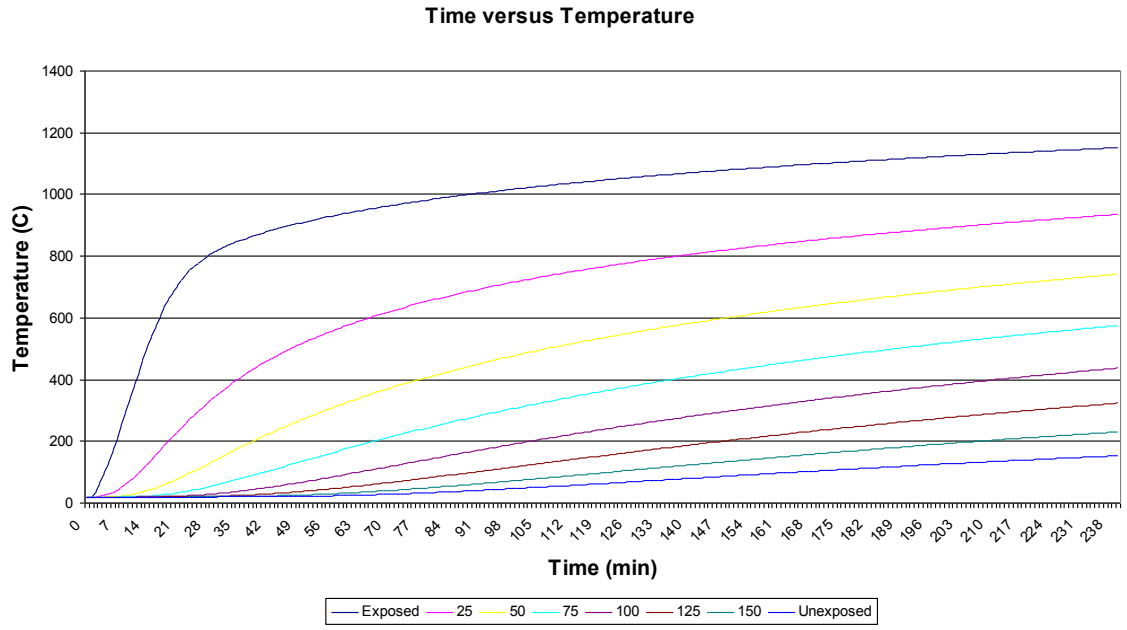

Figure F.4: Temperature Distribution for 175mm Alluvial Quartz Slab with Variable Thermal Conductivity and Constant Upper Bound Specific Heat

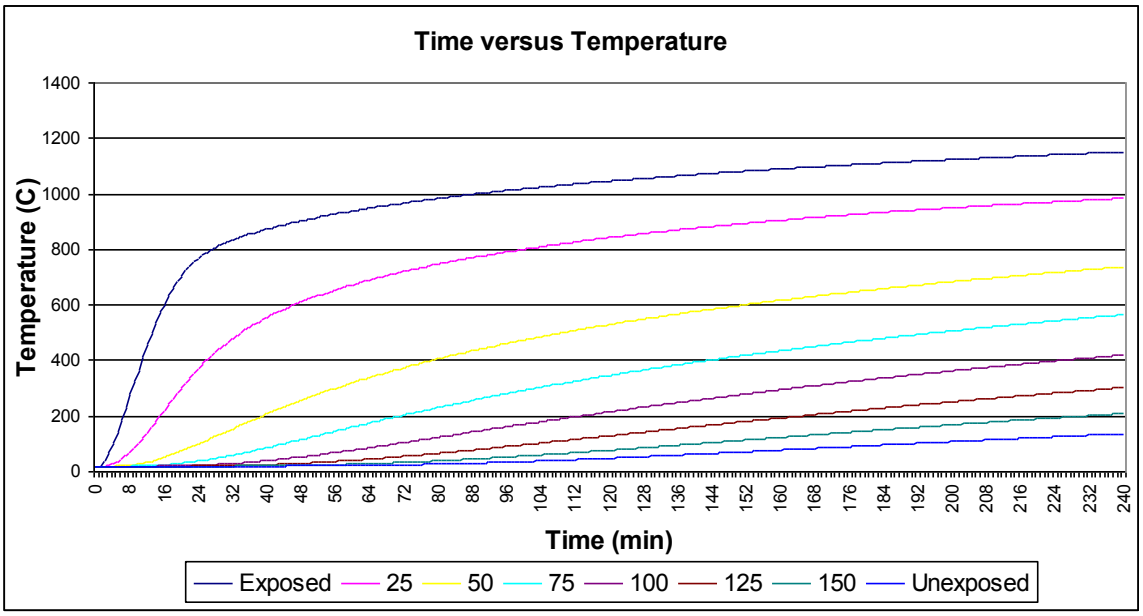

Figure F.5: Temperature Distribution for 175mm Alluvial Quartz Slab with Variable Thermal Conductivity and Constant Average Specific Heat

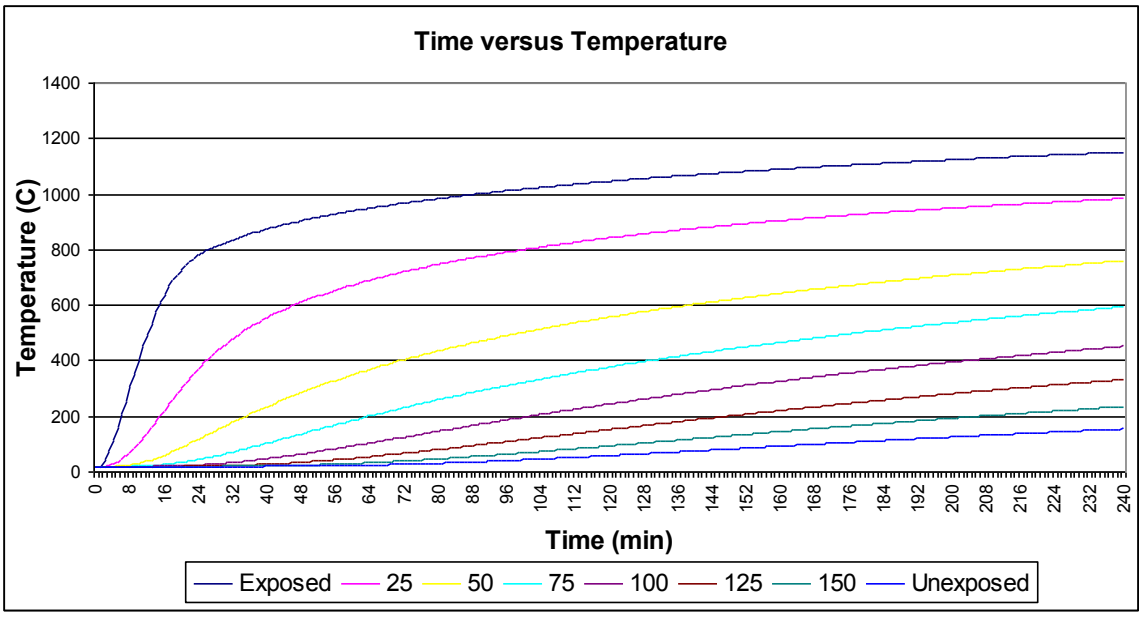

Figure F.6: Temperature Distribution for 175mm Alluvial Quartz Slab with Variable Thermal Conductivity and Constant Lower Bound Specific Heat

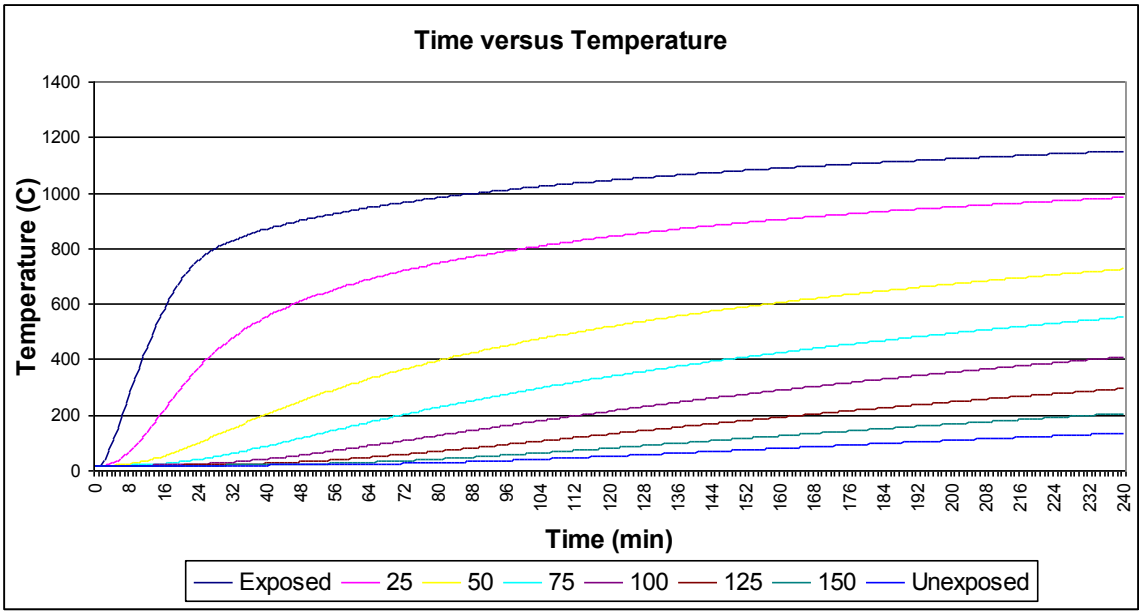

Figure F.7: Temperature Distribution for 175mm Alluvial Quartz Slab with Variable Thermal Conductivity and Variable Specific Heat

Next the affect the time step has on analyses was evaluated for a 175mm siliceous slab. An analysis was performed for both a 30 and 60 second time step. It can be seen from Figures F.8 and F.9 that by reducing the time step temperatures increase faster initially and begin to coincide between 2 and 3 hours of exposure.

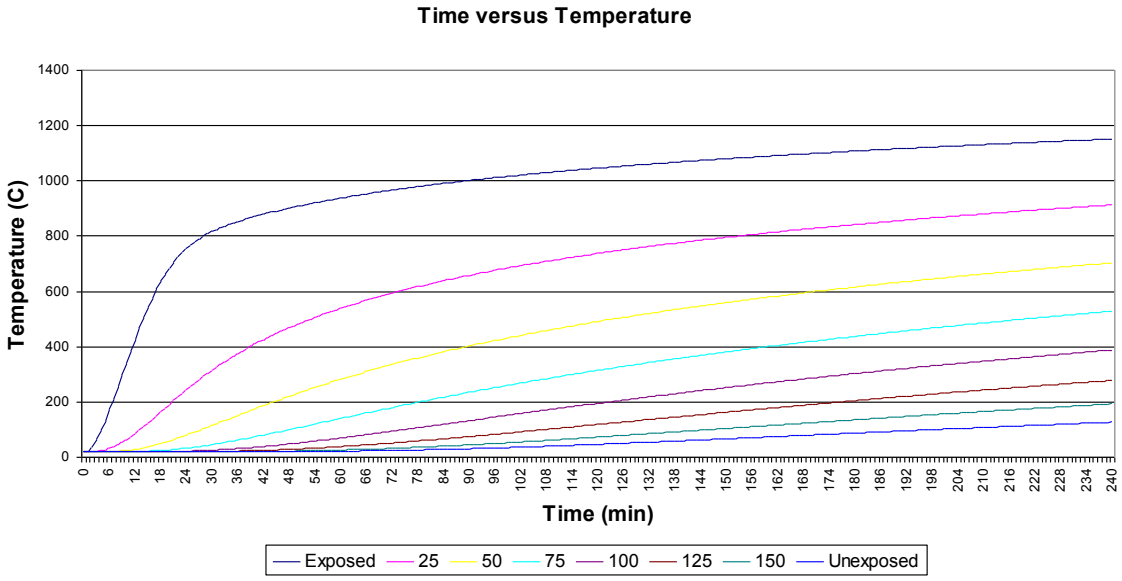

Figure F.8: Temperature Distribution for 175mm Siliceous Slab with a 1 Minute Time Step

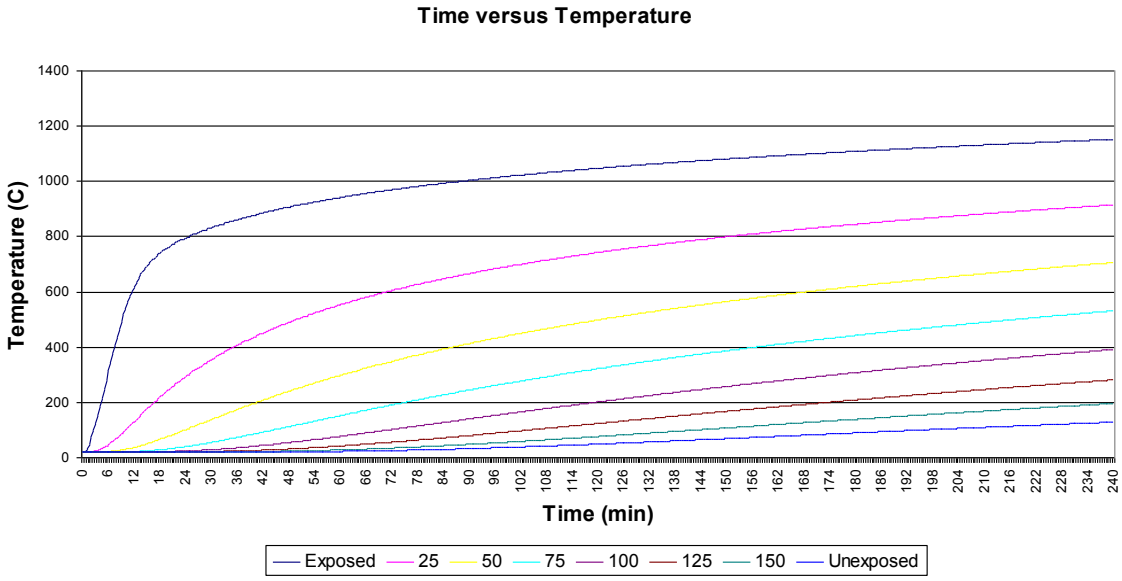

Figure F.9: Temperature Distribution for 175mm Siliceous Slab with a 30 Second Time Step

Finally, the effect the amount of increments the slab is broken into has on temperature analyses was investigated. The analyses were performed for a 175mm shale slab. It can be seen clearly in Figures F.10, F.11, and F.12 that as the increments increase the overall temperature distribution for the slab decreases.

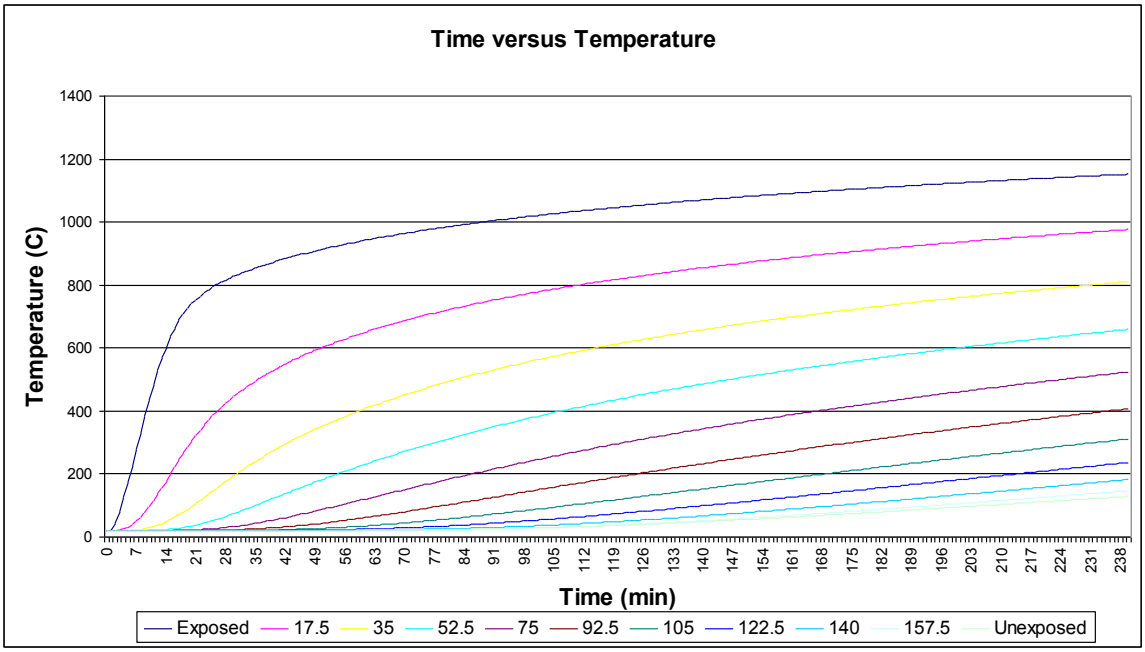

Figure F.10: Temperature Distribution for 175mm Shale Slab Segmented into 10 Increments

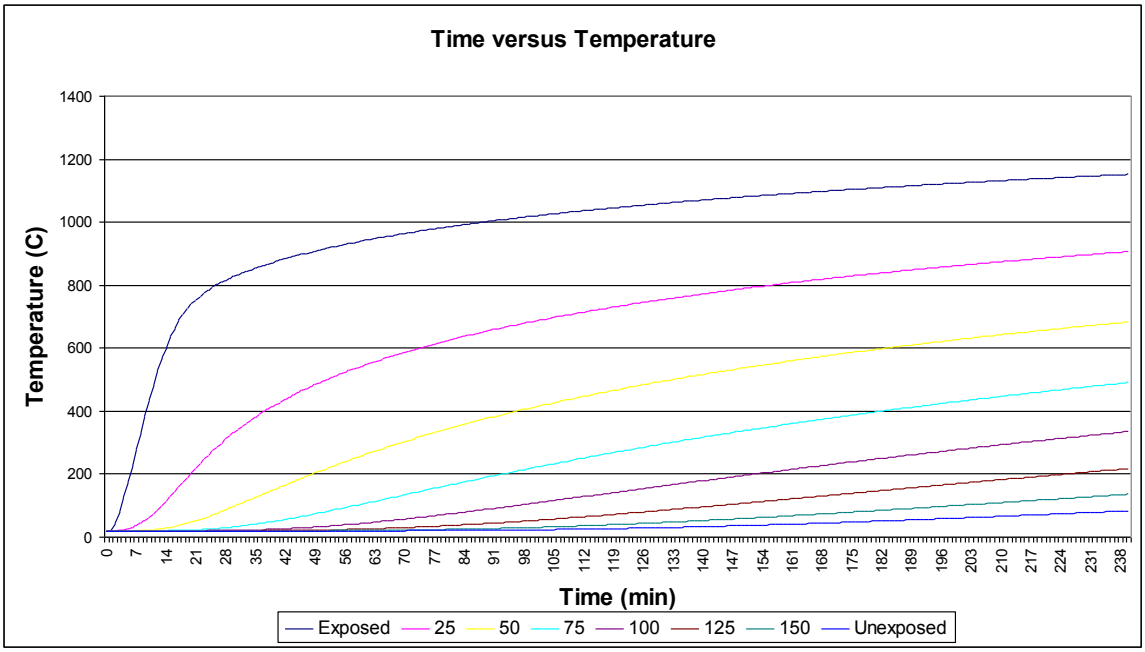

Figure F.11: Temperature Distribution for 175mm Shale Slab Segmented into 7 Increments

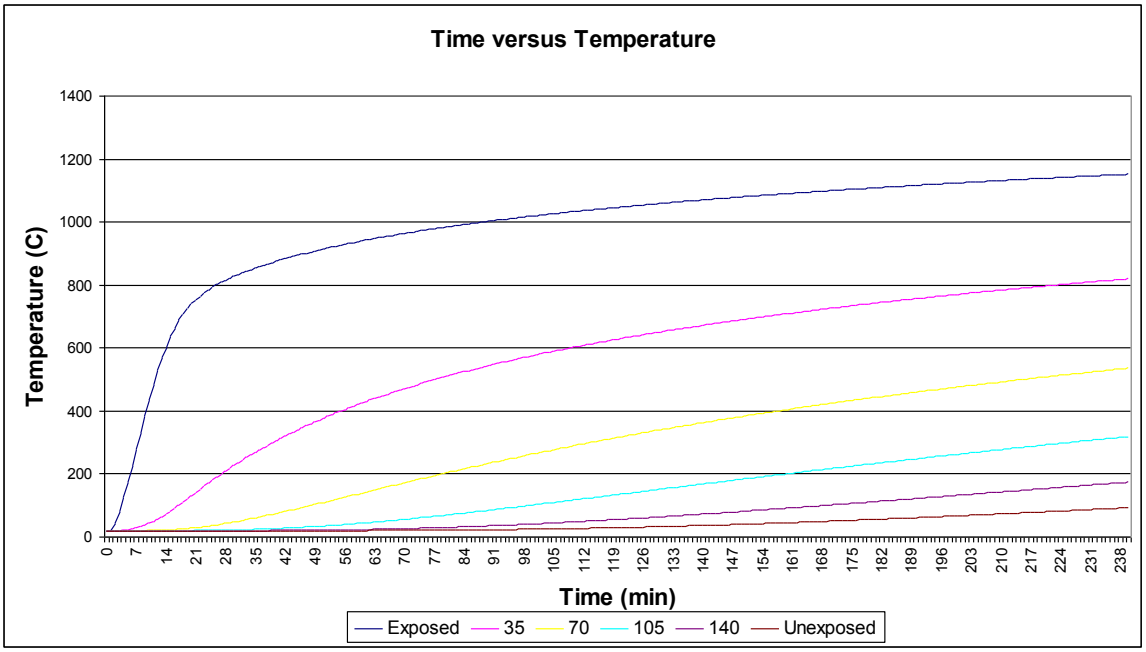

Figure F.12: Temperature Distribution for 175mm Shale Slab Segmented into 5 Increments

G. Experimental Data

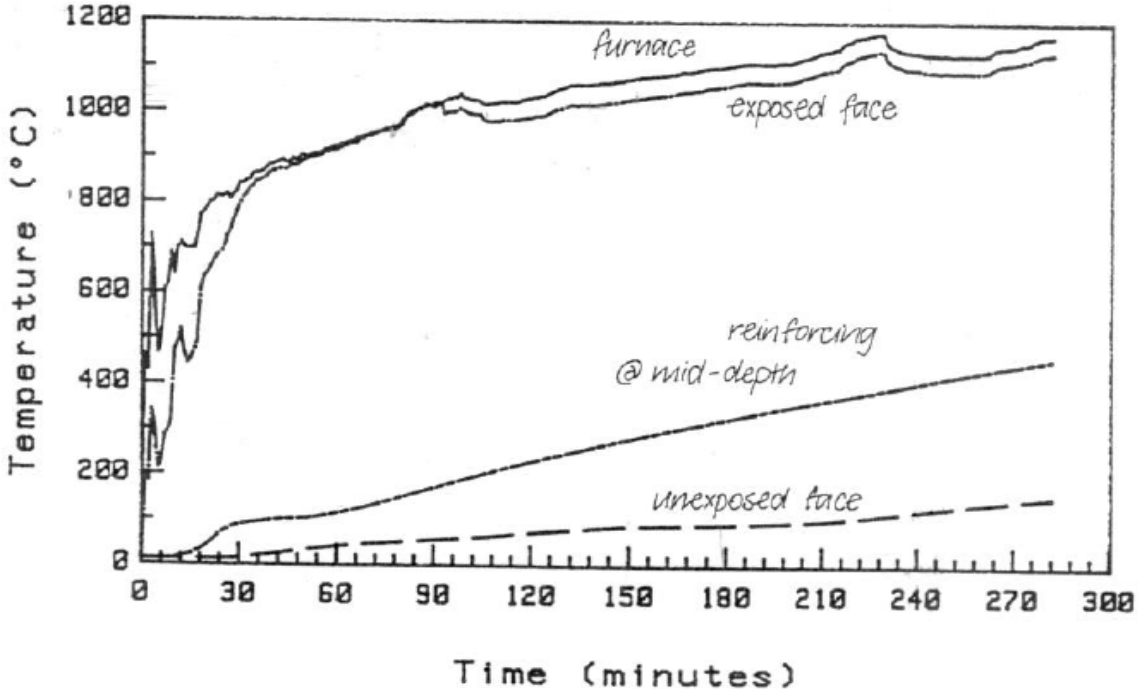

Figure G.1: BRANZ Data for the Temperature of the Unexposed Face, Exposed Face, and Furnace Temperature for a 175mm Alluvial Quartz Slab in ISO 834 Conditions (as taken from Wade 1992)

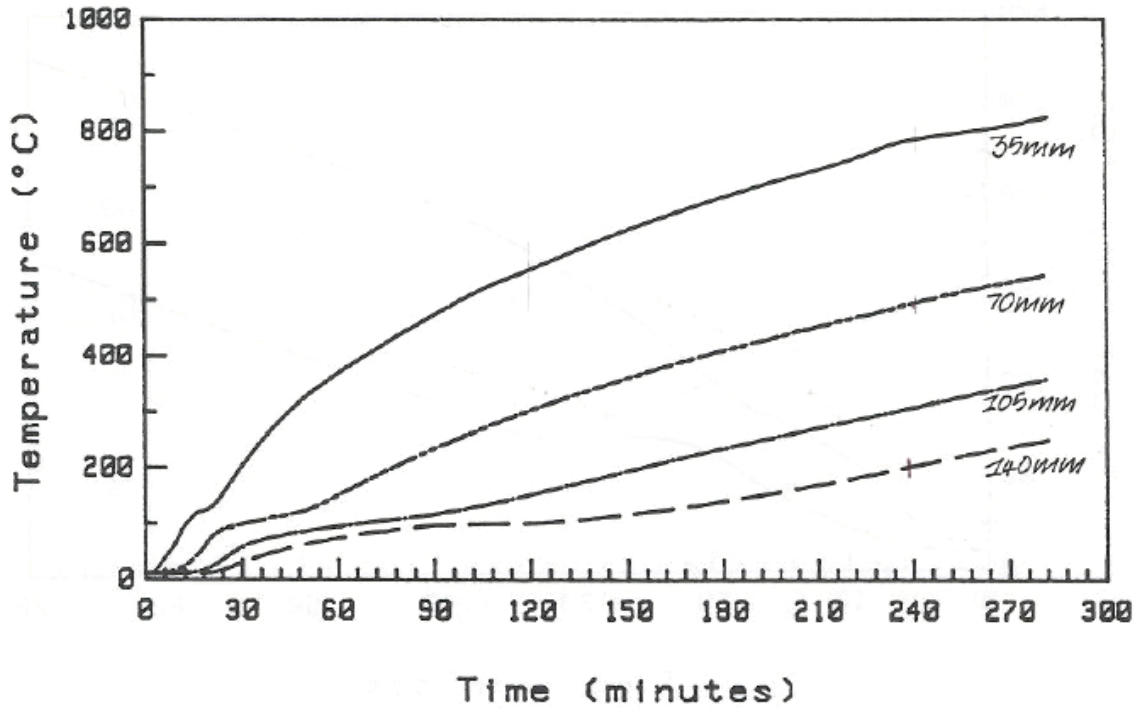

Figure G.2: BRANZ Temperature Distribution Data for a 175mm Alluvial Quartz Slab in ISO 834 Conditions (as taken from Wade 1992)

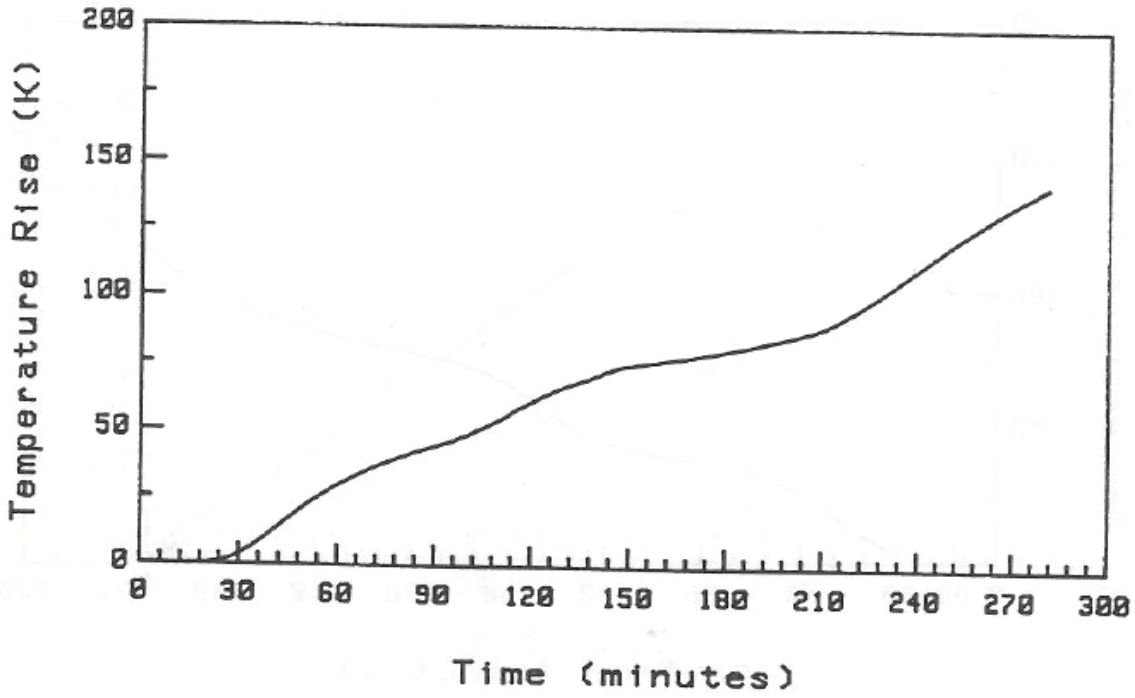

Figure G.3: BRANZ Data for the Temperature of the Unexposed Face of 175mm Alluvial Quartz Slab in ISO 834 Conditions (as taken from Wade 1992)

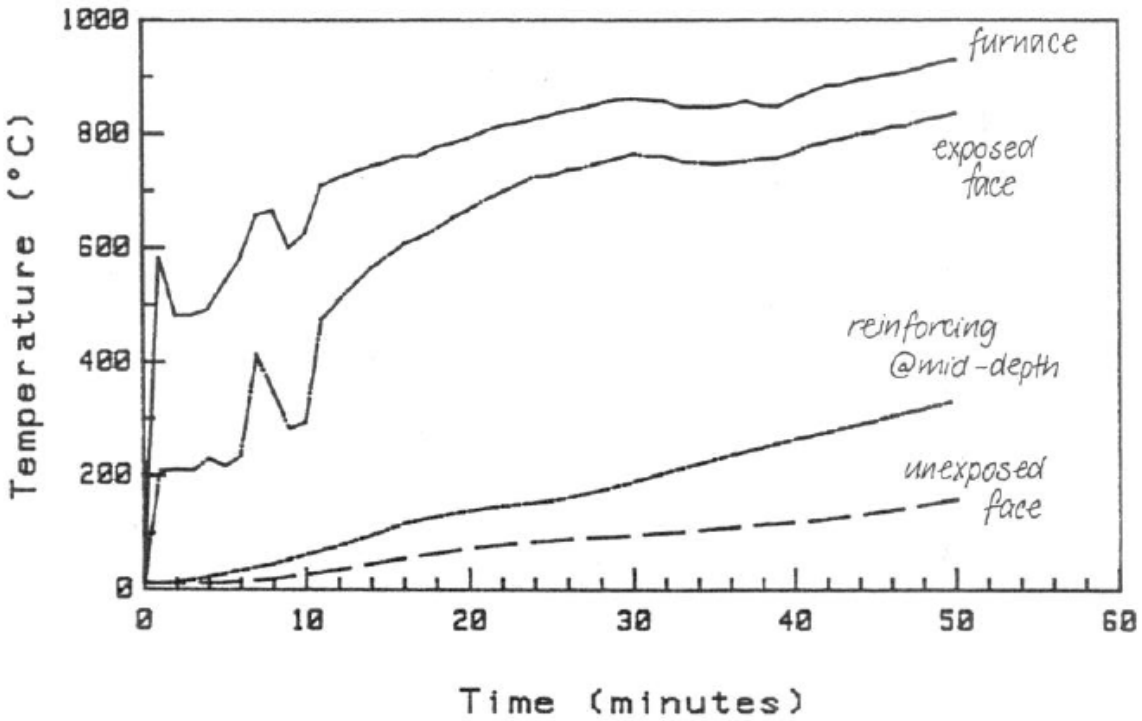

Figure G.4: BRANZ Data for the Temperature of the Unexposed Face, Exposed Face, and Furnace Temperature for a 60mm Alluvial Quartz Slab in ISO 834 Conditions (as taken from Wade 1992)

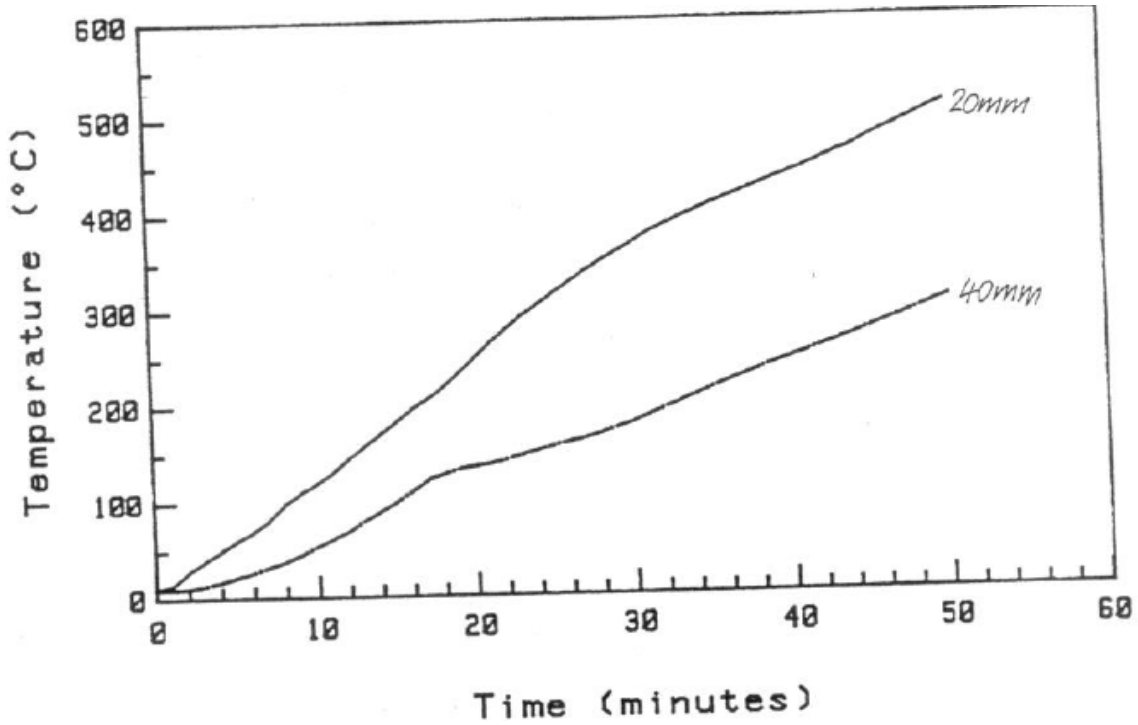

Figure G.5: BRANZ Temperature Distribution Data for a 60mm Alluvial Quartz Slab in ISO 834 Conditions (as taken from Wade 1992)

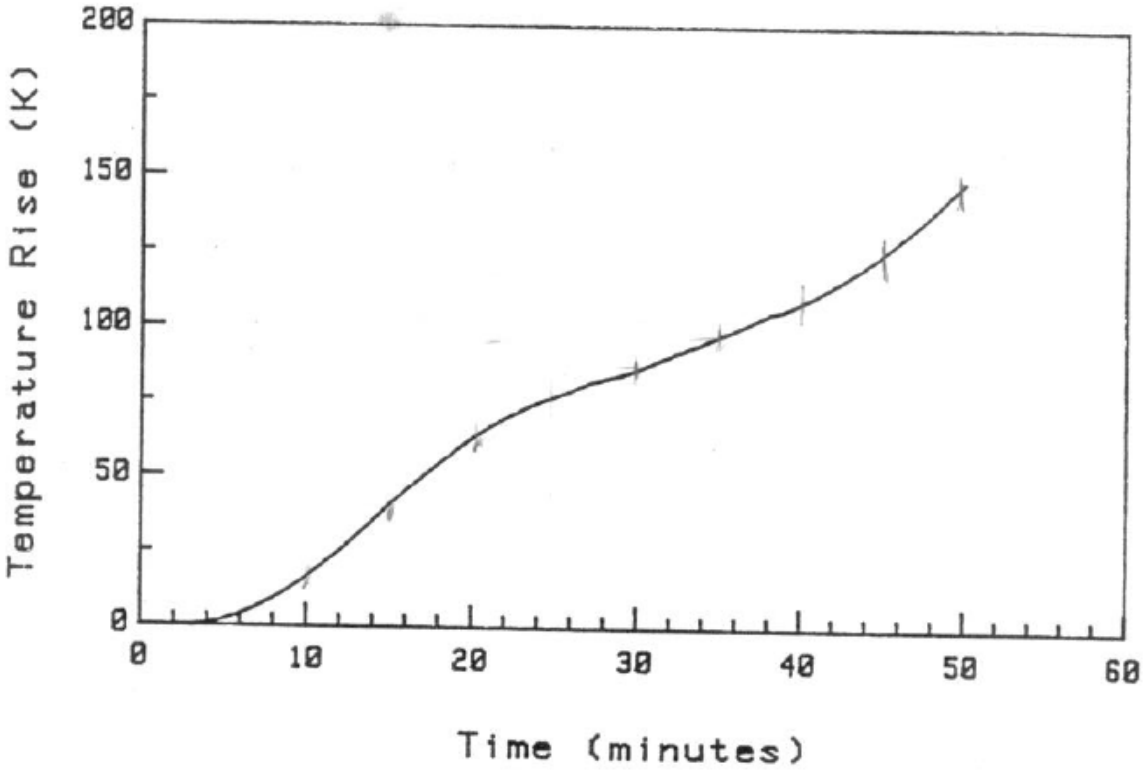

Figure G.6: BRANZ Data for the Temperature of the Unexposed Face of 60mm Alluvial Quartz Slab in ISO 834 Conditions (as taken from Wade 1992)

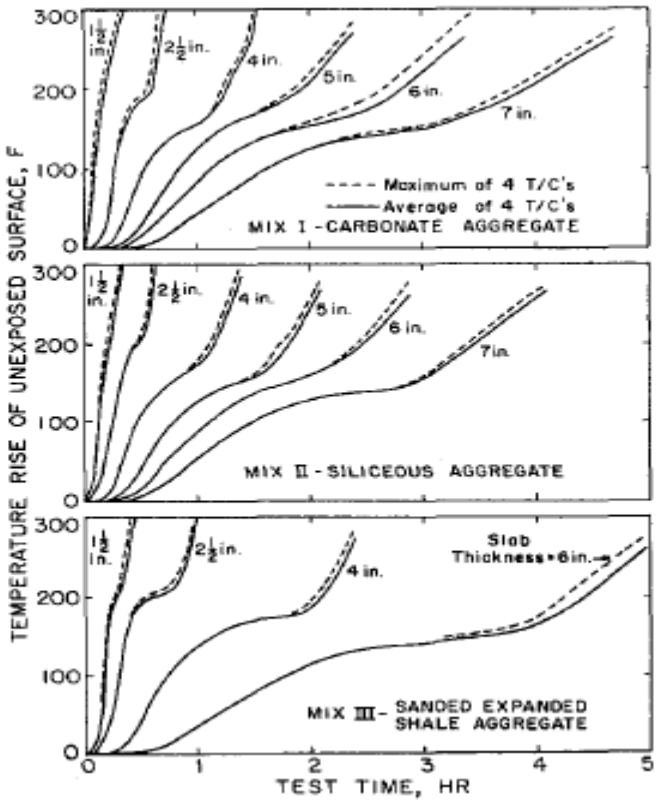

Figure G.7: Time versus Unexposed Surface Temperature for Various Concrete Slabs (as taken from Abrams & Gustaferro 1968)

H. TAS Temperature Distributions

Figures H.1 to H.4 show the modeled slab element in TAS with temperature distributions for 1 and 3 hours of ISO 834 exposure for both examined multiples for the heat release coefficient

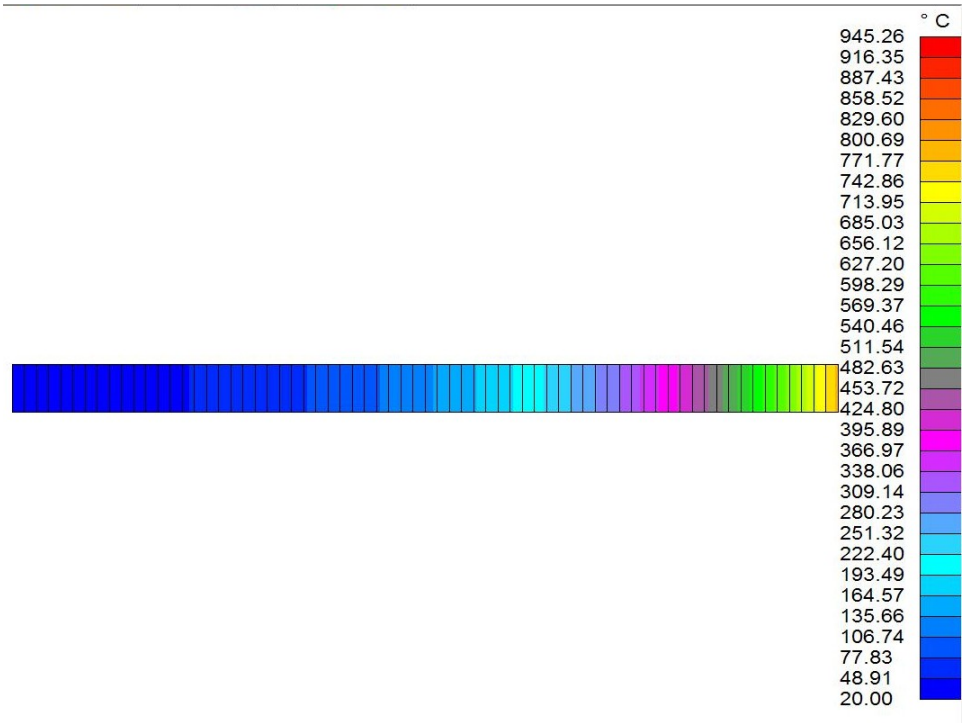

Figure H.1: Temperature Distribution for a 175 mm Alluvial Quartz Slab for 1 Hour Exposure to ISO 834 Conditions with Heat Release Function Multiple of 0.33

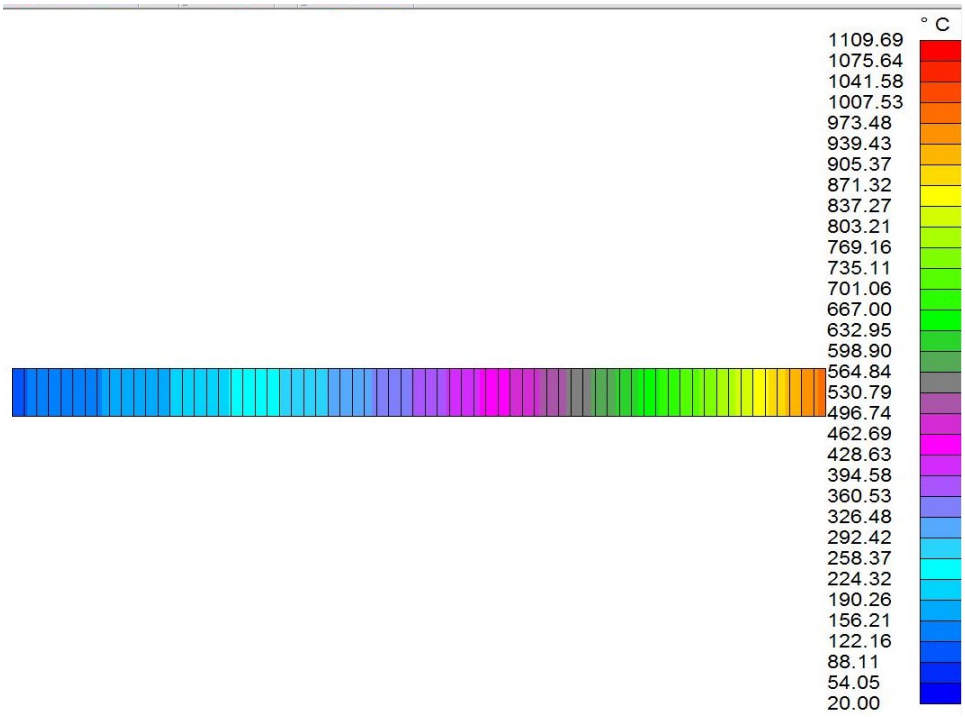

Figure H.2: Temperature Distribution for a 175 mm Alluvial Quartz Slab for 3 Hour Exposure to ISO 834 Conditions with Heat Release Function Multiple of 0.33

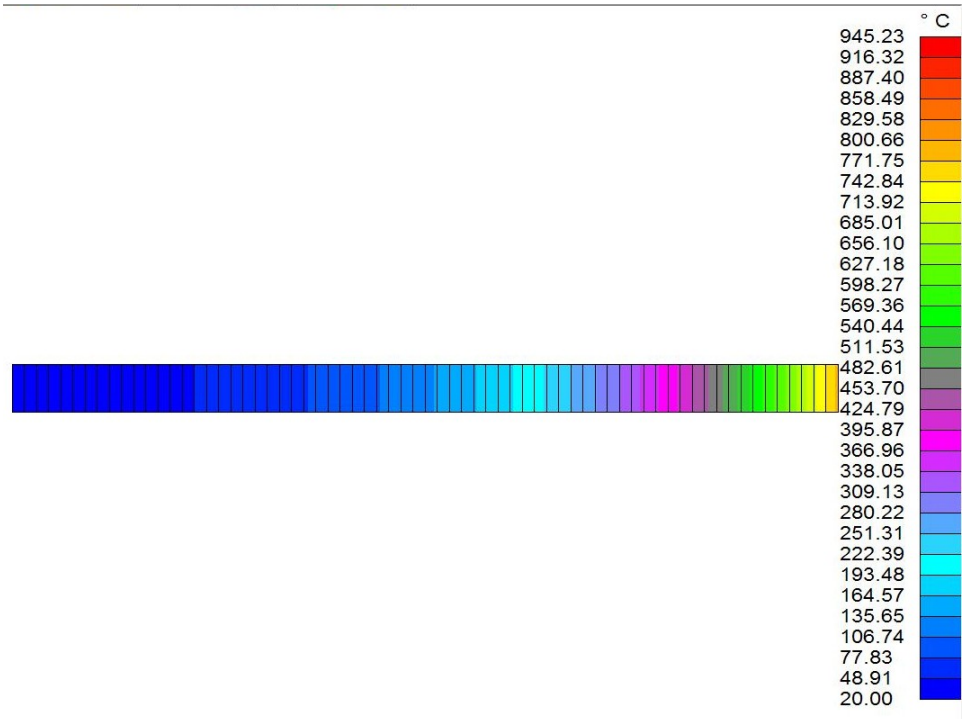

Figure H.3: Temperature Distribution for a 175 mm Alluvial Quartz Slab for 1 Hour Exposure to ISO 834 Conditions with Heat Release Function Multiple of 1

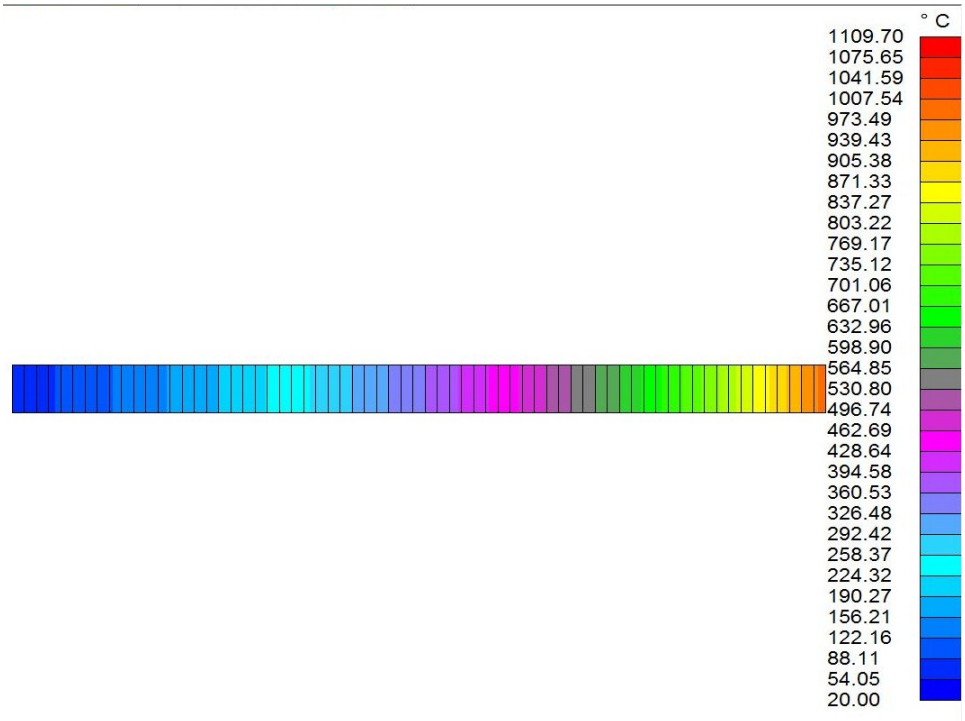

Figure H.4: Temperature Distribution for a 175 mm Alluvial Quartz Slab for 3 Hour Exposure to ISO 834 Conditions with Heat Release Function Multiple of 1